



TRC0401

**The Structural Evaluation of Precast  
Concrete Slab Panels in Bridge  
Superstructures,  
Phase II**

Stephan A. Durham, Ernest Heymsfield, Mark Kuss,  
Jessie X. Jones, Keith D. Tencleve

Final Report

2005

**Stephan A. Durham, Ernest Heymsfield, Mark Kuss,  
Jessie X. Jones, and Keith D. Tencleve**

# **The Structural Evaluation of Precast Concrete Slab Panels in Bridge Superstructures, PHASE II**

**December 2005**

**Sponsored by the  
Arkansas State Highway and  
Transportation Department**

**AHTD TRC 0401**

---

# **Final Report**

---



**Department of Civil Engineering**



**Arkansas State Highway and  
Transportation Department**



# The Structural Evaluation of Precast Concrete Slab Panels in Bridge Superstructures, PHASE II

## PROJECT OBJECTIVES

Prior to the mid 1970's a large number of short span bridges were constructed throughout Arkansas using 19ft. precast, non-prestressed concrete channel beams (PCBs) designed for H15 loading. These beams had no provisions for shear reinforcement. A statewide survey within Arkansas indicates that 389 of these bridges remain in service with nearly one-third experiencing potentially serious deterioration.

The primary objectives of this research project were:

- Determine the extensiveness of PCB deterioration in Arkansas.
- Evaluate potential causes for longitudinal cracking and reinforcing steel corrosion.
- Evaluate shear strengthening techniques for precast channel beams.
- Develop a cost effective retrofit scheme that can easily be implemented at an existing bridge site.

## FINDINGS

Ninety-five bridges containing nearly 2000 channel beams were inspected during a statewide investigation by the UA research team. This examination revealed that approximately 60% of the 2000 beams exhibit longitudinal cracking at the reinforcing steel level. In addition, exposed flexural reinforcing steel was observed in over 20% of the beams. Minimal concrete cover, heavier than designed for live loads, moisture penetration through flexure cracks, and high humidity levels are the major contributing factors for the reinforcing steel corrosion. An investigation of the structural integrity of these beams revealed inadequate shear capacity for the updated HS-20 design loading. Consequently, the major objective of this research work was to improve beam shear strength and ductile behavior.

Three shear strengthening retrofit methods were evaluated. Carbon fiber reinforced polymer strips and a sprayed epoxy coating were each examined as external shear strengthening retrofit methods. A third retrofit alternative involved inserting high strength steel reinforcing (MMFX Steel) "shear" bars internally in each beam stem. Of the three retrofit procedures examined, the shear bar retrofit was found to be the optimal method. The shear bar retrofit approach increased a beam's shear capacity and produced improved ductile beam behavior at failure. Results from a statistical analysis of load tested retrofitted beams, cost, and findings from retrofitting an existing bridge using shear bars substantiates retrofitting using shear bars to improve shear behavior.

**R  
E  
S  
E  
A  
R  
C  
H**

## **Acknowledgements**

The research presented herein was conducted by the University of Arkansas Civil Engineering Department under the direct supervision of the Arkansas State Highway and Transportation Department's Transportation Research Committee.

The contents of this report reflect the views and opinions of the authors and do not necessarily reflect the views of the Arkansas State Highway and Transportation Department.

Special thanks to Mr. James "Scooter" Key; for his involvement in this project to make it successful.

## **The Structural Evaluation of Precast Concrete Slab Panels in Bridge Superstructures, Phase II**

### **Abstract**

Prior to the mid – 1970’s a large number of short span bridges were constructed throughout Arkansas using 19ft. precast, non-prestressed concrete channel beams designed for H15 loading without any provisions for shear reinforcement. A national survey of state departments of transportation found that thirteen additional states have similar bridge elements in their highway inventory. A statewide survey indicates that 389 of these bridges remain in service with nearly one-third experiencing potentially serious deterioration. Ninety-five bridges containing nearly 2000 channel beams were inspected during a statewide investigation by the UA research team. This examination revealed that approximately 60% of the 2000 beams exhibit longitudinal cracking at the reinforcing steel level. In addition, exposed flexural reinforcing steel was observed in over 20% of the beams. Minimal concrete cover, heavier than designed for live loads, moisture penetration through flexure cracks, and high humidity levels are the major contributing factors for the reinforcing steel corrosion. An investigation of the structural integrity of these beams revealed inadequate shear capacity for the updated HS-20 design loading.

Three shear strengthening retrofit methods were evaluated. Carbon fiber reinforced polymer strips and a sprayed epoxy coating were each examined as external shear strengthening retrofit methods. A third retrofit alternative involved inserting high

strength steel reinforcing (MMFX Steel) “shear” bars internally in each beam stem. Four beams retrofitted with CFRP strips, three beams retrofitted with sprayed epoxy coating, and five beams retrofitted with shear bars were load tested to evaluate the effectiveness of each repair method. Both CFRP and shear bar retrofit methods improved deflection behavior when compared to un-retrofitted beams. However, a premature shear failure was experienced in one of the sprayed epoxy coating retrofitted beams. Of the three retrofit techniques, the shear bar retrofit was selected as the optimal shear strengthening method based on structural response, lowest cost, and ease of implementation.

## Table of Contents

<b>List of Figures</b> .....	xi
<b>List of Tables</b> .....	xvii
<b>Chapter 1 Introduction</b> .....	1
<b>Chapter 2 Background</b> .....	5
2.1 National Precast Channel Beam Survey.....	5
2.2 Precast Channel Beam Design.....	6
2.3 Arkansas Precast Channel Beam Survey.....	7
2.4 Structural Evaluation of Existing Channel Beams.....	13
2.4.1 Loading Conditions.....	13
2.4.2 Structural Load Results.....	15
2.4.3 Shear Crack Location.....	16
2.5 Structural Evaluation of New Channel Beams.....	22
2.5.1 Strain Gauge Instrumentation.....	23
2.5.2 Structural Load Results for New Beams.....	25
<b>Chapter 3 Literature Review</b> .....	28
3.1 Effects of Steel Corrosion on Reinforced Concrete Members.....	28
3.2 Shear Strength Evaluation.....	30
3.2.1 Penetration Tests.....	33
3.2.2 Pull-Out Tests.....	33
3.2.3 Pull-Off Tests.....	34
3.2.4 Break-Off Tests.....	34

3.3	Shear Strengthening Techniques.....	35
3.3.1	Sprayed Fiber-Reinforced Polymer Technique.....	36
3.3.2	Externally Placed Fiber-Reinforced Polymer Strips.....	41
3.3.3	Bonded Steel Plates.....	46
3.3.4	Post-Tensioning Strengthening Technique.....	47
3.3.5	Reinforcing Bar Insertion Technique.....	48
3.4	Literature Summary.....	50
<b>Chapter 4 Problem Statement.....</b>		<b>51</b>
<b>Chapter 5 Longitudinal Cracking and Reinforcing Steel Corrosion.....</b>		<b>55</b>
5.1	On-Site Bridge Inspections.....	55
5.1.1	Chloride Content.....	56
5.1.2	Flexure Cracking.....	56
5.1.3	Longitudinal Cracking.....	58
5.1.4	Asphalt Wearing Surface and Deterioration.....	61
5.1.5	PCB Bridge Website Database.....	62
5.2	Bridge Loading Locations and Deterioration.....	66
5.3	Concrete Permeability.....	69
5.3.1	LP-CAP Testing Procedure.....	69
5.3.2	Permeability Results.....	71
5.4	Relative Humidity Data Collection.....	72
5.4.1	Data Collection.....	73
5.4.2	Danville, AR PCB Bridge.....	73
5.4.3	Lakeway, AR PCB Bridge.....	74

5.4.4	Relative Humidity Results.....	75
5.5	In-Situ Moisture Content Determination.....	76
5.5.1	Gravette, AR PCB Bridge.....	77
5.5.2	Moisture Content Results.....	78
5.6	Summary.....	78
<b>Chapter 6</b>	<b>Experimental Design: Shear Strengthening Methods.....</b>	<b>80</b>
6.1	Strength Evaluation.....	81
6.1.1	Moment Capacity and Equivalent HS Truck Loading.....	81
6.1.2	Shear Evaluation.....	84
6.2	Carbon Fiber-Reinforced Polymer Strips.....	87
6.2.1	Material Properties of CFRP Laminates.....	88
6.2.2	Design of the CFRP Strengthening Retrofit.....	88
6.3	MMFX Steel Shear Bar.....	93
6.3.1	Material Properties of MMFX Steel Reinforcement.....	93
6.3.2	Design of the MMFX Shear Bar Retrofit.....	93
6.4	Sprayed Epoxy Coating.....	97
6.4.1	Material Properties of the Sprayed Epoxy Coating.....	97
6.4.2	Design of the Sprayed Epoxy Coating.....	98
<b>Chapter 7</b>	<b>Retrofit Application Procedures.....</b>	<b>101</b>
7.1	Carbon Fiber-Reinforced Polymer Strip Application.....	101
7.1.1	Deteriorated Concrete Surface Repair.....	101
7.1.2	CFRP Strip Application.....	105

7.2 MMFX Steel Shear Bar Application.....	109
7.2.1 Deteriorated Concrete Surface Repair.....	109
7.2.2 MMFX Shear Bar Application.....	111
7.3 Sprayed Epoxy Coating Application.....	116
7.3.1 Deteriorated Concrete Surface Repair.....	116
7.3.2 Sprayed Epoxy Coating Application.....	117
<b>Chapter 8 Data Analysis and Results.....</b>	<b>121</b>
8.1 Beam Characteristics and Retrofit Details.....	121
8.2 Material Properties.....	123
8.3 Structural Results.....	126
8.3.1 Beam Deformation and Yielding.....	127
8.3.2 Load Capacity and Failure Modes.....	129
8.3.3 Shear Crack Location for Retrofit Beams.....	136
8.3.4 Structural Response to Cracking.....	137
8.3.5 Deflection and Energy Ductility.....	141
8.3.6 Failure Types.....	143
8.3.6.1 CFRP Shear Failure.....	144
8.3.6.2 Epoxy Failure.....	144
8.3.6.3 Concrete Bond Failure.....	146
8.3.6.4 Epoxy-Concrete Separation Failure.....	147
8.3.6.5 Concrete Failure.....	147

<b>Chapter 9 Statistical Analysis</b> .....	149
9.1 Statistical Investigation.....	151
9.1.1 Deflection Response.....	152
9.1.1.1 Five Treatment Levels.....	152
9.1.1.2 Sample Size Verification.....	154
9.1.1.3 Four Treatment Levels.....	156
9.1.2 Load Response.....	157
9.1.2.1 Five Treatment Levels.....	157
9.1.2.2 Sample Size Verification.....	159
9.1.2.3 Four Treatment Levels.....	159
9.2 Cost Analysis.....	161
9.3 Summary.....	163
<b>Chapter 10 Field Investigation</b> .....	164
10.1 Bridge Description.....	164
10.2 Retrofitting Deteriorated Panels.....	168
10.3 Instrumentation.....	169
10.4 Loading Procedure.....	174
10.5 Distribution Factors.....	176
10.5.1 No Retrofit.....	178
10.5.2 Retrofit.....	183
10.6 Impact Factors.....	187

<b>Chapter 11 Summary and Conclusions</b> .....	192
11.1 Summary.....	192
11.2 Conclusions.....	193
<b>References</b> .....	198
<b>Appendix A Bridge Inspection Report</b> .....	203
<b>Appendix B Structural Capacity Results for Thirty-Three PCB's</b> .....	207
<b>Appendix C New Beams Load Data and Strain Gauge Results</b> .....	212
<b>Appendix D Retrofit Design Calculations</b> .....	222
<b>Appendix E Retrofit and Control Load Testing Results</b> .....	234
<b>Appendix F Statistical Analysis</b> .....	263
<b>Appendix G Deflection Results from Field Implementation</b> .....	270

## List of Figures

Figure 1.1: Typical PCB Bridge Cross-Section.....	1
Figure 1.2: Cross-Sectional View of Interior Channel Beam.....	2
Figure 1.3: Elevation View of Interior Channel Beam.....	3
Figure 2.1: Ownership of PCB Bridges in Arkansas.....	8
Figure 2.2: Number of PCB Bridges by District and Ownership.....	9
Figure 2.3: PCB Bridges in Each Condition Category by District Location.....	12
Figure 2.4: Loading Configuration.....	14
Figure 2.5: Equivalent Force Diagram.....	14
Figure 2.6: Location of Selected Precast Channel Beams.....	15
Figure 2.7: Typical Shear Crack Behavior.....	17
Figure 2.8: Typical Shear Crack Measurement.....	18
Figure 2.9: Histogram and Normal Probability Plot for Shear Crack Location.....	21
Figure 2.10: Newly Fabricated Precast Channel Beam.....	22
Figure 2.11 Strain Gauge Locations for New Beams.....	23
Figure 2.12: Strain Gauges on Longitudinal Reinforcing Steel.....	24
Figure 2.13: Load versus Deflection Curves for New Beams.....	26
Figure 2.14: Failure Modes for New Beams.....	27
Figure 3.1: Details of CFRP Strengthening of Channel Sections.....	44
Figure 3.2: Strut Installed on Mid-Span Diaphragm.....	48
Figure 4.1: Deterioration of Jenkins' Ferry Bridge.....	52
Figure 4.2: Load vs. Deflection Curves (Poor Condition Beams).....	53

Figure 5.1: Flexure Crack in Mid-Span Region of Beam.....	57
Figure 5.2: Moisture at Beam Stem Base.....	58
Figure 5.3: Longitudinal Cracking and Concrete Spalling in PCB Bridge Beams.....	59
Figure 5.4: Concrete Cover to Reinforcing Bar Diameter Ratio.....	60
Figure 5.5: Moisture at Asphalt-Concrete Interface.....	61
Figure 5.6 Asphalt Wearing Surface and Beam Deterioration.....	62
Figure 5.7: Website Database.....	63
Figure 5.8: Detailed Bridge Checklist on Website.....	64
Figure 5.9: Bridge Site Photos on Website.....	65
Figure 5.10: Traffic Monitoring.....	66
Figure 5.11: Bridge Loading Location and Deterioration.....	68
Figure 5.12: LP-CAP Testing Device.....	69
Figure 5.13: Temperature and Humidity Gauge.....	73
Figure 5.14: Longitudinal Cracking on Danville PCB Bridge.....	74
Figure 5.15: Danville PCB Bridge Temperature and Humidity Data.....	75
Figure 5.16: Lakeway PCB Bridge Temperature and Humidity Data.....	76
Figure 5.17: Moisture Content Determination.....	77
Figure 6.1: HS-20 Axle Spacing and Wheel Line Loads.....	82
Figure 6.2: Wheel Load Position for Maximum Live Load Moment.....	82
Figure 6.3: Equivalent HS Truck Wheel Line Loads at Operating Level.....	84
Figure 6.4: Wheel Load Positions for Maximum Live Load Shear Force.....	85
Figure 6.5: Shear Strength Deficiency.....	87
Figure 6.6: CFRP Strengthening Retrofit.....	89

Figure 6.7: CFRP Strengthening Retrofit (Three Component System).....	90
Figure 6.8: Vertical and Diagonal Arrangement of CFRP Strip Application.....	92
Figure 6.9: MMFX Shear Bar Retrofit.....	95
Figure 6.10: Enlarged Schematic of MMFX Shear Bar Retrofit.....	96
Figure 6.11: MMFX Shear Bar Placement along Length of Beam.....	97
Figure 6.12: Side View of Beam with Sprayed Epoxy Retrofit.....	100
Figure 7.1: Fiber Reinforced Polymer Application Flow Chart.....	102
Figure 7.2: Repair Material and Beam Preparation.....	104
Figure 7.3: Concrete Patch Repair Procedure.....	105
Figure 7.4: Surface Preparation for CFRP Application.....	106
Figure 7.5: CFRP Retrofit Application Procedure.....	108
Figure 7.6: CFRP Vertical and Diagonal Retrofitted Beams.....	109
Figure 7.7: MMFX Steel Shear Bar Application Flow Chart.....	110
Figure 7.8: Beam Preparation for MMFX Shear Bar Retrofit.....	112
Figure 7.9: Reinforcing Bar Preparation.....	112
Figure 7.10 Epoxy Dispensing Tool.....	113
Figure 7.11: Epoxy Application and Bar Insertion.....	114
Figure 7.12: MMFX Steel Shear Bar Retrofit Process.....	114
Figure 7.13: Sprayed Epoxy Coating Application Flow Chart.....	116
Figure 7.14: Surface Repair Using Shotcrete Technique.....	118
Figure 7.15: Sprayed Epoxy Coating Retrofit Process.....	120
Figure 8.1: Regression Curve and Prediction Equation.....	126
Figure 8.2: Load versus Deflection Curves.....	127

Figure 8.3: Enlarged View of Load versus Deflection Curves.....	128
Figure 8.4: Vertical CFRP Retrofitted Beams at Failure.....	131
Figure 8.5: Diagonal CFRP Retrofitted Beams at Failure.....	132
Figure 8.6: Shear Bar Retrofitted Beams at Failure.....	133
Figure 8.7: Sprayed Epoxy Coating Retrofitted Beams at Failure.....	135
Figure 8.8: Control Beams at Failure.....	135
Figure 8.9: Shear Crack Location Histogram.....	138
Figure 8.10: Deflection and Energy Ductility Ratios.....	143
Figure 8.11: CFRP Shear Failure.....	144
Figure 8.12: Epoxy Failure.....	146
Figure 8.13: Concrete Bond Failure.....	147
Figure 8.14: Epoxy-Concrete Separation.....	148
Figure 8.15: Concrete Block Failure.....	148
Figure 10.1: Flat Hollow Branch Bridge Looking East.....	165
Figure 10.2: Flat Hollow Branch Bridge Looking North.....	165
Figure 10.3: Plan View of Flat Hollow Branch Bridge.....	166
Figure 10.4: Deteriorated Bridge Beam.....	167
Figure 10.5: Bridge Approach.....	168
Figure 10.6: Detail of Beams Retrofitted with Shear Bar Application.....	170
Figure 10.7: Strain Gage Location and Orientation.....	171
Figure 10.8: 15-Channel Data Acquisition System.....	172
Figure 10.9: Computers used for Data Collection.....	173
Figure 10.10: LVDT Setup for Measuring Beam Deflections.....	173

Figure 10.11: Truck Wheel Configuration.....	174
Figure 10.12: Static Load Positions Along the Length of the Beam.....	175
Figure 10.13: Loading Position and LVDT Instrumentation.....	176
Figure 10.14: Mid-Span Deflection vs. Longitudinal Position for Span 4 [1].....	181
Figure 10.15: Quarter-Span Deflection vs. Longitudinal Position for Span 4 [1].....	181
Figure 10.16: Beam 2 of Span 4.....	182
Figure 10.17: Mid-Span Deflection vs. Longitudinal Position for Span 4 [2].....	182
Figure 10.18: Quarter-Span Deflection vs. Longitudinal Position for Span 4 [2].....	183
Figure 10.19: Mid-Span Deflection vs. Longitudinal Position for Span 4 [1].....	184
Figure 10.20: Quarter-Span Deflection vs. Longitudinal Position for Span 4 [1].....	185
Figure 10.21: Mid-Span Deflection vs. Longitudinal Position for Span 4 [2].....	186
Figure 10.22: Quarter-Span Deflection vs. Longitudinal Position for Span 4 [2].....	186
Figure 10.23: Deflection Measurements for Truck Velocities Before Retrofit [1]....	188
Figure 10.24: Deflection Measurements for Truck Velocities After Retrofit [1].....	189
Figure 10.25: Deflection Measurements for Truck Velocities Before Retrofit [2]....	189
Figure 10.26: Deflection Measurements for Truck Velocities After Retrofit [2].....	190
Figure B1: Load vs. Deflection Curves for Jenkins' Ferry Bridge Beams.....	208
Figure B2: Load vs. Deflection Curves for Little Osage Creek Bridge Beams.....	209
Figure B3: Load vs. Deflection Curves for Gentry Maintenance Yard Beams.....	210
Figure B4: Load vs. Deflection Curves for Carlisle Ferry Bridge Beams.....	211
Figure C1: Load vs. Deflection Curves for New Beams.....	213
Figure C2: Load and Strain Results for Beam N1 with Shear Reinforcement.....	215
Figure C3: Load and Strain Results for Beam N2 with Shear Reinforcement.....	217

Figure C4: Load and Strain Results for Beam N3 without Shear Reinforcement.....	219
Figure C5: Load and Strain Results for Beam N4 without Shear Reinforcement.....	221
Figure E1: Load vs. Deflection Curves for CFRP Retrofitted Beams.....	235
Figure E2: Load vs. Deflection Curves for MMFX Shear Bar Retrofitted Beams...	236
Figure E3: Load vs. Deflection Curves for Sprayed Epoxy Coating Retrofitted Beams.....	237
Figure E4: Load vs. Deflection Curves for Control Beams.....	238

## List of Tables

Table 2.1: States with Precast Channel Beam Bridges.....	6
Table 2.2 Precast Channel Beam Details.....	7
Table 2.3 Condition Rating System [FHWA].....	10
Table: 2.4: Number of Beams in Each Condition Category.....	12
Table 2.5: Shear Crack Measurements.....	18
Table 2.6: Distance to Shear Crack at Mid-Height from Beam End.....	19
Table 2.7 Theoretical Frequency for Shear Crack Location.....	20
Table 2.8: Horizontal Crack Length.....	21
Table 2.9: New Beam Load Results.....	25
Table 3.1: Testing Matrix and Experimental Results.....	39
Table 3.2: Reinforcement Pattern.....	49
Table 5.1: Bridge Loading Locations for Lakeway Bridge.....	67
Table 5.2: Permeability Testing Results.....	71
Table 5.3: LP-CAP Test Results for 0.60 w/cm Mixtures.....	72
Table 5.4: Moisture Content Data.....	78
Table 6.1: CFRP Strengthening System Material Properties.....	89
Table 6.2: MMFX Steel Rebar Material Properties.....	94
Table 6.3: Sprayed Epoxy Coating Material Properties.....	99
Table 7.1: Patch Repair Material Properties.....	103
Table 7.2: Epoxy Curing Times.....	115
Table 8.1: Beam Characteristics.....	122
Table 8.2: Concrete Compressive Strength Values.....	124

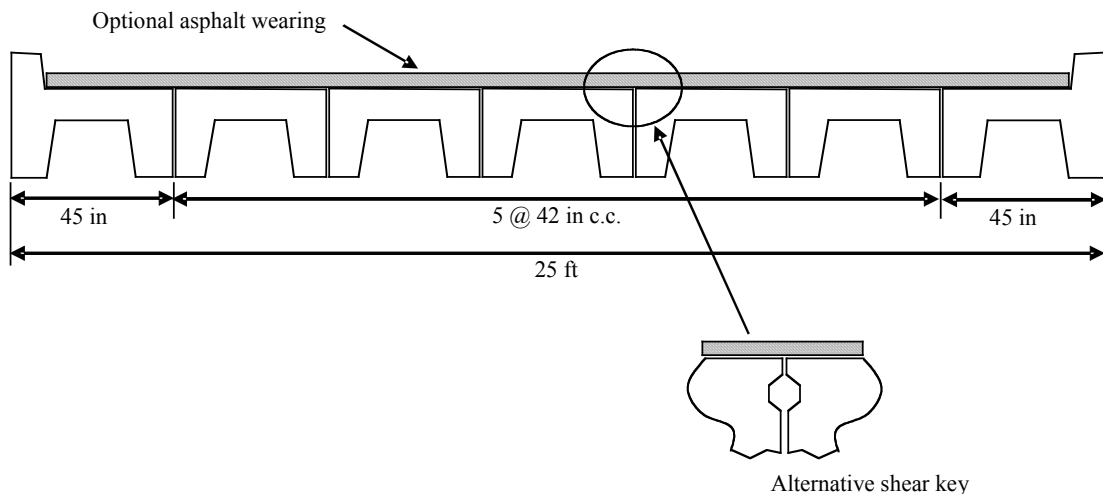
Table 8.3: Actual and Predicted Compressive Strength Values.....	125
Table 8.4: Maximum Mid-Span Deflections.....	129
Table 8.5: Actual Load Capacity Values.....	130
Table 8.6: Shear Crack Locations for Hope Beams.....	137
Table 8.7: Load Response to Cracking.....	139
Table 8.8: Deflection Response to Cracking.....	140
Table 8.9: Deflection and Energy Ductility.....	142
Table 8.10: Failure Mode and Description.....	145
Table 9.1: Testing Matrix.....	149
Table 9.2: ANOVA for Five Treatment Levels – Deflection.....	153
Table 9.3 Retrofit Rankings for Deflection with Five Treatment Levels.....	153
Table 9.4: Sample Size Adequacy for Deflection.....	155
Table 9.5: ANOVA for Four Treatment Levels – Deflection.....	156
Table 9.6: Retrofit Rankings for Deflection with Four Treatment Levels.....	157
Table 9.7: ANOVA for Five Treatment Levels – Load Capacity.....	158
Table 9.8: Retrofit Rankings for Load Capacity with Five Treatment Levels.....	159
Table 9.9: Sample Size Adequacy for Load Capacity.....	159
Table 9.10: ANOVA for Four Treatment Levels – Load Capacity.....	160
Table 9.11: Retrofit Rankings for Load Capacity with Four Treatment Levels.....	161
Table 9.12: Cost Comparison per Beam.....	162
Table 10.1: Distribution Factors for Beams 2, 3, and 4 .....	178
Table 10.2: Distribution Factors for Beams 4, 5, and 6.....	179

Table B1: Structural Load Results for Jenkins' Ferry Bridge Beams.....	208
Table B2: Structural Load Results for Little Osage Creek Bridge Beams.....	209
Table B3: Structural Load Results for Gentry Maintenance Yard Beams.....	210
Table B4: Structural Load Results for Carlisle Ferry Bridge Beams.....	211
Table C1: Structural Load Results for New Beams.....	213
Table E1: Structural Load Results for CFRP Retrofitted Beams.....	235
Table E2: Structural Load Results for MMFX Shear Bar Retrofitted Beams.....	236
Table E3: Structural Load Results for Sprayed Epoxy Coating Retrofitted Beams...	237
Table E1: Structural Load Results for Control Beams.....	238
Table G1: S4B2 Mid-Span Deflection Values.....	271
Table G2: S4B2 Quarter-Span Deflection Values.....	271
Table G3: S4B2R Mid-Span Deflection Values.....	272
Table G4: S4B2R Quarter-Span Deflection Values.....	272
Table G5: S4B6 Mid-Span Deflection Values.....	273
Table G6: S4B6 Quarter-Span Deflection Values.....	273
Table G7: S4B6R Mid-Span Deflection Values.....	274
Table G8: S4B6R Quarter-Span Deflection Values.....	274

## Chapter 1

### Introduction

Precast, non-prestressed, channel beams have been widely used in Arkansas for rural highway bridge superstructures due to their ease of construction and practical configuration. Prior to 1974, approximately 400 bridges of this type were constructed in Arkansas using 1952 AHTD bridge details. The bridge cross-section is comprised of seven beam sections, Figure 1.1. Interior sections measure 42-inch in width while the exterior section, which includes a built-in curb, has a width of 45in. The sections are bolted side-to-side to form the bridge cross-section and end-to-end to form multiple spans. The stem portion of the beam resists both flexure and shear forces, and the flange acts as the bridge deck. Load is distributed between sections through either friction and in some cases longitudinally grouted keyways.



**Figure 1.1: Typical PCB Bridge Cross-Section**

In the 1952 AHTD bridge details, a typical beam cross-section consists of two No. 9, Grade 40 longitudinal reinforcing bars in each stem, however lacks any shear reinforcement. Secondly, longitudinal reinforcement anchorage is developed only through embedment length since the longitudinal reinforcing bars do not have hooked ends. These beams were designed for a maximum H15 AASHTO loading. Both a detailed cross-section and elevation view of a single interior beam section are shown in Figures 1.2 and 1.3 respectively. Because the beams were fabricated without shear reinforcement, the shear strength is fully dependent upon the concrete compressive strength.

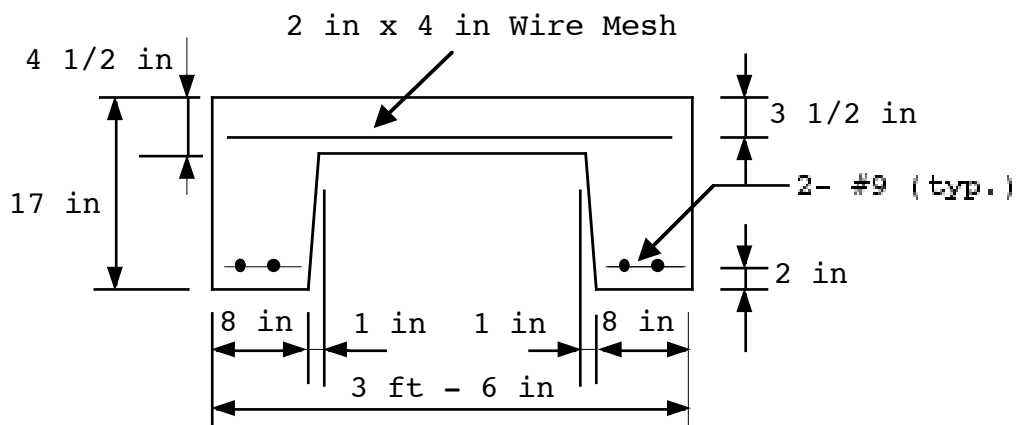


**Figure 1.2: Cross-Sectional View of Interior Channel Beam**

Within the past several years, the Arkansas State Highway and Transportation Department (AHTD) discovered that numerous precast channel beam (PCB) bridge superstructures are experiencing widespread and potentially serious deterioration. The major contributing factor to this severe deterioration is extensive concrete degradation

and longitudinal reinforcing steel corrosion. An added concern is that these beams were designed for a maximum AASHTO H15 loading.

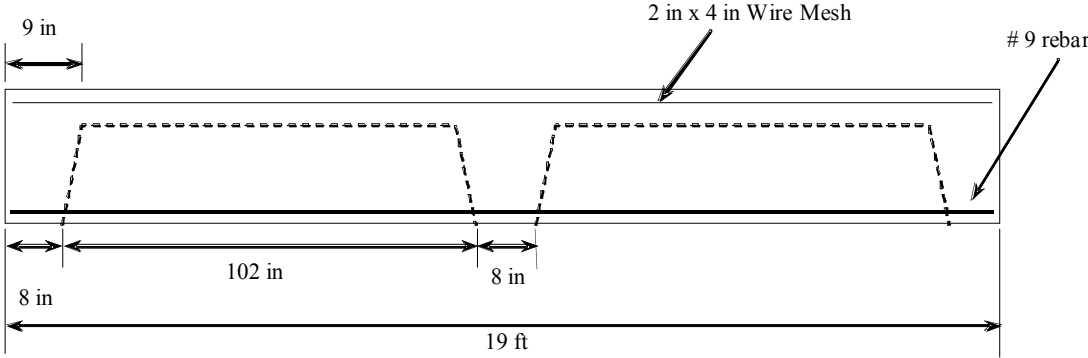


**Figure 1.3: Elevation View of Interior Channel Beam**

An earlier study revealed that these PCB beams have inadequate shear capacity to ensure ductile behavior [Durham, Heymsfield, and Schemmel, 2003]. In addition, many of the beams have extensive spalling with corroded longitudinal reinforcing steel creating the possibility of bond failure between the flexural reinforcement and concrete.

This report considers the deficiencies inherent to these type of beams, and then develops retrofit approaches to remedy these problems. To accomplish this task, research was performed to, establish beam strength, examine potential causes for the extreme beam deterioration, and develop three retrofit applications to increase beam shear strength. The primary objective of this current research is to determine the contributing factors to the extensive deterioration that many of these beams exhibit

and then develop a cost effective shear strengthening retrofit that can be easily implemented in the field.

This report includes:

- Detailed information on thirty-three PCBs that were load tested at the University of Arkansas Engineering Research Center.
- A comprehensive literature review of existing shear strengthening retrofit techniques.
- A research statement and description of tasks.
- An investigation into potential causes for longitudinal cracking and reinforcing steel corrosion.
- An experimental design of three shear strengthening techniques: carbon fiber reinforced polymer strips, micro-composite multi-structural formable steel reinforcing bars, and a sprayed epoxy coating.
- A detailed procedure for each retrofit application.
- Structural load testing of twelve retrofitted beams and four control “un-retrofitted” beams.
- A statistical analysis to determine the optimal retrofit method.
- Field implementation of the optimal retrofit method.

## **Chapter 2**

### **Background**

Throughout the past 50 years, precast concrete channel beams have been used by the AHTD for bridge construction. In the following sections, information regarding state and national surveys is reviewed to summarize the usage level of these beam types. In addition, results from a previous study, which includes load testing results on formerly in-service beams and newly fabricated beams, are discussed.

#### **2.1 National Precast Channel Beam Survey**

A national survey of state highway departments was conducted by the author to gather knowledge of PCB usage within the United States [Durham, Heymsfield, and Schemmel, 2003]. The survey consisted of questions ranging from the number of precast channel beam bridges that are included in their state's highway system to questions of deterioration problems and methods of rehabilitation. Of the twenty-six states that responded to the survey, fourteen have used precast concrete channel beam bridges. States which have used precast channel sections are listed in Table 2.1. Results of the survey found the use of the PCB bridge superstructure represents a small percentage of the total number of bridges in the states surveyed. Percentages ranged from 0.2% to 8.5% with the typical age of these bridges ranging from 5 years in Louisiana to 50 years in Iowa. However, the average bridge age for most states is 30 years or older.

Survey results found that longitudinal cracking, concrete spalling and steel corrosion are evident in eleven of the fourteen states. This type of deterioration is similar to that seen in Arkansas in which concrete delaminations and reinforcing steel corrosion have been identified. Repair strategies that these states are using include patching and bridge replacement.

**Table 2.1: States with Precast Channel Beam Bridges**

Arkansas*	Illinois*	Indiana*	Iowa*
Kentucky*	Louisiana	Minnesota*	Mississippi*
Missouri*	Nebraska*	North Dakota	Pennsylvania
South Dakota*	Wyoming*		

\* Indicates States with PCB Deterioration

## **2.2 Precast Channel Beam Design**

The AHTD design details for 19-ft precast channel beams in bridge superstructures have been revised since the original 1952 AHTD bridge details. Modifications to the original design details include shear reinforcement and an increase in: concrete compressive strength, reinforcing steel yield strength, and design loading. Revisions to the bridge details are summarized in Table 2.2. Most notable for beams constructed prior to 1974 is the fact that the design did not include requirements for shear reinforcement. In 1974, the design was modified to include shear reinforcement. The beams examined in this report were constructed in the pre-1974 era. The lack of shear reinforcement in these sections along with increased truck loads has raised a serious concern for the structural behavior of these beams.

**Table 2.2 Precast Channel Beam Details**

Year	Concrete Compressive Strength $f_c$ (ksi)	Longitudinal Reinforcing Steel Strength $f_y$ (ksi)	Design Truck Loading (Axle Load)	Shear Reinforcement
1952	3	40	H15 (6k - 24k)	No
1974	3	40	H15 (6k - 24k)	Yes
1993	3.5	60	H20 (8k - 32k)	Yes
1997	4	60	HS20 (8k-32k-32k)	Yes

### **2.3 Arkansas Precast Channel Beam Survey**

A statewide survey was conducted to determine the number of pre-1974 precast channel beam bridges, constructed without shear reinforcement, that exist in the state from bridge inventory data obtained from the AHTD [Jones, 2004]. The number of PCB bridges located within each county throughout the state was determined and the data was then separated into each of the state's 10 highway districts.

Currently, 503 of the total 1,955 PCB bridges in the Arkansas highway system consist of 19-foot beams. Upon further review, 389 of the 503 bridges contain beams designed using the 1952 AHTD bridge details, which did not require shear reinforcement. Approximately 77% of the 389 PCB bridges are under state ownership while counties and cities own 18% and 5% respectively, Figure 2.1.

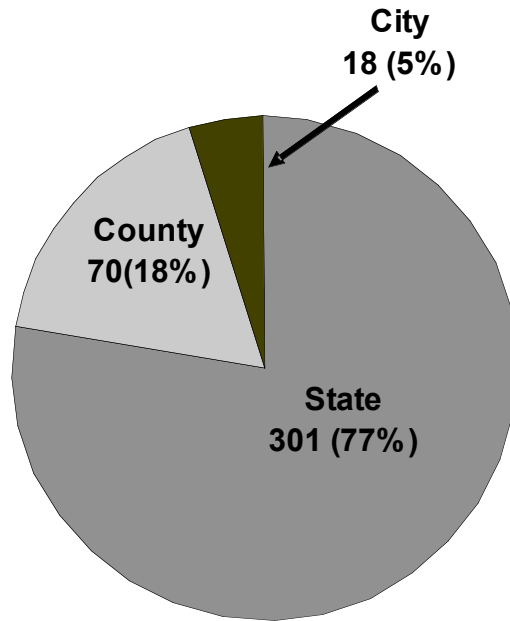


**Figure 2.1: Ownership of PCB Bridges in Arkansas**

The number of bridges significantly varied between districts. District 7 has the largest number of PCB bridges with 120 as compared with District 4 which only has 11 bridges. Similar to findings in Figure 2.1, the state owns the majority of the bridges in each district except District 4. The number of bridges in each district and their ownership is shown in Figure 2.2.

The condition of the 389 PCB bridges statewide was expected to vary based on preliminary observations at several bridge sites. To examine the condition of all 389 PCB bridges, AHTD field inspection reports were reviewed to classify the bridges into condition categories ranging from new to poor condition. The AHTD inspection

reports include condition ratings for the deck, superstructure, substructure, and river channel.

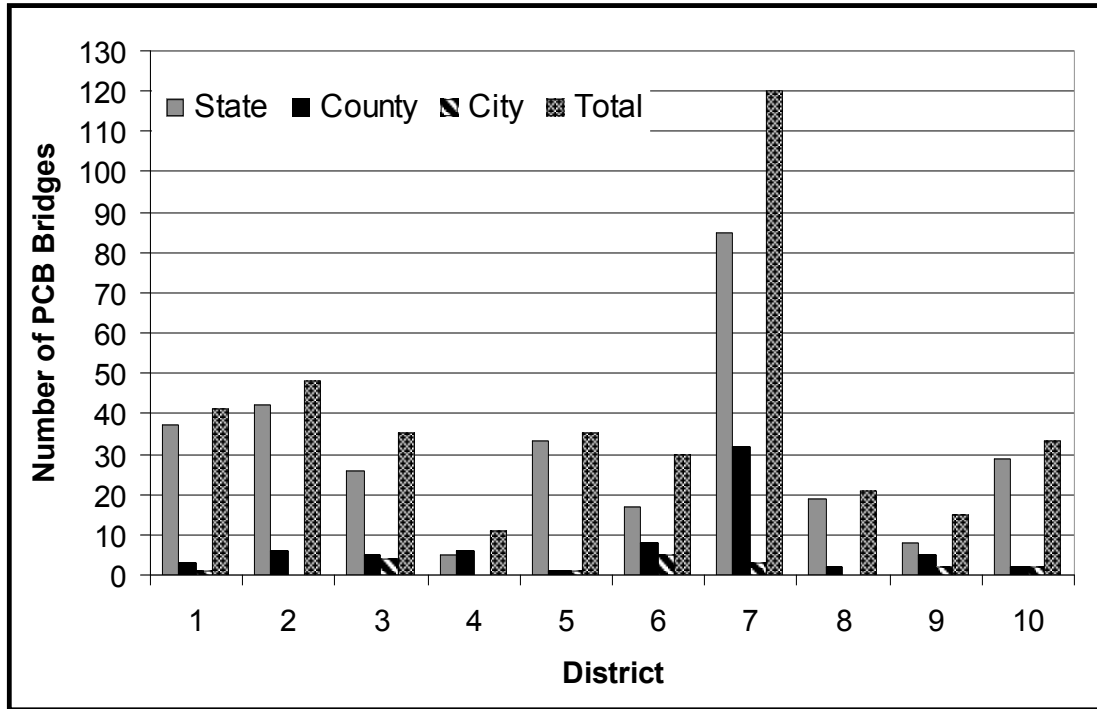


**Figure 2.2: Number of PCB Bridges by District and Ownership**

A typical bridge inspection report is shown in Appendix A. In this study, only the superstructure was of interest in the inspection reports. Information on the bridge superstructure from the field inspection reports include:

- Stringers
- **Girders or beams**
- Floorbeams
- Trusses
- Rivets or bolts
- Welds
- Concrete cracks
- Timber decay
- Collision damage
- Deflection under load
- Vibration under load
- Alignment of members
- Bearing devices

To identify the beam condition for a bridge, the rating for the “girders and beams” subsection was used as the overall rating of the beam. A rating system developed by the Federal Highway Administration, which is also used by AHTD, includes the qualitative definitions given in Table 2.3 [Federal Highway Administration, 1988].

**Table 2.3 Condition Rating System [FHWA]**

<b>Rating</b>	<b>Description</b>
<b>N</b>	<b>Not Applicable</b>
<b>9</b>	<b>Excellent Condition</b>
<b>8</b>	<b>Very Good Condition</b> - no problem noted.
<b>7</b>	<b>Good Condition</b> - some minor problems.
<b>6</b>	<b>Satisfactory Condition</b> - structural elements show minor deterioration.
<b>5</b>	<b>Fair Condition</b> - all primary structural elements are sound but may have minor section loss, cracking, spalling, or scour
<b>4</b>	<b>Poor Condition</b> - advanced section loss, deterioration, spalling, or scour.
<b>3</b>	<b>Serious Condition</b> - loss of section, deterioration, spalling, or scour have seriously affected primary structural components. Local failures are possible. Fatigue cracks in steel or shear cracks in concrete may be present.
<b>2</b>	<b>Critical Condition</b> - advanced deterioration of primary structural elements. Fatigue cracks in steel or shear cracks in concrete may be present or scour may have removed substructure support. Unless closely monitored it may be necessary to close the bridge until corrective action is taken.
<b>1</b>	<b>"Imminent" Failure Condition</b> - major deterioration or section loss present in critical structural components, or obvious vertical or horizontal movement affecting structural stability. Bridge is closed to traffic but corrective action may put bridge back in light service.
<b>0</b>	<b>Failed Condition</b> - out of service; beyond corrective action.

The FHWA rating system was used to classify the beams into 4 condition categories: new, good, average, and poor. A numerical rating of 9 was given for a new beam that was recently manufactured. Good beams were rated as 8 or 7 based on having little to no evidence of deterioration. An average condition beam was rated as 6 or 5. An average beam may be defined as having slight deterioration with minor section loss and cracking. Channel beams experiencing major concrete spalling, cracking, and extensive reinforcing steel corrosion were denoted as being in poor condition. Depending on the severity of the condition, poor sections were rated 4 or below.

Based on the AHTD bridge inspection reports, 69% (267) of the 389 bridges contain beams in good condition. In addition, 24% (94) consist of beams in average condition, and 7% (28) have poor beams. Table 2.4 lists the number of bridges in the four condition categories and their respective districts. This data is also shown in Figure 2.3 as a bar chart. Most notable, is the fact that 31% (15) of the bridges in District 2 are classified in poor condition. In addition, these represent 53% of the total number of bridges statewide in poor condition.

Considering that these inspections were conducted by multiple AHTD bridge inspectors, it is likely that subjectivity entered into the inspection process. Due to this subjectivity, beams classified in the average and poor conditions were examined by the UA research team first hand using on-site bridge inspections. This investigation is discussed in Chapter 5.

**Table: 2.4: Number of Beams in Each Condition Category**

Condition	New	Good	Average	Poor	
Rating	9	8-7	6-5	4-1	
District					Total
1	0	36	3	2	41
2	0	22	11	15	48
3	0	17	15	3	35
4	0	7	3	1	11
5	0	20	15	0	35
6	0	18	6	6	30
7	0	109	11	0	120
8	0	11	10	0	21
9	0	5	9	1	15
10	0	22	11	0	33
Total	0	267	94	28	389
Percent	0	69%	24%	7%	

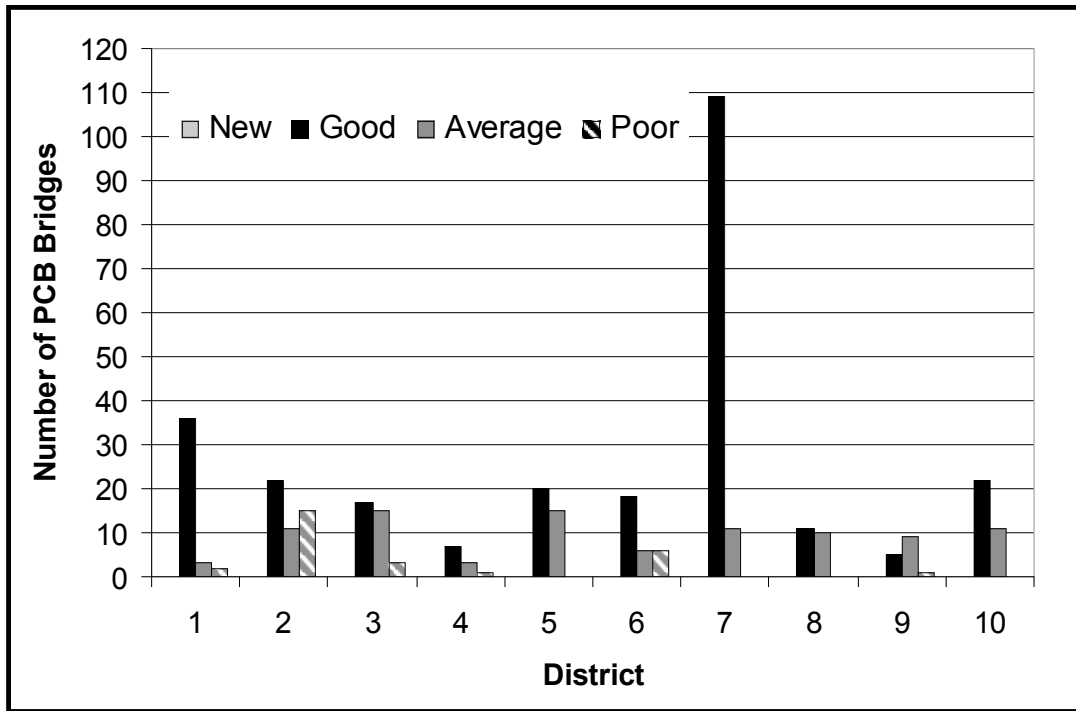


**Figure 2.3: PCB Bridges in Each Condition Category by District Location**

## **2.4 Structural Evaluation of Existing Channel Beams**

In a previous investigation, thirty-three formally in-service PCB's, ranging in condition category from good to poor, were load tested to evaluate their structural behavior [Durham Heymsfield, Schemmel, and Jones 2003]. Results from this earlier investigation were used to identify beam failure characteristics.

### **2.4.1 Loading Configuration**

The channel beams were load tested using a four-point loading setup, Figure 2.4. The applied load, mid-span deflection, and mode of failure were all monitored and digitally recorded throughout each test duration.

The load testing consisted of applying equal point loads,  $P$ , approximately 5.5-ft from either end of the beam. The concentrated force,  $P$ , was applied by two, 200-kip reversible hydraulic jacks linked in parallel. This loading configuration resulted in a linearly varying moment and constant shear in the end regions, and a mid-span of constant maximum moment and zero shear. The loading, bending moment, and shear diagrams are presented in Figure 2.5.

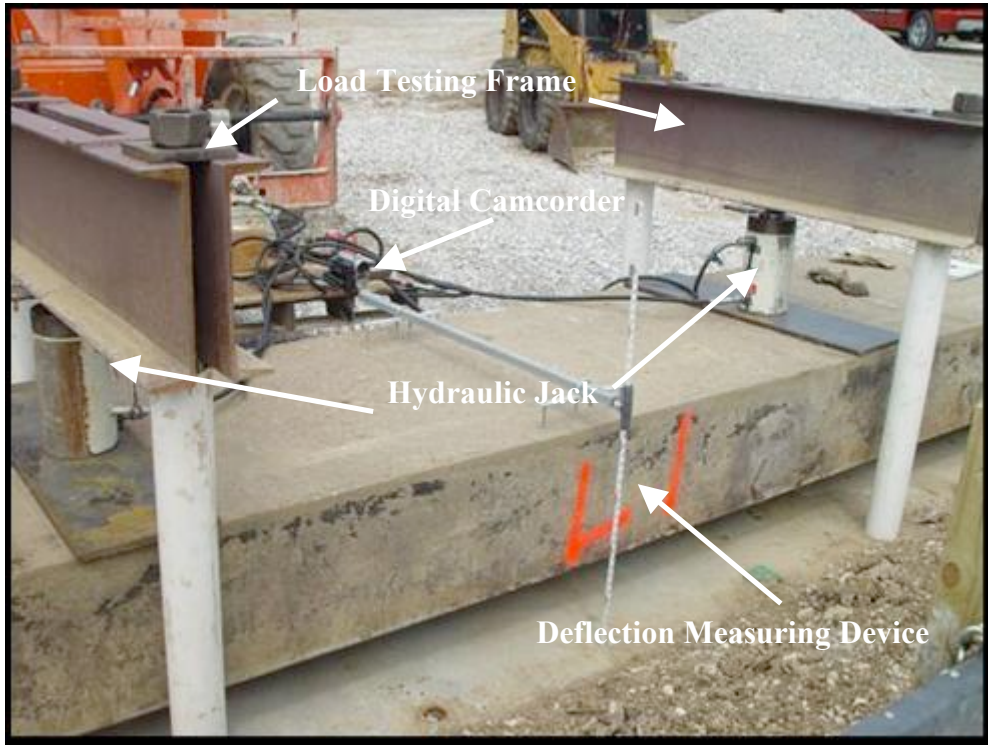


**Figure 2.4: Loading Configuration**

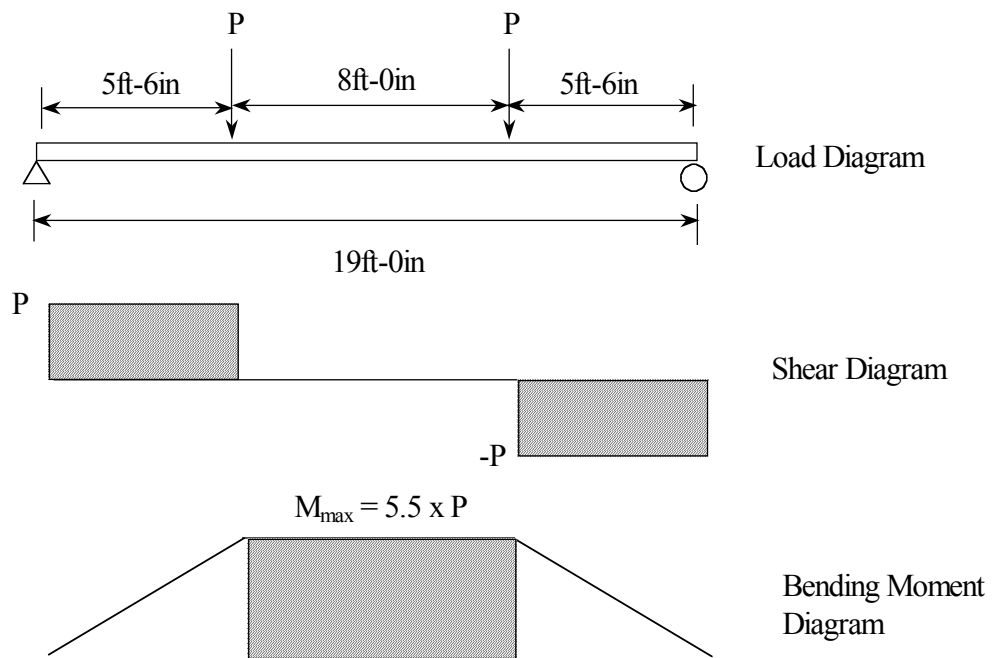


**Figure 2.5: Equivalent Force Diagram**

### 2.4.2 Structural Load Results

Beams were chosen to be load tested from four locations, Figure 2.6. The condition of these beams taken from each site is listed to the right of Figure 2.6. Visual inspection was used to categorize the beam sections as good, average, poor, or repaired. Beams in varying states of deterioration were tested to produce load and deflection data as a function of beam condition.

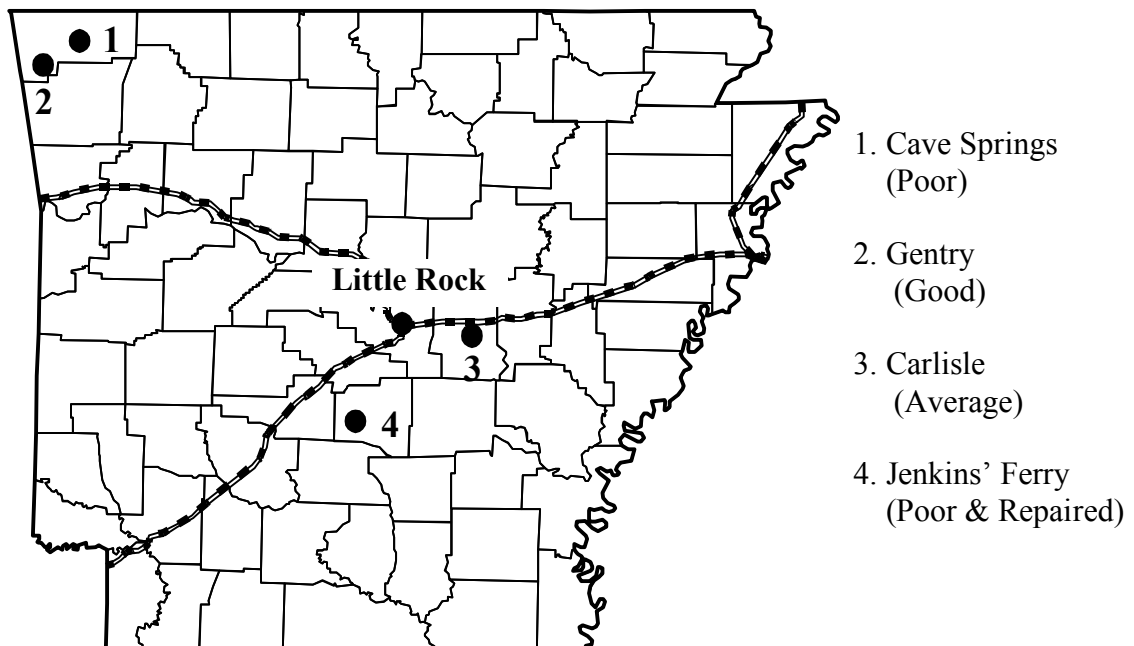


**Figure 2.6: Location of Selected Precast Channel Beams**

Similarities were identified as to the type and amount of deterioration between the thirty-three beams, and their corresponding load capacities. The total load carrying capacity,  $2P$ , for a beam in either good or average condition ranged from 94-kip to 124-kip, with a mean of approximately 100-kip. Beams rated as poor or repaired had considerably lower capacity,  $2P$ , ranging from 40-kip to 100-kip, with an average of

74-kip. Mid-span deflections were generally consistent with the load carrying capacity of a section ranging from 2-in to 6-in in good and average condition beams. Conversely, the mid-span deflections were significantly lower in poor or repaired sections ranging from 0.875-in to 4.5-in with an average of 1.8-in. Results for the thirty-three load tested beams are presented in Appendix B.

Load testing revealed that thirty-one of the thirty-three tested beams ultimately failed in shear. Further, five beams did not experience a yield plateau prior to failure. Failures not exhibiting a yield plateau are discussed in more detail in Chapter 4. Since there was no shear reinforcement present in these beams, the beam shear strength is directly dependent upon the shear strength of the concrete.

#### 2.4.3 Shear Crack Location

Shear crack locations from the thirty-three load tested beams were examined and used to establish criteria for shear crack locations [Jones et al, 2004]. Theoretically, shear cracks develop at a distance approximately  $d$  from the face of the support, where  $d$  is the depth from the extreme compression fiber to the centroid of the longitudinal reinforcing steel. The shear crack theoretically propagates upward at an approximately  $45^\circ$  angle toward the extreme compression fiber in the beam and defines a principal axis [ACI, 2002]. Figure 2.7 illustrates the theoretical shear crack behavior for beams in this study. The depth  $d$  for the beams examined in this research is 15-in. It is assumed that a shear crack for these beams will develop at approximately  $d$ , 15-in, from the support. During load testing, the beams rested on two 8-in x 8-in solid oak

timbers. Therefore, this configuration shifts the base of the shear crack origin to 23in. from the beam ends.

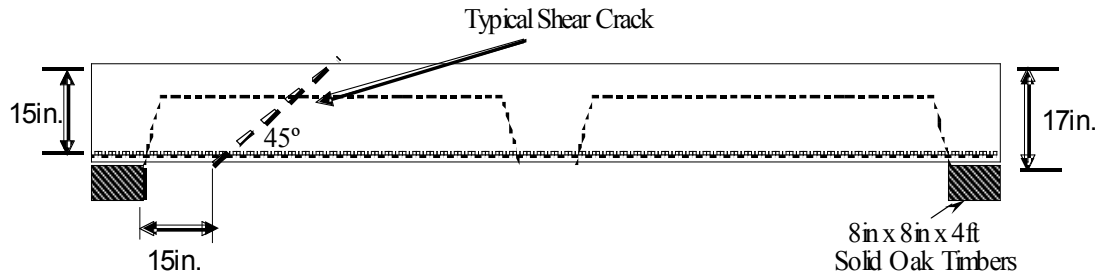


**Figure 2.7: Typical Shear Crack Behavior**

To more accurately determine shear crack locations, top and bottom shear crack distances were measured from each tested beam end. A single shear crack could be identified on twenty-three of the thirty-three beams. In addition, three beams exhibited shear cracks on both beam ends. Table 2.5 lists the top and bottom distances and resulting angles of the twenty-nine measured shear cracks. In some cases, the bottom distance was approximated by extending the diagonal crack to the bottom face of the beam where debonding between the concrete and reinforcing steel occurred, Figure 2.8.

As noted in Table 2.5 with an asterisk, nine (31%) shear cracks developed less than the estimated 23-in from the beam end. In sample 7, a shear crack developed only 4-in from the beam end, which is directly over the beam support.

**Table 2.5: Shear Crack Measurements**

Jenkins' Ferry				Little Osage Creek				Gentry				Carlisle							
No.	Bot. (in)	Top (in)	Angle (°)	No.	Bot. (in)	Top (in)	Angle (°)	No.	Bot. (in)	Top (in)	Angle (°)	No.	Bot. (in)	Top (in)	Angle (°)				
1	29	47	43	3	34	59	34	11	30	54	35	19	30	44	51				
2	31	60	30	4	32	61	30	12*	10	55	21	20*	22	38	47				
				5*	16	63	20	13	34	46	55	21	26	49	36				
				6*	12	48	25	14	38	54	47	22	29	47	43				
				7	24	51	32	15*	18	48	30	23	28	45	45				
				8	27	68	23	16*	18	47	30	24	29	53	35				
				9*	4	49	21	17	24	46	38	25	24	49	34				
				10*	9	50	23	18	23	50	32	26	24	46	38				
																27	25	56	29
																28	27	57	30
												29*	17	39	38				

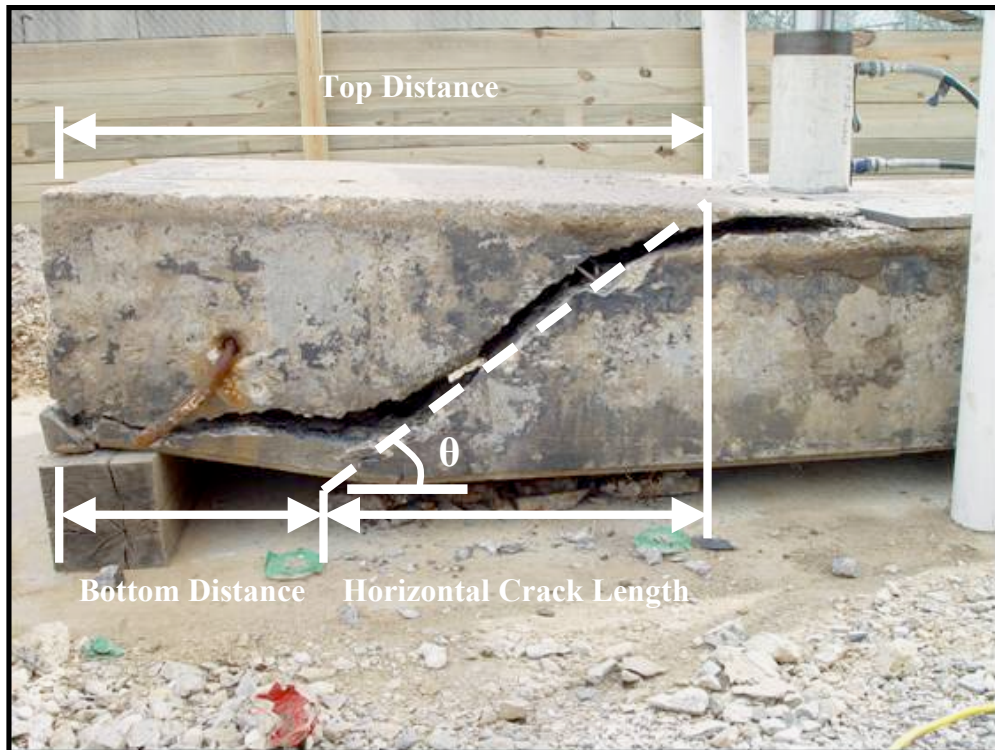


**Figure 2.8: Typical Shear Crack Measurement**

Also shown in Table 2.5 are shear crack angles computed from the bottom and top distance measurements. Most notable is that only five (17%) of the shear cracks resulted in an angle equal to or greater than 45° with 55° being the largest.

The collected data was used to produce a shear crack location histogram and normal probability plot for the retrofitting phase of this study. Table 2.6 lists the twenty-nine samples and their corresponding distances measured from the beam end to the mid-height of the shear crack.

**Table 2.6: Distance to Shear Crack at Mid-Height from Beam End**

No.	Bot. (in.)	Top (in.)	Mid-Height (in.)	No.	Bot. (in.)	Top (in.)	Mid-Height (in.)
1	29	47	38.0	16	18	47	32.5
2	31	60	45.5	17	24	46	35.0
3	34	59	46.5	18	23	50	36.5
4	32	61	46.5	19	30	44	37.0
5	16	63	39.5	20	22	38	30.0
6	12	48	30.0	21	26	49	37.5
7	24	51	37.5	22	29	47	38.0
8	27	68	47.5	23	28	45	36.5
9	4	49	26.5	24	29	53	41.0
10	9	50	29.5	25	24	49	36.5
11	30	54	42.0	26	24	46	35.0
12	10	55	32.5	27	25	56	40.5
13	34	46	40.0	28	27	57	42.0
14	38	54	46.0	29	17	39	28.0
15	18	48	33.0				

The data from Table 2.6 was grouped into class intervals. The frequency of the mid-height shear crack location within each class interval is listed in Table 2.7. The theoretical frequency for each class interval is plotted on the normal probability chart shown in Figure 2.9.

**Table 2.7 Theoretical Frequency for Shear Crack Location**

Class Interval (in)	Frequency	Percentage	Midpoints (in)	Prob. < x	Theoretical Probability	Theoretical Frequency
20-24	0	0.0%	22	0.0102	0.0102	0.2961
24-28	2	6.9%	26	0.0516	0.0414	1.1995
28-32	3	10.3%	30	0.1733	0.1218	3.5311
32-36	5	17.2%	34	0.4004	0.2271	6.5846
36-40	10	34.5%	38	0.6687	0.2683	7.7816
40-44	4	13.8%	42	0.8697	0.2010	5.8292
44-48	5	17.2%	46	0.9651	0.0954	2.7671
48-52	0	0.0%	50	0.9938	0.0287	0.8319
52-56	0	0.0%	54	0.9993	0.0055	0.1582

From this statistical analysis, the shear crack mid-height is most likely to occur, 96% probability, at a distance between 20-in and 48-in from the beam end. Further, there is over a 99% probability that a shear crack will develop within 50-in of the beam end.

The horizontal crack length, as shown in Figure 2.8, was determined by subtracting the crack distance at the top of the beam from the bottom distance. This data was used to estimate the horizontal shear crack length measured from the crack origin on the tension face to the compression face of the beam. Table 2.8 lists the horizontal crack lengths for the twenty-nine samples. The probability of a shear crack propagating through the entire depth of the beam in a 12-in horizontal length is approximately 6%.

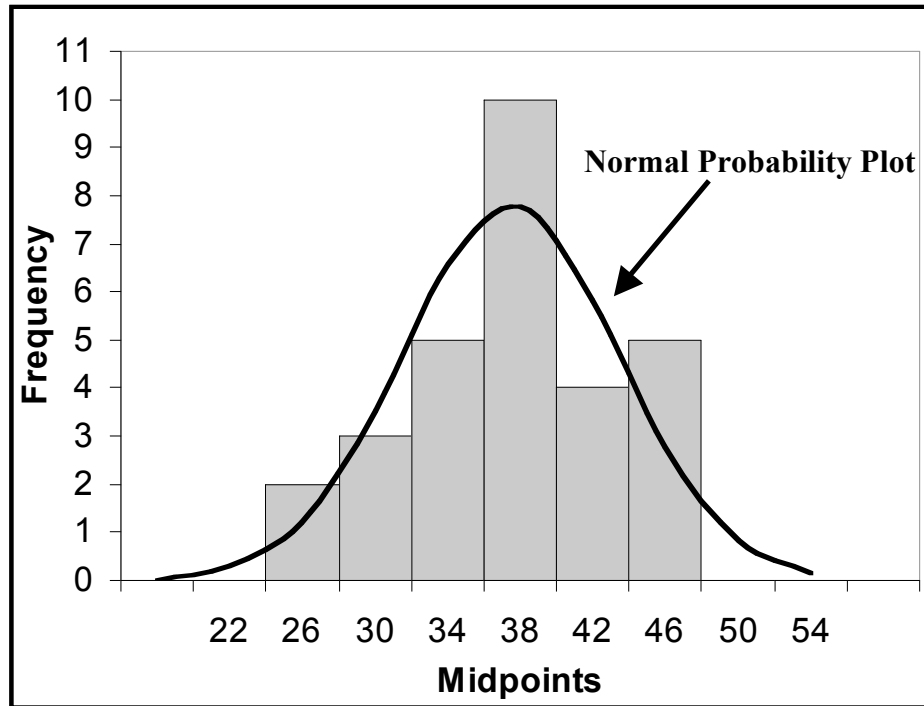


Figure 2.9: Histogram and Normal Probability Plot for Shear Crack Location

Table 2.8: Horizontal Crack Length

Class Interval	Frequency	Percentage	Prob. < x
<12	0	0.0%	0.0583
12-16	3	10.3%	0.1245
16-20	3	10.3%	0.2308
20-24	6	20.7%	0.3746
24-28	4	13.8%	0.5386
28-32	6	20.7%	0.6962
32-36	1	3.4%	0.8238
36-40	0	0.0%	0.9109
40-44	2	6.9%	0.9611
44-48	3	10.3%	0.9854
> 48	0	0.0%	0.9854

## **2.5 Structural Evaluation of New Channel Beams**

Four new precast channel beams were fabricated by Hanson Pipe and Products, Figure 2.10. Two fabricated beams were designed using the pre-1974 AHTD details and two were cast similarly however using shear reinforcement. Due to availability, grade 60 reinforcing steel, instead of grade 40, was used for all four beams. The two beams without shear reinforcement resembled the thirty-three beams tested in the structural investigation. The two sections with shear reinforcement were fabricated using #3 stirrups spaced every 8-in. During the fabrication process, concrete cylinders were cast to determine the compressive strength. In addition, documentation was obtained from Hanson Pipe and Products regarding the steel strength characteristics. The overall average concrete compressive strength for the newly fabricated beams was 7695-psi.



**Figure 2.10: Newly Fabricated Precast Channel Beam**

### 2.5.1 Strain Gauge Instrumentation

To monitor the behavior of the reinforcing steel during load testing, strain gauges were placed on the reinforcing steel. Strain gauges were located approximately 18-in, 78-in, and 114-in from both beam ends in each stem. Furthermore, two strain gauges were placed at stirrup mid-height in the shear reinforced beams. This configuration resulted in using twelve gauges in a shear reinforced channel beam and ten gauges in a beam without stirrups. A detail of this placement is shown in Figure 2.11. Figure 2.12 shows the strain gauges installed on the longitudinal reinforcing steel of (a) a beam without shear reinforcement and (b) a beam including stirrups.

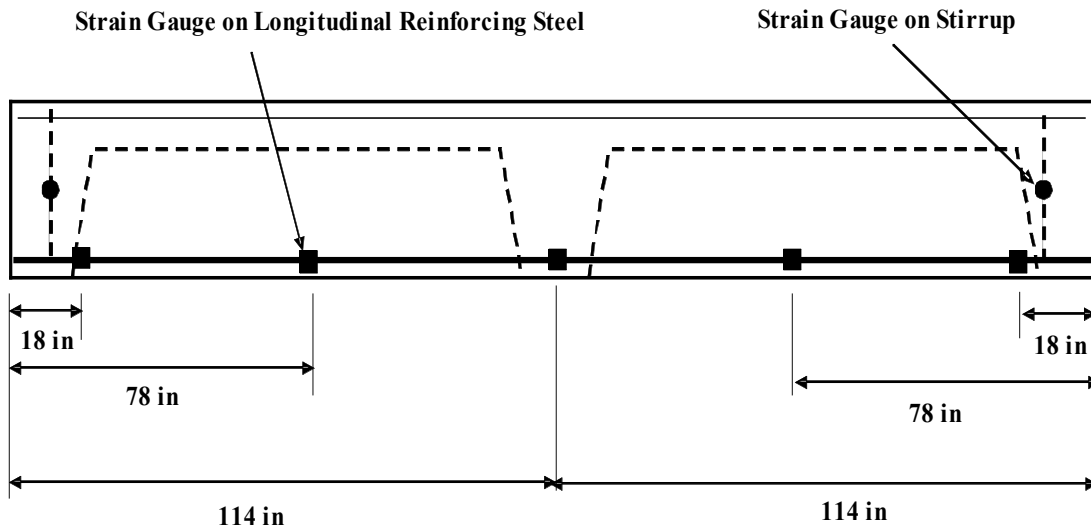


**Figure 2.11 Strain Gauge Locations for New Beams**

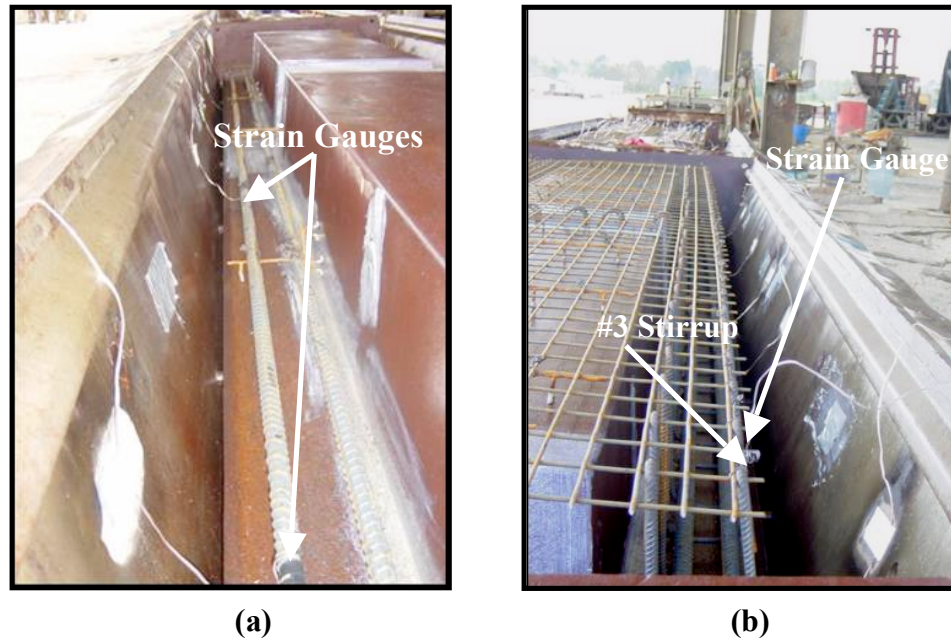


**Figure 2.12: Strain Gauges on Longitudinal Reinforcing Steel**

Strain gauges along the length of the longitudinal reinforcing steel were positioned to be able to monitor the behavior of the reinforcing steel during yielding. During load testing, some strain gauges were found faulty. These faulty gauges were a result of either the installation process or gauge damage during the concrete placement procedure. The results from this investigation showed that during load testing, very little change in strain occurred in the shear regions until failure and this only in the beams without shear reinforcement. In the flexure region of the beam, there was a strain increase only in beams containing shear reinforcement. As the beam yielded and flexure cracks developed along the mid-region, the amount of load carried by the longitudinal reinforcement increased until compression failure in the deck surface occurred in compression. Strain gauge results for beams with and without shear reinforcement are found in Appendix C. A moving average of every 20 data points

was used in the chart due to the amount of noise in the wires connecting the strain gauges to the data acquisition system.

2.5.2 Structural Load Results for New Beams

The ultimate load capacity values for the new beams are summarized in Table 2.9. There is a considerable difference between the shear reinforced and non-shear reinforced beams. The shear reinforced beams reached load capacities, 2P, of approximately 140 kips with an average deflection of 6.13-in. Shear cracks developed in the shear reinforced beams at approximately 72-kip, but were constrained due to the shear stirrups. Conversely, beams without stirrups failed at an average of 78-kip and 1.09-in of deflection. This failure load corresponds very well with the calculated failure load of 80-kip based on the measured concrete compressive strength. The load versus deflection plots for the new beams are shown in Figure 2.13.

**Table 2.9: New Beam Load Results**

Beam	Stirrups	Load, 2P @ First Flexure Crack (kip)	Load, 2P @ First Shear Crack (kip)	Failure Load, 2P (kip)	Mode of Failure
N1	Yes	-	68	140	Flexure Deck Compression
N2	Yes	24	76	130	Flexure Deck Compression
N3	No	24	60	80	Shear
N4	No	-	63	78	Shear

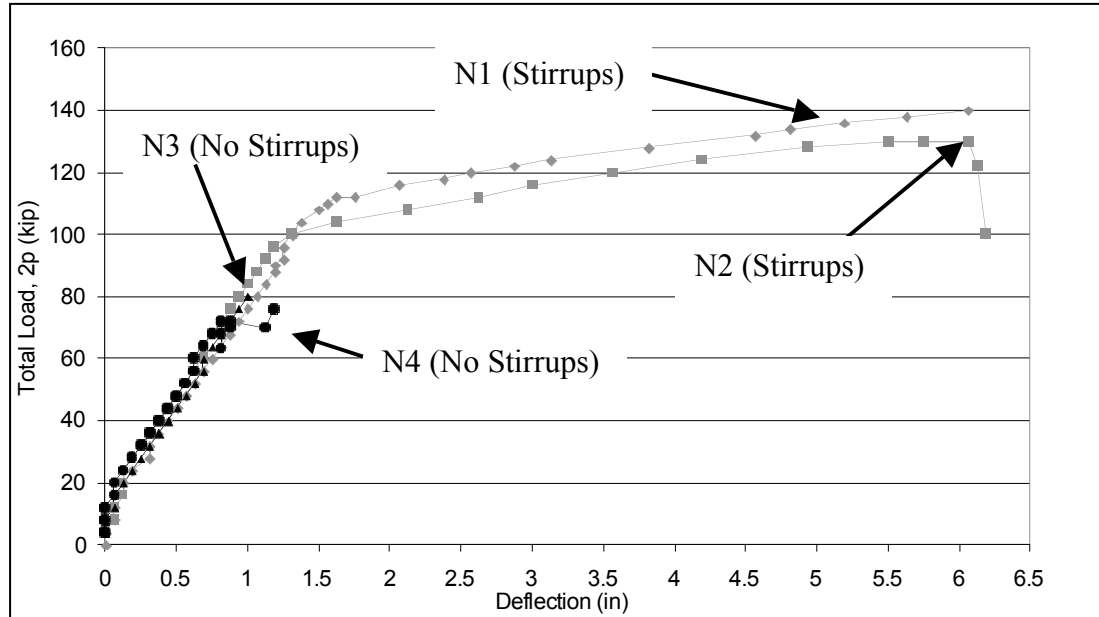


**Figure 2.13: Load versus Deflection Curves for New Beams**

Beams N1 and N2, which include shear stirrups, displayed a ductile behavior easily identified by the yield plateaus shown in Figure 2.13. Conversely, beams N3 and N4, without stirrups, failed suddenly in shear without reinforcing steel yielding. Figure 2.14 shows the two types of failure experienced with the new beams, (a) with and (b) without shear reinforcement.

With the addition of the shear reinforcement, there was a 42% increase in total load capacity,  $2P$ , and an 82% increase in deflection. In conclusion, shear deficiency coupled with brittle failure exhibited in beams excluding shear reinforcement warrants the need to develop a shear strengthening method for beams not having shear reinforcement.



(a)



(b)

**Figure 2.14: Failure Modes for New Beams**

## **Chapter 3**

### **Literature Review**

Much research has been performed recently on the repair or rehabilitation of concrete structures. This abundance in research is due in large part to an overwhelming majority of concrete bridges, nationally, reaching the end of their design life. However, research on the retrofitting of precast channel beam bridges is limited due to the relatively small number of such bridges nationwide. In the following, research examining potential reasons for steel corrosion in reinforced concrete members, shear strength evaluation and determination, and retrofit techniques on concrete structures is reviewed.

#### **3.1 Effects of Steel Corrosion on Reinforced Concrete Members**

Corrosion leads to the reduction of cross-sectional area of the reinforcing steel and may cause stress concentrations in the steel resulting in decreased ductility of the structural member [Yoon et al, 2000]. Yoon et al report findings that suggests the rate of corrosion may be a function of the applied load. Further, once the degree of steel corrosion exceeds 3% of the steel cross-sectional area, the remaining loading capacity of a reinforced concrete member may decrease as a percentage of the reinforcing steel weight loss. Tsukahara and Uomoto evaluated the corrosion rate of steel reinforcement in cracked concrete [Tsukahara and Uomoto, 2000]. Tsukahara and Uomoto suggest that cracks have the greatest impact on accelerating the deterioration of concrete structures.

Auyeung, Balaguru, and Chung acknowledge two mechanisms that result in strength loss [Auyeung et al, 2000]. These include a loss of reinforcement cross-sectional area and reduction in bond between the concrete and steel reinforcement. Therefore, besides the corrosion of the reinforcing steel, another important aspect is the bond behavior between the corroded reinforcing steel and the concrete. Four types of bond failures can be experienced in reinforced concrete structures: pullout without concrete splitting, pullout along a pre-existing crack due to corrosion, simultaneous splitting of the concrete and pullout failure, and concrete tension failure between long and short bars. At the initial stages of corrosion, bond slip behavior was improved due to friction at the bar-concrete interface. However, beyond 2% corrosion, a higher amount of slip between the reinforcement and concrete is seen. This additional slip is believed to occur due to tearing of the corroded reinforcing steel skin. Other research has also shown that longitudinal cracking occurs when reinforcing steel corrosion reaches approximately 2%. Al-Sulaimani, et al, examined the influence of corrosion and cracking on reinforcing steel bond behavior [Al-Sulaimani et al, 1990]. Their findings are similar to that of Auyeung, et al, in that the bond strength between the steel reinforcement and concrete increases up to approximately 1% corrosion and decreases there after. The initial increase in bond strength was attributed to the increased bar roughness due corrosion. In research conducted by Al-Sulaimani, et al, the cover-to-bar diameter ratio was a critical corrosion protection factor. Results of the study showed that four percent corrosion is needed to initiate concrete cracking when the  $c/d$  ratio is 7, whereas only 1 percent is needed for a  $c/d$  ratio of 3 [Al-Sulaimani et al, 1990, Emmons, 1993].

### **3.2 Shear Strength Evaluation**

Shear behavior in reinforced concrete has been studied since the early 1900's [Valerio and Ibell, 2003]. Despite extensive research over the last fifty years, the problem of how shear failure actually occurs in reinforced concrete members still remains indefinite [Zararis and Papadakis, 2001]. Ritter and Morsch, two of the first to conduct research in this area, believed that diagonal cracks in concrete were formed when the tensile strength of the concrete was exceeded [Valerio and Ibell, 2003]. In later years, the truss model was a widely accepted method of determining shear strength. In this model, the shear resistance is assumed to be provided by the concrete,  $V_c$ , and by the transverse shear reinforcement,  $V_s$ . However, in the truss model, shear reinforcement strength is not considered until the concrete is cracked. Zararis et al explain that reinforced concrete members without web reinforcement subjected to load will typically fail due to a crack that is formed from two shear cracks [Zararis and Papadakis, 2001]. The first branch is an inclined shear crack that originates near the supports occurring after the onset of flexural cracking. The second branch is initiated just prior to failure at the tip of the first branch and propagates toward the load. This type of failure is often found in beams where the shear span to depth ratio ( $a/d$ ) is greater than 2.5 where "a" is the distance to the load and "d" is the effective depth of the flexural steel reinforcement. Zararis et al proposed that the shear stress at failure is a function of the ratio of the neutral axis depth to the effective depth of the beam times the splitting tensile strength of the concrete, Equation 3.1.

$$v_u = \frac{V_u}{bd} = \frac{c}{d} f_{ct} \quad \text{Eq. 3.1}$$

where:  $V_u$  = shear force, lb  
 $v_u$  = shear stress, psi  
 $b$  = width of the beam, in  
 $c$  = depth of compression zone above the tip of the diagonal crack, in.  
 $d$  = effective depth to reinforcement, in.  
 $f_{ct}$  = splitting tensile strength of concrete, psi

For non-prestressed members, the American Association of State Highway and Transportation Officials (AASHTO) uses Equation 3.2 for concrete's contribution to shear resistance [ACI, 2002, AASHTO, 1996, Wang and Salmon, 1998]. This represents the typically accepted theoretical shear strength value of a beam without shear reinforcement.

$$V_c = 2\sqrt{f'_c} b_w d \quad \text{Eq. 3.2}$$

where:  $b_w$  = web width, in.  
 $d$  = effective depth to reinforcement, in.  
 $f'_c$  = concrete compressive strength, psi.  
 $V_c$  = concrete shear resistance

Some researchers feel that Equation 3.2 does not accurately account for the behavior between the arch action of a short beam and the beam action of a long beam [ACI, 2002]. Therefore, it only predicts the cracking shear strength and not the ultimate shear strength of the concrete. Consequently, Rebeiz, et al, have presented a new ultimate shear prediction equation, applicable to both normal and high strength concrete for concrete sections without shear reinforcement [Rebeiz et al, 2000]. Their

proposed equation is an empirical relationship developed from work using a dimensional analysis and a non-linear multiple regression analysis. Their relationship includes an interpolation function with a shape adjustment factor. The use of a shape adjustment factor was included to account for the arch action of short beams and beam action of long beams.

Three variables are included in the Rebeiz, et al shear prediction equation: the span-to-depth ratio ( $a/d$ ), the compressive strength ( $f'_c$ ), and the tensile reinforcement ratio ( $\rho$ ), Equation 3.3.

$$Vu = 57 + \sqrt{f'_c \rho (d/a)} [120 - 36 A_d] \quad \text{Eq. 3.3}$$

where:  $A_d$  = shear shape adjustment factor, =  $a/d$  for  $1.0 < a/d < 2.5$ , =  
 $2.5$  for  $a/d \geq 2.5$   
 $a$  = shear span, in.  
 $b_w$  = web width, in.  
 $d$  = distance from extreme compression fiber to centroid of  
longitudinal tension reinforcement, in.  
 $f'_c$  = specified compressive strength of concrete, psi.  
 $V_u$  = ultimate shear force, lb.  
 $\rho$  = flexural reinforcement ratio

As previously discussed, there are multiple methods for determining the shear strength of reinforced concrete members without shear reinforcement. However, the shear strength is a function of the concrete compressive strength,  $f'_c$ . Therefore, for existing concrete structures cast without shear reinforcement, non-destructive tests must be conducted for in-situ compressive strength values. There are numerous tests available to provide reasonably accurate values. Many of these tests termed “non-destructive”

in fact cause some minimal localized surface damage [Bungey, 1993]. However, these non-destructive strength assessment tests result in less damage than that of a cored specimen. Non-destructive test methods are divided into four broad categories: penetration resistance, pull-out tests, pull-off tests, and break-off tests. A description of each category is described below.

### 3.2.1 Penetration Tests [Bungey, 1993]

Penetration tests are based on the rationale that the depth of penetration of a projectile into a mass of concrete is inversely proportional to the concrete's compressive strength. Two tests that follow this approach are the Windsor probe test and Windsor penetrometer. The Windsor probe test involves driving a 3-in x 0.25-in hardened steel alloy bolt into the concrete surface. Disadvantages of this procedure include skewed results due to aggregate characteristics, curing, and concrete age. The Windsor penetrometer test differs in that it uses a smaller pin to drive into the concrete surface. Therefore, the Windsor penetrometer test is only applicable for fine grained materials and not particularly suitable for concrete containing aggregates.

### 3.2.2 Pull-Out Tests [Bungey, 1993]

Pull-out tests measure the tensile force capacity of a device embedded in concrete. The embedded device may be placed before or after the concrete is cured. The most common pull-out tests include the internal fracture test, Lok test, and Capo test. Of the two, the cast-in place Lok test is the more common of the tests. This test involves positioning a 1-in diameter metal disk 1in. below the concrete surface before casting.

After concrete hardening, the disk is pulled from the concrete using a hydraulic jack. The measured resistance is then correlated to produce an in-situ compressive strength. This test method is the most accurate of the all non-destructive testing methods. The Capo-test is a similar version of the Lok test; however, it is instead designed for determining the compressive strength of existing concrete structures. This test involves drilling a hole into the concrete producing a groove in which a compressed steel split ring expands producing a setup similar to the previously mentioned Lok test. Due to its accuracy and procedural ease, this method is gaining popularity. Soutsos et al reports that the Capo test produces similar strength values as the Lok testing procedure [Soutsos et al, 2000].

### 3.2.3 Pull-Off Tests [Bungey, 1993]

Pull-off tests measure the tensile force required to separate a metal disk bonded to the concrete surface. This test involves loading in tension a 2-in metal disk through a reaction ring system bearing on the concrete surface. The nominal concrete tensile strength is then a function of the force needed to remove the disk. This value is then converted to a compressive strength using a correlation chart. One disadvantage to this test is that surface preparation and proper bonding is essential to obtain reliable results.

### 3.2.4 Break-Off Tests [Bungey, 1993]

The break-off test measures the transverse force applied to the top of a concrete cylinder. The cylinder is either made using a partial coring or from fresh concrete.

The cylinder is 2.2-in in diameter and 2.75-in in length. The force is applied to the top of the cylinder by a hydraulic jack attached to the concrete surface. The compressive strength from this procedure is influenced by whether the test specimen was drilled or formed.

### **3.3 Shear Strengthening Techniques**

In general, six traditional shear strengthening methods of concrete members are currently used in practice. The first method involves slab removal above the beam so to allow for new stirrup placement around the existing beam. After stirrup placement, new concrete is cast or sprayed onto the member to form a composite section. One disadvantage with this technique is assurance of a proper bond between the new and old concrete. A second method involves inserting steel tendons through the slab portion and bolting plates to the top and bottom of the beam. Thirdly, shotcrete with fibers is applied to the face of the beam. The shortcoming of this method is that the shotcrete-fiber composite is not anchored in the compression zone of the concrete member. A fourth method involves mounting steel plates on both sides of the reinforced concrete member. Another option includes drilling a hole completely through the member and anchoring a plate at the top and bottom of the beam. Lastly, steel straps may be wrapped around the entire cross-section. In this case the repair may be sensitive to impact loads. In the following sections, various strengthening techniques that are most commonly used for reinforced concrete structures are discussed in detail.

### 3.3.1 Sprayed Fiber-Reinforced Polymer Technique

An innovative repair method has been developed at the University of British Columbia by Banthia et al using sprayed fiber reinforced polymer (SFRP) coatings [Banthia et al, 2002]. The method consists of simultaneously spraying a polymer and short, randomly distributed fibers on the concrete surface. The spray produces multi-directional fibers along the repaired surface. The procedure includes mixing a resin and catalyst which are then introduced into a spray gun. Next, fiber sheets are placed into a chopping unit attached to the spray gun which allows the cut fibers to be placed into the resin/catalyst stream. The fibers may be cut at lengths from 0.31in to 1.9in. By applying multiple coating layers, the SFRP repair can be built-up to any desired thickness.

Banthia, Nandakumar, and Boyd 2002 examined this repair through field and laboratory testing. The field examination involved applying the technique to a bridge consisting of precast channel beams needing shear strengthening. It was noted that surface preparation is minimal when using the spray technique. Results from the laboratory investigation revealed that the fiber wrap increased the ultimate flexural load carrying capacity by 33%. However, the sprayed graphite fiber-reinforced polymer, GFRP, method had a 96% increase in the overall flexural load capacity.

Banthia et al compared the sprayed FRP application with a similar continuous fiber wrap on compression loaded cylinders [Banthia and Boyd, 2000]. In this article, the authors found that the sprayed FRP technique is ideal for rehabilitation of concrete

exposed to harsh environmental conditions. In addition, the application is useful for concrete structures where concrete expansion and spalling has occurred due to the presence of chlorides and reinforcement corrosion. Banthia et al evaluated the FRP wrap procedure as a function of fiber orientation and the number of wrap layers. The orientation of the wrap was examined at 0, 45, and 90 degrees to the longitudinal axis of the cylinders. The stress-strain curves for the wraps showed less variability than curves for the FRP spray. Possible reasons for this variability are the difficulty of applying a consistent spray layer thickness, and controlling the fiber content in the spray. The cylinder specimens retrofitted with the FRP spray exhibited far superior strength and energy absorption than specimens retrofitted with both a one and two layer wrap. Therefore, the FRP spraying technique improved member ductility. The FRP spray retrofit was found to produce equally, if not better results than the traditional wrap for both small and large cylinders. Tension properties of the sprayed fiber reinforced polymers were also examined in the Banthia and Boyd study. Tests were conducted on tension coupons as a function of fiber lengths ranging from 5/16-in to 1 7/8-in to evaluate their effectiveness. Test results showed that an increase in the fiber amount increased both the FRP composite elastic modulus and its tensile strength.

Harries and Young conducted a similar investigation to the Banthia et al study by evaluating the effectiveness of sprayed fiber reinforced polymers for infrastructure rehabilitation [Harries and Young, 2003]. The authors found that even though randomly oriented chopped fiber composites do not have the ultimate strength or

stiffness of unidirectional fiber composites, they show significantly larger strains at failure due to non-linear behavior. This fiber characteristic results in a more ductile concrete member. Harries and Young recommend using a SFRP application to: stabilize deteriorated structures, increase the load carrying capacity of in-service structures, in situations where minimal disruption is desired, and retrofitting structures with complex geometries. Harris and Young state that most structural rehabilitation using FRP materials consists of fabrics and sheets of continuous fibers. However, continuous fiber sheets are undesirable in some instances due linear stress-strain behavior and small rupture strains. Consequently, the material provides little warning prior to failure. The Harries and Young procedure for applying the SFRP is similar to that of Banthia, Nandakumar, and Boyd 2002 [Banthia et al, 2002]. As noted by Harries and Young, epoxy sprays are commonly used for the rehabilitation and lining of pipes and liquid storage systems. Although system strength improvement is not the main objective in this application, strength and stability of some pipe systems are enhanced. Harries and Young evaluated concrete specimens strengthened with the SFRP for strength, stiffness, and behavior as a function of fiber length, fiber loading, and coating thickness.

Results from the Harries and Young investigation indicated that the failure mode changed from pullout to rupture as the fiber length increased. Three fiber loading densities and coating thicknesses were used in the investigation. The densities included of 5, 10, and 15% by volume with 0.125, 0.250, and 0.500-in coating thicknesses. The testing matrix and results for this investigation are shown in Table

3.1. The results are summarized as the ratio between the experimental specimen to the control specimen.

An increase in load capacity was seen in all retrofitted specimens. In comparison with no treatment, a considerable increase in load carrying capability is shown in Table 3.1 for beams with only the epoxy spray, specimens 0-125, 0-250, and 0-500. The optimum thickness for the epoxy spray was 0.250-in resulting in a 40% increase in load capacity; however, the 0.125-in epoxy sprayed specimen resulted in improved bending stiffness.

**Table 3.1: Testing Matrix and Experimental Results**

Specimen	Fiber Length (in.)	% Fiber (%)	Coating Thickness (in.)	Load	Deflection	Strain Energy Absorbed
0-0	0	0	0	1.00	1.00	1.00
0-125	0	0	0.125	1.30	1.12	1.59
0-250	0	0	0.250	1.40	1.12	1.23
0-500	0	0	0.500	1.25	1.20	3.82
L-125	0.75	5	0.125	1.25	0.96	1.15
L-250	0.75	5	0.250	1.19	1.38	2.44
M-125	0.75	10	0.125	1.25	1.08	1.33
M-250	0.75	10	0.250	1.32	1.20	9.93
H-125	0.75	15	0.125	1.30	1.32	8.33
H-250	0.75	15	0.250	1.44	1.20	3.11

Though the peak load for specimens retrofitted with an epoxy-fiber composite resulted in slightly lower load values than that of the epoxy only specimens, the epoxy-fiber specimens exhibited much greater deflections with improved ductility. Harries and Young made the following conclusions from their study:

- The sprayed fiber reinforced polymer increases the load carrying capacity and deflection when compared to plain concrete beams.
- The optimum thickness for an epoxy only application is 0.250 in.
- Though chopped fibers did not have a significant effect on the load carrying capacity when compared to the epoxy only application, the fibers did increase beam ductility.
- The SFRP retrofit was well suited for applications involving deteriorated concrete structures.
- The SFRP application is applied with relative ease and minimal surface preparation.

Factors that Harries and Young found to impact the effectiveness of the SFRP retrofit were worker's skill in applying the epoxy-fiber composite, epoxy temperature, application orientation, and fiber type.

Numerical investigations on damaged reinforced concrete bridge beams retrofitted with spray fiber reinforced polymers were made by Lee, Avila, and Montanez [Lee et al, 2004]. Lee et al developed a computational model that simulates the SFRP retrofit and resulting performance. The analysis was developed to analyze retrofitted beams for both flexure and shear capacity. Lee et al concluded that the coating thickness had a significant impact on the load-carrying capacity and energy absorption capacity of the beams, which validates the Harries and Young findings [Harries and Young,

2003]. Lee et al demonstrated similar characteristics between sprayed fiber reinforced polymer and woven fabrics in bridge applications.

### 3.3.2 Externally Placed Fiber-Reinforced Polymer Strips

Flexible fabrics have been used as a wrap for reinforced concrete structures. Stallings, Tedsco, El-Mihilmy, and McCauley examined the use of externally placed fiber reinforced plastic laminates for the rehabilitation of an existing concrete bridge in need of structural strengthening [Stallings et al, 2000]. The focus of the investigation was to evaluate the effectiveness of FRP repairs on existing concrete bridge structures. The investigation included load testing of a bridge both before and after repair. The retrofitted bridge was monitored for vertical deflections, strains in the longitudinal reinforcement, and strains on the FRP laminates. The strains and deflections were recorded before and after the FRP repairs, using two identical trucks of known weight and loading configuration considering static and dynamic load conditions.

Carbon fiber reinforced polymer plates were attached along the bottom of each girder along the bridge. Additionally, graphite fiber reinforced polymer, GFRP, plates were attached to the sides of the girders; however, the composite plates were not wrapped along the edges of the beams. Prior to applying the FRP composite plates, the concrete surface of the girders were smoothed and abraded until the coarse aggregate was visible. The bonding side of the FRP plates was roughened using a sanding device. The plates were applied to the girders by rolling the composites in-place. The plates were then subjected to an applied pressure using a vacuum bag to ensure

proper bonding. Traffic was detoured for approximately one week while the retrofitting process was performed.

To monitor the effect of truckloads on the bridge, strain gauges were placed on the reinforcing bars, FRP plates, and the concrete surface. Strain gauges were placed at mid-span except for four gauges placed at the FRP splice locations. Linear variable differential transformers (LVDT's) were used to measure mid-span deflections of the bridge girders.

Load tests were conducted on the bridge both before and after the FRP application by subjecting the bridge to a load of 78-kip using two trucks. Truck loads were distributed between three axles per truck. The bridge testing consisted of static and dynamic load tests. The static tests were conducted by positioning the middle axle of each truck at mid-span in four transverse load positions to produce the largest load condition possible for the span. Dynamic tests were also conducted having the two trucks travel at 50-mph side-by-side across the bridge.

Results from the static field load testing indicated that a slight reduction in reinforcement stress was found due to the FRP application. The minimum and maximum percent difference in reinforcement stress before and after the retrofit was 4% and 12% respectively. In addition, mid-span deflection was reduced by at least 2% and not more than 12% when compared with the un-retrofitted load tests. The dynamic load tests revealed a reduction in mid-span deflection; however, the peak

deflection readings exhibited more scatter than those found in the static investigation. Strain measurements from both the flexural reinforcement and the CFRP plates were approximately similar assuring proper bond between the CFRP plates and the concrete.

Stallings et al concluded that the application of CFRP plates to reinforced concrete bridge girders reduced the flexural reinforcement bar stress and mid-span deflections. Secondly, the GFRP plates applied to the girder sides caused a greater reduction in stress and deflection.

Three bridges in Boone County, Missouri, were retrofitted. The bridges were constructed between 1970 and 1976 using single-span, simply supported precast reinforced concrete channel sections [Alkhrdaji, 2002]. A 15-ton load rating was established in 1979 for the bridges. Replacement of the sections was not an option due to the high costs associated with bridge replacement. Therefore, it was determined instead to use carbon fiber reinforced polymer (CFRP) composites as a solution to this strengthening problem. A CFRP composite was used along the beam sides to provide shear strength and along the stem bases for flexural strength. Details of this strengthening method are shown in Figure 3.1. Load tests showed smaller mid-span deflections after strengthening. In addition, the retrofitted members experienced reduced internal stresses indicating improved beam stiffness.

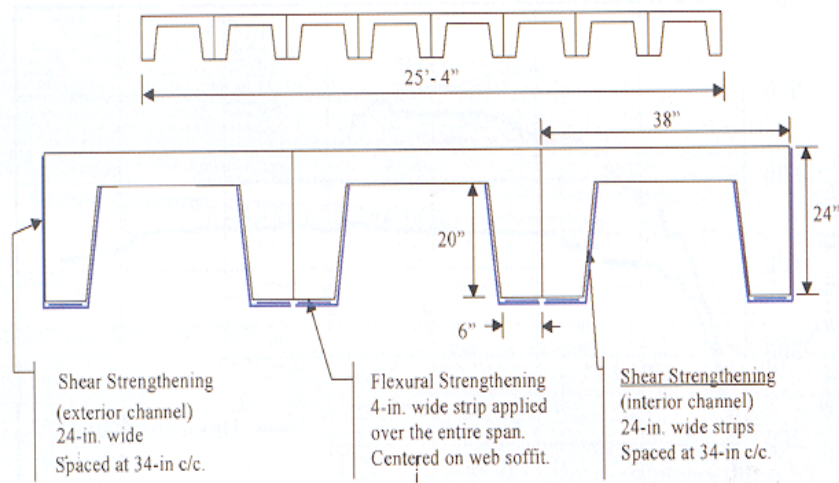


**Figure 3.1: Details of CFRP Strengthening of Channel Sections [Alkhrdaji, 2002]**

A Swiss federal laboratory has developed an externally bonded L-shaped CFRP plate used to strengthen concrete beams in shear [Czaderski, 2000]. These L-shaped plates are prefabricated consisting of carbon fibers with an epoxy resin. The plates have a 90-degree bend with a radius of 1-in. To validate the shear strengthening design, large-scale tests were conducted on beams with minimal shear reinforcement. The tests showed improved ductile behavior. Further tests are currently being conducted to evaluate the mechanical and composite behavior of the CFRP plates.

Bousselham and Chaallal examined parameters that have the most significant impact on reinforced concrete member shear behavior strengthened with externally bonded fiber reinforced polymers [Bousselham and Chaallal, 2004]. To evaluate behavior of strengthened members, their research included testing over one hundred samples.

Parameters that were examined included beam cross-section (rectangular or T-section), span length, concrete and reinforcing steel properties, FRP type, and strengthening scheme. Their research revealed that parameters other than those associated with the FRP and shear steel reinforcement had a significant impact on member strength. The shear span ratio, longitudinal steel reinforcement ratio, and beam cross-section all influenced shear behavior. When shear is increased, the contribution of the FRP composite is more significant in regular beams than in deep beams with an  $a/d < 2.5$ . The importance of the shear span ratio lies in the fact that during failure of a concrete beam, beam rotation occurs prior to shear failure, which is dependant upon the  $a/d$  ratio [Ibell et al, 1997]. Also, beam rotation is more evident at isolated beams (edge beams) than at interior beams in a bridge superstructure.

The importance of fiber direction was examined by Norris et al in an investigation of flexural and shear strengthening of reinforced concrete members [Norris et al, 1997]. Their research found an increase in strength and stiffness in existing concrete beams when FRP strips were bonded to the web and tension face of the beam; however, strength improvement was directly related to the fiber orientation. When the fiber strips were placed perpendicular to longitudinal cracks, a large increase in stiffness and strength was observed in the beam. However, in this orientation a brittle failure occurred near the end of the CFRP strips due to concrete rupture. When the strips were applied diagonally, a smaller increase in strength and stiffness was observed; however, the beam ductility increased. O. Chaallal et al validated this result where diagonal CFRP strips resulted in improved shear strength in comparison to a vertical

strip arrangement [Chaallal et al, 1998]. Further, strips in a diagonal arrangement experienced premature failure due to strip peeling from the concrete near the end of the strip. Chaallal et al suggests the use of FRP U strips or U jackets for extreme loading cases. In other work, Taljsten recommends that fiber strips be placed perpendicular to the shear crack if possible [Taljsten, 2003].

### 3.3.3 Bonded Steel Plates

Bonded steel plates have been used to strengthen reinforced concrete members for over 40 years [Emmons et al, 1998]. The retrofit consists of a steel plate mounted to the concrete surface using a two component epoxy. This produces a three part composite system: steel, epoxy, and concrete. Bonded steel plates are an attractive retrofit method due to high strength epoxy adhesives available in today's market, ease of implementation, and minimal change to the overall cross-section of the concrete member. Three important factors must be present for a steel plate retrofit to be effective:

- The surface to be bonded must be clean.
- The epoxy should have a bond strength equal to or greater than the concrete.
- Plates should be long and thin to prevent a brittle plate separation failure.

Though bonding of steel plates to concrete has shown great strengthening success, several problems are associated with this technique. First, the weight and geometry of steel plates can be cumbersome in the field. In addition, restrictions on the length and

width must be enforced for handling purposes, and steel plate bonding is difficult for concrete structures with complex shapes. Secondly, bond durability and the potential for corrosion at the steel-epoxy adhesive interface is an issue. Thirdly, plate separation has been found to occur due to high localized stresses at the bond interface resulting in debonding near the steel plate ends [Jones et al, 1988].

#### 3.3.4 Post-Tensioning Strengthening Technique

A recent study conducted at Iowa State University, ISU, examined strengthening precast concrete deck bridges located in Iowa [Klaiber, et al, 2001]. In addition to hooked longitudinal reinforcing bars, beams found in these bridges contained shear reinforcement. A strengthening system was designed by ISU to reinforce the deteriorated bridges. The retrofit consisted of a strut located on the diaphragm and a post-tensioned tendon extending the length of each panel, Figure 3.2.

Load tests were conducted on a model bridge retrofitted with this post-tensioning method. Stretching the post-tensioning strand beneath the strut produces tension in the tendon that induces an upward force on the precast section. The magnitude of the upward force depends on the amount of tension in the strand, height of the strand, and length of the beam. Therefore, a moment can be applied equal and opposite to the moment produced from the beam self weight. This eliminates the effect of dead load, which allows for an increase in the live load capacity.

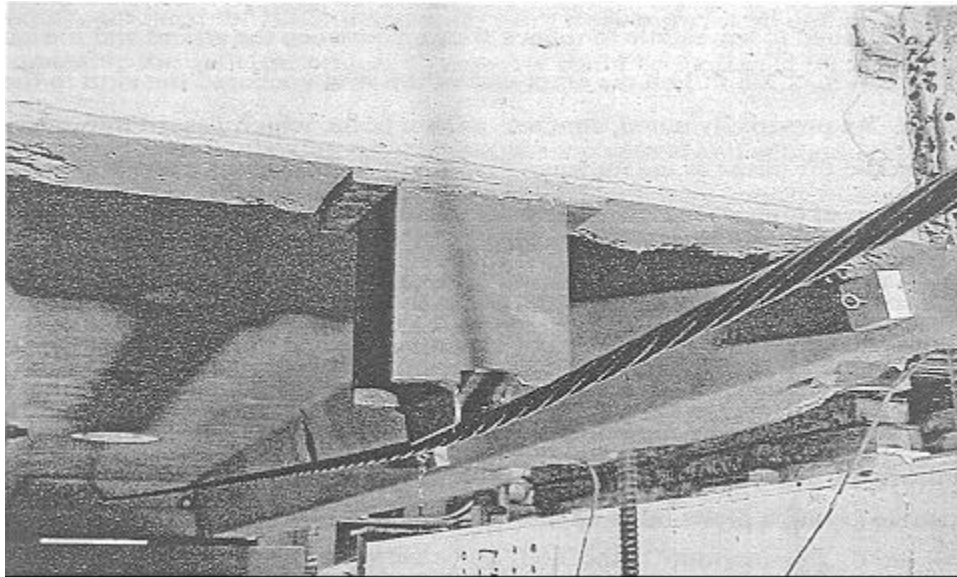


**Figure 3.2: Strut Installed on Mid-Span Diaphragm [Klaiber et al, 2001]**

### 3.3.5 Reinforcing Bar Insertion Technique

Valerio and Ibell examined shear strengthening of concrete bridges by inserting reinforcing bars into pre-drilled holes through the bridge deck [Valerio and Ibell, 2003]. In order to prevent corrosion, the use of FRP rods was used as an alternative to traditional steel reinforcing bars. Manitoba's Department of Highways and Transportation estimates that bridge beams can be retrofitted using imbedded FRP bars at about 15% of member replacement cost [Mufti et al, 2002].

Table 3.2 lists the reinforcement pattern for each of the specimens tested in their investigation.

Results from the load testing revealed that there was negligible difference between the load capacities of the un-retrofitted beam (Specimen 1) and a beam with drilled, unfilled holes (Specimen 2), 10.1-kip and 9.4-kip respectively. Therefore, the bridge is not structurally weakened during the retrofitting process.

**Table 3.2: Reinforcement Pattern**

Specimen No.	Transverse Reinforcement per Shear Span
1	none
2	5 holes
3	5 (10mm) FRP vertical bars
4	5 (10mm) steel vertical bars
5	3 (10mm) FRP bars angled 60°
6	3 (10mm) FRP vertical bars
7	3 (10mm) steel vertical bars
8	2 (10mm) FRP vertical bars
9	2 (7.5mm) FRP vertical bars
10	1 (10mm) FRP vertical bar

The addition of five FRP bars (Specimen 3) or steel bars (Specimen 4) increased the load capacity over 8kips. Further, the use of embedded bars altered the failure mode from a shear to a flexural failure. Mid-span deflection values improved when compared to the un-retrofitted beam. The reduction in transverse steel used in specimens 5, 6, and 7 proved insignificant for load capacity and mid-span deflection when compared to specimens 3 and 4. Specimens 3-7 failed in flexure. However, specimens 8 and 9, each containing 2 internal bars, and specimen 10, containing a single internal bar per shear zone, experienced a shear failure. The load capacity in specimens 8-10 increased by over 4-kip, but the mid-span deflection was similar to the un-retrofitted beam.

### **3.4 Literature Summary**

Reinforcing steel corrosion is the leading cause for concrete bridge structure repair. Contributing factors to corrosion of reinforcing steel are higher than designed for applied loads, concrete cracking, and cover-to-bar diameter ratio. Much research has been conducted in this area over the last 50 years. Many of the strengthening applications require bonding to the concrete surface and include: spray fiber-reinforced polymer, fiber-reinforced polymer strips, and steel plates. To improve shear strength, reinforcing bars can be placed internally in concrete members lacking shear strength.

## **Chapter 4**

### **Problem Statement**

There are 503 of bridges in Arkansas that were built using 19ft. non-prestressed concrete channel beams [Jones et al, 2004]. Of these bridges, 389 were constructed prior to 1974 with design details that excluded shear reinforcement. In the same study by Jones et al, approximately one-third of these existing PCB bridges are experiencing extensive deterioration. At the national level, a U.S. survey of state highway and transportation departments indicates that at least thirteen states besides Arkansas have precast channel beam structures in their bridge inventory [Durham, Heymsfield, and Schemmel, 2003]. Of these thirteen states, nine states are experiencing deterioration similar to that found in Arkansas PCB bridges.

An October, 2000 inspection of a channel beam bridge located near Jenkins' Ferry, Arkansas, revealed exposed corroded longitudinal reinforcing steel in the beam stems, Figure 4.1. As a result of what was found at the Jenkins' Ferry Bridge, the AHTD decided to investigate the condition of other precast concrete bridges. In an inspection of a limited number of bridges, it was concluded by AHTD that a widespread problem existed for these types of precast concrete sections. The most prevalent conditions observed in field observations were extensive longitudinal cracking at the level of the longitudinal reinforcing steel and concrete spalling.

Research has been summarized in this study evaluating the structural capacity of sections from several precast concrete beam bridges in varying deterioration conditions.



**Figure 4.1: Deterioration of Jenkins' Ferry Bridge**

This research has provided insight on possible failure modes and beam behavior. Results from the structural investigation of thirty-three load tested beams found twenty-eight of the beams experienced yielding prior to failure and five failed without experiencing a yield plateau. The five beams that did not experience yielding were extremely deteriorated and visually categorized as being in poor condition. All five beams failed in shear. A total of thirty-one of the thirty-three beams ultimately failed in shear. Load-deflection curves for six sections removed from a bridge site are shown in Figure 4.2. All six sections were classified in poor condition by visual inspection because of their extensive deterioration. Only three of the six beams experienced longitudinal steel yielding before failure.

The extensive deterioration found by the AHTD at PCB bridges statewide, warranted the need for an approach to remedy this problem. A PCB bridge survey, on-site bridge inspections, local relative humidity data collection, in-situ moisture content determination, and concrete permeability tests were conducted on beams state-wide to investigate the extensiveness of the problem and propose possible solutions.

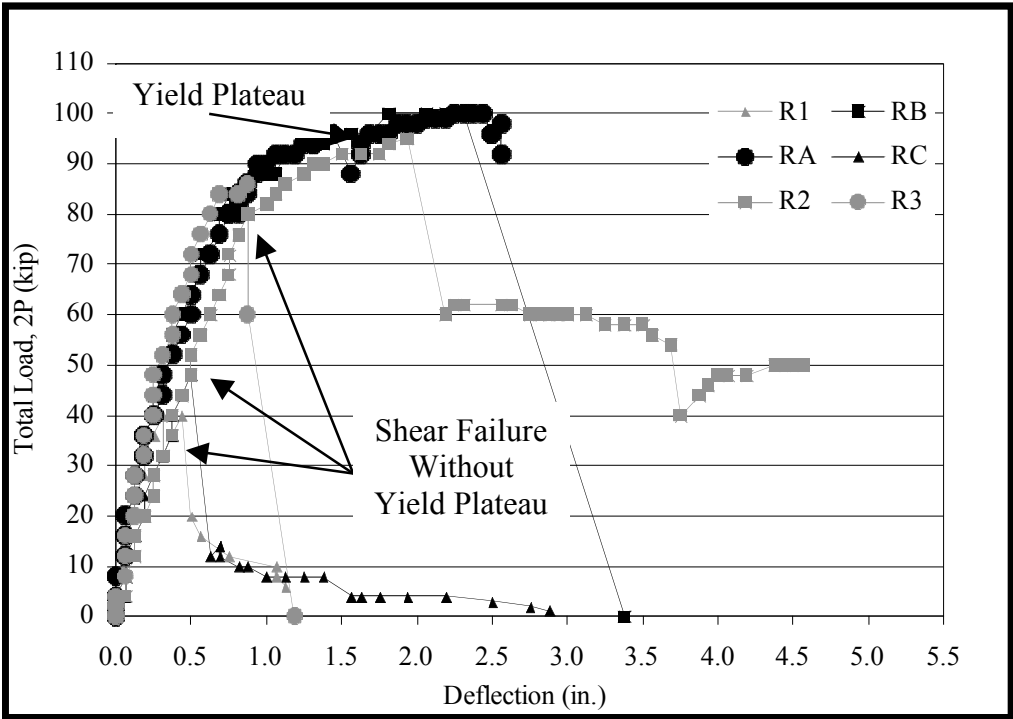


**Figure 4.2: Load vs. Deflection Curves (Poor Condition Beams)**

This report examines potential shear strengthening methods that can be implemented for precast concrete channel beams used in bridge superstructures. To accomplish this task, thirty-three beams from bridge sites within the state along with data from four newly fabricated beams were reviewed to examine locations and angles of shear

cracks. The shear strength deficiency in these beams was then used to retrofit the beam to ensure flexural failure.

Three retrofit techniques are developed and explained in detail herein. The overall aim of this research project was to develop an innovative, cost-effective shear strengthening technique that can be easily implemented in the field.

## Chapter 5

### **Longitudinal Cracking and Reinforcing Steel Corrosion**

Approximately 1,200 of the 1,981 PCBs inspected by the UA research team classified in poor or average condition by AHTD are exhibiting longitudinal cracking at the height of the flexural reinforcing steel. In addition, in many of these beams reinforcing steel corrosion has become evident. Reasons for such deterioration were examined in this investigation and are presented herein. This investigation included: on-site bridge inspections, determining transverse live loading positions, concrete permeability tests, collecting local relative humidity data, and determining the in-situ beam moisture content. Beams were examined in both laboratory and field settings.

#### **5.1 On-Site Bridge Inspections**

As noted in Chapter 2, there are currently 389 precast channel beam bridges in Arkansas designed using the 1952 AHTD bridge details of which 122 are classified by AHTD personnel as in either average or poor condition. Of the 122 bridges, on-site inspections were performed at 95 PCB bridges by University of Arkansas (UA) personnel. These on-site inspections were used to uniformly examine the condition of these PCBs in greater detail and remove subjectivity between district inspections. The inspections included taking photographs and collecting data on longitudinal, flexure, and shear cracking.

### 5.1.1 Chloride Content

Approximately 94% of Arkansas' PCB bridges are located in rural locations. Only seven bridges classified in poor or average condition were located on U.S. Numbered State Highways or inside towns with a population greater than 1,000. Because such a large number of these bridges are located in rural areas, chloride penetration from deicing salts was examined. Concrete samples were taken from six formerly in-service beams and analyzed for chloride content. Three samples were taken from each beam from the side of the beam stem at 1.5in depth increments (1.5-in, 3.0-in, 4.5-in). The maximum chloride content based on the minimum amount of cement for the concrete mixture specified in the 1952 bridge details is 488ppm [Tencleve, 2005]. Of the eighteen samples examined (3 samples per beam, 6 beams), only one was found to be greater than this maximum chloride content value. These minimal chloride contents indicate that chloride was not the primary contributor to the reinforcing steel corrosion. These minimal values also suggest that chloride-based set accelerators were probably not used during beam casting.

### 5.1.2 Flexure Cracking

UA field inspections revealed that 713 of the 1981 PCBs inspected, 36%, contained visible flexure cracks. These cracks are most likely the result of higher than designed live loads. Excluding an asphalt wearing surface, the shear and moment capacities for the beams designed under H15 truck loading are approximately 60% and 44%, respectively, deficient when compared to HS-20 truck loading. Even with this deficiency, only 3% of PCB bridges are load posted within Arkansas [Jones et al,

2004]. Typical flexure cracks begin at the stem base and propagate up the beam stem. Flexure cracks provide access for moisture and oxygen to the reinforcing steel. Figure 5.1 shows a flexure crack on the inside portion of the beam stem. The darkness surrounding the flexure crack is moisture seeping from inside the beam stem.

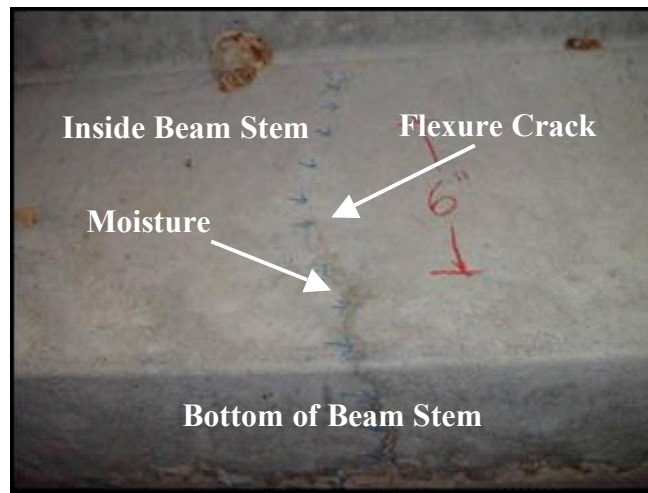


**Figure 5.1: Flexure Crack in Mid-Span Region of Beam**

During the field inspection, many flexure cracks contained water staining around the cracks. This observation led to an investigation of water seepage into these cracks. Four bridge sites were visited after varying amounts of rainfall to compare the amount of precipitation with the amount of moisture present at the stem base. Two extremely different rainfalls, 0.06-in and 0.38-in, were examined at the bridge sites. The temperature during each of these visits was approximately 80°F. At both rainfall levels, moisture was observed on the base of the beam stems, Figure 5.2 (a). In many cases, beam separation as shown in Figure 5.2 (b) was observed between adjacent beams allowing a moisture pathway to the stem base. The amount of moisture present

during the 0.38in. rainfall resulted in the entire stem base being completely saturated. Besides moisture at the stem base, moisture was observed exiting flexure cracks on the inside portion of the beam stem.

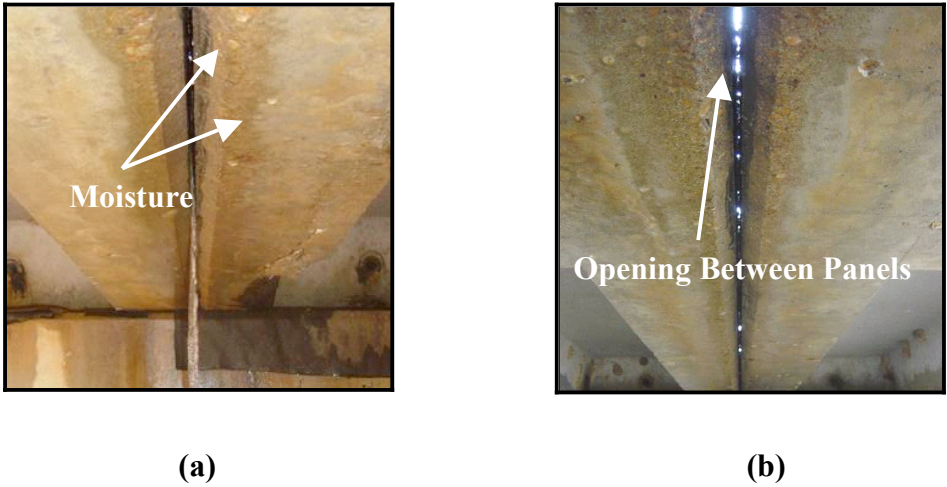
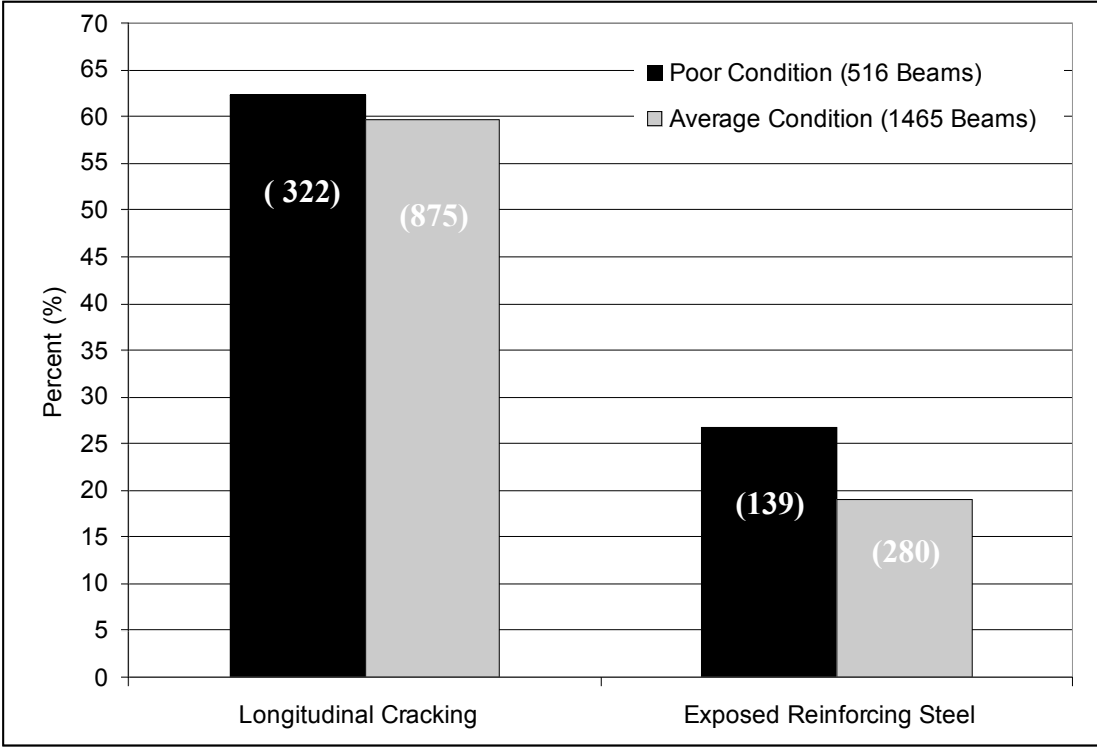


**Figure 5.2: Moisture at Beam Stem Base**

5.1.3 Longitudinal Cracking

Of the 1,981 beams examined during the UA on-site bridge inspections, 516 beams were from bridge superstructures classified in “poor” condition by AHTD officials and the remaining 1465 beams were from “average” condition bridges. Figure 5.3 illustrates the percentage of beams classified as poor and average that were experiencing longitudinal cracking and concrete spalling. Cracking at the level of the flexural reinforcing steel was found in 62.4% of “poor” beams and 59.7% of “average” beams. Further, exposed reinforcing steel as a result of concrete spalling was observed in 26.9% of “poor” beams and 19.1% of “average” beams. This statistic

indicates that there is not a significant difference between “average” and “poor” beams for longitudinal cracking and concrete spalling.



\* Number of beams in parenthesis.

**Figure 5.3: Longitudinal Cracking and Concrete Spalling in PCB Bridge Beams**

UA field inspections revealed that longitudinal cracking typically occurred on the inside stem portion of the channel beam rather than along the bottom. In addition, it was concluded that when a single reinforcing bar was exposed in a beam stem, it was predominately the inside reinforcing steel bar. The predominant reason for this is the limited reinforcing steel concrete cover. A laboratory investigation of formerly in-service beams revealed that the concrete cover for the inside reinforcing bar was at least 0.75in less than that of the outer bar. In addition, at some of the channel beams

the reinforcing bar cover varied along the span length. The minimum concrete cover specified by ACI for precast concrete beams with #9 reinforcing bars manufactured under plant control conditions is 1.5-in. It may be the case that some beams in this study may not have been manufactured under plant control conditions; therefore, requiring a 2-in minimum concrete cover for cast in-place concrete. With the bar alignment variability and placement found in the beams of this study, many times the 2-in. cover requirement was not satisfied.

The concrete cover ( $c$ ) to bar diameter ( $d_b$ ) ratio is an indicator for potential longitudinal concrete cracking and spalling, Figure 5.4 [Emmons, 1993]. Concrete begins cracking when the corrosion level reaches 4% for a  $c/d_b$  ratio of 7. As the  $c/d_b$  is lowered to 3, cracking begins at only 1% corrosion.

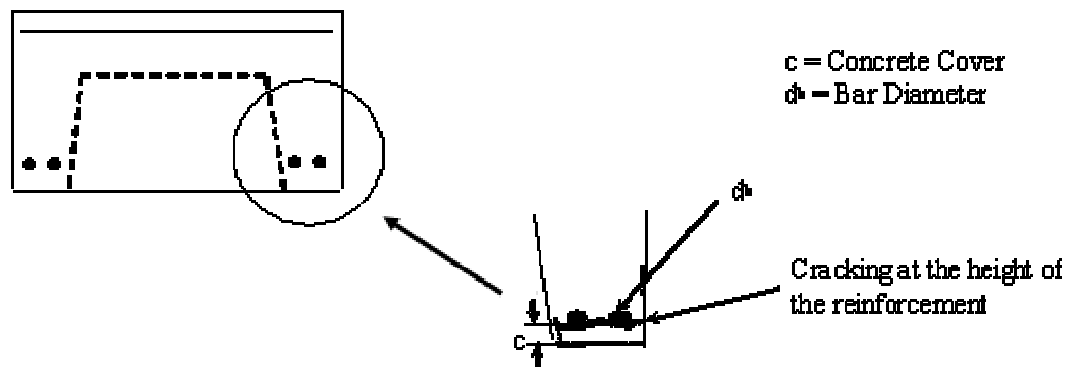


**Figure 5.4: Concrete Cover to Reinforcing Bar Diameter Ratio**

The  $c/d_b$  ratio for the beams examined in this research ranged from 1.3 to 1.7, suggesting that very little corrosion is required to initiate cracking.

#### 5.1.4 Asphalt Wearing Surface and Deterioration

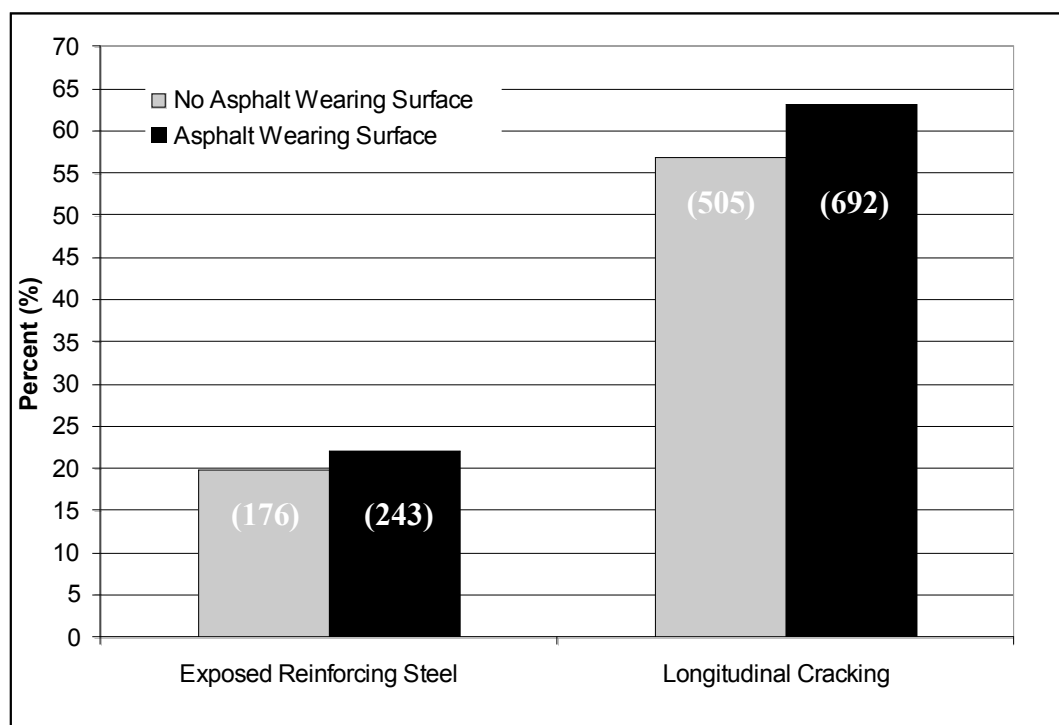
Asphalt wearing surface removal from formerly in-service beams revealed substantial water ponding at the asphalt-concrete interface, Figure 5.5. Currently, AHTD specifies that bridge decks shall not have an asphalt wearing surface. However, a large number of PCB bridges were placed prior to this specification and therefore include an asphalt wearing surface. In these cases, moisture permeates through the asphalt layer at a much faster rate than that of concrete. This permeability difference results in moisture collecting at the asphalt-concrete interface and producing a water source which eventually seeps into the concrete beam.



**Figure 5.5: Moisture at Asphalt-Concrete Interface**

Data was collected in this study from on-site bridge inspections comparing bridges with and without asphalt wearing surfaces having longitudinal cracking and exposed reinforcing steel. Results from this investigation are shown in Figure 5.6. Beams with an asphalt wearing surface exhibited longitudinal cracking 6.2% more often than

beams without. In addition, exposed reinforcing steel occurred 2.3% more often in beams with an asphalt wearing surface. The increase in longitudinal cracking and concrete spalling was determined to be statistically insignificant when comparing PCB bridges with and without asphalt wearing surfaces.



\* Number of beams in parenthesis.

**Figure 5.6 Asphalt Wearing Surface and Beam Deterioration**

#### 5.1.5 PCB Bridge Website Database

The data collected from the 95 UA on-site PCB bridge inspections were compiled and incorporated into an existing AHTD bridge web database. The website-accessed database, Figure 5.7, contains information on existing bridges throughout the state. The specific bridge number and location is found by pointing at a red locator dot on

the map which represents a particular PCB bridge. Additional information including concrete deterioration, reinforcing steel corrosion, asphalt wearing surface, drainage, and bridge site photos of problem areas associated with beam deterioration are also included with the bridge description, Figure 5.8 and Figure 5.9.

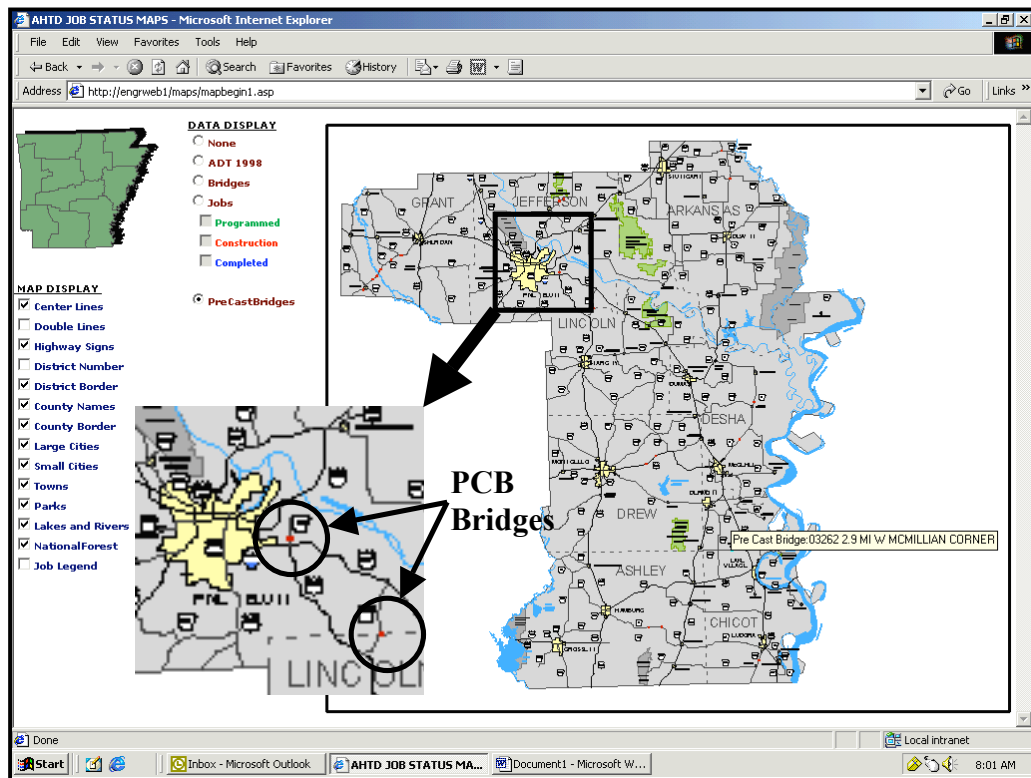


Figure 5.7: Website Database

## Bridge Checklist

Report No.: 03262  
Inspector ID: Keith Tenclave  
Date: 37797  
Structure Type: Precast Concrete Channel Beam Bridge  
Location: 144+2 + 5.70 - LOST LAKE/LAKE VILLAGE

### Deck Elements

Asphalt wearing surface present? YES  
Drainage system adequate? NO, CLOGGED ON NORTH SIDE  
Is dirt found on bridge surface? NO  
Are joints between panels filled with grout sufficiently? N/A

### Superstructure Elements

Any type of bearing for beams resting on abutments and piers? NEOPRENE  
Are channel beams bolted together? Are they corroded? YES; VERY LITTLE  
Concrete deterioration? NO  
Steel corrosion? NO  
Collision damage present? NO  
Are utilities present on bridge? YES - ~3" PIPE

### Substructure Elements

High water mark? 6' BELOW BEAMS  
Concrete deterioration? NO  
Scour/Undermining? NO - STREAM DRY

### Environmental Concerns

Is bridge elevation higher in one direction than other? NO  
Is bridge located in low region of area? NO

**Figure 5.8: Detailed Bridge Checklist on Website**

Bridge #: 03262

Location: 144-2 + 5.70

On site inspection pictures – May not contain pictures of all problem areas on each beam.



Deck



Span 1 Beam 1 (S1B1)

1

**Figure 5.9: Bridge Site Photos on Website**

## **5.2 Bridge Loading Locations and Deterioration**

A relationship between beams located within the wheel path and beam deterioration was analyzed. To examine this correlation, traffic was monitored at a bridge site near Lakeway, Arkansas, to determine transverse wheel load locations on PCBs within the bridge cross-section. This was accomplished using a digital video camera fixed on a tripod in the rear bed of a truck parked approximately 300-ft northwest of the bridge. The camera setup and bridge are shown in Figure 5.10. Continuous video was taken for one hour during which thirty-four various sized vehicles passed over the bridge.



**Figure 5.10: Traffic Monitoring**

The locations of the wheel path were approximated using close-up photographs previously taken at the bridge site. Surface discoloration was used to approximate beam locations. These values were compared with traffic loadings, Table 5.1, taken from the traffic video of the Lakeway Bridge. The Lakeway traffic loadings revealed that the majority of live loadings occurred within the inner five beams of the seven

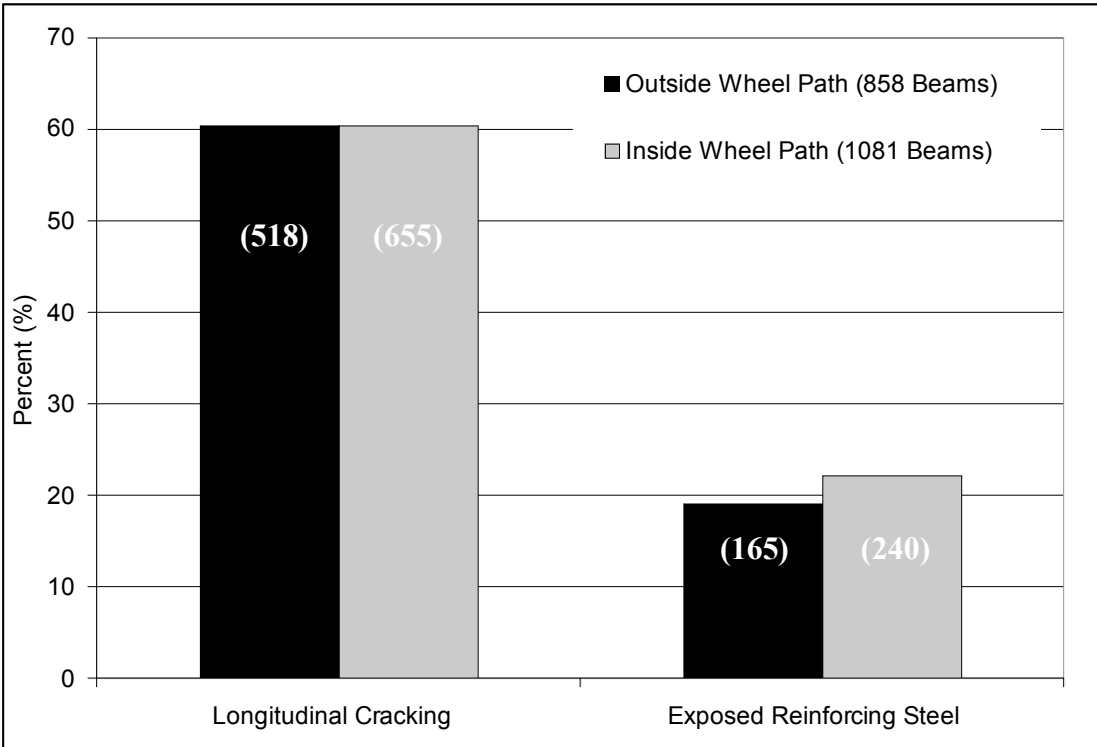
beam cross-section and that a large number of these loadings occurred over the joints of adjacent beams.

**Table 5.1: Bridge Loading Locations for Lakeway Bridge**

Vehicle	Vehicle Type	Beam Number													
		1	1-2*	2	2-3*	3	3-4*	4	4-5*	5	5-6*	6	6-7*	7	
1	Light Truck														
2	Car														
3	Light Truck														
4	Truck														
5	Truck														
6	Van														
7	Heavy Truck														
8	Heavy Truck														
9	Car														
10	Truck														
11	Truck														
12	Truck														
13	Car														
14	Car														
15	Truck														
16	Truck														
17	Van														
18	Car														
19	Van														
20	Car														
21	Truck														
22	Semi-Truck														
23	Truck														
24	Truck														
25	Car														
26	Car														
27	Car														
28	Truck														
29	Truck														
30	Van														
31	Truck														
32	Light Truck														
33	Truck														
34	Car														

\* Indicates joint between adjacent beams.

From the Lakeway traffic loading data, beams 2 through 6 were determined to be inside the wheel path. Conversely, beams 1 and 7 were considered to be outside the wheel path. UA inspection data for the 95 PCB bridges was examined and revealed a difference of only 0.2% in longitudinal cracking and 3.0% for exposed reinforcing steel when comparing beams within and outside the wheel path based on the determined loading locations. The percent of beams experiencing this deterioration is shown in Figure 5.11. A statistical paired t-test with a 95% level of significance indicates no significant difference between traffic loading locations and beam deterioration. Therefore, the transverse live load position within the bridge cross-section was determined to not be the primary factor for beam deterioration.



\* Number of beams in parenthesis.

**Figure 5.11: Bridge Loading Location and Deterioration**

### **5.3 Concrete Permeability**

Concrete permeability tests were performed on twenty-nine of the load tested beams discussed in Chapter 2. Tests were conducted on the deck surface to examine a possible moisture path to the reinforcing steel. A Low Pressure Concrete Air Permeameter (LP-CAP), shown in Figure 5.12, was used for this investigation [Hale and Kuss, 2004]. The LP-CAP was used for testing instead of other devices due to its low vacuum pressure, which provides a more realistic pressure head differential than high vacuum pressure systems.

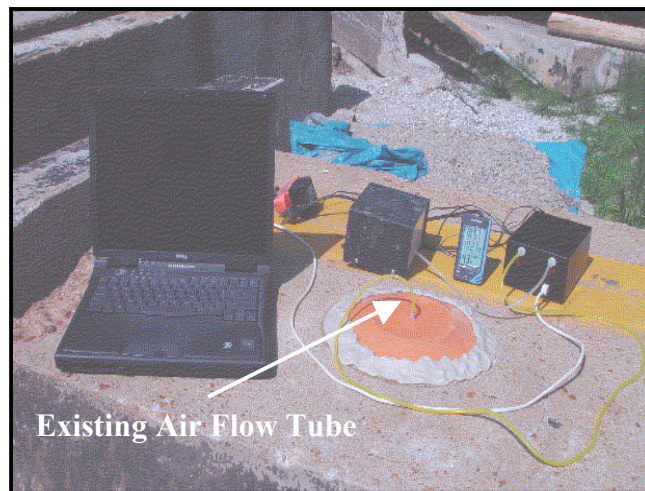


**Figure 5.12: LP-CAP Testing Device**

#### **5.3.1 LP-CAP Testing Procedure**

The LP-CAP system applies a low pressure vacuum over a 63.5-in<sup>2</sup> circular area. The circumference of this area is developed by spraying a 2-in ring with a non-permeable spray sealant. Next, a 10-in diameter plate is placed over the sealed area to form the vacuum area. The plate is sealed to the impermeable ring using putty. The plate

contains a hole at the top-center for exiting air flow, Figure 5.12. During permeability testing, suction is induced forcing air from outside the sealed ring into the vacuumed area and through the exiting air flow tube. The air flow rate is measured during this process to give a measure of material permeability.

Each LP-CAP tests requires one-half hour for test set up and execution. During the test, real-time data is collected on a laptop computer. The computer program used for data collection produces a graph that allows the user to determine when the flow rate reaches steady state. The flow rate measurement is recorded in mL/min.

Factors affecting the permeability reading include changes in either ambient atmospheric pressure or existing concrete moisture at the time of testing. To overcome atmospheric pressure changes, the test duration was extended beyond the normal time interval needed for flow rate equilibrium. Secondly, a 48 hour time interval was used between testing and any precipitation to ensure the permeability reading was not affected by concrete moisture.

Because of concrete's heterogeneous state, multiple permeability tests were performed on each of the 29 beams. The equivalent permeability for the beam was then computed as the average of these tests. Presently, a standard has not been developed for the LP-CAP test; however, protocol similar to the rapid chloride penetration test (RCPT) was used for this investigation. RCPT requires permeability readings from

the same mixture to be within 42% of one another. Therefore, this percent was used for the test series using the LP-CAP test.

5.3.2 Permeability Results

Results from the permeability testing are listed in Table 5.2. The average air flow rate determined using the LP-CAP device ranged between 2 to 11-mL/min for all but a single beam; this single beam had an average air flow rate of 24-mL/min. This high value is still reasonable considering the lower than typical compressive strength of 2.3-ksi.

**Table 5.2: Permeability Testing Results**

Jenkins' Ferry		Little Osage Creek		Gentry		Carlisle		New		Hope	
No.	Flow Rate	No.	Flow Rate	No.	Flow Rate	No.	Flow Rate	No.	Flow Rate	No.	Flow Rate
	(mL/min)		(mL/min)		(mL/min)		(mL/min)		(mL/min)		(mL/min)
RC	4	C7	5	G3	9	L3	4	N1	7	H1	3
		C8	24	G5	8	L4	8	N2	11	H2	3
				G6	7	L5	10	N4	10	H4	8
				G7	8	L7	5			H5	4
						L9	2			H6	5
						L10	5			H8	3
						L11	3			H9	3
						L12	3			H10	5
										H11	7
										H12	7

When compared to laboratory mixtures with known permeability readings from both the LP-CAP and RCPT, values determined for the PCBs were considered impermeable. Table 5.3 lists 28-day and 90-day permeability results from three mixtures having a w/c of 0.60. The 90-day laboratory permeability values were much larger than values experienced on PCBs ranging from 17 to 45-mL/min. These results

indicate that water permeation from the deck surface is not the primary contributor to reinforcing steel corrosion.

**Table 5.3: LP-CAP Test Results for 0.60 w/cm Mixtures**

Mixture	28-Days	90-Days
100% portland cement	22	29
10% silica fume replacement	12	17
25% fly ash replacement	22	45

#### **5.4 Relative Humidity Data Collection**

Humidity was evaluated as a possible factor for reinforcing steel corrosion. The warm Arkansas climate coupled with stagnate stream water below many PCB bridges provides ideal conditions for high humidity levels. This environment combined with existing flexure cracks in the beams provides the necessary conditions needed for reinforcing steel corrosion. Humidity within concrete pores and the relative humidity in the surrounding air reach equilibrium [Menzel, 1955]. As the humidity within the concrete reaches a level between 70 and 85%, adequate moisture is present for reinforcing steel corrosion [Stark, 1989]. Methods for determining relative humidity within the concrete pores were not economical for this research project. Instead, the ambient relative humidity at the concrete surface was measured and assumed to be in equilibrium with the concrete.

#### 5.4.1 Data Collection

Temperature and humidity gauges were placed beneath two PCB bridges to determine the possibility of humidity being the source of moisture for corrosion. The gauges were placed in a plastic box attached to the inside beam stem of a PCB using a quick-set epoxy adhesive, Figure 5.13. Ten 1 in diameter holes were drilled into the plastic box to ensure proper air flow to the gauge. The gauges recorded temperature and humidity hourly for a 3 month duration beginning in June, 2004. The PCB bridges evaluated were located in Danville, AR, and Lakeway, AR.

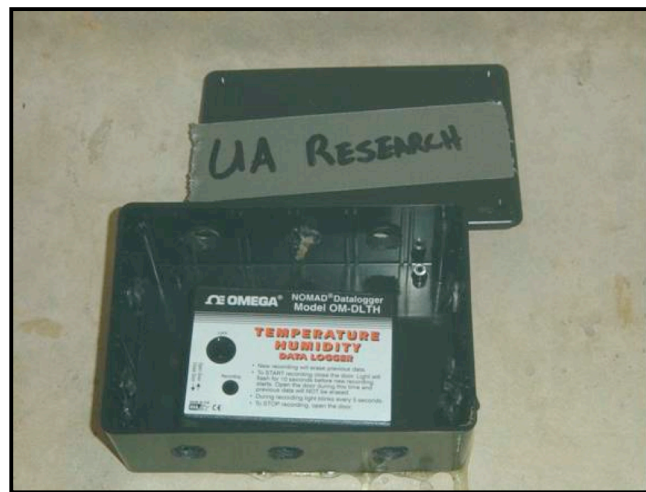


**Figure 5.13: Temperature and Humidity Gauge**

#### 5.4.2 Danville, AR PCB Bridge

A five span bridge near Danville, AR, was used in the humidity investigation. A greater truck traffic volume was observed at this bridge when compared to other PCB

bridge locations. Site conditions included a stream approximately 15ft below the base of the PCBs. High summer temperatures and humidity is typical for this river valley area. A majority of the beams, 36 of 42, exhibited longitudinal cracking at the level of the flexural reinforcing steel, Figure 5.14. In addition, exposed reinforcing steel was observed in 11 beams.



**Figure 5.14: Longitudinal Cracking on Danville PCB Bridge**

#### 5.4.3 Lakeway, AR PCB Bridge

Humidity was recorded at a four span PCB bridge near Lakeway, AR. A stream exists approximately 12-ft below the base of the PCBs. The mountainous area produces a stream that is typically flowing rather than stagnant. Of the 28 PCBs, 20 beams contained longitudinal cracking. Exposed reinforcing steel was observed in 10 beams. This bridge was selected to implement of the shear strengthening retrofit and is discussed in greater detail in Chapter 10.

#### 5.4.4 Relative Humidity Results

Relative humidity at both sites was consistently above 70%. Results from the humidity data collection are shown in Figures 5.15 and 5.16 for Danville, AR, and Lakeway, AR, respectively. As a result of humidity levels exceeding 70%, data indicates that adequate moisture is available for active reinforcing steel corrosion. Therefore, the combination of humidity and existing flexure cracks provides the warranted conditions for reinforcing steel corrosion.

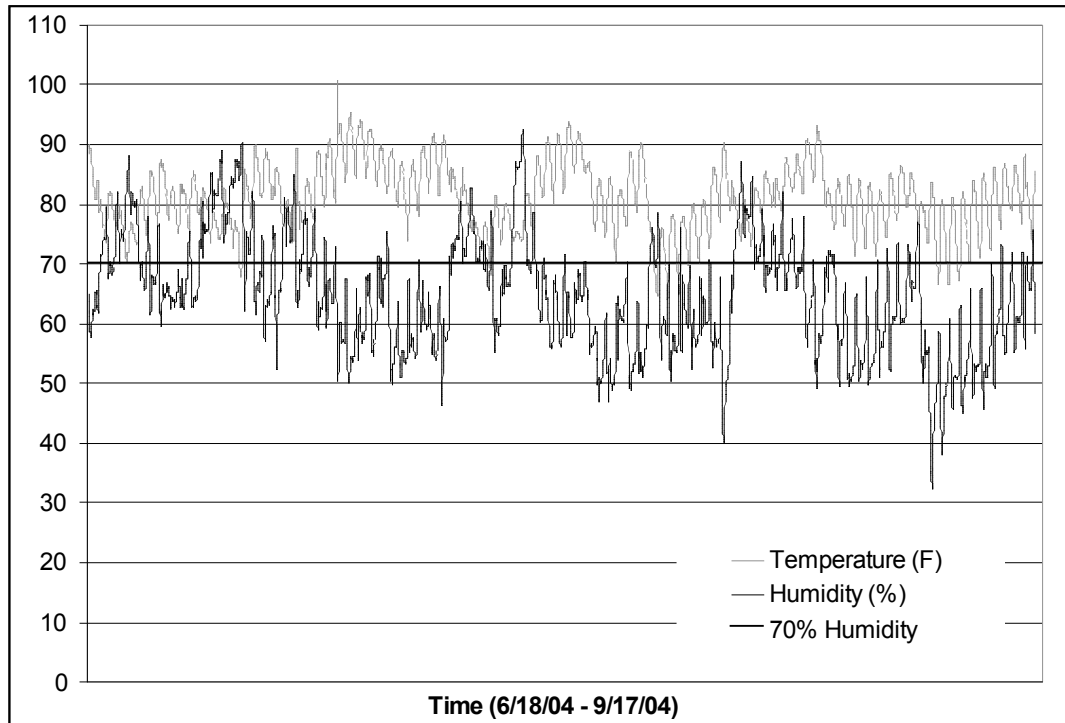


**Figure 5.15: Danville PCB Bridge Temperature and Humidity Data**

**5.5 In-Situ Moisture Content Determination**

Moisture contents were obtained from in-service beams at three PCB bridge locations. The locations used for this investigation included Danville, AR; Lakeway, AR; and Gravette, AR. Four locations were evaluated for moisture content at each bridge superstructure. Two samples were taken from the same exterior beam and two samples were taken from separate interior beams at each bridge site.

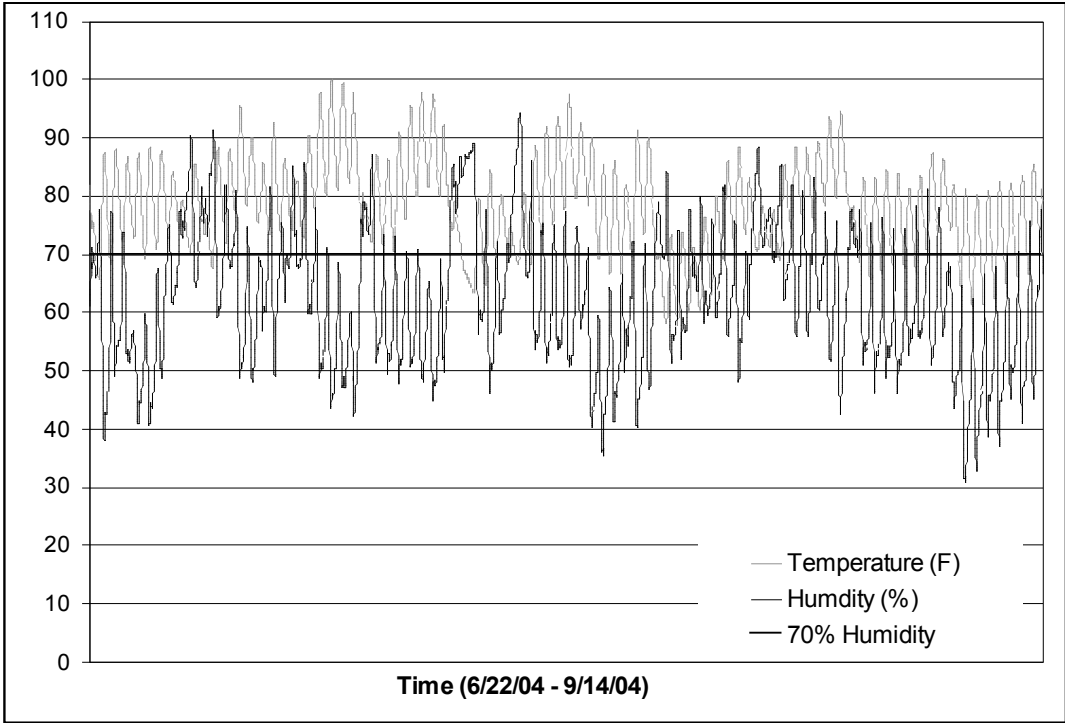


**Figure 5.16: Lakeway PCB Bridge Temperature and Humidity Data**

Drilling for a concrete sample was performed on the inside beam stem at mid-depth to evaluate the variability of moisture throughout the beam stem width. The inside beam stem was investigated in this study since deterioration was most often found at the

inside reinforcing steel bar. A 20-gram sample was taken at 1.5-in increments to a total depth of 4.5-in, Figure 5.17, using a 3/4-in drill bit attached to a hammer drill. The samples were collected and sealed in small plastic containers. They were then tested at the UA laboratory for moisture content.

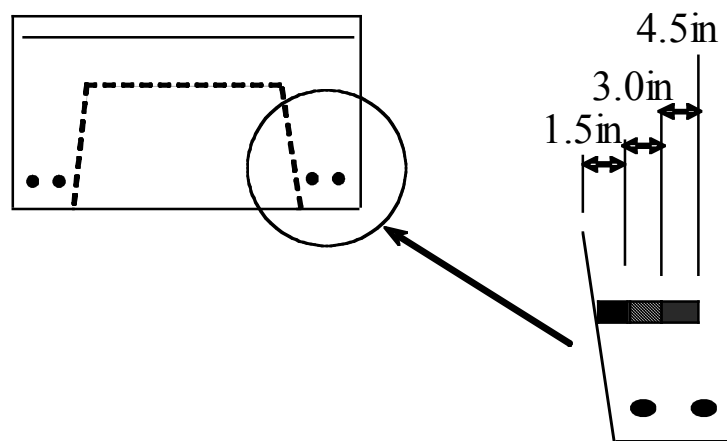


**Figure 5.17: Moisture Content Determination**

#### 5.5.1 Gravette, AR PCB Bridge

The Danville and Lakeway PCB bridges were previously described in section 5.4. The Gravette PCB Bridge contained three spans for a total of 21 beams. The bridge typically experiences light traffic with minimal heavy truck loadings. The bridge is in good condition with minimal longitudinal cracking and no exposed reinforcing steel. The stream water level is approximately 8-ft below the base of the beam stems.

### 5.5.2 Moisture Content Results

Results from the moisture content investigation of the three bridge sites are listed in Table 5.4. The moisture content was approximately constant throughout the depth tested indicating that water seepage from runoff was not the major contributor to the reinforcing steel corrosion.

**Table 5.4: Moisture Content Data**

Location	Depth (in)	Gravette	Danville	Lakeway
Exterior 1	0-1.5	3.55%	3.16%	2.90%
	1.5-3.0	4.44%	3.76%	2.78%
	3.0-4.5	4.25%	3.81%	3.29%
Exterior 2	0-1.5	4.73%	3.52%	3.02%
	1.5-3.0	5.37%	3.86%	3.30%
	3.0-4.5	6.10%	4.49%	3.07%
Interior 1	0-1.5	2.45%	1.82%	3.20%
	1.5-3.0	2.50%	2.01%	3.89%
	3.0-4.5	3.05%	1.78%	2.77%
Interior 2	0-1.5	3.41%	2.11%	2.77%
	1.5-3.0	2.72%	2.59%	3.92%
	3.0-4.5	3.14%	2.18%	3.24%

### 5.6 Summary

From the longitudinal cracking and reinforcing steel corrosion investigation, several conclusions were made.

- Longitudinal cracking is initiated by reinforcing steel corrosion. This deterioration ultimately leads to concrete spalling and exposed reinforcing steel.
- Flexure cracking is the result of heavier than designed for live loads.

- Moisture penetrates flexure cracks at the base of the beam stems by traveling from the deck surface through the joints at adjacent beams.
- High humidity levels present at bridge sites creates an ideal condition for reinforcing steel corrosion.
- Beam deterioration of in-service PCB bridges throughout Arkansas using the 1952 AHTD bridge details is much greater than originally suspected.
- Asphalt wearing surfaces were found to be statistically insignificant as a contributing factor for longitudinal cracking and reinforcing steel corrosion.
- Transverse traffic loading locations within the bridge cross-section have no impact on beam deterioration.
- Minimal chloride content indicates that chlorides from deicing salts or set accelerators are not contributing factors for beam deterioration.

## Chapter 6

### Experimental Design: Shear Strengthening Methods

Given the extreme nature of deterioration exhibited by many PCB's throughout the state, along with the lack of shear reinforcement, it was vital to develop a retrofit system to improve shear strength. The objective for a successful retrofit system for beams examined in this study was to increase shear capacity and beam ductility, thereby reducing the risk of a catastrophic shear failure. Three retrofit approaches were examined in this research project: (1) carbon fiber reinforced polymer strips, (2) microcomposite multistructural formable steel, MMFX, reinforcing bars, and (3) sprayed epoxy coating. Carbon fiber reinforced polymer strips and a sprayed epoxy coating were each examined as external shear strengthening methods. Conversely, the use of MMFX reinforcing bars was examined as internal shear reinforcement. Each of these strengthening methods can be easily implemented in the field providing a more efficient method of increasing shear capacity rather than beam replacement with shear reinforcement. The required shear improvement for these retrofit methods was to improve beam strength in shear so that failure would occur in bending. Therefore, maximum live load was based on the maximum truckload experienced by the beam in flexure over the life of the structure. This truck load was then used as the minimum design load for the shear retrofit. Consequently, this approach results in a beam that is stronger in shear than in bending and ensures a ductile failure rather than a catastrophic shear failure.

## **6.1 Strength Evaluation**

Results from thirty-three load tested PCBs confirmed the potential for a catastrophic shear failure. Of major concern were beams that did not exhibit ductile behavior prior to shear failure. To remedy this condition, the beam shear strength was increased to ensure longitudinal reinforcing steel yielding, based on the calculated beam moment capacity, prior to shear failure.

### *6.1.1 Moment Capacity and Equivalent HS Truck Loading*

Beam moment capacity was determined based on maximum live loading. Beam load ratings were performed to determine the equivalent truck loading for beams in their present condition. Load rating factors were calculated using the “Manual for Condition Evaluation of Bridges” [AASHTO, 1994]. The beams were examined at both an inventory and operating level for a standard HS-20 truck with a total gross weight of 36-tons. Axle spacing along with wheel loads for a HS-20 truck are presented in Figure 6.1. Inventory level rating factors represent the ability of a bridge to safely sustain a vehicular load for an indefinite period of time. Conversely, the operating level rating factor is the ability for a bridge to safely carry a vehicle a limited number of times.

To calculate either of the two rating factors, the factored moment,  $M_U$ , dead load moment,  $M_{DL}$ , and live load moment with impact,  $M_{LL+I}$  are required. The dead load moment and live load moment with impact were calculated to be 20.7-kip-ft and 98.8-kip-ft respectively. The dead load moment was calculated using only the beam self

weight to determine a maximum live load. The live load moment with impact was determined based on the HS-20 design truckload assuming no load distribution between beams in the bridge cross-section and an impact factor of 1.3 as per AASHTO specifications [AASHTO, 1996]. The maximum live load moment for the HS-20 truck configuration occurs when the 16 kip wheel load is positioned at mid-span, Figure 6.2.

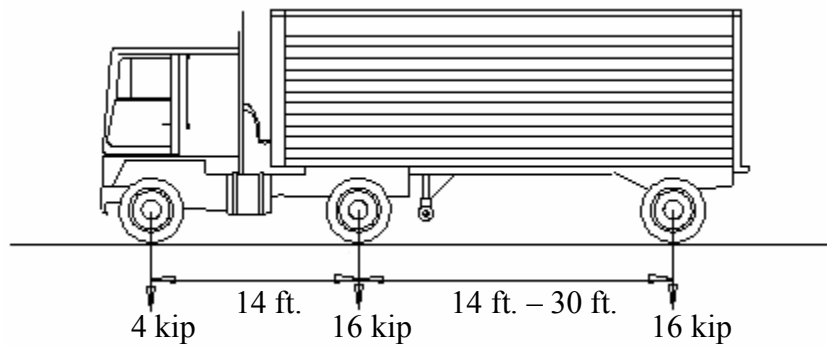


**Figure 6.1: HS-20 Axle Spacing and Wheel Line Loads**

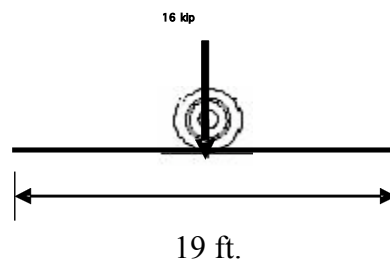


**Figure 6.2: Wheel Load Position for Maximum Live Load Moment**

Using the 1974 bridge details with a specified concrete compressive strength,  $f'_c$ , of 3,000-psi and a reinforcing steel yield strength,  $f_y$ , equal to 40ksi the factored moment capacity is 190.0-kip-ft. Including the AASHTO strength reduction factor, 0.9, for bending, the factored nominal moment is then 171.0-kip-ft.

Using Equation 6.1, the inventory level rating factor is 0.672.

$$RF_I^{LF} = \frac{M_u - A_1 M_{DL}}{A_2 M_{LL+I}} \quad \text{Eq. 6.1}$$

where:

- $RF_I^{LF}$  = load factor rating at inventory level
- $M_u$  = factored nominal moment capacity
- $M_{DL}$  = moment due to dead load
- $M_{LL+I}$  = moment due to live load and impact
- $A_1$  = load factor of dead load, 1.3
- $A_2$  = load factor of live load, 2.17

While the operating level rating factor is 1.122 using Equation 6.2:

$$RF_O^{LF} = \frac{M_u - A_1 M_{DL}}{A_2 M_{LL+I}} \quad \text{Eq. 6.2}$$

where:

- $RF_O^{LF}$  = load factor rating at operating level
- $A_1$  = load factor of dead load, 1.3
- $A_2$  = load factor for live load, 1.3

Considering the 1.122 operating level rating factor, Figure 6.3 illustrates the equivalent HS truck wheel load for a HS-22.5 live load. Therefore, for beam strength based on bending, the beam is required to have adequate strength for a HS truck load

of 24.1-tons at the inventory level and 40.5-tons at the operating level. These are the loads used to develop the required retrofit shear strength.

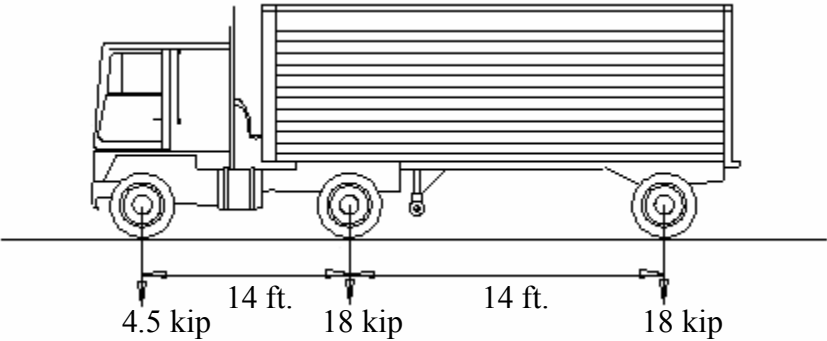


**Figure 6.3: Equivalent HS Truck Wheel Line Loads at Operating Level**

6.1.2 Shear Evaluation

The maximum factored shear force,  $V_u$ , is expressed as the function of the factored shear force due to dead load,  $V_{DL}$  and HS-22.5 live load with impact,  $V_{LL+I}$ , Equation 6.3:

$$V_u = 1.3V_{DL} + 1.67V_{LL+I} \qquad \text{Eq. 6.3}$$

The maximum factored shear force due to live load occurs when the rear cab wheel and trailer wheel loads are spaced 14-ft from one another with the trailer wheel positioned at the beginning of the span, Figure 6.4. This loading configuration results in a maximum shear force due to live load with impact, 1.3, of 29.6-kip. The dead

load shear force due to beam weight is 4.4-kip. Therefore, the maximum factored shear force, using Equation 6.3, is 55-kip.

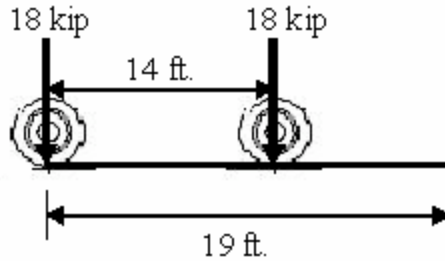


**Figure 6.4: Wheel Load Positions for Maximum Live Load Shear Force**

The required nominal shear strength of the beam is determined using Equation 6.4. The shear strength reduction factor,  $\phi = 0.85$ , is applied to the maximum factored shear force, 55-kip. Consequently, the required nominal shear strength is 64.8-kip.

$$V_n(\text{required}) = \frac{V_u}{\phi} \quad \text{Eq. 6.4}$$

The nominal shear capacity strength of the beam represents the actual tested beam strength and is the combination of the concrete shear capacity,  $V_c$ , and the shear capacity provided by the steel reinforcement,  $V_s$ , Equation 6.5. In this study, the beams are deficient of shear reinforcement and the nominal shear capacity is solely dependant upon the shear contribution by the concrete. Concrete's contribution to shear strength is expressed in Equation 6.6 and is dependant upon the concrete compressive strength. The nominal shear capacity of a single PCB is 26.3-kip based

on the pre-1974 bridge details which included a concrete compressive strength of 3,000-psi.

$$V_n = V_c + V_s \quad \text{Eq. 6.5}$$

where:

- $V_n$  = nominal shear capacity
- $V_c$  = shear capacity provided by the concrete
- $V_s$  = shear capacity provided by the transverse steel

$$V_c = 2\sqrt{f'_c} b_w d \quad \text{Eq. 6.6}$$

where:

- $f'_c$  = concrete compressive strength
- $b_w$  = web width
- $d$  = distance from extreme compression fiber to the centroid of the longitudinal tension reinforcement

When compared to the required nominal capacity of 64.8-kip, based on bending strength, the calculated nominal shear capacity of the beams is approximately 60% deficient. This shear deficiency is illustrated in Figure 6.5. Laboratory results revealed that thirty-one of the thirty-three load tested un-retrofitted beams failed in shear below the 64.8-kip nominal shear capacity value. The two other beams failed in flexure due to existing flexure cracks prior to load testing.

The three proposed retrofit methods to improve beam shear strength included: carbon fiber reinforced polymer strips, microcomposite multi-structural formable reinforcing

steel bars, and using a sprayed epoxy coating. The design of each retrofit is described in the following.

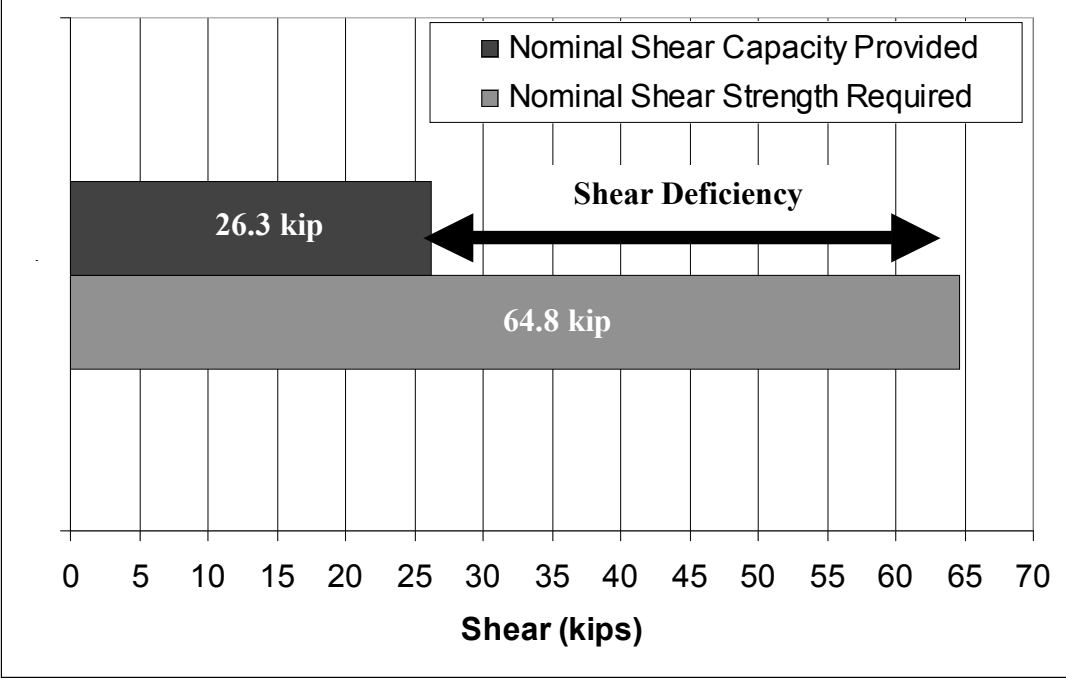


Figure 6.5: Shear Strength Deficiency

**6.2 Carbon Fiber-Reinforced Polymer Strips**

In recent times, repair of damaged bridge superstructures or strengthening of bridge superstructures to improve load capacity has been encouraged over beam replacement. Therefore, not only must repairs to bridge structures satisfy structural strengthening requirements, but also must be performed quickly to minimize traffic operation disruptions. Using carbon fiber reinforced polymer strips satisfies these requirements. Carbon fiber reinforced polymers (CFRP) are favorable materials for bridge

superstructure repair because of their superior mechanical properties and low density [Emmons et al, 1998].

### 6.2.1 Material Properties of CFRP Laminates

Fiber reinforced polymer materials have been generally used for concrete beam repair or strengthening with the objective of increasing the flexural strength of the structure; however, for this research, they are instead considered for shear strengthening purposes. CFRP laminates consist of unidirectional carbon fibers combined with an epoxy resin. A commercially available CFRP system, Sika CarboDur, was used as the retrofit material in this research project. Material properties supplied by the manufacturer are listed in Table 6.1. CFRP laminates are extremely effective in retrofitting deteriorated concrete structures due to their high strength-to-weight ratio, chemical resistance, lightweight, and handling ease. In addition, a CFRP laminate application results in minimal interruption time. In comparison, the cost of a CFRP repair is considerably less than the overall cost of structural replacement.

### 6.2.2 Design of the CFRP Strengthening Retrofit

Carbon fiber reinforced polymer strips were applied externally to the interior portion of the channel beam stems, Figure 6.6. By applying these strips externally, a three element composite system is formed: concrete, epoxy, and CFRP strip, Figure 6.7. Two CFRP strip configurations were investigated. One arrangement consisted of the CFRP strips aligned vertically and the second in a diagonal orientation.

**Table 6.1: CFRP Strengthening System Material Properties**

<b>Carbon Fiber Reinforced Polymer Strip</b>	
Design Tensile Strength	406 ksi (2799 MPa)
Design Modulus of Elasticity	23.9 x 10 <sup>3</sup> ksi (165 GPa)
Elongation at Break	1.69%
Thickness	0.047 in. (1.19 mm)
Width	1.97 in. (50.0 mm)
Fiber Volumetric Content	> 68%
Temperature Resistance	> 300°F (149°C)
<b>Epoxy</b>	
Tensile Strength @ 7 Days	3.6 ksi (24.8 MPa)
Elongation at Break @ 7 Days	1%
Modulus of Elasticity @ 7 Days	650 ksi (4482 MPa)
Flexural Strength @ 14 Days	6.8 ksi (46.9 MPa)
Tangent Modulus of Elasticity in Bending @ 14 Days	1700 ksi (11.7 GPa)
Shear Strength @ 14 Days	3.6 ksi (24.8 MPa)

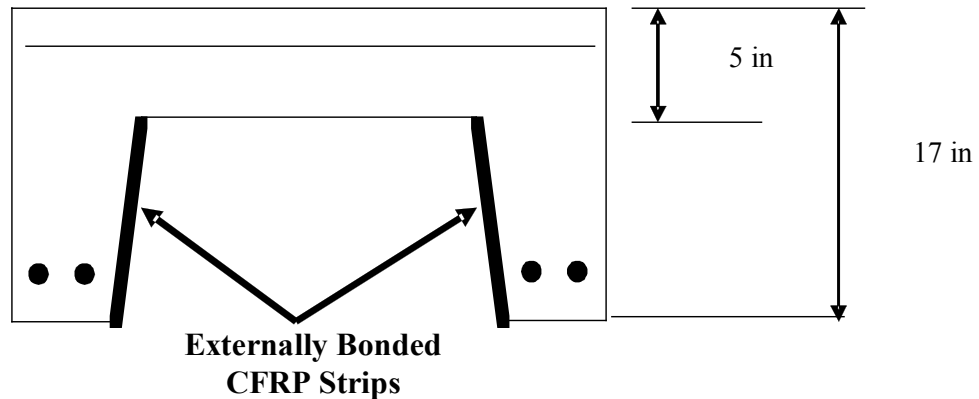


**Figure 6.6: CFRP Strengthening Retrofit**

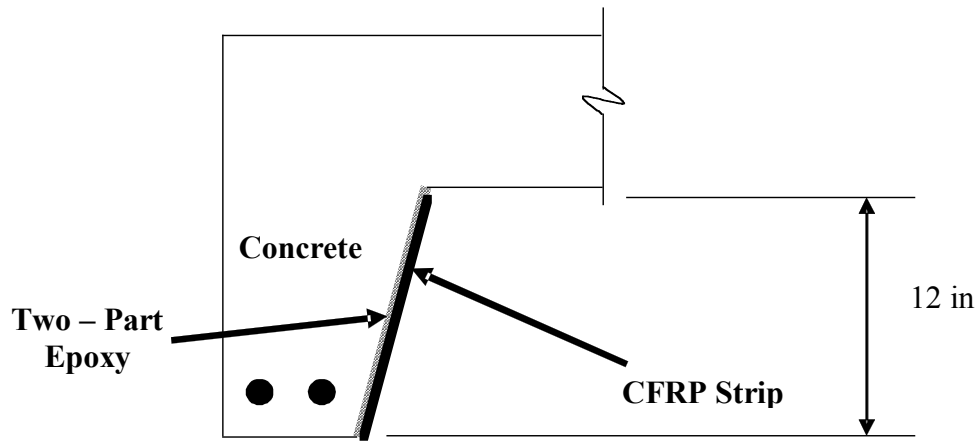


**Figure 6.7: CFRP Strengthening Retrofit (Three Component System)**

The required shear improvement to assure ductile beam failure is based on HS-22.5 truck live load. The design of the external CFRP strengthening technique was based on the AASHTO internal stirrup design procedure [AASHTO, 1994]. A conservative approach was taken in designing the external spacing for the CFRP strips. Because of its deteriorated state, the contribution of shear by the concrete was excluded from the required shear strength  $V_n$ . Consequently, this provides shear strength independent of the concrete condition.

Shear capacity provided by the CFRP,  $V_{CFRP}$ , for the vertical arrangement was determined using Equation 6.6:

$$V_{CFRP}(\text{vertical}) = \frac{A_f f_f d}{S} \quad \text{Eq. 6.6}$$

where:

- $A_f$  = area of the CFRP strip,  $2t_f w_f$
- $f_f$  = CFRP design tensile strength
- $s$  = CFRP strip spacing
- $t_f$  = thickness of a single CFRP strip
- $w_f$  = width of the CFRP strip

The shear capacity provided by the CFRP,  $V_{CFRP}$ , for the diagonal arrangement ( $\alpha = 45^\circ$ ) was computed using Equation 6.7:

$$V_{CFRP}(diagonal) = \frac{A_f f_f (\sin \alpha + \cos \alpha) d}{S} \quad \text{Eq. 6.7}$$

where:

- $\alpha$  = angle between an inclined CFRP strip and longitudinal axis of the member

To ensure ductile behavior, the CFRP shear strength was limited by Equation 6.8:

$$V_{CFRP} < 8\sqrt{f'c} b_w d \quad \text{Eq. 6.8}$$

The carbon fiber reinforced polymer strips were spaced to prevent the full formation of a diagonal crack between two adjacent strips. Therefore, the maximum spacing permitted for the vertical arrangement is:

$$s = w_f + \frac{d}{4} \quad \text{Eq. 6.9}$$

and for the diagonal arrangement:

$$s = w_f + \frac{d}{2 \tan \alpha} \quad \text{Eq. 6.10}$$

A 1.97-in width CFRP strip was used in this project. From Equation 6.9, the vertical arrangement has a maximum spacing of 5.5-in. This spacing results in a shear contribution of 103-kip by the CFRP and is well above the required nominal shear capacity of 64.8-kip. The diagonal arrangement has a maximum 8-in. spacing, Equation 6.10, which results in a shear contribution of 100-kip by the the CFRP strip.

Arrangement of the fiber strips in the vertical and diagonal orientation is illustrated in Figure 6.8. In both cases, the base of the first strip was located 15-in. from the beam end.

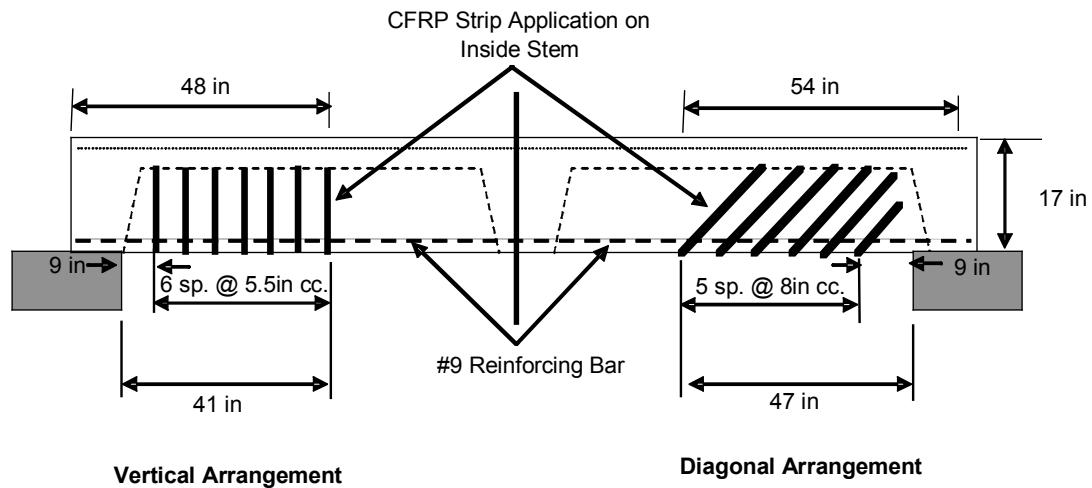


**Figure 6.8: Vertical and Diagonal Arrangement of CFRP Strip Application**

### **6.3 MMFX Steel Shear Bar**

Advanced high-strength corrosion-resistant steel has been developed by the MMFX Steel Corporation of America [El-Hacha and Rizkalla, 2002]. This relatively new high performance steel is becoming increasingly popular in the United States for use in bridges, highways, and parking structures.

#### **6.3.1 Material Properties of MMFX Steel Reinforcement**

Microcomposite multistructural formable steel (MMFX) has superior mechanical properties over traditional steels. These microcomposite steels are composed of a patented chemical composition and a proprietary steel microstructure that produces steel with a higher yield strength than traditional steel. In addition to its high strength, MMFX steel is extremely corrosion resistant. MMFX steel contains less than one percent of carbon and between eight and ten percent chrome. Its high yield strength of 120-ksi requires less steel cross-sectional area when designing concrete structures. Because of its corrosive resistant behavior, MMFX steel is effective in both highly corrosive environments and permeable concretes. Due to its superior material properties, MMFX reinforcing steel was selected as the material for the shear bar retrofit. The material properties determined by an independent testing facility are shown in Table 6.2 [El-Hacha and Rizkalla, 2002].

#### **6.3.2 Design of the MMFX Shear Bar Retrofit**

Shear strengthening of the channel beams was examined using straight sections of MMFX steel bars as internal shear reinforcement. An attractive characteristic of this

retrofit approach is that the shear bar retrofit can be installed from above the bridge deck and therefore reduce equipment costs. Traditionally, a #3 Grade 60 U-stirrup is used for shear reinforcement in concrete beams. However, a #5 MMFX reinforcement bar was selected based on its cross-sectional area and availability. A #3 Grade 60 stirrup will resist a shear crack with two cross-sectional areas and therefore provides slightly more area than a single #5 reinforcing bar; however, area difference is compensated for by the yield strength of the MMFX reinforcing bar.

**Table 6.2: MMFX Steel Rebar Material Properties**

<b>Microcomposite Multistructural Formable Steel (MMFX) Reinforcing Bar</b>	
Yield Tensile Strength (0.2% Offset)	120 ksi (1111 MPa)
Strain @ 0.2% Offset Yield Strength	0.60%
Ultimate Tensile Strength	177 ksi (1220 MPa)
Strain @ Ultimate Stress	12%
Young's Modulus of Elasticity (Tension)	29,000 ksi (200 GPa)
Yield Compressive Strength (0.2% Offset)	145 ksi (1000 MPa)
Young's Modulus of Elasticity (Compression)	29,000 ksi (200 GPa)
Shear Strength	110 ksi (758 MPa)
Poisson's Ratio	0.26
<b>Epoxy</b>	
Shrinkage During Cure	0.00051 (in/in)
Compressive Strength	10.3 ksi (71.0 MPa)
Heat Deflection Temperature	140°F (60°C)

Similar to the previously discussed CFRP strengthening retrofit, a conservative approach was used to determine the shear bar spacing. The design of the internal MMFX shear bar strengthening retrofit followed the AASHTO internal stirrup design procedure [AASHTO, 1994]. Neglecting the contribution of shear due to the concrete,

adequate spacing of the shear bars was determined using the required nominal shear capacity,  $V_n$ , of 64.8-kip and Equation 6.11.

$$S_{MMFX} = \frac{A_s f_y d}{V_n} \quad \text{Eq. 6.11}$$

where:

- $S_{MMFX}$  = MMFX shear bar spacing
- $A_s$  = area of the shear bar
- $f_y$  = yield strength of the MMFX shear bar
- $d$  = distance from extreme compression fiber to the centroid of the longitudinal tension reinforcement
- $V_n$  = nominal required shear strength

Figure 6.9 illustrates a cross-section of a precast channel beam retrofitted with shear bars. An enlarged retrofitted cross-section of a single beam stem is shown in Figure 6.10.

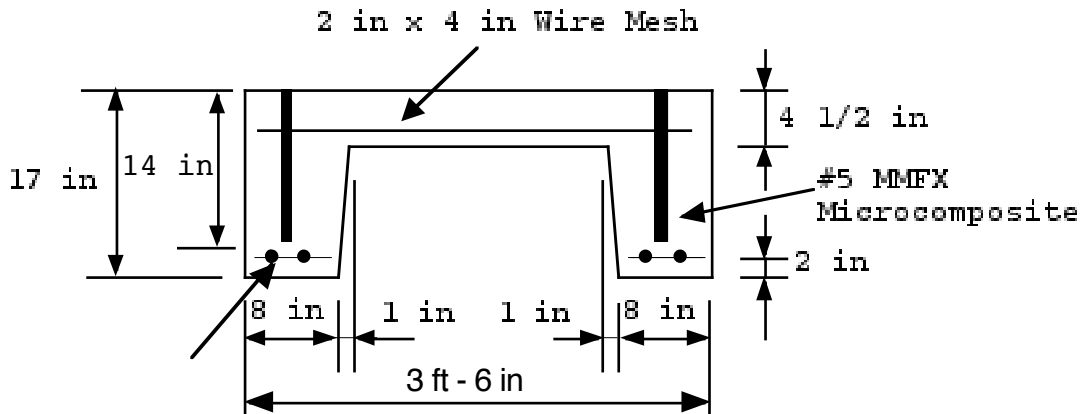


**Figure 6.9: MMFX Shear Bar Retrofit**

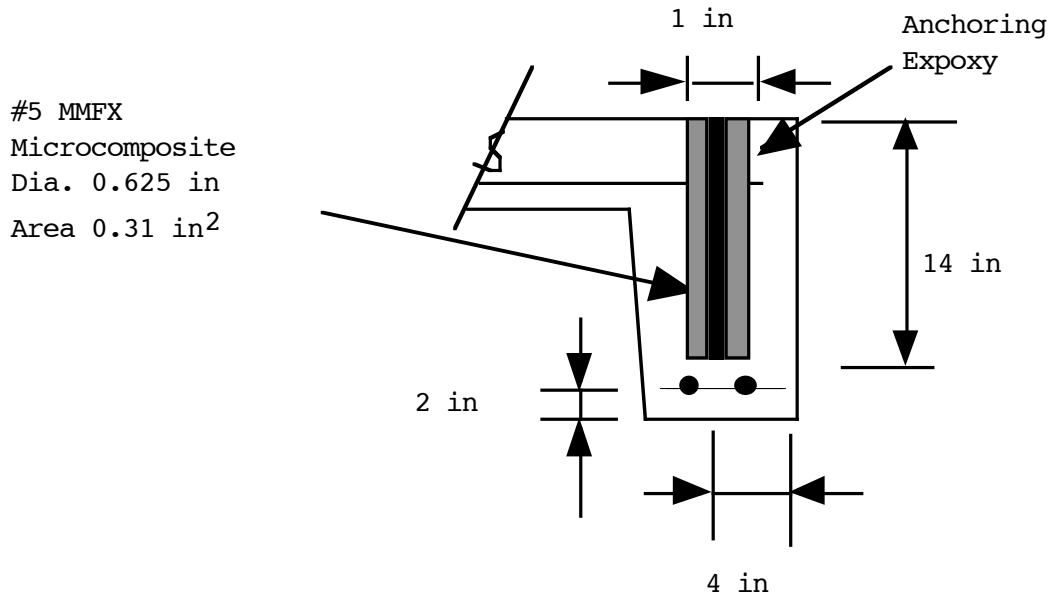


**Figure 6.10: Enlarged Schematic of MMFX Shear Bar Retrofit**

Using Equation 6.11, the shear bar spacing was determined to be 17.1-in.; however to be conservative and for ease of installation a spacing of 12-in. was selected for this application. This spacing allows for bar spacing measurements to be easily performed in the field. The 12-in. spacing does exceed the specified maximum for shear stirrups provided by AASHTO; however many researchers have shown that spacing less than the effective depth, in this case 15-in., is adequate [Batchelor and Kwun, 1981]. In other research by Swamy, the most efficient spacing has been found to be 0.75d, which is approximate to the 12-in spacing used in this application [Swamy and Qureshi, 1973]. Similar to the CFRP retrofit approach, the design was limited by Equation 6.8 to ensure beam ductility. A 12-in spacing provides shear capacity of

93.0-kip. Arrangement of the embedded shear bars is illustrated in Figure 6.11. The first bar is located 14-in. from the beam end. Shear bars were discontinued 50-in. from the beam end at a point in which required shear strength is adequately provided for by the concrete.

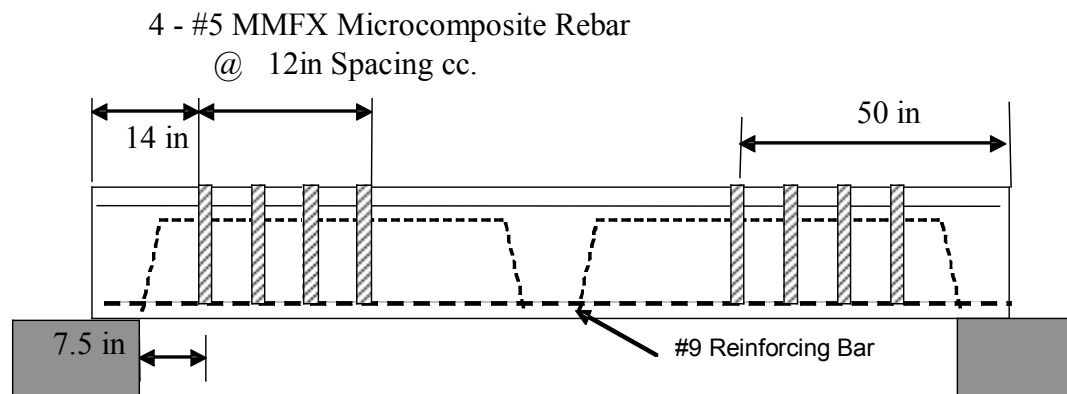


**Figure 6.11: MMFX Shear Bar Placement along Length of Beam**

#### **6.4 Sprayed Epoxy Coating**

The final repair method involved spraying an epoxy coating along the inside portion of the beam stems. The sprayed epoxy coating method was selected for its minimal surface preparation and application ease. Sprayed epoxy coatings have been typically used for rehabilitation of existing structures where structural enhancement is desirable.

##### **6.4.1 Material Properties of the Sprayed Epoxy Coating**

The coating material used for the retrofitting was Raven 405. Raven 405 is a solvent-free, ultra high build epoxy coating developed by Raven Lining Systems. The epoxy

exhibits superior bond to concrete, steel, masonry, and fiberglass even when moisture is present on the concrete surface. Recommended thicknesses vary between 40 mils to 250-mils for different applications; however for overhead applications a maximum thickness of 200-mils is advised to reduce sagging. The epoxy consists of 100% solids allowing for zero shrinkage to occur resulting in the same wet film thickness and final dry thickness. After the resin (Part A) and the hardener (Part B) are mixed at temperatures up to 200°F., the epoxy goes through a gelling stage where the coating becomes extremely sticky. This stage is followed by the initial set of the epoxy occurring typically within 6 hours at 70°F. At 6 hours the epoxy strengthening system can withstand light traffic or flow, but curing continues for several days. Typically, the maximum properties shown in Table 6.3 are achieved within 8 hours of application. When applying several coats to attain a desired thickness, the maximum time between coatings should not exceed 24 hours. Adherence is a function of temperature; therefore, concrete surface temperature should be at least 40°F and not more than 120°F at application time.

#### 6.4.2 Design of the Sprayed Epoxy Coating

Sprayed epoxy coatings have typically been used for the rehabilitation of existing structures for strength enhancement and protection from environmental conditions; however, a design procedure for epoxy thicknesses and coverage has not been standardized.

**Table 6.3: Sprayed Epoxy Coating Material Properties**

<b>Raven 405 Sprayed Epoxy Coating</b>	
Flexural Strength	13 ksi (89.63 Mpa)
Compressive Strength	18 ksi (124.1 Mpa)
Tensile Strength	7.6 ksi (52.4 Mpa)
Tensile Ultimate Elongation	1.50%
Hardness, Shore D	88
Water Vapor Transmission	3.2 gms/sq.m per 24 hr. (0.0105 oz/sq.ft. per 24 hr.)
Abrasion	<112 mg loss (0.004 oz loss)
Adhesion (Concrete)	Substrate Failure
Temperature Resistance	200°F (93.3°C)

Research has shown that an epoxy thickness of 0.25 inches increases the load capacity of concrete members over 40% [Harries and Young, 2003]. Further, an epoxy thickness of 0.125-in has demonstrated improved bending stiffness. From strength curves of the epoxy material used in the project, the epoxy thickness was selected to be 0.125-in and was applied along the inside portion of the channel stems to replicate field application. The 60-in end segments of each stem was sprayed with the epoxy coating. Figure 6.12 illustrates this retrofit method.

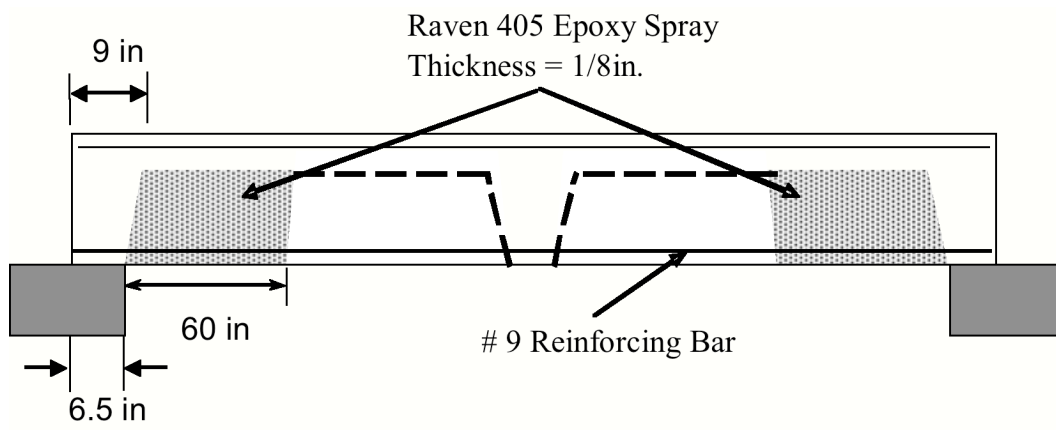


**Figure 6.12: Side View of Beam with Sprayed Epoxy Retrofit**

## Chapter 7

### Retrofit Application Procedures

In any retrofitting process, improved strength, ease of implementation and minimal traffic disruption are major factors in determining the success of a retrofit procedure. In this chapter, the procedure for each of the three retrofit techniques discussed, examined, and illustrated in detail.

#### **7.1 Carbon Fiber-Reinforced Polymer Strip Application**

The application procedure for the carbon fiber-reinforced polymer (CFRP) retrofit is described using the flow chart shown in Figure 7.1. In the following sections, each procedure step is discussed.

##### *7.1.1 Deteriorated Concrete Surface Repair*

Because of the highly stiff behavior of the carbon fiber-reinforced polymer strips, the concrete surface must be smooth and free of surface irregularities to ensure proper bonding at the strip-concrete interface. The maximum allowable deviation within a 3ft segment in which the strip will be applied must not be greater than 0.25in., and not more than 0.125-in per foot. Furthermore, any sharp edges within the concrete surface formed during construction must be ground smooth and flush with the surrounding area. In cases when the concrete surface has deteriorated to such a degree that a smooth surface is unattainable, the spalled area must be filled with a mortar based material. The manufacturers of the CFRP strip recommend the use of SikaTop®123. This material is a two-component, polymer-modified, portland

cement, fast-setting, non-slag mortar used to repair deteriorated concrete structures, Figure 7.2 (a).

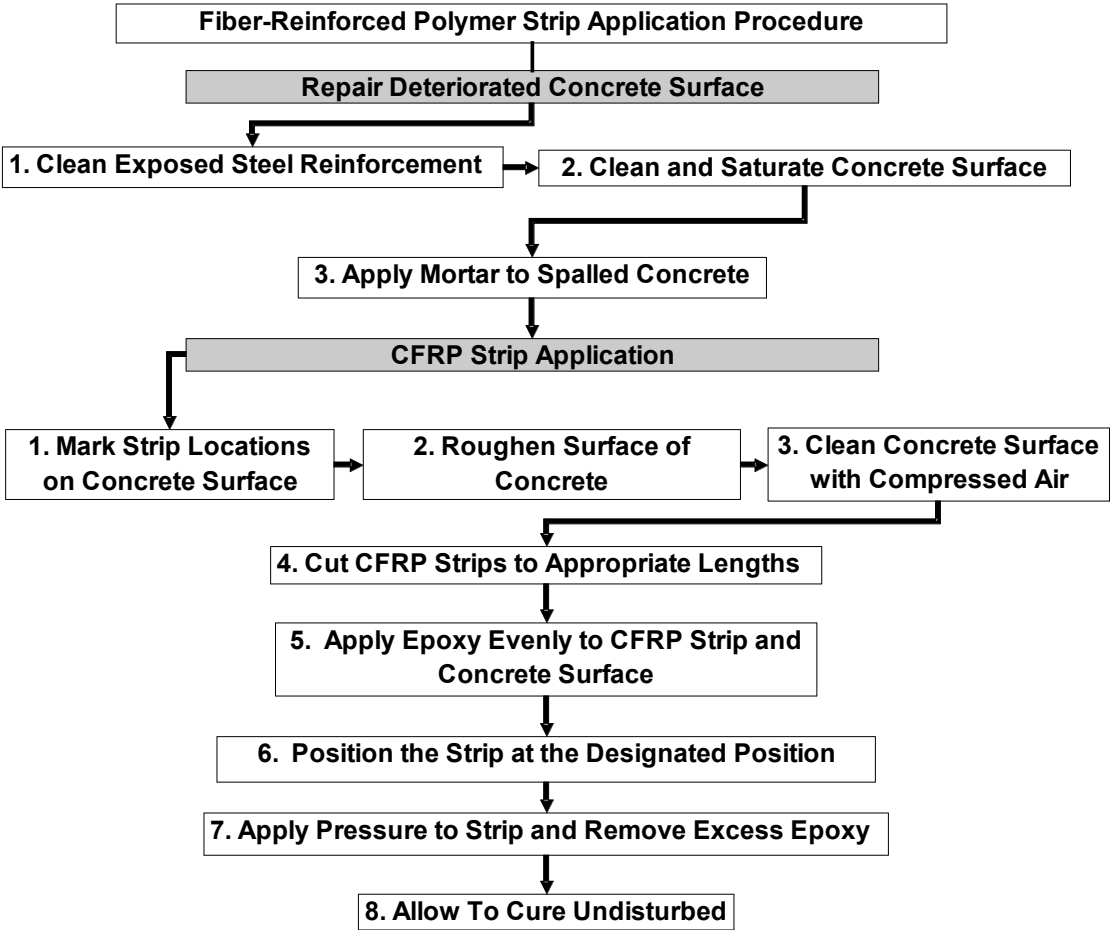


Figure 7.1: Fiber Reinforced Polymer Application Flow Chart

In addition to the material properties shown in Table 7.1, SikaTop®123 contains FerroGard 901, a penetrating corrosion inhibitor. Advantages of this mortar material include:

- High compressive and flexural strengths





(a)



(b)



(c)

**Figure 7.2: Repair Material and Beam Preparation**

The concrete substrate of the spalled area was primed using a scrub coat to ensure that all voids and pores were filled with the mortar mixture. The mortar was applied to the repaired area in 1.5-in maximum lifts. Each lift was allowed to cure for 30 minutes before the next lift was applied. The surface of each preceding lift was saturated with water and roughened to produce an interlocking bond at the layer interface. The final layer of the mortar repair was finished to the desired shape by using hand trowels and wooden boards. Figure 7.3 shows a spalled area being repaired with the mortar

material: (a) priming, (b) application of a single layer of mortar, (c) finishing, (d) and finally the repaired surface.

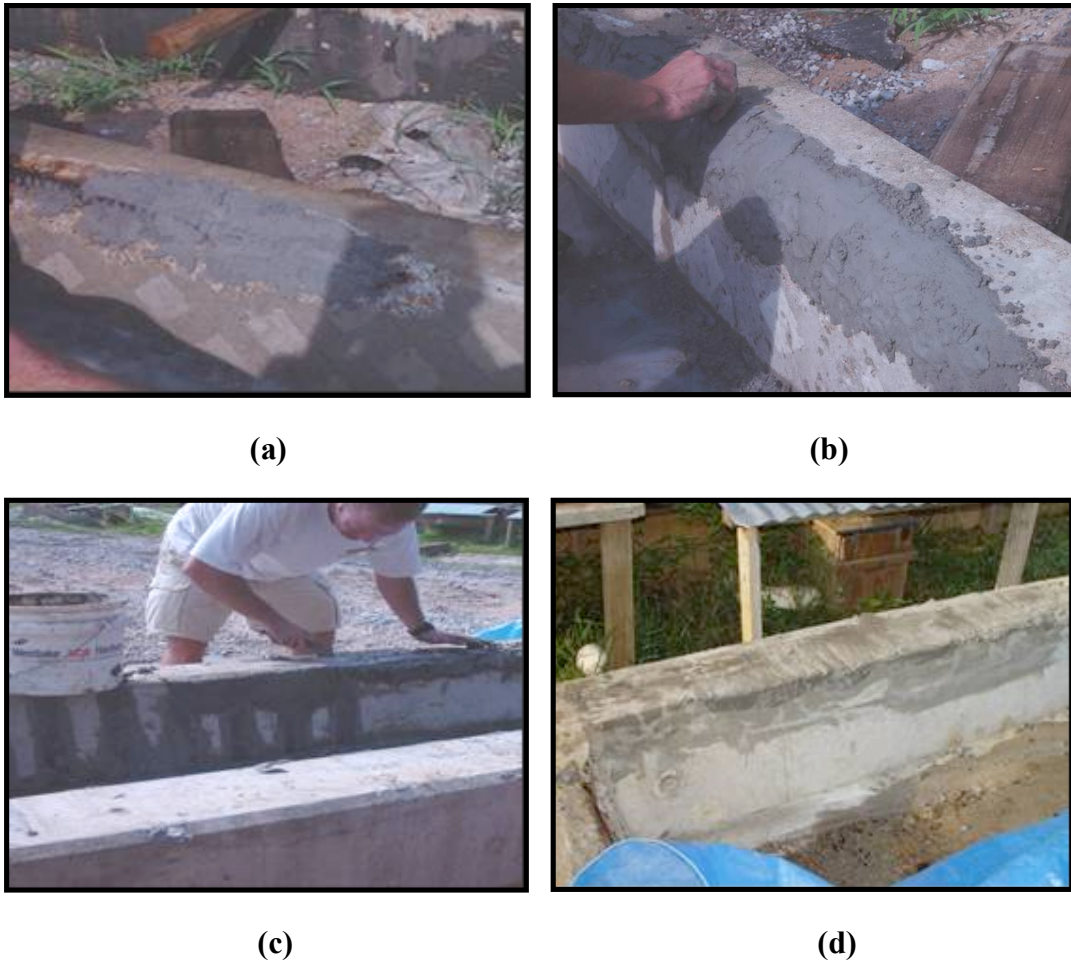


**Figure 7.3: Concrete Patch Repair Procedure**

### 7.1.2 CFRP Strip Application

The first step in the CFRP strip application procedure was to clearly mark the strip locations on the inside portion of the beam stems. Next a hand held grinder was used to roughen the concrete surface within the strip application areas, Figure 7.4 (a). The

roughened areas were made slightly larger than the actual CFRP strip to ensure that an adequate bonding area was available during the strip application.

Contaminants from the grinding process were removed using compressed air, Figure 7.4 (b). The prepared surfaces for the vertical and diagonal CFRP arrangements are shown in Figure 7.4 (c,d) respectively.



(a)



(b)



(c)



(d)

**Figure 7.4: Surface Preparation for CFRP Application**

The CFRP strips were cut to their appropriate lengths and dimensions prior to application. The strips were cut so as not to create splitting between fibers. The best method to perform this operation was by using a heavy-duty sheet trimmer, Figure 7.5 (a). Afterwards, the cut CFRP strips were cleaned with acetone to remove any carbon dust that would prevent proper bonding.

Manufacturers of the CFRP strip recommended that Sikadur 30, a two-component epoxy be used to bond the strips to the beam stem. This epoxy resin was thoroughly mixed to a paste-like consistency removing any air bubbles in the mixture. Figure 7.5 (b) shows the epoxy mixing. The epoxy was applied to the concrete with a uniform thickness of approximately 1/16-in using a spatula. Next, the epoxy was applied to the CFRP strip with a uniform thickness of 1/16-in, Figure 7.5 (c). High temperatures reduce epoxy bonding time. Because of high temperatures at the time of strip placement, strip application was rushed. The strips were then placed on the concrete while applying uniform pressure to ensure an epoxy-to-epoxy contact throughout the length of the strip, Figure 7.5 (d). Pressure was initially induced using a hard painter's roller and then a wooden roller as shown in Figure 7.5 (e, f). This pressure from the rollers was used to force excess epoxy from the strip-concrete interface. Excess epoxy was removed such that the epoxy thickness did not exceed 1/8-in.



(a)



(b)



(b)



(d)



(e)



(f)

**Figure 7.5: CFRP Retrofit Application Procedure**

The newly applied external shear strip reinforcement was protected from ambient conditions and allowed to cure undisturbed according to the manufacturer's

recommendation. After seven days, the epoxy reached its final design strength. Beams retrofitted with the diagonal and vertical retrofits are shown in Figure 7.6 (a, b), respectively.



**Figure 7.6: CFRP Vertical and Diagonal Retrofitted Beams**

## **7.2 MMFX Steel Shear Bar Application**

The procedure for inserting the microcomposite multistructural formable steel bars into the stems of precast channel beams through the deck surface is illustrated using the flow chart found in Figure 7.7. Each step of the procedure is explained in the following sections.

### **7.2.1 Deteriorated Concrete Surface Repair**

Though this repair material does not require the spalled concrete surfaces be repaired, repair should still be made since it protects the beam from further reinforcing steel corrosion. A similar repair procedure for the spalled areas as described previously in the CFRP application should be used. In this study, surface repair was not performed

on the retrofitted beams since preservation for long term effects were not the major objective of this research.

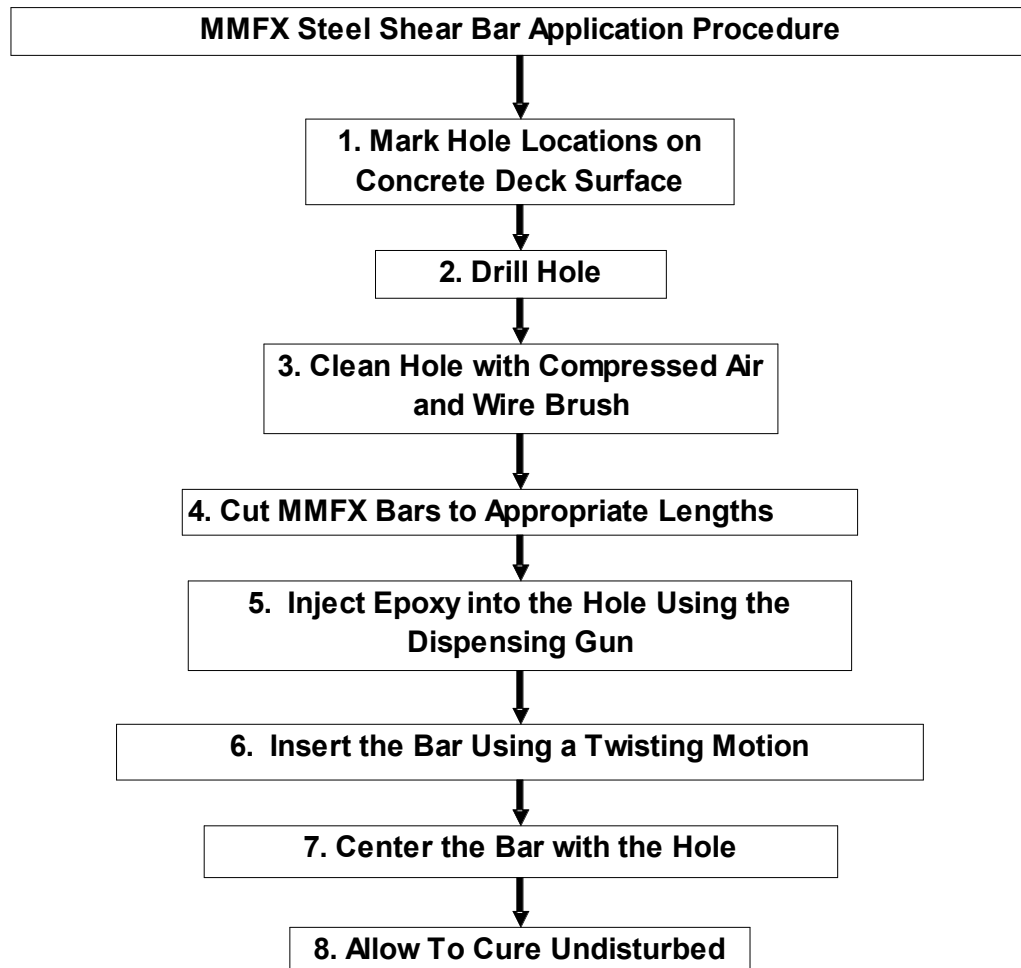
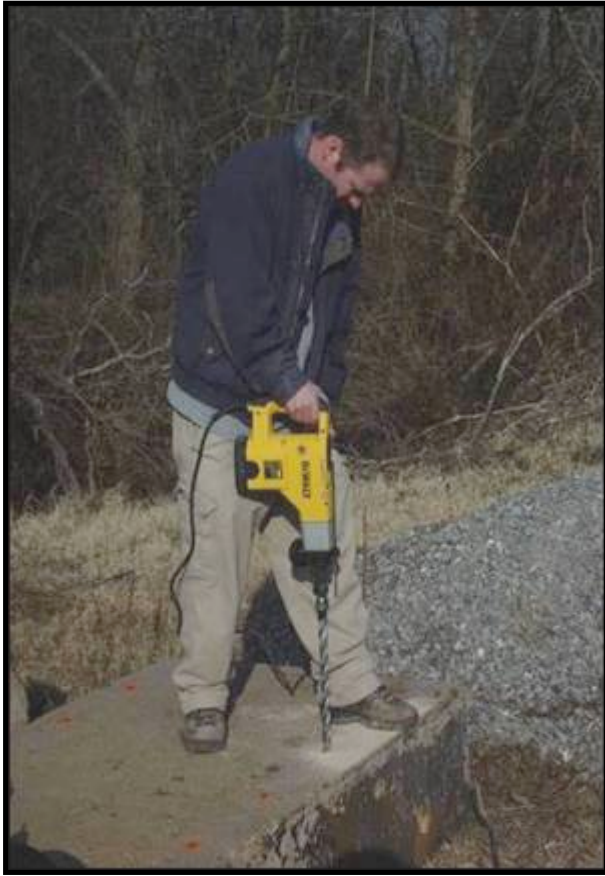


**Figure 7.7: MMFX Steel Shear Bar Application Flow Chart**

### 7.2.2 MMFX Shear Bar Application

The first step in the MMFX steel shear bar application procedure was to mark the locations of the holes on the deck surface at which internal reinforcement is to be placed. Next a Dewalt® DW530 rotary hammer drill with a 1-in diameter 4-cutter spline carbide tip drill bit was used to drill holes at predetermined locations, Figure 7.8 (a). Compressed air was used to remove all fines within the holes created during the drilling process. An extended air nozzle was used to supply large concentrated amounts of air to the bottom of the hole, Figure 7.8 (b). A wire brush, Figure 7.8 (c), was then used to clean the sides of the holes to remove any dust or slurry to ensure a proper bond between the epoxy and concrete.

The MMFX steel reinforcing bar was cut to their appropriate lengths prior to installation. The reinforcing steel was cut using a chop saw with a fast cutting reinforced blade made for steel cutting. The cutting process is shown in Figure 7.9 (a). The bar ends were ground to a smooth finish for handling safety during steel bar placement, Figure 7.9 (b). The cut steel reinforcing bars were cleaned with a cloth to remove any contaminants that would prevent sufficient bonding between the reinforcing steel and epoxy.



(a)



(b)



(c)

**Figure 7.8: Beam Preparation for MMFX Shear Bar Retrofit**



(a)



(b)

**Figure 7.9: Reinforcing Bar Preparation**

The Red Head® C6 Adhesive Anchoring System was used as the bonding material. The epoxy is applied using a dually loadable ratchet caulking gun with a nozzle, Figure 7.10. To assure quality, when starting a new cartridge or nozzle, excess epoxy was dispensed and discarded until a uniform dark gray color, fully mixed material, was identified.



**Figure 7.10 Epoxy Dispensing Tool**

Next, the nozzle was inserted into the bottom of the hole and slowly removed from the hole until half the hole depth was filled with epoxy. Finally, the reinforcing bar was slowly inserted by hand into the bottom of the hole with a slow twisting motion to fill voids and crevices uniformly. This procedure is illustrated in Figure 7.11 and shown in Figure 7.12 (a, b).

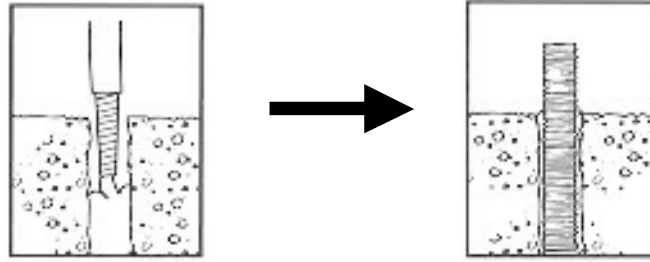


**Figure 7.11: Epoxy Application and Bar Insertion**



**(a)**



**(b)**



**(c)**



**(d)**

**Figure 7.12: MMFX Steel Shear Bar Retrofit Process**

Once the MMFX steel reinforcing bar was centered in the hole, care was taken to ensure that the bar is approximately flush with the concrete surface. In cases in which the bar was not, a hand held grinder was used to round the top of the bar. Excess epoxy seen in Figure 7.12 (c) was used to cover the top surface of the bar to provide a smooth vehicle riding surface at the bar locations. A beam retrofitted with the MMFX shear bar strengthening system is shown in Figure 7.12 (d).

The retrofit was allowed to cure as recommended by the manufacturers. Table 7.2 lists the working and final cure times required for the epoxy as a function of temperature. At the temperatures between 0°F and 50°F, the manufacturer recommends heating the epoxy to room temperature prior to its use. Working time is the minimum time required before the structure can be in service for limited loading. Large over loaded trucks are not permitted on the bridge structure until full epoxy strength is reached.

**Table 7.2: Epoxy Curing Times**

<b>Temperature (°F / °C)</b>	<b>Working Time (Minutes)</b>	<b>Full Cure Time (Hours)</b>
120 / 49	4	1
90 / 32	5	1
70 / 20	7	1
60 / 16	10	2
50 / 10	20	24
40 / 4	45	32

### **7.3 Sprayed Epoxy Coating Application**

The procedure for applying a sprayed epoxy coating on the inside stem portions of the beam is described in the flow chart presented in Figure 7.13. Each step of the procedure is discussed in detail in the following sections.

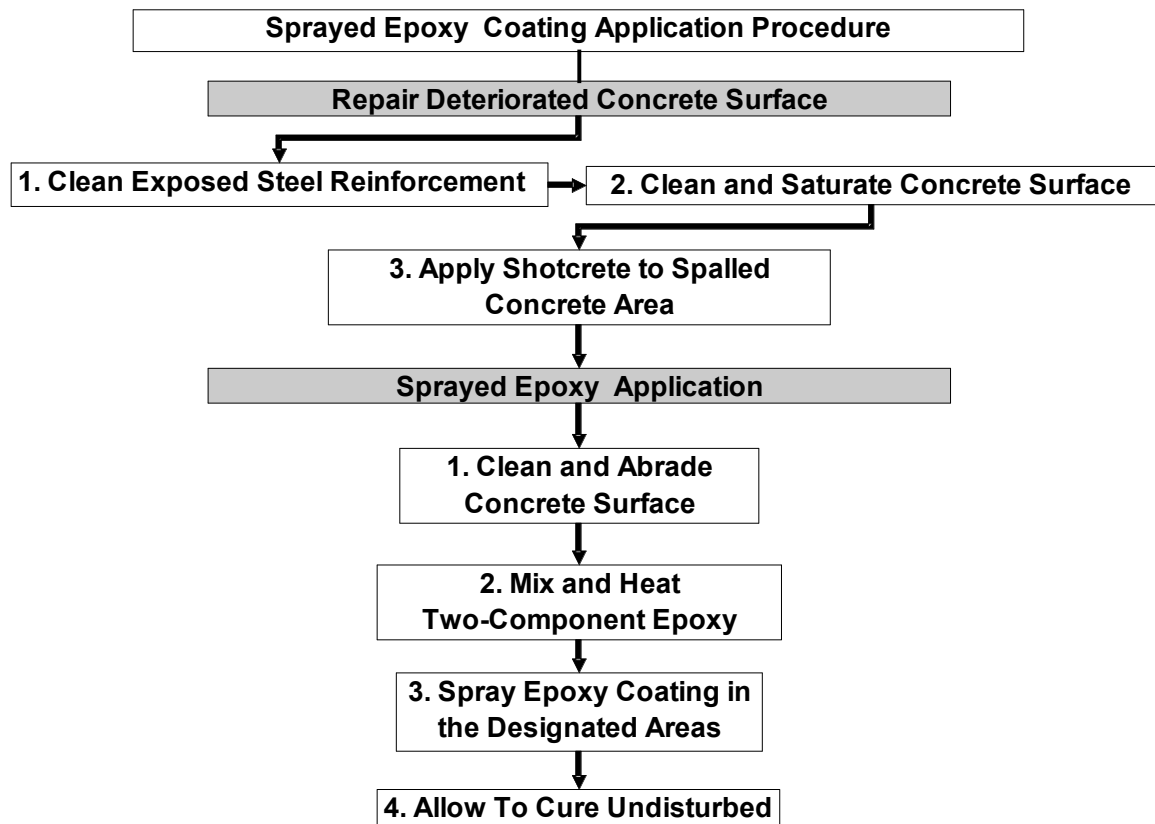


**Figure 7.13: Sprayed Epoxy Coating Application Flow Chart**

#### **7.3.1 Deteriorated Concrete Surface Repair**

In order for the sprayed epoxy coating repair procedure to work properly, the spalled concrete areas were repaired. The manufacturer of the epoxy coating recommends that concrete surface repair be performed when any of three conditions are present.

First, any area that exhibits cracking due to expansion or contraction should be patched. Second, exposed reinforcing steel should be cleaned. All concrete surfaces that contain exposed reinforcing steel with spalling greater than 0.75-in deep, or cracks greater than 0.375-in wide, should be patched with a quick setting, high strength cement mortar. Third, any concrete degraded by chemical reaction or other environmental conditions should be removed and replaced with sound concrete.

The procedure for repairing damaged concrete areas was similar to the CFRP retrofit application. During the sprayed epoxy coating retrofit process, the reinforcing steel was cleaned using a high pressure water jet. This process removed any loose steel fragments from the existing reinforcing steel and thoroughly cleaned the corroded reinforcing steel. Next, the concrete area around the reinforcing steel was cleaned to remove any loose particles that would inhibit bonding of the shotcrete repair. This process is shown in Figure 7.14 (a). The shotcrete mixture was applied to the spalled areas pneumatically combining the dry concrete mixture with water at the sprayer nozzle. Figures 7.14 (b) and 7.14 (c) show the shotcrete procedure and the final repaired surface respectively.

### 7.3.2 Sprayed Epoxy Coating Application

With any coating procedure, proper surface preparation is essential to ensure proper bonding between the epoxy coating and the concrete surface. The surface was prepared to provide a clean and roughened surface for the epoxy coating to adhere to. High pressure water jetting to the level of 5,000-psi at 4-gpm was used for surface

preparation, Figure 7.15 (a). Alternatively, mechanical methods such as abrasive blasting, shotblasting, grinding or scarifying could be used. Care was taken so that all oils, grease, or other contaminants were removed from the concrete surface.



(a)



(b)



(c)

**Figure 7.14: Surface Repair Using Shotcrete Technique**

A Raven® application spray system shown in Figure 7.15 (b) was used to apply the epoxy coating to the inside portions of the beam stems. The spray system was a multi-component airless spray application system that pre-heats the resin and hardener prior

to application. The system then mechanically proportions the resin and hardener (3 part resin, 1 part hardener) and pumps the two components through a heated hose to a mixing block. The mixture becomes homogeneously blended and transported through a hose and applied to the concrete substrate using an air-assisted spray gun, Figure 7.15 (c). Mixture of the two components creates a chemical reaction generating large amounts of heat. It is recommended that epoxy application begin immediately after mixing. The spray gun nozzle applies a uniform layer of epoxy over an approximately 1ft length, Figure 7.15 (d). During the spraying application, the epoxy thickness was measured using a wet film thickness gauge shown in Figure 7.15 (e). A beam retrofitted with the sprayed epoxy coating retrofit is shown in Figure 7.15 (f).



(a)



(b)



(c)



(d)



(e)



(f)

**Figure 7.15: Sprayed Epoxy Coating Retrofit Process**

## Chapter 8

### Data Analysis and Results

Twelve formerly in-service channel beams were retrofitted using the methods discussed in Chapters 6 and 7. These beams were load tested to failure to measure the effectiveness of each retrofit application by comparing the retrofitted beams with an additional four control “un-retrofitted” beams under the same loading configuration.

#### **8.1 Beam Characteristics and Retrofit Details**

The sixteen beams examined in this investigation were removed from a bridge near Hope, Arkansas. The channel beams had the same dimensions and longitudinal reinforcing steel as the thirty-three load tested beams discussed in Chapter 2. As in Chapter 2, these beams did not include shear reinforcement. The sixteen beams exhibited similar deterioration which included concrete spalling and longitudinal reinforcing steel corrosion. Details of each beam are listed in Table 8.1 and discussed in the following.

Beams H1 and H4 were shear strengthened with vertical CFRP strips, whereas beams H2 and H6 were retrofitted with diagonal CFRP strips. Areas of spalled concrete and exposed reinforcing steel in beams H1, H2, and H4 were repaired with SikaTop 123 Plus prior to the strip application. This repair was critical for proper bonding between the CFRP strip and the concrete surface.

**Table 8.1: Beam Characteristics**

<b>Beam</b>	<b>Retrofit Method</b>	<b>Description</b>
H1	Vertical CFRP 12in x 2in x 0.047in	Existing longitudinal cracks Repaired with Sika Top 123 Plus
H2	Diagonal CFRP 17in x 2in x 0.047in	Two existing flexure cracks at approximately the third points Repaired with Sika Top 123 Plus
H3	No Retrofit	Visible evidence of asphalt wearing surface Excessive concrete spalling and corrosion of longitudinal reinforcing steel
H4	Vertical CFRP 12in x 2in x 0.047in	Visible evidence of asphalt wearing surface Excessive concrete spalling and corrosion of longitudinal reinforcing steel Repaired with Sika Top 123 Plus
H5	No Retrofit	Slight concrete spalling and corrosion of longitudinal reinforcing steel
H6	Diagonal CFRP 17in x 2in x 0.047in	Existing flexure crack 3ft - 6in from beam end
H7	MMFX Shear Bar #5 Rebar (14in Length)	Existing longitudinal cracks Excessive concrete spalling and corrosion of longitudinal reinforcing steel
H8	MMFX Shear Bar #5 Rebar (14in Length)	Existing longitudinal cracks Excessive concrete spalling and corrosion of longitudinal reinforcing steel
H9	MMFX Shear Bar #5 Rebar (14in Length)	Visible evidence of asphalt wearing surface Excessive concrete spalling and corrosion of longitudinal reinforcing steel near the beam end
H10	Sprayed Epoxy Coating 12in x 60in x 0.125in	Excessive concrete spalling and corrosion of longitudinal reinforcing steel Repaired using shotcrete technique
H11	Sprayed Epoxy Coating 12in x 60in x 0.125in	Excessive concrete spalling and corrosion of longitudinal reinforcing steel Repaired using shotcrete technique
H12	MMFX Shear Bar #5 Rebar (14in Length)	Excessive concrete spalling and corrosion of longitudinal reinforcing steel
H13	Sprayed Epoxy Coating 12in x 60in x 0.125in	Excessive concrete spalling and corrosion of longitudinal reinforcing steel Repaired using shotcrete technique
H14	MMFX Shear Bar #5 Rebar (14in Length)	Existing longitudinal cracking Slight concrete spalling and corrosion of longitudinal reinforcing steel
H15	No Retrofit	Slight concrete spalling and corrosion of longitudinal reinforcing steel
H16	No Retrofit	Slight concrete spalling and corrosion of longitudinal reinforcing steel Two existing flexure cracks at approximately the third points

Beams H7, H8, H9, H12, and H14 were retrofitted with the MMFX shear bar design. Areas of spalled concrete were not repaired since the concrete surface had no influence on the shear strengthening system. Longitudinal reinforcing steel corrosion was most evident in the mid-span region of the beams; however, beam H12 had exposed reinforcing steel throughout the entire length of the beam.

The sprayed epoxy coating retrofit was applied by an outside contractor to beams H10, H11, and H13 on the inside face of the beam stem. A shotcrete repair was made where concrete spalling had taken place. The repair included cleaning the reinforcing steel and applying the repair to provide a smooth beam surface.

Control beams were tested to evaluate the effectiveness of the shear strengthening retrofit designs. The un-retrofitted beams H3, H5, H15, and H16 exhibited deterioration similar to the retrofitted beams. It was expected that these control beams would fail in shear and produce similar results as those found in Chapter 2.

## **8.2 Material Properties**

The concrete compressive strength and the theoretical shear strength contribution provided by the concrete,  $V_c$ , for the sixteen beams are listed in Table 8.2. The concrete compressive strength was determined by coring 4in. diameter samples from the beam stems in thirteen of the sixteen beams. A non-destructive testing device was used to determine the concrete compressive strength for beams H14, H15, and H16.

**Table 8.2: Concrete Compressive Strength Values**

<b>Beam</b>	<b>Concrete Compressive Strength (ksi)</b>	<b>Theoretical Shear Strength P (kip)</b>
H1	11.6	51.8
H2	13.1	54.9
H3	6.9	39.8
H4	8.7	44.7
H5	8.6	44.6
H6	10.9	50.0
H7	10.6	49.4
H8	9.2	46.1
H9	9.9	47.8
H10	10.5	49.3
H11	12.7	54.0
H12	13.7	56.2
H13	10.8	49.8
H14*	11.0	50.2
H15*	11.9	52.3
H16*	11.1	50.7

\* Indicates predicted concrete compressive strength from rebound hammer.

For non-destructive testing, a rebound hammer was used to develop a prediction equation for the determination of concrete compressive strength. A rebound value, R, was obtained by measuring the concrete's hardness using the spring-loaded device. Three sample groups of R-values were taken throughout each beam. Each sample group consisted of the average of ten measurements. The three sample groups were then averaged to provide an equivalent R-value for the beam. R-values and actual concrete compressive strength values were plotted and a regression analysis was used to create a prediction equation. The prediction equation was limited to the values obtained from the beams examined in this investigation. For this method to produce

reliable results in the field, more beams are needed to substantiate accuracy of the equation. Actual and predicted concrete compressive strength values along with the resulting R-values are listed in Table 8.3. The regression curve and prediction equation are shown in Figure 8.1.

**Table 8.3: Actual and Predicted Compressive Strength Values**

Beam	Actual	R-Value	R-Value	R-Value	Average	Predicted
	Compressive Strength	#1	#2	#3	R-Value	Compressive Strength
	(ksi)					(ksi)
H1	11.6	48.5	48.2	48.2	48.3	11.3
H2	13.1	49.3	49.3	49.8	49.5	12.7
H3	6.9	40.5	39.9	40.2	40.2	7.2
H4	8.7	43.4	43.8	44.6	43.9	7.9
H5	8.6	44.4	45	45.5	45.0	8.4
H6	10.9	48	48.2	48.6	48.3	11.3
H7	10.6	48	48.2	48.5	48.2	11.2
H8	9.2	46.6	47.4	47.3	47.1	10.1
H9	9.9	46.7	47.1	47	46.9	9.9
H10	10.5	47.1	47.4	46.8	47.1	10.1
H11	12.7	49	49.5	49.3	49.3	12.5
H12	13.7	49.5	49.9	49.6	49.7	13.0
H13	10.8	48.3	48.6	48.6	48.5	11.6
H14	-	48	48.2	47.7	48.0	11.0
H15	-	49	48.4	48.9	48.8	11.9
H16	-	48.1	48.1	48.2	48.1	11.1

A paired t-test statistical analysis with a 95% level of significance was performed to determine if the equation predicted reliable concrete compressive strength values. A test statistic of 0.005 was found to be significantly less than the critical test statistic of 2.179. Therefore, the equation presented in Figure 8.1 is a valid prediction for the concrete compressive strengths of these beams.

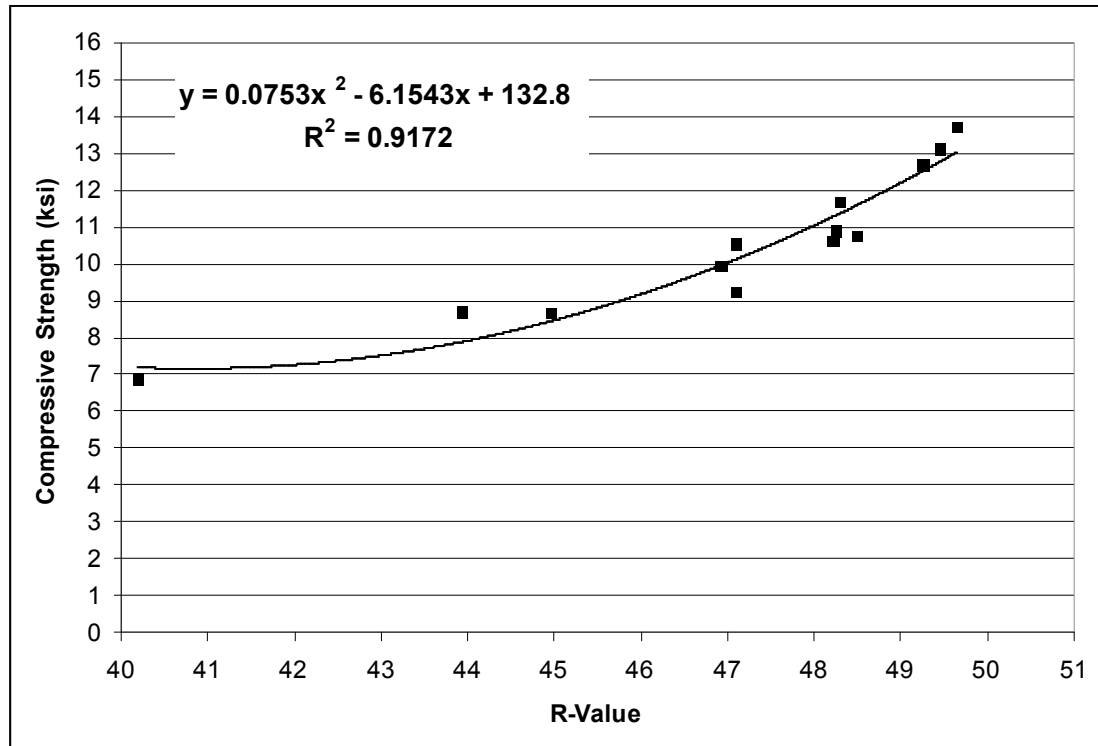


**Figure 8.1: Regression Curve and Prediction Equation**

### **8.3 Structural Results**

Three shear strengthening techniques were applied to a total of twelve beams and load tested. These results were compared with load testing results of four un-retrofitted beams. During the structural investigation, load and deflection values were continuously recorded using a digital camcorder. In addition, the mode of failure and behavior of the strengthening materials at failure were documented. The results are presented in the following.

8.3.1 Beam Deformation and Yielding

As expected, the load capacity of the retrofitted beams surpassed that of the control beams. More importantly, a yield plateau, ductile behavior, was observed for all the retrofitted beams with the exception of a single sprayed epoxy coating retrofitted beam. Conversely, two of the four control beams failed in shear without exhibiting a yield plateau. Load versus mid-span deflection curves for the sixteen beams are shown in Figure 8.2. Figure 8.3 shows the same curves for a limited deflection range.

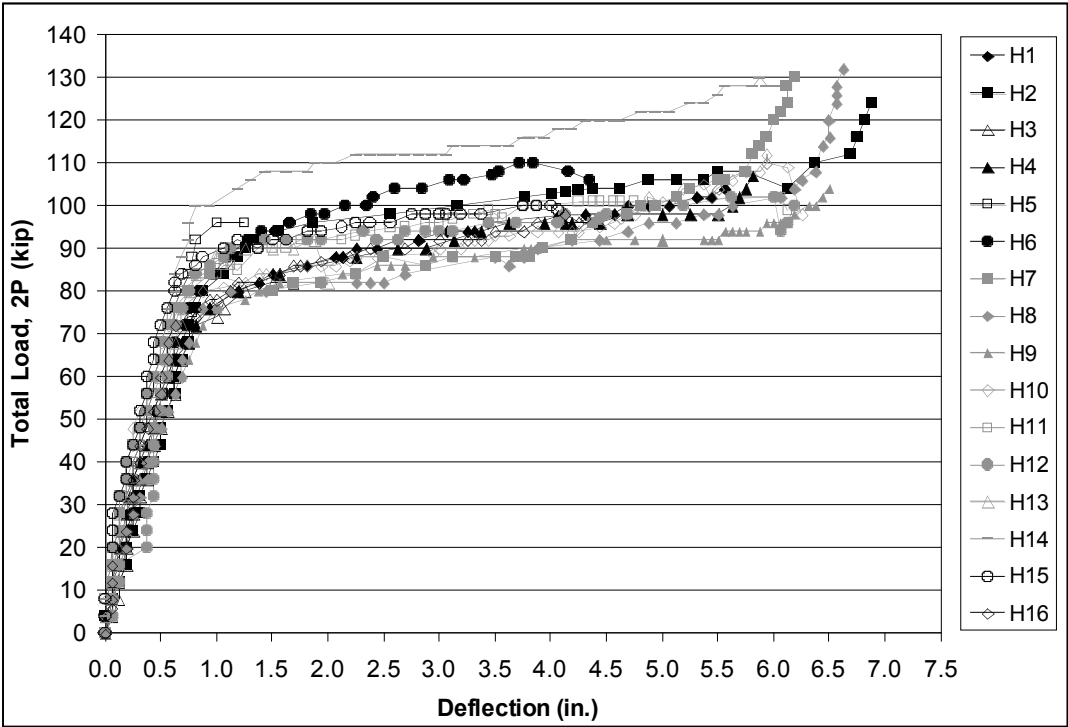


**Figure 8.2: Load versus Deflection Curves**

Maximum mid-span deflections were increased as a result of the retrofit methods. When compared with the best performing control beam, H16, the shear bar retrofit had

the greatest percent increase in mid-span deflection with a cumulative average of just over 47%. In comparison, the CFRP retrofit increased mid-span deflections over 31% and only two of the three sprayed epoxy retrofitted beams increased mid-span deflection. Table 8.4 lists the maximum deflection values, percent increase in mid-span deflection of the retrofitted beams, and the measured residual deflection after load removal.

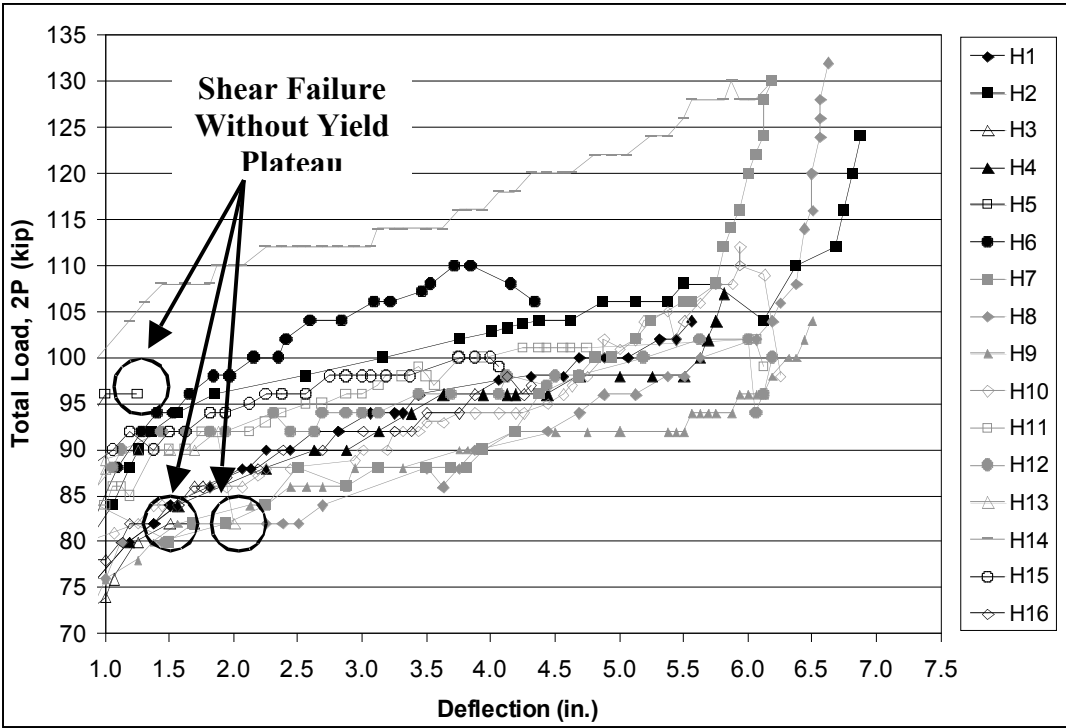


**Figure 8.3: Enlarged View of Load versus Deflection Curves**

Results from Table 8.4 indicate that the CFRP and shear bar retrofit methods significantly increase beam deflection at failure. In addition, these methods produce ductile behavior. Conversely, the sprayed epoxy retrofit method for the thickness

coating used, was determined to be unreliable in preventing shear failure prior to yielding.

**Table 8.4: Maximum Mid-Span Deflections**

<b>Beam</b>	<b>Maximum Deflection (in.)</b>	<b>Percent Increase in Deflection (%)</b>	<b>Residual Deflection (in.)</b>
H1	5.56	29%	0.81
H2	6.88	60%	1.13
H3	1.69	-	-
H4	5.81	35%	1.06
H5	1.25	-	-
H6	4.34	1%	0.87
H7	6.19	44%	0.81
H8	6.63	54%	0.88
H9	6.50	51%	1.06
H10	6.25	45%	0.94
H11	6.13	42%	1.00
H12	6.19	44%	1.00
H13	2.00	-54%	-
H14	6.19	44%	1.31
H15	4.06	-	-
H16	4.31	-	-

### 8.3.2 Load Capacity and Failure Modes

An increase in load capacity, 2P, was observed for all but one of the retrofitted beams when compared with the control beams. The total load capacity, 2P, at failure for each of the beams is listed in Table 8.5. In addition, the percent increase when compared with the control beam, H15, which experienced the largest ultimate load, is also shown. Of the retrofitted beams, only beam H13, retrofitted with the sprayed epoxy coating application, failed at a lower load capacity than the control beam H15.

Beam H1 with vertical CFRP strips obtained a maximum load,  $2P$ , of 104kip at failure with a shear crack forming prior to failure between two adjacent CFRP strips. Though the beam ultimately failed in shear, Figure 8.4 (a), the CFRP strips provided the beam with additional shear resistance to support more load and provide sufficient ductility prior to failure. A composite failure shown in Figure 8.4 (b) between the CFRP strip and the beam concrete was observed in beam H1.

**Table 8.5: Actual Load Capacity Values**

<b>Beam</b>	<b>Total Load Capacity 2P (kip)</b>	<b>Percent Increase in Load Capacity (%)</b>
H1	104.0	4%
H2	124.0	24%
H3	82.0	Control Beam
H4	107.0	7%
H5	96.0	Control Beam
H6	110.0	10%
H7	130.0	30%
H8	132.0	32%
H9	104.0	4%
H10	112.0	12%
H11	102.0	2%
H12	102.0	2%
H13	92.0	-8%
H14	130.0	30%
H15	100.0	Control Beam
H16	98.0	Control Beam

However, a ductile behavior was more obvious in beam H4. The formation of a shear crack was observed intercepted by two adjacent vertical CFRP strips in beam H4, preventing further shear crack development, Figure 8.4 (c). Ultimately the beam failed

in flexure as a result of concrete crushing in the compression zone between the two load applicators. This failure is shown in Figure 8.4 (d). Beam H4 reached a maximum 2P load of 107-kip.

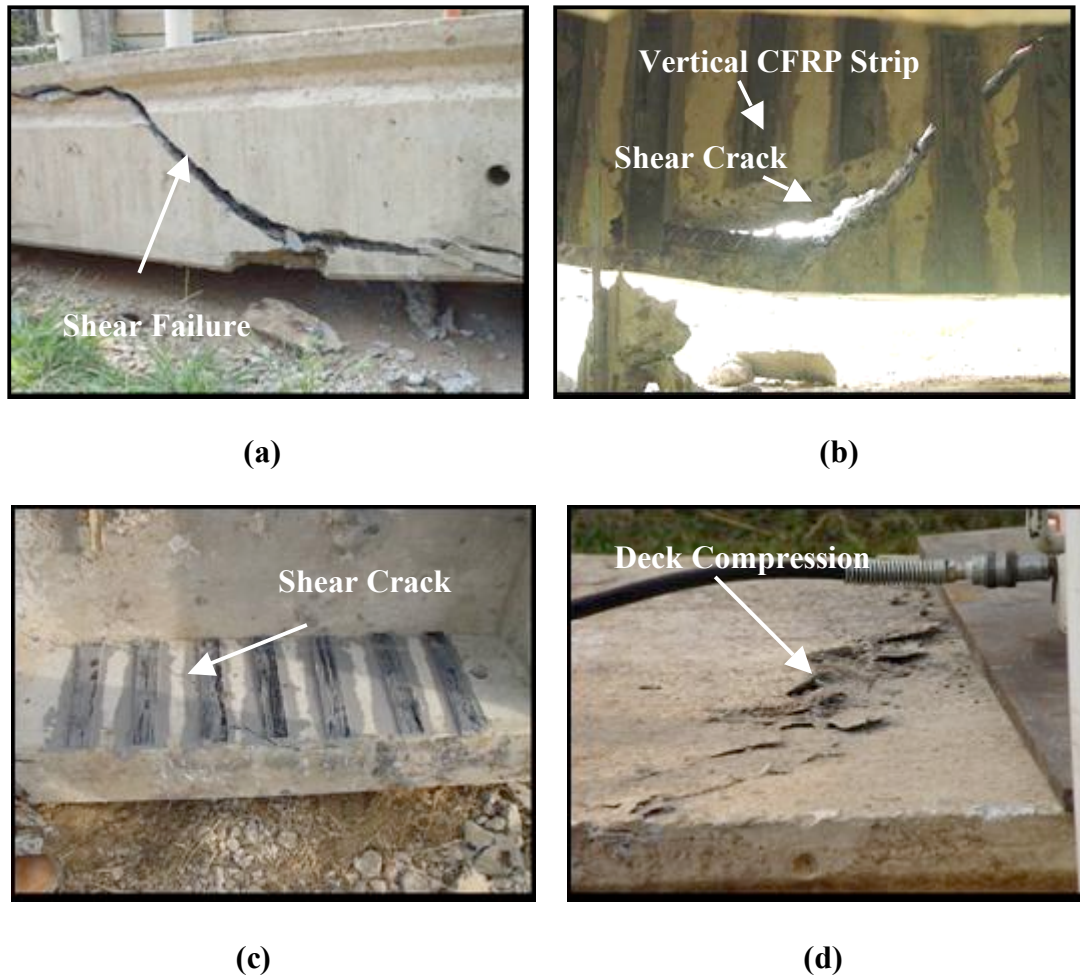


**Figure 8.4: Vertical CFRP Retrofitted Beams at Failure**

Beam H2 retrofitted with diagonal CFRP strips was extremely ductile with a total load, 2P, of 124-kip and nearly 7-in deflection. A flexure-shear crack, Figure 8.5 (a), developed approximately 5.5-ft from the beam end. The crack was restrained as it

passed through a CFRP strip as shown in Figure 8.5 (b). Beam H6 experienced less ductility than other retrofitted beams with a mid-span deflection of 4.34in; however, had a maximum load capacity,  $2P$ , of 110-kip. Beam H6 failed in shear due to debonding between the CFRP strips and the concrete surface, Figure 8.5 (c) and (d).

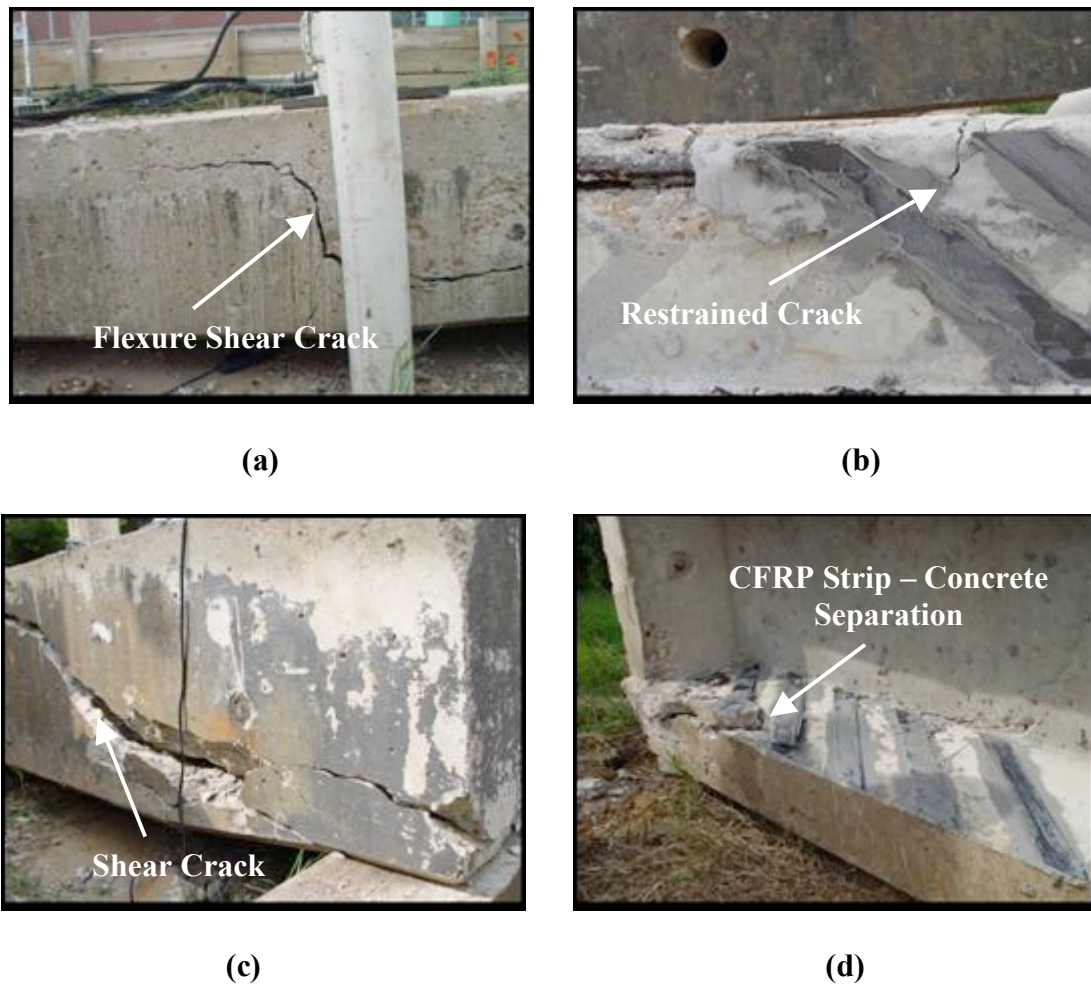


**Figure 8.5: Diagonal CFRP Retrofitted Beams at Failure**

The MMFX shear bar retrofitted beams outperformed the other retrofit methods in both load capacity and mid-span deflections. The behavior between shear bar

retrofitted beams was similar. Beams H7, H8, and H14 obtained similar maximum loads,  $2P$ , of 130-kip, 132-kip and 130-kip respectively. Similar ductile behavior was observed in the three beams with each ultimately failing in flexure. Shear bar retrofitted beams H9 and H12 failed at lower load capacities of 104-kip and 102-kip respectively; however, mid-span deflections were equal or higher than beams H7, H8, and H14. A single hairline shear crack developed in each of the shear bar retrofitted beams; however, was restrained from growth by the internal shear bars, Figure 8.6 (a). Each of the shear bar retrofitted beams exhibited concrete crushing between the two loading points. Compression failure shown in Figure 8.6 (b) was the failure mode for each of the beams.

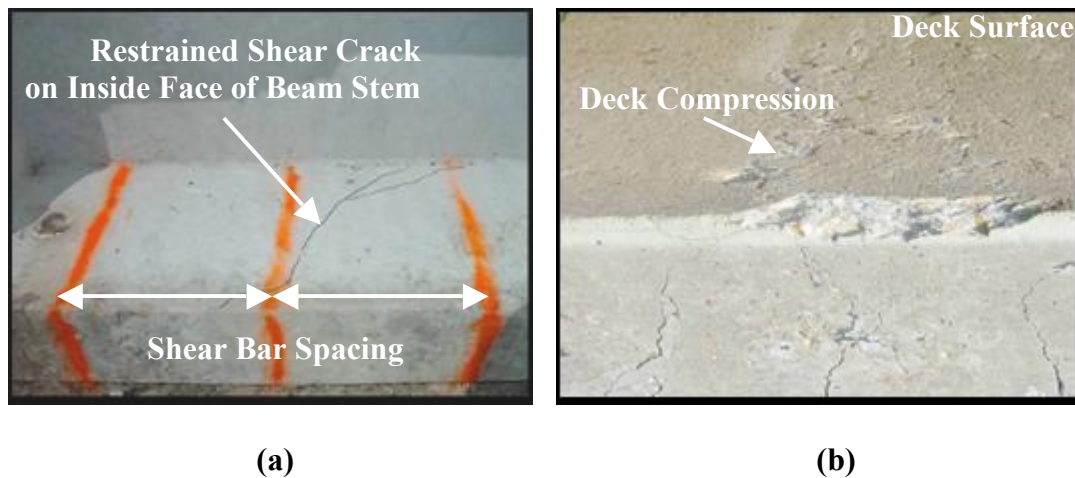
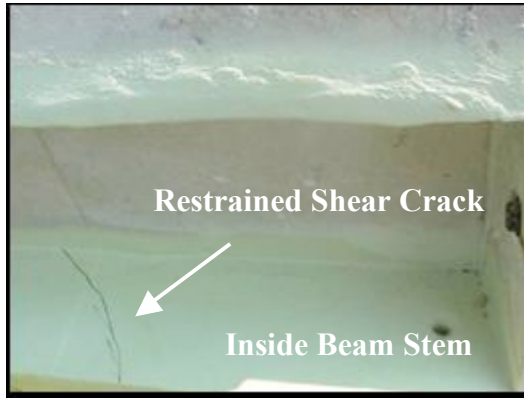


**Figure 8.6: Shear Bar Retrofitted Beams at Failure**

The sprayed epoxy coating method reached load capacities,  $2P$ , in excess of 100-kip. Epoxy coated beams H10 and H11 experienced ductile behavior similar to the CFRP and shear bar retrofit methods. Beam H10 obtained a maximum load capacity,  $2P$ , of

112-kip and a mid-span deflection of 6.25-in. A shear crack shown in Figure 8.7 (a) developed; however, the sprayed epoxy restricted the growth of the crack. The beam ultimately failed in compression due to concrete crushing within the constant moment region between the two loading points. Beam H11 obtained a load capacity of 102-kip with a mid-span deflection of over 6-in. A shear crack never developed, but instead the beam failed in flexure, Figure 8.7 (b). Beam H12 behaved differently than beams H10 and H11. The beam experienced limited ductility with a mid-span deflection of only 2.0in. The maximum load,  $2P$ , of 92-kip was the lowest capacity of any retrofitted beam. At failure, the H12 beam experienced shear failure, Figure 8.7 (c).

The four control beams failed in shear with a maximum load capacity,  $2P$ , of 100-kip (beam H15) and minimum of 82-kip (beam H3). Beams H3 and H5 failed in shear without exhibiting a yield plateau, Figure 8.8 (a). During loading testing small hair-line cracks, as shown in Figure 8.8 (b), developed in the end segment of the beam. As additional load was applied, the cracks became larger until failure. Conversely, beams H15 and H16 experienced distinct yield plateaus prior to failure. Similar to beams H3 and H5, beams H15 and H16 failed in shear.



(a)



(b)



(c)

**Figure 8.7: Sprayed Epoxy Coating Retrofitted Beams at Failure**



(a)



(b)

**Figure 8.8: Control Beams at Failure**

With the exception of beam H13, each retrofit resulted in an increase in load capacity. When compared to the control “un-retrofitted” beam H15, the shear bar retrofit averaged a 19.6% increase in load capacity. This increase in load capacity was considerably larger than the CFRP and sprayed epoxy coating retrofit methods with average increases of 11.25% and 2%, respectively, as compared to the control. For the CFRP application, the percent increase in load capacity was higher for the diagonal oriented CFRP application (10%) in comparison to the vertical (7%).

### 8.3.3 Shear Crack Location for Retrofitted Beams

Shear crack locations were measured for each beam using the same procedure as discussed in Chapter 2. The location measurements and mid-height crack locations are summarized in Table 8.6. Figure 8.9 shows the shear crack locations for the retrofitted beams superimposed on the shear crack histogram from Chapter 2.

Thirteen of the sixteen beams experienced shear cracks within the projected range. Two beams, H2 and H12, developed shear cracks outside this range and a single beam (H11) did not contain shear cracks. Two shear cracks from beam H2 developed closer to the mid-span region than the end of the beam. A shear crack in beam H12 developed outside the projected range; however, was restrained by the internal shear bars.

**Table 8.6: Shear Crack Locations for Hope Beams**

<b>Beam</b>	<b>Bottom Distance (in)</b>	<b>Top Distance (in)</b>	<b>Mid-Height Distance (in)</b>
H1	28	44	36
H2	60	72	66
H2	48	60	54
H3	28	49	38.5
H4	32	57	44.5
H5	28	45	36.5
H6	22	48	35
H7	29	45	37
H8	32	45	38.5
H9	27	38	32.5
H10	36	47	41.5
H11	-	-	-
H12	49	65	57
H13	32	61	46.5
H14	26	47	36.5
H15	34	52	43
H15	31	57	44
H16	38	55	46.5

8.3.4 Structural Response to Cracking

The beam behavior after flexure and shear cracks developed was documented during the structural investigation of the Hope beams. The corresponding loads for each beam at first flexure crack, reinforcing steel yielding, and first shear crack are listed in Table 8.7. The percentage of each load with respect to the ultimate load capacity of the beam is included in the table. Similarly, to summarize deflection behavior, Table 8.8 lists the deflection values for each beam at first flexure crack, reinforcing steel yielding, and first shear crack. The percentage of the maximum deflection value is also listed.

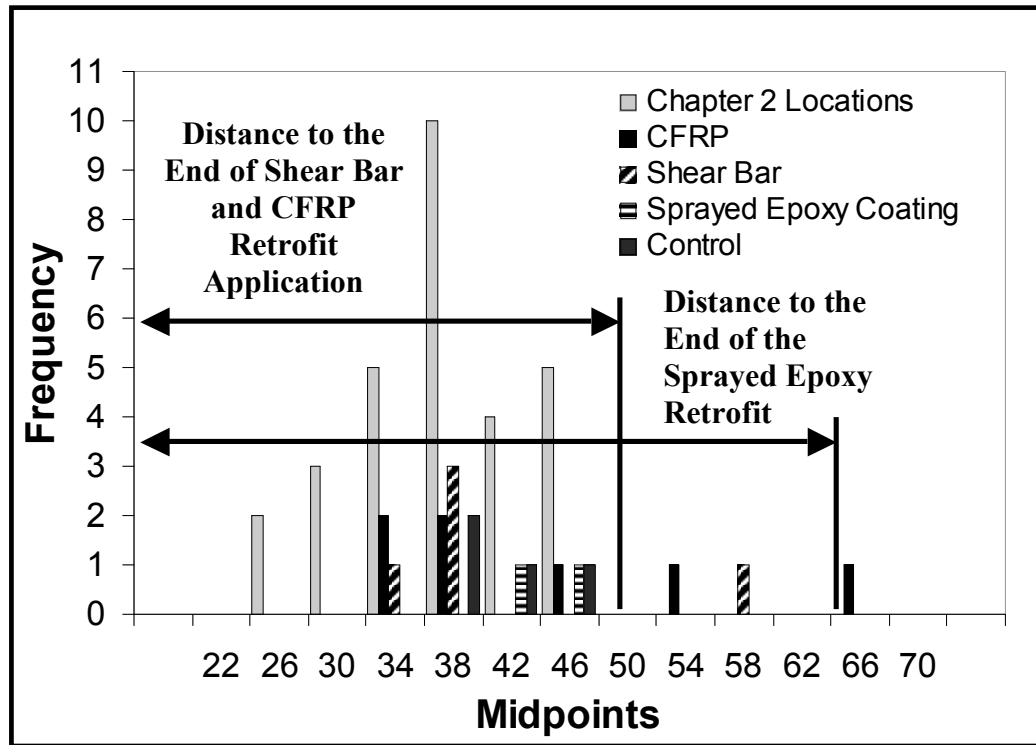


**Figure 8.9: Shear Crack Location Histogram**

Results from the structural response investigation revealed that the retrofitted beams were able to carry additional load and deflection after a shear crack developed. In many cases, over 10% of the beam’s ultimate load capacity was measured after the initiation of a shear crack. In beam H12, a shear crack was not discovered until after beam failure. Further, when compared to the control beams, the retrofitted beams exhibited improved ductile response after a shear crack developed.

**Table 8.7: Load Response to Cracking**

<b>Beam</b>	<b>Load at First Flexure Crack (kip)</b>	<b>Load at Flexural Steel Yielding (kip)</b>	<b>Load at First Shear Crack (kip)</b>	<b>Ultimate Load Capacity 2P (kip)</b>
H1	40.0	76.0	92.0	104.0
Percent of 2P	38.5%	73.1%	88.5%	-
H2	44.0	84.0	80.0	124.0
Percent of 2P	35.5%	67.7%	64.5%	-
H3	52.0	80.0	82.0	82.0
Percent of 2P	63.4%	97.6%	100.0%	-
H4	40.0	76.0	86.0	107.0
Percent of 2P	37.4%	71.0%	80.4%	-
H5	64.0	92.0	96.0	96.0
Percent of 2P	66.7%	95.8%	100.0%	-
H6	Pre-Existing Cracks	84.0	106.0	110.0
Percent of 2P		76.4%	96.4%	-
H7	72.0	84.0	88.0	130.0
Percent of 2P	55.4%	64.6%	67.7%	-
H8	60.0	76.0	76.0	132.0
Percent of 2P	45.5%	57.6%	57.6%	-
H9	48.0	76.0	90.0	104.0
Percent of 2P	46.2%	73.1%	86.5%	-
H10	44.0	80.0	82.0	112.0
Percent of 2P	39.3%	71.4%	73.2%	-
H11	Not Recorded	84.0	No Shear Crack	102.0
Percent of 2P		82.4%		-
H12	44.0	90.0	Discovered After Testing	102.0
Percent of 2P	43.1%	88.2%		-
H13	44.0	88.0	84.0	92.0
Percent of 2P	47.8%	95.7%	91.3%	-
H14	Not Recorded	100.0	100.0	130.0
Percent of 2P		76.9%	76.9%	-
H15	44.0	92.0	98.0	100.0
Percent of 2P	44.0%	92.0%	98.0%	-
H16	Pre-Existing Cracks	82.0	98.0	98.0
Percent of 2P		83.7%	100.0%	-

**Table 8.8: Deflection Response to Cracking**

Beam	Deflection at First Flexure Crack (in)	Deflection at Flexural Steel Yielding (in)	Deflection at First Shear Crack (in)	Maximum Deflection (in)
H1	0.31	0.94	2.81	5.56
Percent of Max	5.6%	16.9%	50.5%	-
H2	0.50	1.06	0.88	6.88
Percent of Max	7.3%	15.4%	12.7%	-
H3	0.56	1.06	1.50	1.69
Percent of Max	33.1%	62.7%	88.8%	-
H4	0.31	0.94	1.88	5.81
Percent of Max	5.3%	16.2%	32.3%	-
H5	0.50	0.81	1.00	1.25
Percent of Max	40.0%	64.8%	80.0%	-
H6	Pre-Existing Cracks	0.97	3.22	4.34
Percent of Max		22.4%	74.2%	-
H7	0.56	0.94	2.50	6.19
Percent of Max	9.0%	15.2%	40.4%	-
H8	0.69	1.00	0.88	6.63
Percent of Max	10.4%	15.1%	13.3%	-
H9	0.50	1.00	3.75	6.50
Percent of Max	7.7%	15.4%	57.7%	-
H10	0.25	0.88	1.25	6.25
Percent of Max	4.0%	14.1%	20.0%	-
H11	Not Recorded	0.85	No Shear Crack	6.13
Percent of Max		13.9%		-
H12	0.44	1.13	Discovered After Testing	6.19
Percent of Max	7.1%	18.3%		-
H13	0.38	1.00	0.81	2.00
Percent of Max	19.0%	50.0%	40.5%	-
H14	Not Recorded	0.94	0.94	6.19
Percent of Max		15.2%	15.2%	-
H15	0.25	1.19	3.38	4.06
Percent of Max	6.2%	29.3%	83.3%	-
H16	Pre-Existing Cracks	1.2	4.1	4.3
Percent of Max		27.6%	95.8%	-

### 8.3.5 Deflection and Energy Ductility

The retrofitted beams experienced a substantial increase in beam ductility manifested by the greater mid-span deflections shown in Table 8.8. To examine this behavior in more detail, the deflection ductility was determined using Equation 8.1 and expressed as the ratio of the maximum deflection value at ultimate load to the deflection at reinforcing steel yielding.

$$\mu_{\Delta} = \frac{\Delta_{ult}}{\Delta_{yield}} \quad \text{Eq. 8.1}$$

where:

$$\begin{aligned} \mu_{\Delta} &= \text{Deflection ductility} \\ \Delta_{ult} &= \text{Deflection at ultimate load} \\ \Delta_{yield} &= \text{Deflection at yielding} \end{aligned}$$

In addition, the energy ductility, defined as the ratio of the area under the load-deflection curve at failure to the area under the curve at yielding, was calculated using Equation 8.2. A retrofit's success was dependent on if its energy ductility was greater than that of the control beams.

$$\mu_E = \frac{E_{ult}}{E_{yield}} \quad \text{Eq. 8.2}$$

where:

$$\begin{aligned} \mu_E &= \text{Energy ductility} \\ E_{ult} &= \text{Area under the load-deflection curve at ultimate} \\ &\text{load} \\ E_{yield} &= \text{Area under the load-deflection curve at yielding} \end{aligned}$$

The ductility and ductility ratios of the retrofitted beams when compared to the control, H16, are summarized in Table 8.9. To demonstrate the significant increase in ductility exhibited by the retrofitted beams, the ratios are plotted in Figure 8.10.

**Table 8.9: Deflection and Energy Ductility**

Beam	Retrofit Method	Deflection Ductility $\mu_{\Delta}$	Deflection Ductility Ratio	Energy Ductility, $\mu_E$	Energy Ductility Ratio
H1	Vertical CFRP	5.91	1.63	10.42	2.00
H2	Diagonal CFRP	6.49	1.79	12.55	2.41
H3	No Retrofit	1.35	0.37	1.56	0.30
H4	Vertical CFRP	6.18	1.71	10.91	2.10
H5	No Retrofit	1.54	0.43	1.97	0.38
H6	Diagonal CFRP	4.47	1.23	8.24	1.58
H7	MMFX Shear Bar	6.58	1.82	10.01	1.93
H8	MMFX Shear Bar	6.63	1.83	12.19	2.34
H9	MMFX Shear Bar	6.50	1.80	11.81	2.27
H10	Sprayed Epoxy	7.09	1.96	11.36	2.18
H11	Sprayed Epoxy	6.96	1.92	11.86	2.28
H12	MMFX Shear Bar	5.48	1.51	9.11	1.75
H13	Sprayed Epoxy	2.00	0.55	2.63	0.51
H14	MMFX Shear Bar	6.59	1.82	11.44	2.20
H15	No Retrofit	3.41	0.94	4.42	0.85
H16	No Retrofit	3.62	1.00	5.2	1.00

The shear bar retrofit increased the structural ductility by at least 151% for deflection and 175% for energy. Similarly, the CFRP retrofit increased ductility by at least 123% for deflection and 153% for energy. Though the ductility increased for two sprayed epoxy coating retrofitted beams, beam H13 was found to be less ductile than the control. Beam H8 retrofitted with the shear bar retrofit had the maximum energy ductility ratio of 234%.

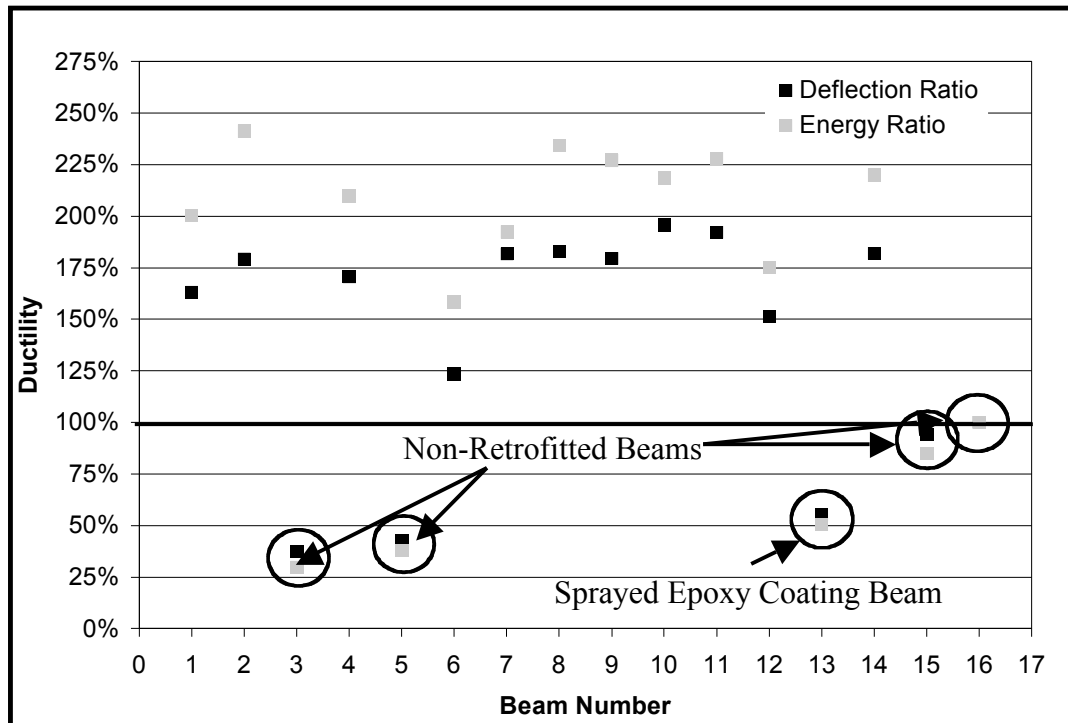


**Figure 8.10: Deflection and Energy Ductility Ratios**

8.3.6 Failure Types

The failure mode for each beam is summarized in Table 8.10. Nine of the twelve retrofitted beams failed in flexure while three ultimately failed in shear. In addition, the four control “un-retrofitted” beams all failed suddenly in shear. Intrinsic failures were observed in the CFRP and sprayed epoxy coating retrofitted beams with respect to the strengthening materials. Each failure type is included in Table 8.10 and discussed in greater detail in the following.

### 8.3.6.1 CFRP Shear Failure

CFRP shear failure occurred between the resin rich top layer and the remaining portion of the strip in beams H1, H4, and H6. In these beams a thin layer of black carbon fiber remained on the epoxy surface. Shear failure of a CFRP strip is shown in Figure 8.11.

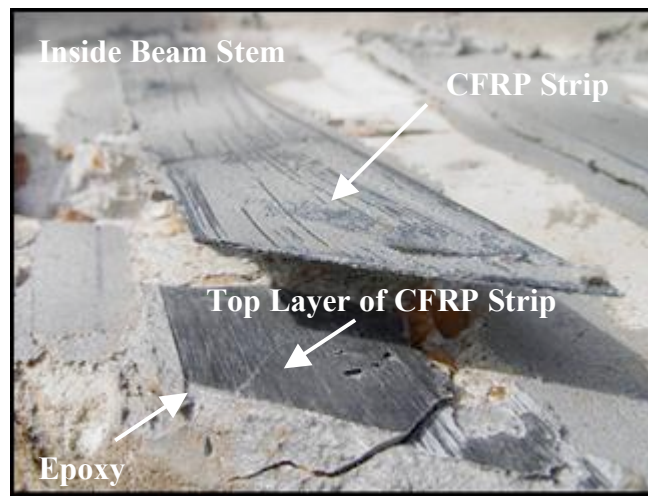


**Figure 8.11: CFRP Shear Failure**

### 8.3.6.2 Epoxy Failure

Epoxy failure was observed in beams H10 and H13. Shown in Figure 8.12, this type of failure resulted in the sprayed epoxy coating cracking. In both beams, H10 and H13, shear cracks in the concrete developed subsequently at the locations of the epoxy failure. After this failure in beam H13, the percent load increase was minimal.

**Table 8.10: Failure Mode and Description**

<b>Beam</b>	<b>Mode of Failure</b>	<b>Description</b>
H1	Shear	CFRP Shear Failure
		Concrete Block Failure
H2	Flexural	Compression Failure in Deck Surface Between Loading Points
		Concrete Bond Failure
		Epoxy-Concrete Separation Failure
		Concrete Block Failure
H3	Shear	Sudden Failure
H4	Flexural	Compression Failure in Deck Surface Between Loading Points
		CFRP Shear Failure
		Concrete Bond Failure
		Concrete Block Failure
H5	Shear	Sudden Failure
H6	Shear	CFRP Shear Failure
		Concrete Bond Failure
		Concrete Block Failure
H7	Flexural	Compression Failure in Deck Surface Between Loading Points
H8	Flexural	Compression Failure in Deck Surface Between Loading Points
H9	Flexural	Compression Failure in Deck Surface Between Loading Points
H10	Flexural	Compression Failure in Deck Surface Between Loading Points
		Epoxy Failure
H11	Flexural	Compression Failure in Deck Surface Between Loading Points
H12	Flexural	Compression Failure in Deck Surface Between Loading Points
H13	Shear	Epoxy Failure
		Concrete Bond Failure
		Epoxy -Concrete Separation Failure
		Concrete Block Failure
H14	Flexural	Compression Failure in Deck Surface Between Loading Points
H15	Shear	Sudden Failure
H16	Shear	Sudden Failure

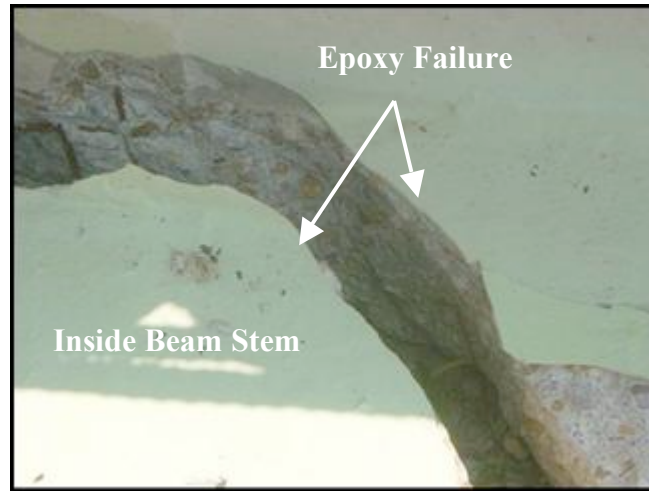


**Figure 8.12: Epoxy Failure**

#### *8.3.6.3 Concrete Bond Failure*

Concrete bond failure at the epoxy-concrete interface was observed in beams H2, H4, H6, and H13. In this case, the epoxy was able to resist the stress better than the concrete at the concrete-epoxy interface; therefore, causing a thin layer of concrete to peel away with the epoxy. In this type of failure, the strength of the CFRP strips and the sprayed epoxy coating are not fully utilized. Concrete bond failure is illustrated for a CFRP retrofitted beam and a sprayed epoxy beam in Figure 8.13 (a) and (b) respectively.

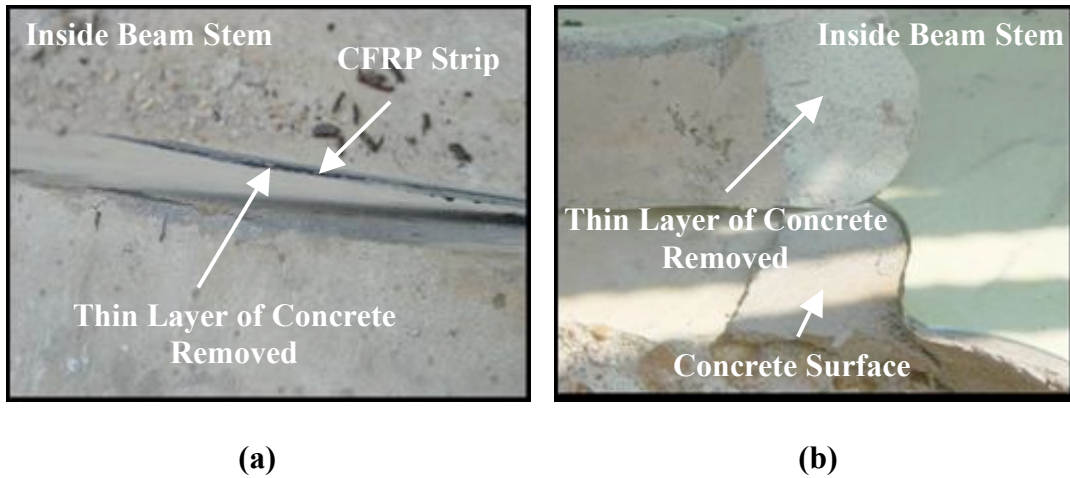


**Figure 8.13: Concrete Bond Failure**

#### *8.3.6.4 Epoxy-Concrete Separation Failure*

Complete separation of the epoxy from the concrete surface occurred in beams H2 and H13. This type of failure resulted when the epoxy debonded from the concrete surface without removing concrete from the beam surface. Epoxy-concrete separation failure is due to improper surface preparation. To prevent this type of failure, additional surface preparation including surface grinding and removal of loose particles is necessary. An epoxy-concrete separation failure is shown in Figure 8.14.

#### *8.3.6.5 Concrete Failure*

Several beams exhibited concrete failure. In this type of failure the concrete failed within the beam stem. Unlike the previous failures, this type was not a result of retrofit material or bond failure. Concrete failure manifests itself as concrete blocks in a CFRP retrofitted beam, Figure 8.15 (a), and in a sprayed epoxy retrofitted beam, Figure 8.15 (b).

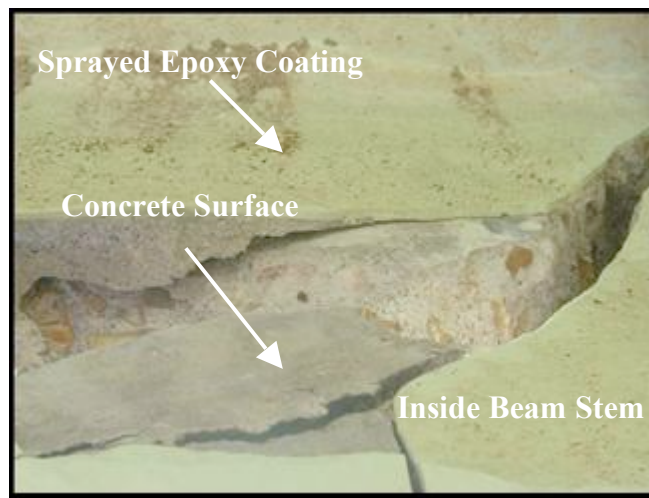


**Figure 8.14: Epoxy-Concrete Separation**

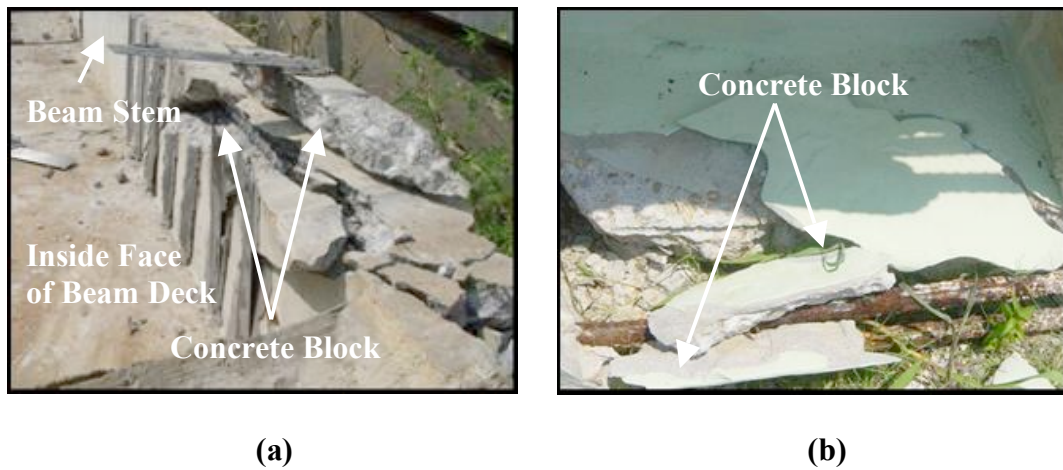


**Figure 8.15: Concrete Block Failure**

## Chapter 9

### Statistical Analysis

The load and deflection data obtained from the experimental testing was statistically analyzed to determine the effectiveness of each retrofit option. The statistical analysis included four treatment options: three retrofit methods and one no retrofit option. This investigation was used to predict the optimal retrofit method for field implementation. The analysis was based on both experimental load capacity and deflection values using the SAS program. In addition to the twelve retrofitted beams, four beams were not retrofitted and used as control specimens in the investigation. The testing matrix for this investigation is shown in Table 9.1.

**Table 9.1: Testing Matrix**

<b>Number of Beams</b>	<b>Retrofit Methods</b>
<b>4</b>	<b>Carbon Fiber-Reinforced Polymer Strips</b>
<b>5</b>	<b>MMFX Shear Bar Application</b>
<b>3</b>	<b>Sprayed Epoxy Coating Application</b>
<b>4</b>	<b>No retrofit Application</b>

A single factor factorial design with fixed effects was selected based on the one factor analysis. A specific number of treatments were chosen resulting in a fixed effects model. The dataset was unbalanced due to missing data. The effects model for this analysis is described using Equation 9.1 [Montgomery, 2001].

$$\text{Model: } y_{ij} = \mu + \tau_i + \varepsilon_{ij} \quad \text{Eq. 9.1}$$

where:  $y_{ij}$  =  $ij$ th observation  
 $\mu$  = overall mean  
 $\tau_i$  =  $i$ th treatment effect  
 $\varepsilon_{ij}$  = random error

The underlying assumptions in this statistical model include: the residual values are normally and independently distributed, a mean equal to zero, and a constant variance.

These assumptions are expressed in Equation 9.2.

$$\varepsilon_{ij} = \text{NID}(0, \sigma^2) \quad \text{Eq. 9.2}$$

where: NID = normally and independently distributed  
0 = mean (assumed to be zero)  
 $\sigma^2$  = variance (assumed to be constant)

After initial data collection, the sample size was investigated to ensure that an adequate number of retrofitted beams were tested to establish a measure of variability. Based on the initial variability, the sample size was found to be inadequate. Therefore, an additional three load tests were conducted to ensure sample size adequacy.

A thorough statistical analysis was performed on the data results obtained through experimental research of the three retrofit methods. The statistical analysis included evaluating the effectiveness of each method when compared to un-retrofitted beams through examination of deflection and load capacity values. Each analysis is discussed in the following.

## **9.1 Statistical Investigation**

The SAS program was utilized in evaluating the effectiveness of each retrofit method. A total of four analyses with two responses was examined, each tested using both a four-treatment and five-treatment evaluation. A five treatment evaluation in which the CFRP retrofit methods were separated by directional strip orientation was analyzed and compared with four treatments where the two CFRP alignment retrofits were grouped together. The treatments examined were: (1) CFRP (vertical), (2) CFRP (diagonal), (3) shear bar, (4) sprayed epoxy, and (5) no retrofit.

Several similarities were found between the four analyses. All analyses were found to be normally distributed as defined by the Shapiro-Wilks test with a constant variance found by examination of the residual plots. Justification of these assumptions validates the analysis of variance. In addition, the Bartlett's test for equality of variance was conducted on the load and deflection results. The variances were found to be equal for the deflection analysis; however, the variances were not equal for the load analysis. Because of this inequality of variances, as well as the practical implications associated with the deflection analysis, more emphasis was placed on the deflection results.

Where significant differences existed, a least square (LS) means test was performed for each to more accurately determine where significant differences exist. An analysis of variance (ANOVA) was performed based on a 95% level of significance ( $\alpha = 0.05$ ). The data was found to be significant when evaluating both load and deflection values.

Significance is experienced when the calculated F statistic is greater than the critical F statistic, and can also be judged based on whether the P-value is less than alpha. The P-value is defined as the smallest level of significance that would lead to rejection of the null hypothesis. A detailed description of each analysis is provided in the following.

### 9.1.1 Deflection Response

#### *9.1.1.1 Five Treatment Levels*

As shown in Table 9.2, the P-value is less than the alpha value of 0.05. A level of significance was found between the retrofit methods and the un-retrofitted beams. To further investigate which methods showed a significant increase in ductility when compared to the control beams the least squares (LS) means test was examined.

The LS means test revealed that the shear bar retrofit had the highest mean value for deflection with 6.34in. and the CFRP-vertical retrofit followed closely with 5.69-in. The control beams had the lowest mean value at 2.83-in. In this analysis, it was found that there was not a significant difference between the two CFRP methods, shear bar, and sprayed epoxy coating retrofits. In addition, there was not a statistical difference between the CFRP-vertical and the CFRP-diagonal retrofits.

**Table 9.2: ANOVA for Five Treatment Levels - Deflection**

**Anova: Single Factor**

SUMMARY

<i>Groups</i>	<i>Count</i>	<i>Sum</i>	<i>Average</i>	<i>Variance</i>
CFRP-Vert	2	11.4	5.69	0.03
CFRP-Dia.	2	11.2	5.61	3.23
Shear Bar	5	31.7	6.34	0.04
Epoxy	3	14.4	4.79	5.86
No Retrofit	4	11.3	2.83	2.49

ANOVA

<i>Source of Variation</i>	<i>SS</i>	<i>df</i>	<i>MS</i>	<i>F</i>	<i>P-value</i>	<i>F crit</i>
Between Groups	29.62	4	7.41	3.60	0.04	3.36
Within Groups	22.61	11	2.06			
Total	52.24	15				

The treatment means for each CFRP retrofit were nearly identical indicating that strip direction had no impact on deflection. There was not a significant difference between the sprayed epoxy coating retrofit and the control. This implies that there is an insignificant increase in ductility when applying the sprayed epoxy; however, significant ductility improvement is shown with the CFRP and shear bar retrofit methods. Table 9.3 lists the treatment means and statistical similarities between treatments.

**Table 9.3 Retrofit Rankings for Deflection with Five Treatment Levels**

<b>Retrofit Method</b>	<b>Rank</b>	<b>Mean Value</b>	<b>Similarity</b>
Shear Bar	1	6.34 in	A
CFRP (Vertical)	2	5.69 in	A
CFRP (Diagonal)	3	5.61 in	A
Sprayed Epoxy	4	4.79 in	AB
No Retrofit	5	2.83 in	B

\*Methods with the same similarity letter are statistically similar.

### 9.1.1.2 Sample Size Verification

The probability of a type II error of the fixed effects model was examined to determine the sample size adequacy used in this research. If the sample size is not statistically adequate, Type II error is expressed as assuming an adequate sample size.

The number of observations,  $n$ , was selected to be five due to the number of tests performed using the shear bar retrofit. The number of beams retrofitted with the shear bar application is larger than the beams used for the other retrofitted approaches due to its lower cost.

To verify sample size, operating characteristics (OC) curves were used to evaluate the probability statement of  $\beta = 1 - P\{\text{Reject } H_0 \mid H_0 \text{ is false}\}$  [Montgomery, 2001]. The OC curves plot the probability of a type II error,  $\beta$ , against the parameter  $\Phi$ , where:

$$\Phi^2 = \frac{n \sum_{i=1}^a \tau_i^2}{a \sigma^2} \quad \text{Eq. 9.3}$$

where:  $\Phi^2$  = Parameter

$n$  = number of observations

$a$  = number of treatments

$\tau$  = average of the individual treatment means

$\sigma^2$  = sample variance

The objective of this study was to develop a retrofit method to provide substantial strength and ductility to beams such that yielding occurs prior to failure. By ensuring

adequate deflection, this objective is validated. For this reason, the sample size adequacy examination for deflection values is the more critical analysis, and was used as the determining criterion. The parameter,  $\Phi$ , was compared with the type II error on a 95% level of significance ( $\alpha = 0.05$ ). The single factor ANOVA provided the sample means and mean square errors needed for determining the parameter,  $\Phi$ , where the mean square error is the best estimate of the sample variance. The ANOVA tables and parameter calculations are included in Appendix F. The results of the sample size adequacy examination are presented in Table 9.4. A power of 0.90 was determined to be sufficient for this experiment based on recommendations found in the reference by Montgomery [Montgomery, 2001].

**Table 9.4: Sample Size Adequacy for Deflection**

<b>Response</b>	<b>Treatment Level</b>	<b><math>\Phi</math></b>	<b><math>\beta</math></b>	<b>Power</b>	<b>Adequacy</b>
Deflection	5	1.89	0.11	0.89	Adequate

The power value was close enough to 0.90 to consider the sample size to be adequate. Thus, it was concluded that a sufficient number of retrofitted beams have been tested based on the probability of a type II error.

### 9.1.1.3 Four Treatment Levels

Because of the adequate sample size with five treatment levels, an analysis with four treatment levels was performed. Using fewer treatment levels increases the degrees of freedom, which ultimately results in a more accurate mean square error. It was further assumed that four treatment levels were sufficient since both CFRP strip orientations resulted in similar deflections.

Table 9.5 identifies the level of significance between the retrofit methods and the un-retrofitted beams. The least squares (LS) means test was used to further determine which methods showed a significant increase in ductility as compared to the control beams.

**Table 9.5: ANOVA for Four Treatment Levels - Deflection**

**Anova: Single Factor**

SUMMARY

<i>Groups</i>	<i>Count</i>	<i>Sum</i>	<i>Average</i>	<i>Variance</i>
CFRP	4	22.6	5.65	1.09
Shear Bar	5	31.7	6.34	0.04
Epoxy	3	14.4	4.79	5.86
No Retrofit	4	11.3	2.83	2.49

ANOVA

<i>Source of Variation</i>	<i>SS</i>	<i>df</i>	<i>MS</i>	<i>F</i>	<i>P-value</i>	<i>F crit</i>
Between Groups	29.62	3	9.87	5.24	0.02	3.49
Within Groups	22.62	12	1.88			
Total	52.24	15				

The highest mean deflection value was experienced by the shear bar retrofit with 6.34-in. The CFRP (vertical & diagonal) retrofits were slightly lower with a mean value of 5.65-in, Table 9.5. The LS means test was used to determine significance between retrofit methods. No significant difference was seen between the shear bar, CFRP, and sprayed epoxy retrofits; however a significant difference was identified when compared to the control. No statistically significant increase in deflection was noted for the sprayed epoxy retrofit when compared to the un-retrofitted beams. Table 9.6 lists the treatment means and statistical similarities for the four treatment level analyses.

**Table 9.6: Retrofit Rankings for Deflection with Four Treatment Levels**

<b>Retrofit Method</b>	<b>Rank</b>	<b>Mean Value</b>	<b>Similarity</b>
Shear Bar	1	6.34 in	A
CFRP	2	5.61 in	A
Sprayed Epoxy	3	4.79 in	AB
No Retrofit	4	2.83 in	B

\*Methods with the same similarity letter are statistically similar.

### 9.1.2 Load Response

#### *9.1.2.1 Five Treatment Levels*

A significant difference was found between the retrofit methods and the un-retrofitted beams based on load capacity. This level of significance is shown in Table 9.7. The least squares (LS) means test was examined to evaluate which methods showed a significant increase in load capacity when compared to the control beams.

The least squares means test revealed that the shear bar retrofit had the highest mean value, 2P, with 119-kip and the CFRP-diagonal retrofit followed closely with 117-kip. The control beams, as expected, had the lowest mean value, 2P, at 94-kip. In this analysis based on load capacity, it was found that there was a significant difference between the retrofit methods and the un-retrofitted beams. However, it was found that the sprayed epoxy coating retrofit and the control were statistically similar as well as the CFRP-vertical and the control. This shows that there was basically no improvement in load capacity using these retrofit methods. Though both the CFRP-vertical and CFRP-diagonal are statistically similar, a trend is evident which indicates a greater improvement in load capacity when using the diagonal orientation. Therefore, in comparing the two CFRP applications, the CFRP diagonal method is better. Table 9.8 lists the treatment means and statistical similarities for the five treatment levels.

**Table 9.7: ANOVA for Five Treatment Levels – Load Capacity**

**Anova: Single Factor**

SUMMARY

<i>Groups</i>	<i>Count</i>	<i>Sum</i>	<i>Average</i>	<i>Variance</i>
CFRP-Vert	2	211	105.5	4.5
CFRP-Dia.	2	234	117.0	98.0
Shear Bar	5	598	119.6	230.8
Epoxy	3	306	102.0	100.0
No Retrofit	4	376	94.0	66.7

ANOVA

<i>Source of Variation</i>	<i>SS</i>	<i>df</i>	<i>MS</i>	<i>F</i>	<i>P-value</i>	<i>F crit</i>
Between Groups	1738.74	4	434.68	3.35	0.05	3.36
Within Groups	1425.70	11	129.61			
Total	3164.44	15				

**Table 9.8: Retrofit Rankings for Load Capacity with Five Treatment Levels**

<b>Retrofit Method</b>	<b>Rank</b>	<b>Mean Value</b>	<b>Similarity</b>
Shear Bar	1	119 kip	A
CFRP (Diagonal)	2	117 kip	A
CFRP (Vertical)	3	105 kip	AB
Sprayed Epoxy	4	102 kip	AB
No Retrofit	5	94 kip	B

\*Methods with the same similarity letter are statistically similar.

#### *9.1.2.2 Sample Size Verification*

The results of the sample size adequacy examination are presented in Table 9.9.

**Table 9.9: Sample Size Adequacy for Load Capacity**

<b>Response</b>	<b>Treatment Level</b>	<b><math>\Phi</math></b>	<b><math>\beta</math></b>	<b>Power</b>	<b>Adequacy</b>
Load	5	1.87	0.11	0.89	Adequate

The power value was determined to be approximately equal to the desired 0.90. Furthermore, it was concluded that a sufficient number of retrofitted beams were tested based on the probability of a type II error for load capacity values.

#### *9.1.2.3 Four Treatment Levels*

Similar to the deflection response, four treatment levels were examined since the sample size was adequate using five treatment levels. A significant difference is noted between the retrofit methods and the control beams in Table 9.10 by the P-value being less than an alpha value of 0.05.

When the CFRP methods were combined, the shear bar retrofits had the highest mean value, 2P, with 119-kip and the CFRP (vertical & diagonal) retrofit was next with 111kips. In this analysis of load capacity, it was determined from the LS means test that there was not a significant difference between the CFRP, shear bar, and sprayed epoxy coating retrofits. It was also found that there was not a significant difference between the CFRP, sprayed epoxy retrofit and the control. This demonstrates that there was no statistically significant improvement in load capacity when applying the CFRP or sprayed epoxy coating retrofits when compared to the control beams. However, improvement in load capacity was observed in the shear bar retrofit when compared to the control. The treatment means and statistical similarities are given in Table 9.11.

**Table 9.10: ANOVA for Four Treatment Levels – Load Capacity**

**Anova: Single Factor**

SUMMARY

<i>Groups</i>	<i>Count</i>	<i>Sum</i>	<i>Average</i>	<i>Variance</i>
CFRP	4	445	111.3	78.3
Shear Bar	5	598	119.6	230.8
Epoxy	3	306	102.0	100.0
No Retrofit	4	376	94.0	66.7

ANOVA

<i>Source of Variation</i>	<i>SS</i>	<i>df</i>	<i>MS</i>	<i>F</i>	<i>P-value</i>	<i>F crit</i>
Between Groups	1606.49	3	535.50	4.12	0.03	3.49
Within Groups	1557.95	12	129.83			
Total	3164.44	15				

**Table 9.11: Retrofit Rankings for Load Capacity with Four Treatment Levels**

<b>Retrofit Method</b>	<b>Rank</b>	<b>Mean Value</b>	<b>Similarity</b>
Shear Bar	1	119 kip	A
CFRP	2	111 kip	AB
Sprayed Epoxy	3	102 kip	AB
No Retrofit	4	94 kip	B

\*Methods with the same similarity letter are statistically similar.

Statistically, there is not a significant difference between the CFRP, shear bar, and sprayed epoxy retrofit methods. In addition, the difference between the CFRP, sprayed epoxy coating and control was insignificant. However, there was a significant difference in comparing the control with the shear bar retrofit method.

## **9.2 Cost Analysis**

Based on strength characteristics, statistically either the CFRP or shear bar method should be used as a shear strength improvement method. Therefore, to decide on the optimal method, other factors must be considered. The major difference between the two retrofit alternatives is material cost. The shear bar retrofit is considerably less expensive than either of the CFRP arrangements or the cost of beam replacement, Table 9.12. In addition, the shear bar retrofit is performed from the deck surface, resulting in a simpler retrofitting method. Excluding traffic control, a two person crew could complete the shear bar retrofit method with relative ease.

Cost data for precast beam placement was provided by the AHTD from a concrete culvert replacement project. The project was at Highway 5 in Bryant, Arkansas, where the failed concrete culvert overpass was replaced with 19-ft precast channel beams. Included in the cost analysis is a \$27.00 per hour labor cost, which includes the cost for manual labor and traffic control. Traffic control equipment was not considered in this cost analysis.

When compared to beam replacement, the CFRP retrofit method provided a cost savings of approximately 33% and 21% for the vertical and diagonal orientations respectively. However, a substantial 80% reduction in cost is achieved when the shear bar retrofit is used instead of beam replacement. Overall cost is reduced with the CFRP and shear bar retrofit methods due to not needing heavy equipment.

**Table 9.12: Cost Comparison per Beam**

Option		Labor Cost \$	Heavy Equipment Cost \$	Material Cost \$	Total Cost \$
Retrofit a Beam	CFRP Vertical Arrangement	760	N.A.	1,120	1,880
	CFRP Diagonal Arrangement	920	N.A.	1,300	2,200
	MMFX Shear Bar	324	N.A.	250	574
Replace a Beam	New Beam	1500	806	1,142	3,448
	Used Beam	1500	806	500	2,806

### 9.3 Summary

From the statistical analysis, several conclusions regarding the effectiveness of the retrofit methods were made.

- The sprayed epoxy coating retrofit was found to be not significantly different than the control “un-retrofitted” beams for both deflection and load effects.
- The CFRP and shear bar retrofits significantly increased the load carrying capacity of the beams when compared to the control beams.
- Although not significantly different, beams retrofitted with the diagonal CFRP strips produced greater load carrying capacities.
- The deflection response was approximately equal for both CFRP strip configurations.
- The CFRP, shear bar, and sprayed epoxy retrofits significantly increased the ductility of the beam in terms of displacement when compared to the control beams.
- The shear bar retrofit produced the highest mean values for load capacity and deflection.
- The shear bar retrofit is the most economical retrofit method.

In summary, the CFRP and shear bar retrofits effectively provided statistically significant increases in terms of load capacity and ductility. Although statistically similar to CFRP, the shear bar retrofit produced the largest load capacity and ductility of the retrofit methods at the lowest cost. Therefore of the investigated retrofit approaches, the shear bar retrofit is considered to be the optimal method.

## Chapter 10

### Field Investigation

Field load tests were conducted on an existing precast concrete channel beam bridge rated by AHTD personnel in poor condition. Bridge #02992 located near Lakeway, Arkansas over the Flat Hollow Branch creek was originally constructed in 1955; however, since initial construction several of the channel beams have been replaced with sections of better condition. Load tests were conducted on the bridge before and after the retrofitting process. Tests included monitoring both concrete and reinforcing steel strains. In addition, beam deflections were recorded. Transverse live load distribution was then calculated based on the measured deflection values. Included in the following is a detailed description of the bridge condition, loading procedure, retrofit scheme, and discussion of results.

#### **10.1 Bridge Description**

The Flat Hollow Branch Bridge is a four span, two lane, precast channel beam bridge located near Lakeway, Arkansas on State Hwy 14. Photographs of the bridge looking east and north are shown in Figures 10.1 and 10.2 respectively. The bridge was categorized by both AHTD personnel and the UA researchers as being in poor condition. A small stream flows beneath the bridge; however, minimal water was present at the time of this investigation.

Each span consisted of five interior channel units and two exterior units. The length of each section was 19 ft–0 in. and the clear distance between the inside portion of the curbs was measured to be 24 ft–0 in. See Figure 10.3.



**Figure 10.1: Flat Hollow Branch Bridge Looking East**



**Figure 10.2: Flat Hollow Branch Bridge Looking North**

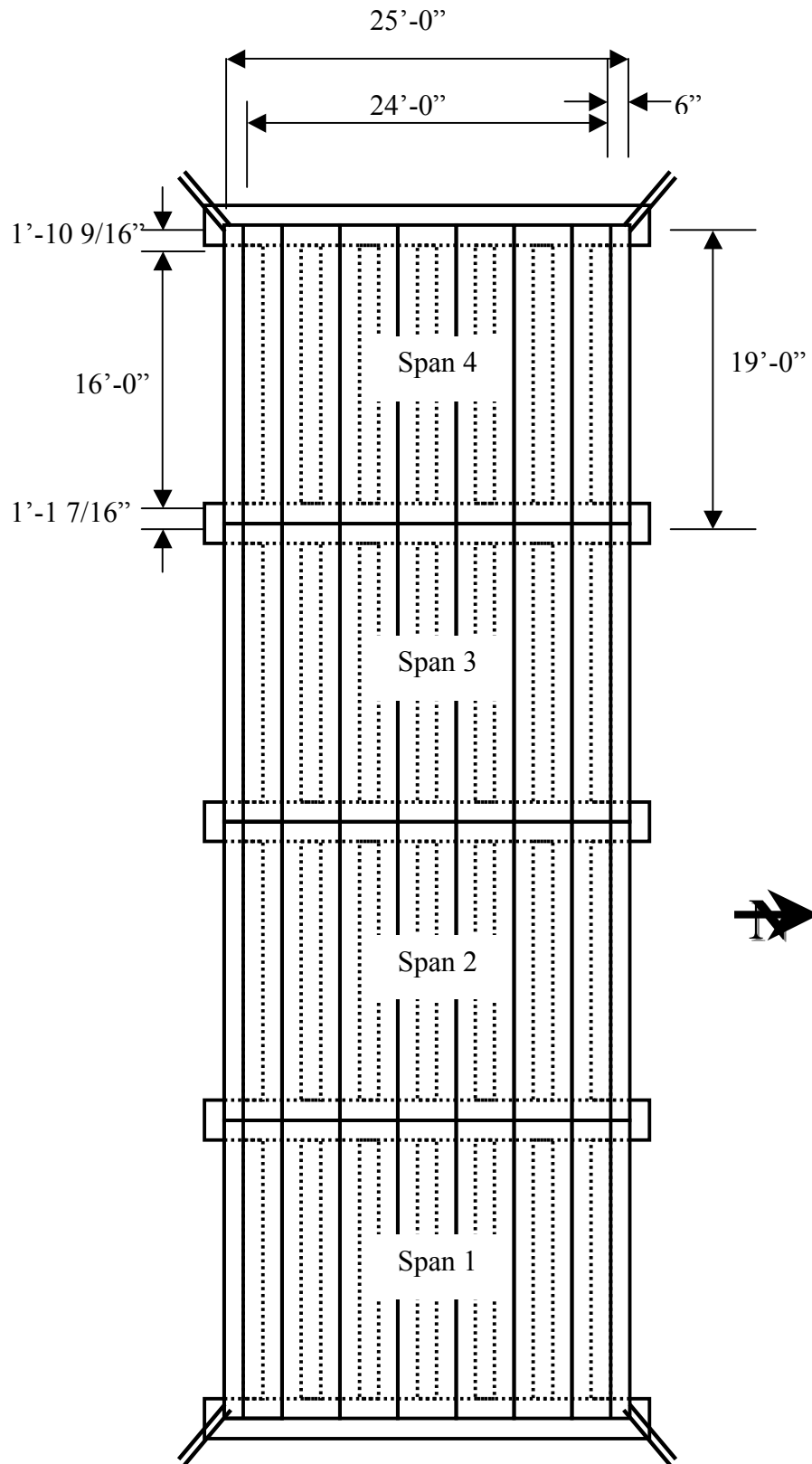


Figure 10.3: Plan View of Flat Hollow Branch Bridge

The beams were bolted to one another in both the longitudinal and transverse directions. The bridge abutments were cast in-place reinforced concrete and the piers consisted of a reinforced concrete cap supported by two rectangular reinforced concrete piles.

Extensive deterioration was observed in 10 of the 28 beams included in the Flat Hollow Branch Bridge. Deterioration included excessive concrete spalling, longitudinal cracking at the flexural reinforcement level, and inadequate flexural reinforcement anchorage. A deteriorated channel beam is pictured in Figure 10.4.



**Figure 10.4: Deteriorated Bridge Beam**

In addition to beam deterioration, the roadway approach to the bridge was lower by as much as 1.5-in at the span 4 bridge – approach joint. This elevation difference is shown in Figure 10.5. This was assumed to have an impact on the dynamic amplification effect on the bridge superstructure.



**Figure 10.5: Bridge Approach**

### **10.2 Retrofitting Deteriorated Panels**

A preliminary investigation of the site revealed ten deteriorated channel beam members in the Flat Hollow Branch Bridge that were in need of strengthening. These beams were classified as Poor Condition due to exposed reinforcement, longitudinal cracking, and inadequate anchorage. Seven of the ten beams were retrofitted using the

shear bar application to determine the suitability of the retrofit technique. The shear bar retrofit was selected for the application due to its superior performance during the laboratory investigation phase of this study and its ease of application. The retrofit process was conducted such that only one lane of the two lane bridge was closed to traffic at a single time. A two person crew drilled holes in the bridge deck at specific locations along the beam. The hole was cleaned and filled with epoxy. Lastly, pre-cut high strength #5 MFX steel reinforcing bars (14-in length) were inserted into each hole. The seven beams retrofitted are shown in Figure 10.6.

### **10.3 Instrumentation**

Concrete and steel reinforcing strains in Span 4 were monitored using electrical resistance strain gauges. Reinforcing steel strain gauges with a two-wire parallel 1.25 in. gauge length and 120-ohm resistance were used. These gauges are appropriate for metal, ceramic, and glass strain measurements. For concrete strain measurements, a single element strain gage consisting of a 2.4-gauge length and 120-ohm resistance was used. Both types of gauges were manufactured by Tokyo Sokki Kenkyujo Company and purchased from Texas Measurements, Inc.

The orientation and location of the strain gauges are shown in Figure 10.7. Multiple gauge configurations were compared. This strain gauge configuration allowed for concrete strains to be monitored in compression and tension zones and near the neutral axis.

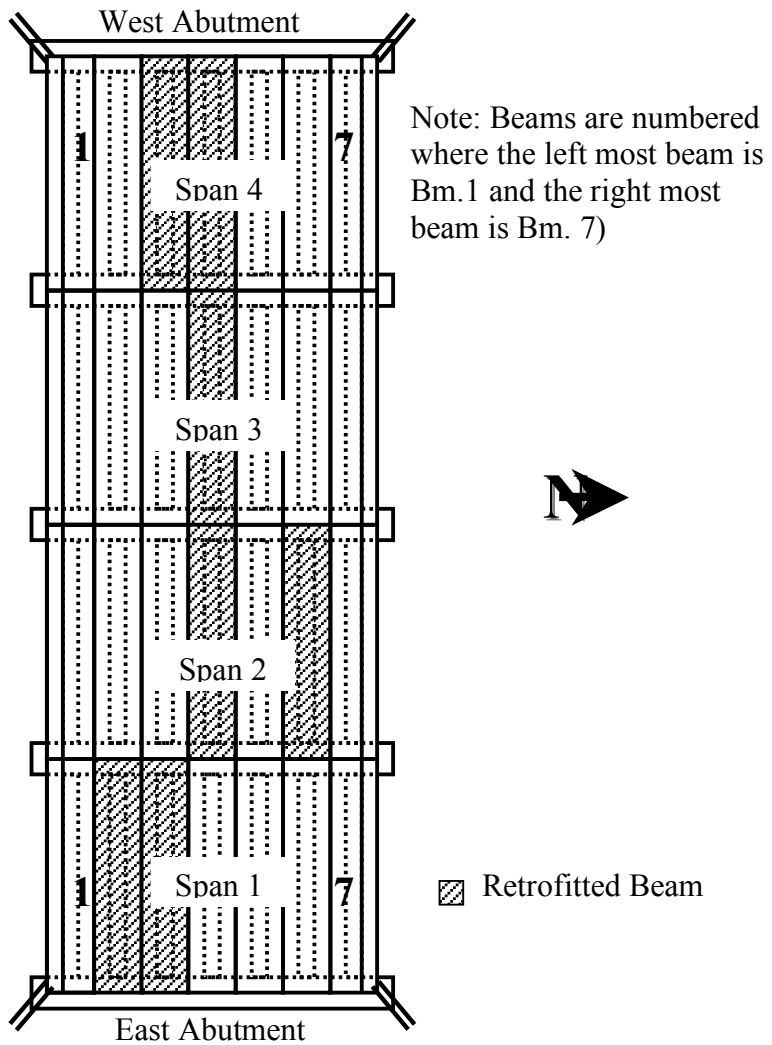


**Figure 10.6: Detail of Beams Retrofitted with Shear Bar Application**

In addition, at mid-span a concrete strain gauge was applied to the beam and two steel strain gauges were placed on the exposed steel reinforcement.

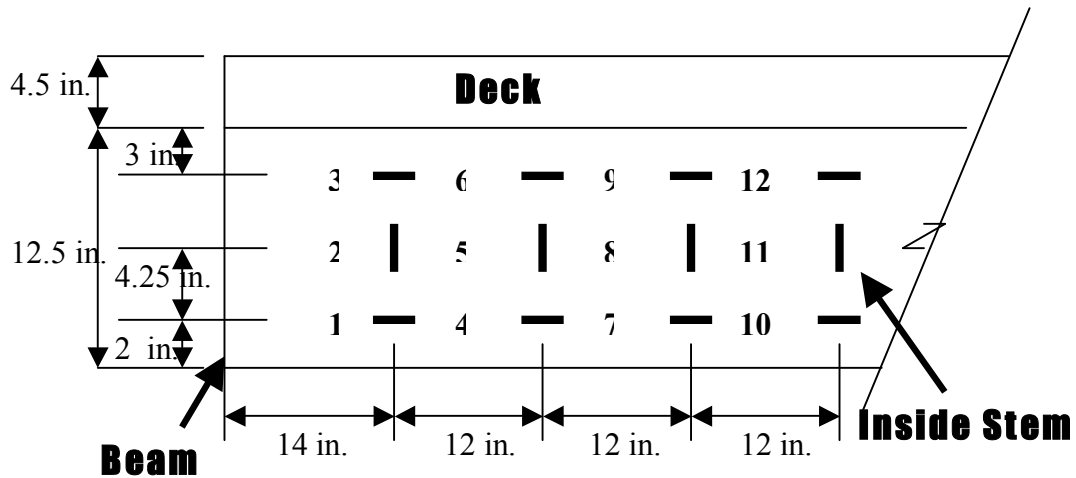


**Figure 10.7: Strain Gauge Location and Orientation**

Prior to application, gauge locations were marked and cleaned to ensure a proper bond at the gauge-concrete surface interface. A two-part epoxy was applied and allowed to cure. The epoxy typically sets within 5 minutes of application.

Reinforcing steel at mid-span was exposed due to concrete spalling. Therefore, concrete removal to expose reinforcing steel at mid-span was not necessary. The first step in applying the strain gauges to the flexural steel reinforcement was to grind the reinforcing steel surface to create a flat, smooth area approximately 0.5-in wide and 1.5-in long. The steel surface was cleaned to remove any dust left from the grinding process and the gauges applied using the same two-part epoxy as used for the concrete strain gauge application.

The strain gauge leads were connected to a 15-channel data acquisition system, Figure 10.8, which was connected to a Gateway E4200 desktop computer, Figure 10.9. This

configuration allowed for both the concrete and steel strain gages to be tested at the same time.

Linear variance displacement transducers (LVDT's) linked to a data acquisition system were used to measure mid-span and quarter-span deflections. The displacement transducers were supported beneath the channel beam stem using camera tripods. This setup configuration is shown in Figure 10.10.

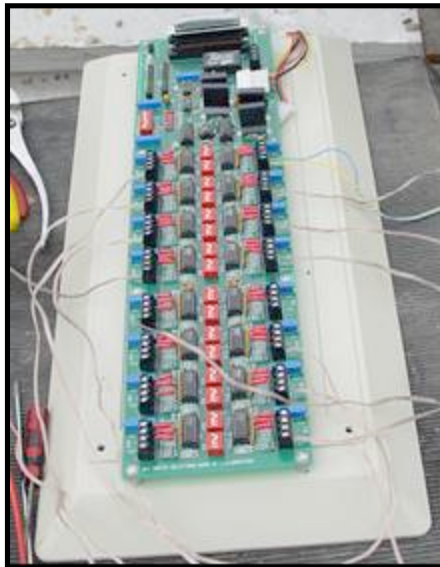


**Figure 10.8: 15-Channel Data Acquisition System**

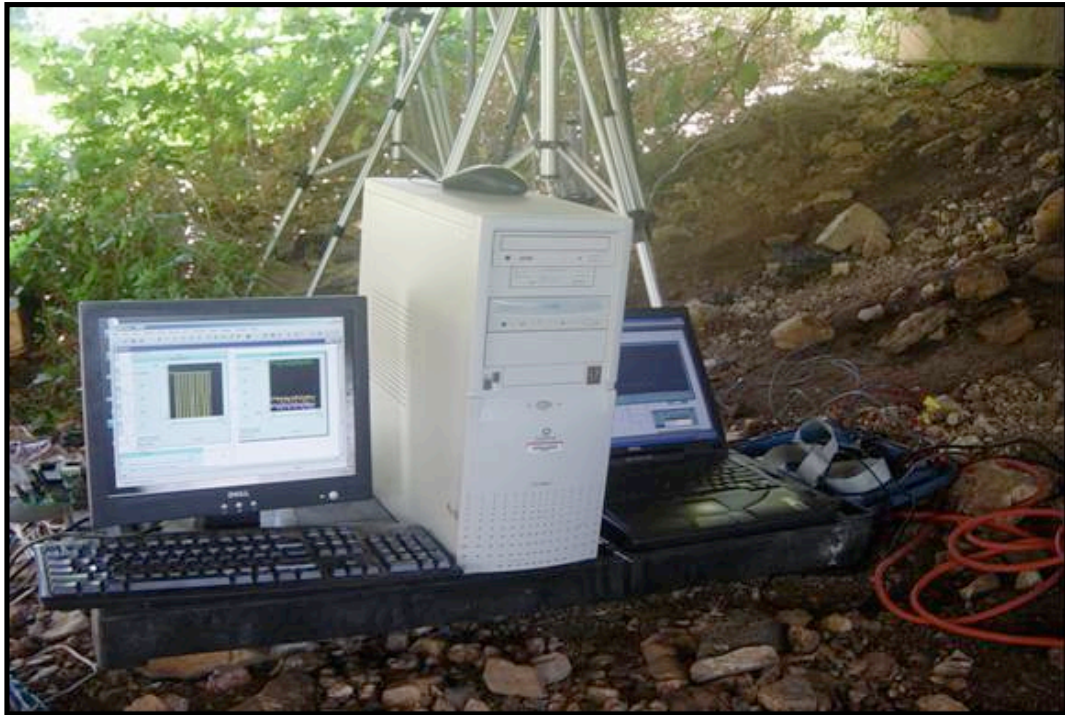


**Figure 10.9: Computers used for Data Collection**



**Figure 10.10: LVDT Setup for Measuring Beam Deflections**

**10.4 Loading Procedure**

A rear single-axle dual tire dump truck was used for the field load tests at the Flat Hollow Branch Bridge. The dump truck was provided and operated by AHTD personnel. Dump truck wheel weights were determined using portable wheel scales supplied by the Arkansas State Police. The research team measured distances between wheels and axle spacing. Wheel loads and configuration are illustrated in Figure 10.11.

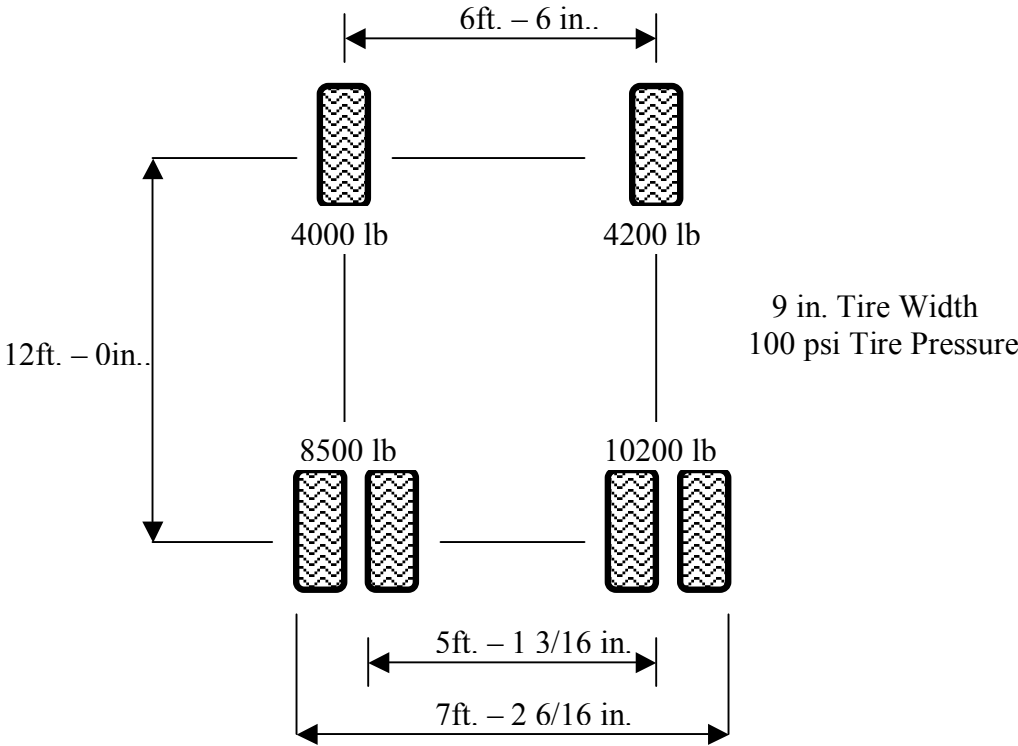


**Figure 10.11: Truck Wheel Configuration**

A series of static and dynamic load tests using the dump truck were performed on the bridge both before and after the retrofitting process. For the static load tests, the truck was positioned such that a pair of rear tires would travel over a single beam.

Care was taken to ensure that the centerline of the wheel line was along the centerline of beam being monitored. Static truck load positions along the beam corresponded to the shear bar retrofit locations within the 5-ft end span region and overall quarter points within the un-retrofitted beam section, Figure 10.12.

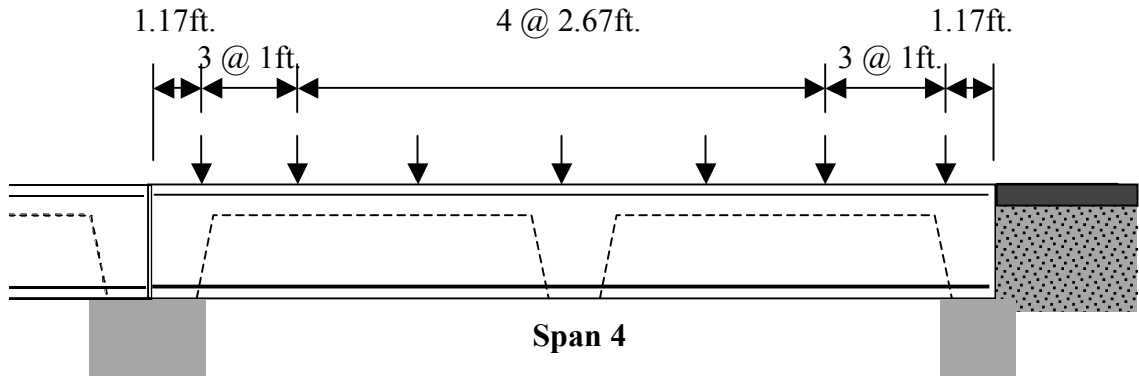


**Figure 10.12: Static Load Positions Along the Length of the Beam**

Dynamic load tests were conducted to determine the impact factor for the beam type used at this bridge. The dynamic load testing consisted of driving the single-axle dump truck across the bridge at varying speeds: creep, 5, 10, 20, 30, 40, and 50-mph. Care was taken to ensure that the truck tires passed over the centerline of the specific beam being evaluated.

A series of static and dynamic load tests were performed for two transverse load positions within the same bridge span. Figure 10.13 shows the loading positions within the cross-section of the bridge and the LVDT locations.

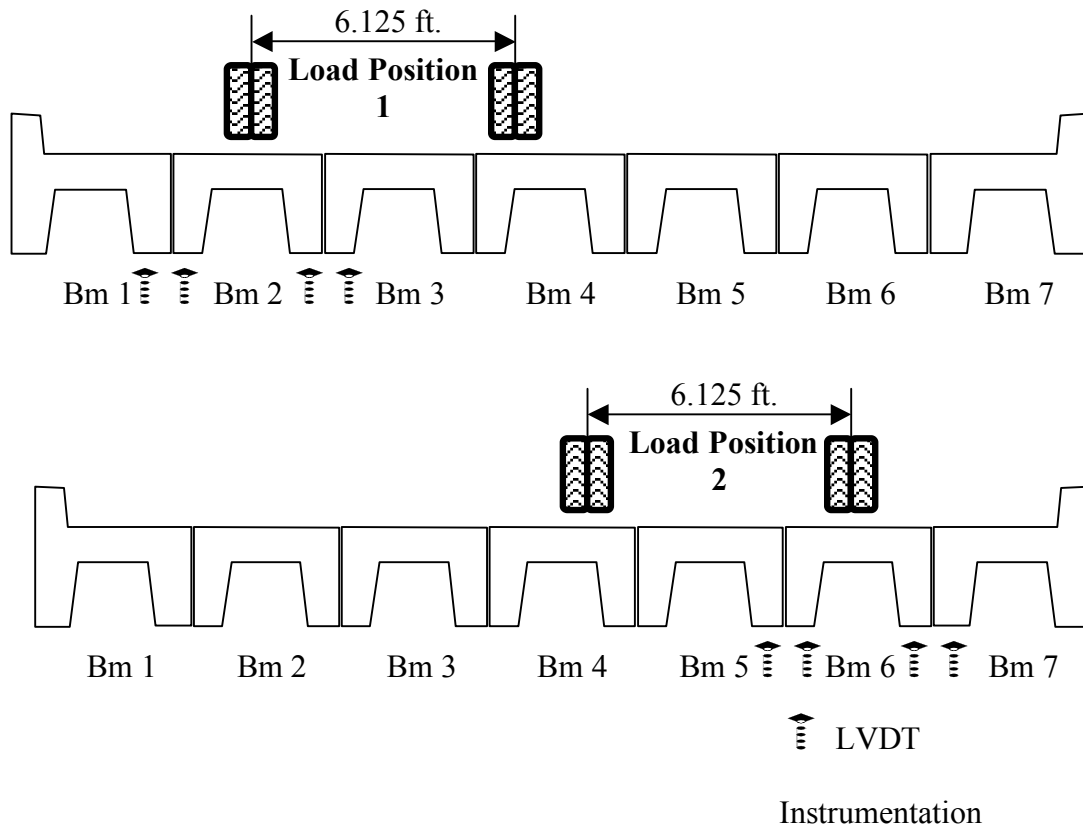


**Figure 10.13: Loading Position and LVDT Instrumentation**

### **10.5 Distribution Factors**

The major objective in the field load testing was to evaluate the effectiveness of the shear bar retrofit and its applicability in a field setting. Additional information was obtained to investigate load distribution between adjacent beams and live load impact factors. This information was collected both before and after the retrofiting process. AASHTO describes the calculation of the distribution factors as a function of beam

geometry, span length and bridge cross-section [AASHTO, 1998]. Distribution factors for a bridge superstructure such as the one being evaluated in this study must meet the following requirements:

- Constant deck width
- Number of beams is not less than four
- Parallel beams having approximately the same stiffness
- The roadway part of the overhang does not exceed 3.0ft.

The bridge evaluated in this field implementation study complies with these requirements. Experimental transverse distribution factors were calculated using Equation 10.1 and the deflection readings from the LVDT's at mid-span and quarter-span of the bridge. It was assumed that the total load of the truck was carried entirely by the two precast channel beams directly underneath the wheel loads and the beam between these two.

$$DF_i = \frac{\Delta_i}{\sum_{j=1}^n \Delta_j} \quad \text{Eq. 10.1}$$

where:  $DF_i$  = Distribution factor for the  $i$ th precast channel beam  
 $\Delta_i$  = Deflection of the  $i$ th precast channel beam  
 $\Delta_j$  = Deflection of the  $j$ th precast channel beam  
 $n$  = Number of precast channel beams (3)

Deflection readings were recorded for both beam stems of the beam under the wheel load and at adjacent stems. For load position 1 shown in Figure 10.13, both stems of Beam 2 and adjacent stems of Beam 1 and Beam 3 were monitored as the wheel load

passed over Beam 2. The two stem deflections for the beam under the wheel load were averaged to give a single beam deflection. This deflection value was assumed to be the same as the beam deflection under the unmeasured rear wheel load.

10.5.1 No Retrofit

Distribution factors as a percentage of rear axle load were calculated for load positions 1 and 2 of span 4 and given as a function of the longitudinal position of the truck.

Table 10.1 lists the distribution factors for beams 2, 3, and 4 for load position 1 at both mid-span and quarter-span.

**Table 10.1: Distribution Factors for Beams 2, 3, and 4 Before Retrofitting**

Position	Distribution Factors			Position	Distribution Factors		
ft.	Beam 2	Beam 3	Beam 4	ft.	Beam 2	Beam 3	Beam 4
1.2	0.46	0.08	0.46	1.2	0.46	0.08	0.46
2.2	0.46	0.10	0.46	2.2	0.46	0.08	0.46
3.2	0.45	0.13	0.45	3.2	0.46	0.08	0.46
4.2	0.45	0.15	0.45	4.2	0.46	0.08	0.46
6.8	0.45	0.17	0.45	6.8	0.46	0.08	0.46
9.5	0.45	0.18	0.45	9.5	0.46	0.08	0.46
12.2	0.45	0.18	0.45	12.2	0.45	0.10	0.45
14.9	0.44	0.14	0.44	14.9	0.43	0.13	0.43
15.9	0.44	0.13	0.44	15.9	0.43	0.15	0.43
16.9	0.43	0.10	0.43	16.9	0.41	0.17	0.41
17.9	0.43	0.07	0.43	17.9	0.40	0.21	0.40

**Mid- Span Distribution Factors**

**Quarter-Span Distribution Factors**

Table 10.2 lists the distribution factors for beams 4, 5, and 6 for load position 2, Figure 10.13, at both mid-span and quarter-span.

**Table 10.2: Distribution Factors for Beams 4, 5, and 6 Before Retrofitting**

Position ft.	Distribution Factors			Position ft.	Distribution Factors		
	Beam 4	Beam 5	Beam 6		Beam 4	Beam 5	Beam 6
1.2	0.38	0.24	0.38	1.2	0.41	0.19	0.41
2.2	0.38	0.24	0.38	2.2	0.40	0.19	0.40
3.2	0.39	0.22	0.39	3.2	0.40	0.19	0.40
4.2	0.40	0.21	0.40	4.2	0.40	0.20	0.40
6.8	0.41	0.18	0.41	6.8	0.40	0.20	0.40
9.5	0.41	0.17	0.41	9.5	0.41	0.18	0.41
12.2	0.42	0.17	0.42	12.2	0.42	0.16	0.42
14.9	0.42	0.17	0.42	14.9	0.43	0.15	0.43
15.9	0.42	0.17	0.42	15.9	0.43	0.14	0.43
16.9	0.42	0.16	0.42	16.9	0.43	0.14	0.43
17.9	0.43	0.15	0.43	17.9	0.43	0.14	0.43

**Mid- Span Distribution Factors**

**Quarter-Span Distribution Factors**

The largest load fractions were observed on the first half of the span when the entire truck was placed on the span and the rear axle was positioned 1.2-ft from the west abutment for loading position 1 and conversely for loading position 2. The maximum load fractions determined experimentally were determined to be 0.46 lanes/bridge for both mid-span and quarter-span during load position 1 and 0.43-lanes/bridge for both mid-span and quarter-span during load position 2. This value is greater than the 0.35 lanes/beam calculated using the AASHTO Bridge Design Specifications [AASHTO, 1998].

Deflection measurements were recorded on three adjacent panels for each load position. This information was useful not only for calculating distribution factors, but evaluating the significance that deterioration, particularly of the steel reinforcement, has on the structural response of the beam. The mid-span and quarter-span deflection measurements used in calculating the distribution factors for load position 1 are shown

in Figure 10.14 and Figure 10.15 respectively. Deflection readings were recorded as a function of the load position longitudinally along the span. As expected, maximum deflections were observed at mid-span loading with deflection readings decreasing as the load position was moved to the outer region of the span.

Deflection measurements during load position 1 were slightly different between the two stems of beam 2. The deflection reading for the right stem was 0.013-in greater than the left stem of Beam 2 in Figure 10.13. Several factors contribute to this difference such as beam deterioration, unsymmetrical beam loading, and friction between adjacent beams. The right stem of beam 2 had considerably more concrete spalling and exposed steel reinforcement than the left stem. The deteriorated beam 2 is shown in Figure 10.16.

The mid-span and quarter-span deflection measurements used in calculating the distribution factors for load position 2 are shown in Figure 10.17 and Figure 10.18 respectively. Beam 6 had considerably less deterioration than that of beam 2. Consequently, overall beam deflections were smaller for beams 4, 5, and 6 during load position 2 in comparison to beams 2,3, and 4 during load position 1.

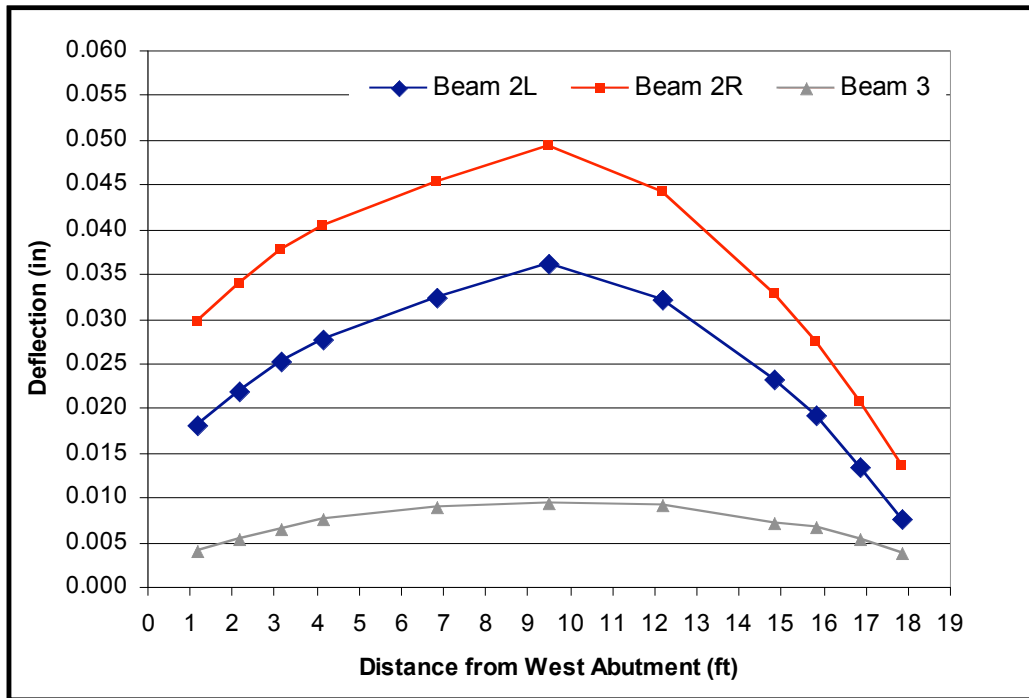


Figure 10.14: Mid-Span Deflection vs. Longitudinal Position for Span 4 [1]

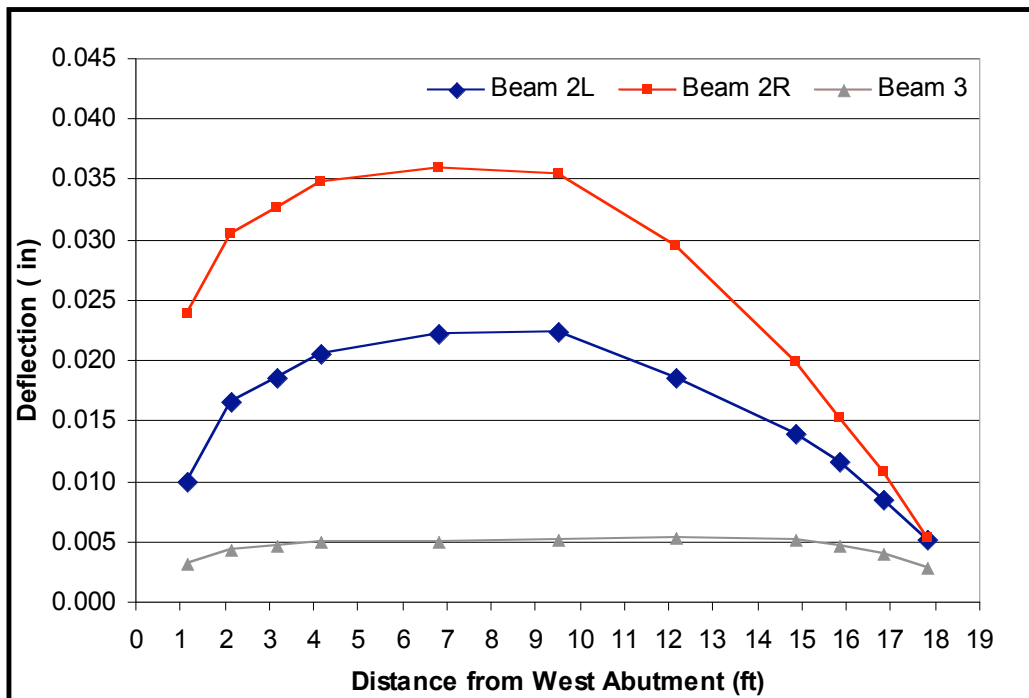
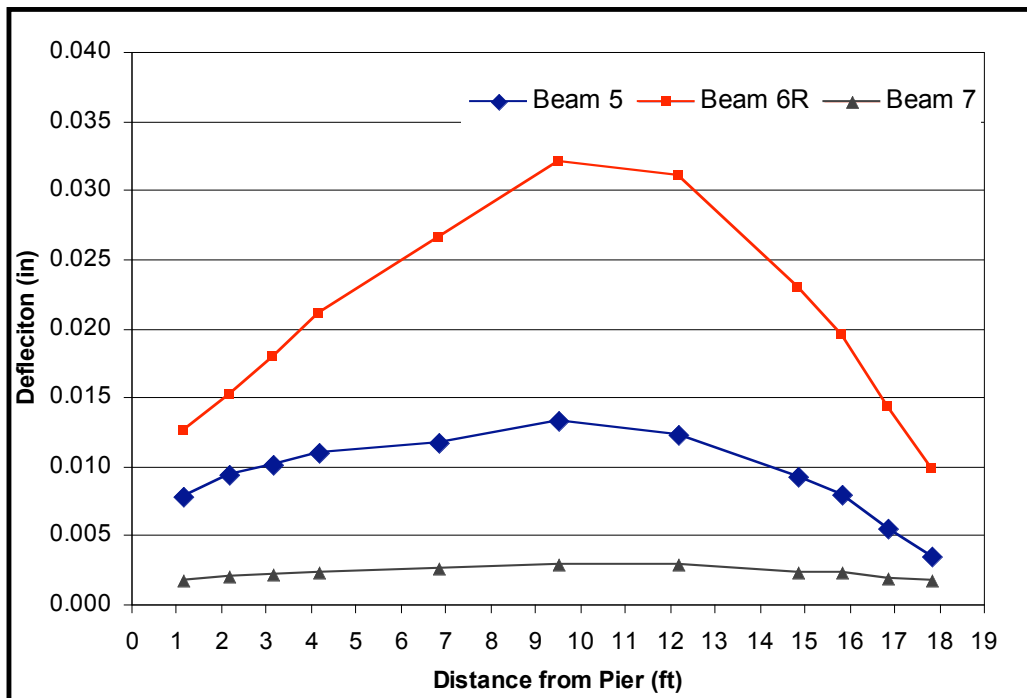


Figure 10.15: Quarter-Span Deflection vs. Longitudinal Position for Span 4 [1]



**Figure 10.16: Beam 2 of Span 4**



**Figure 10.17: Mid-Span Deflection vs. Longitudinal Position for Span 4 [2]**

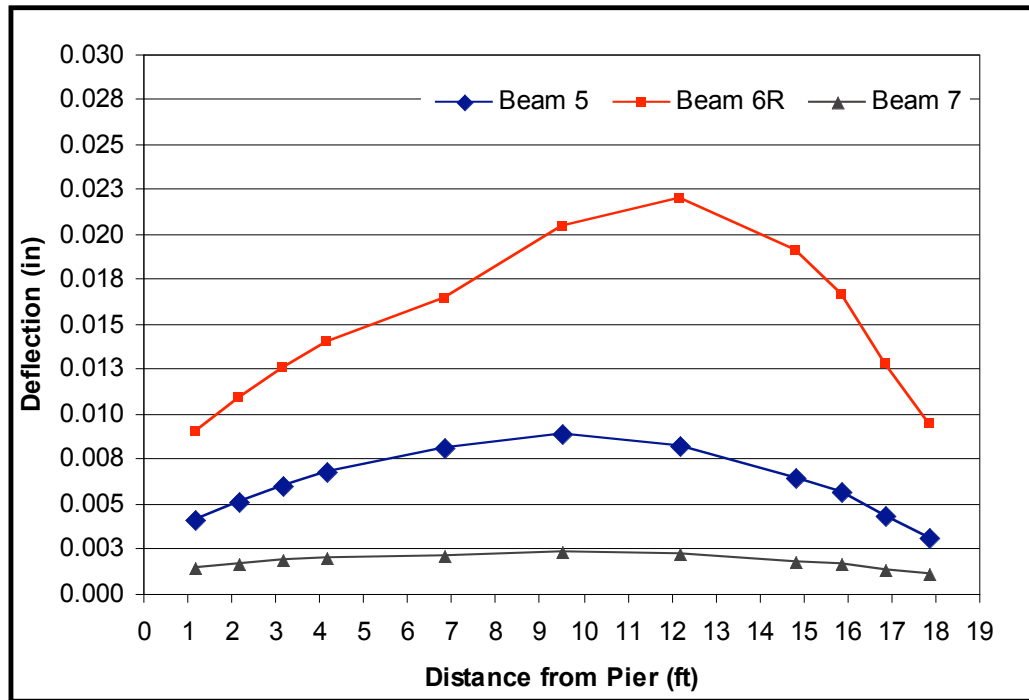


**Figure 10.18: Quarter-Span Deflection vs. Longitudinal Position for Span 4 [2]**

10.5.2 Retrofit

Once the selected beams were retrofitted using the shear bar retrofit approach, the same truck was used to load the beams to evaluate the effectiveness of the retrofit. Beams 2 and 5 were the only beams retrofitted using the shear bar application in span 4. Results from this load case provided information on how the retrofit affects beam stiffness.

Deflection readings decreased as a result of the retrofitting process, Figures 10.19 and 10.20. This is particularly evident in beam 2 as the total average deflection for beam 2 decreased from 0.043-in to 0.035-in.

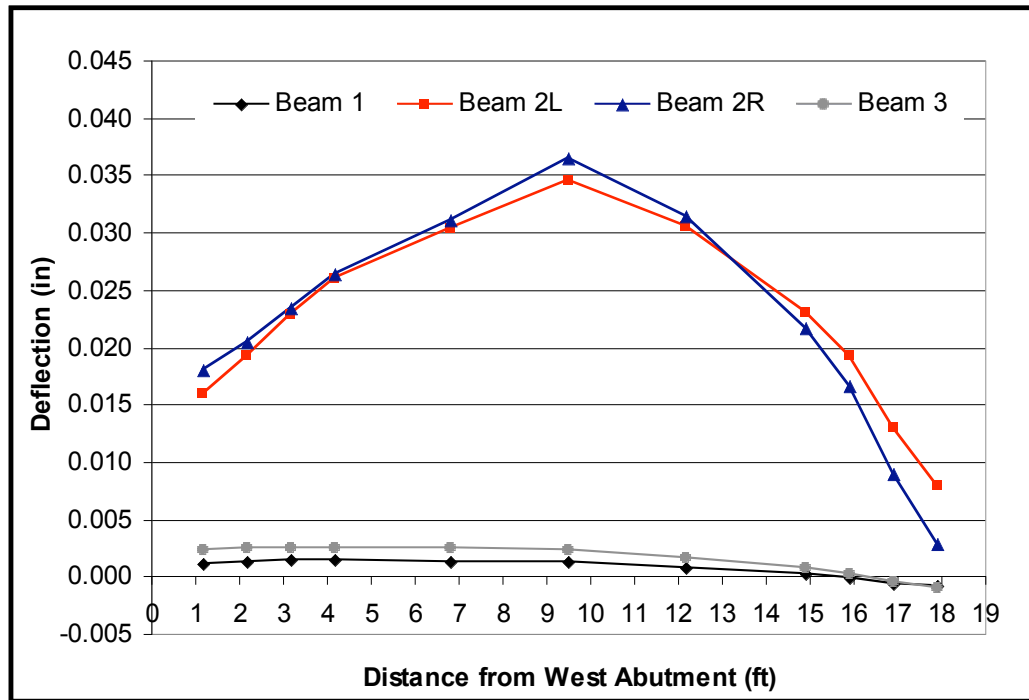


**Figure 10.19: Mid-Span Deflection vs. Longitudinal Position for Span 4 [1]**

The addition of the shear bars to the beam cross-section changes the effective moment of inertia,  $I$ , of the beam. The increase in the moment of inertia due to the retrofit is calculated from the change in the deflection curves. A 20% increase in bending stiffness was calculated based on before and after retrofit deflection readings. In addition, the difference in deflection between the deteriorated stems of beam 2 is considerably less after the retrofit than before the retrofit.

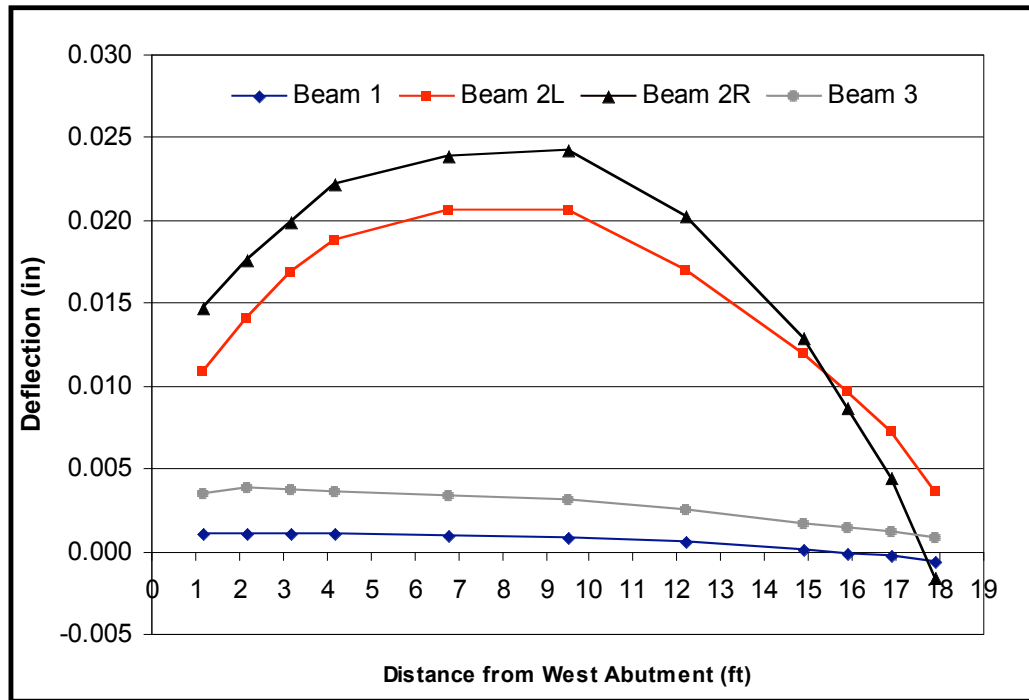


**Figure 10.20: Quarter-Span Deflection vs. Longitudinal Position for Span 4 [1]**

Smaller deflections were also experienced in the retrofitted beam 5. The deflection reading was 0.005-in less than the deflection prior to the retrofit. However, deflection readings of adjacent beams were unchanged due to the stiffening of beam 5. Mid-span and quarter-span deflection readings are shown in Figures 10.21 and 10.22.

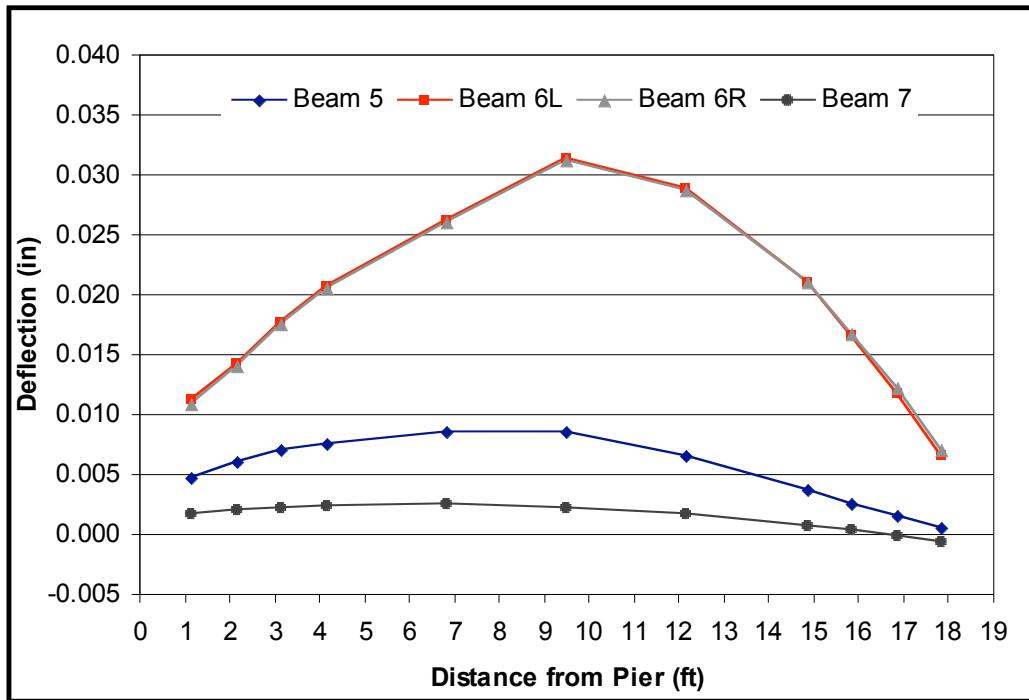


Figure 10.21: Mid-Span Deflection vs. Longitudinal Position for Span 4 [2]

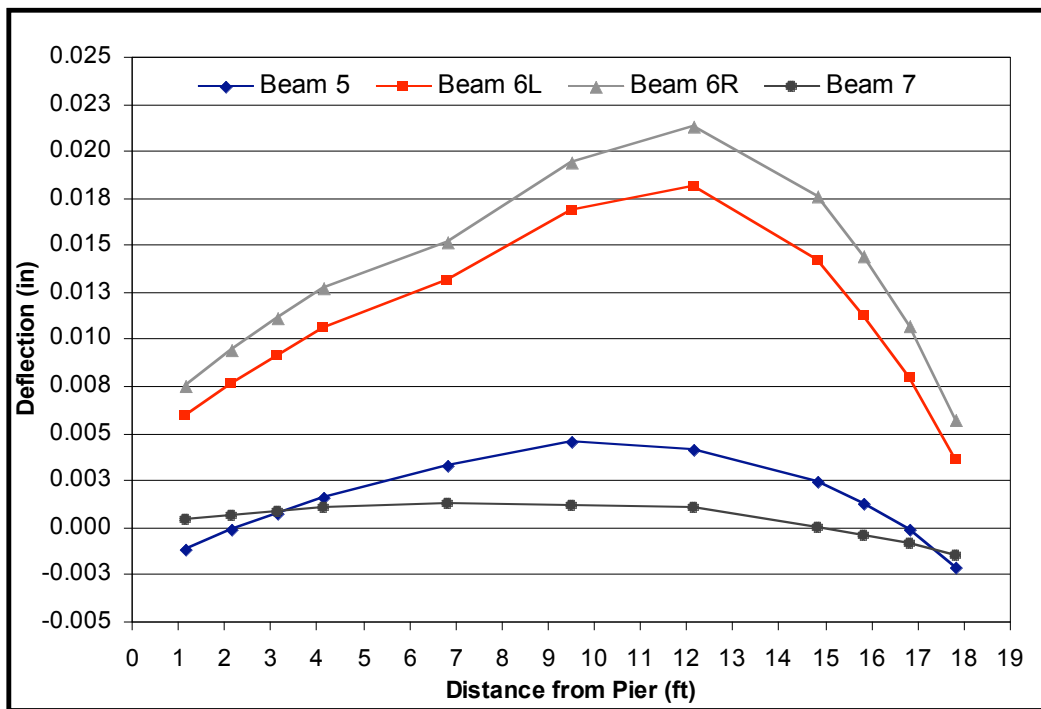


Figure 10.22: Quarter-Span Deflection vs. Longitudinal Position for Span 4 [2]

## **10.6 Impact Factors**

The AASHTO dynamic load allowance, impact factor, is applied to static wheel loads to account for the dynamic influence of a moving vehicle. AASHTO states that these dynamic effects are due to hammering effects and the dynamic response of the bridge as a whole. The hammering effect is the dynamic response caused by discontinuities in the bridge deck surface. Such discontinuities occur at joints, cracks, potholes, and concrete delamination in the deck surface. It can also be due to an uneven transition between the road surface and the bridge. This elevation difference may be caused by settlement of fill beneath the approach roadway surface. The maximum increase for impact specified by AASHTO is 0.33 for bridge beams.

To evaluate the dynamic load allowance factor for this bridge, the fully loaded truck passed over the bridge at varying speeds of 10, 30, and 50 mph. At each speed interval, mid-span deflection was recorded. The impact factor is then determined by the difference between the mid-span static and dynamic deflection. Of particular interest is the slight approach roadway settlement at the west abutment. The same two locations as previously discussed within the cross-section of the bridge were used in evaluating the impact factors; however, the truck traveled in the same direction approaching span 4 from the west for both transverse load positions.

The mid-span deflection values recorded while the truck traveled at 10-mph are similar to that of the static condition. For load position 1, deflection values drastically increased as the truck velocity increased to 50-mph, meaning that the dynamic

response on the bridge is dependent on truck velocity. However, this trend is not seen for load position 2. A decrease in mid-span deflection similar to the static condition is seen with the addition of the shear bar retrofit. Deflection readings recorded for load position 1 before and after retrofitting are shown in Figures 10.23 and 10.24. Similarly, deflection readings are shown for load position 2 in Figures 10.25 and 10.26.

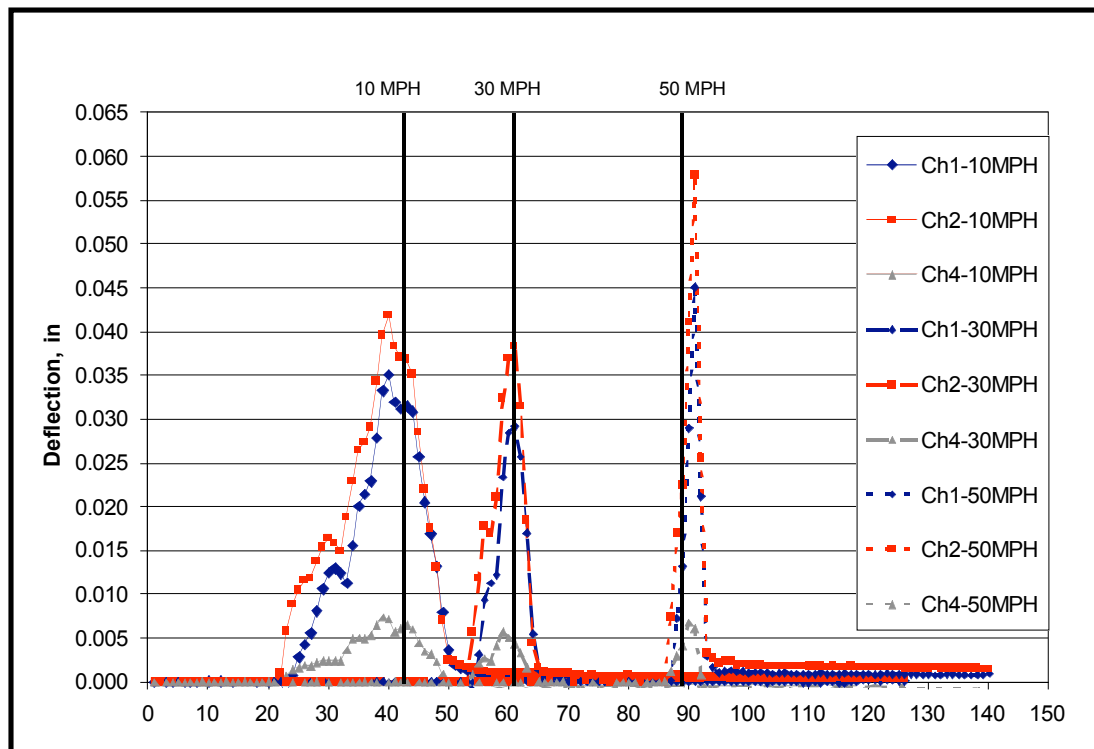


**Figure 10.23: Deflection Measurements for Truck Velocities Before Retrofit [1]**

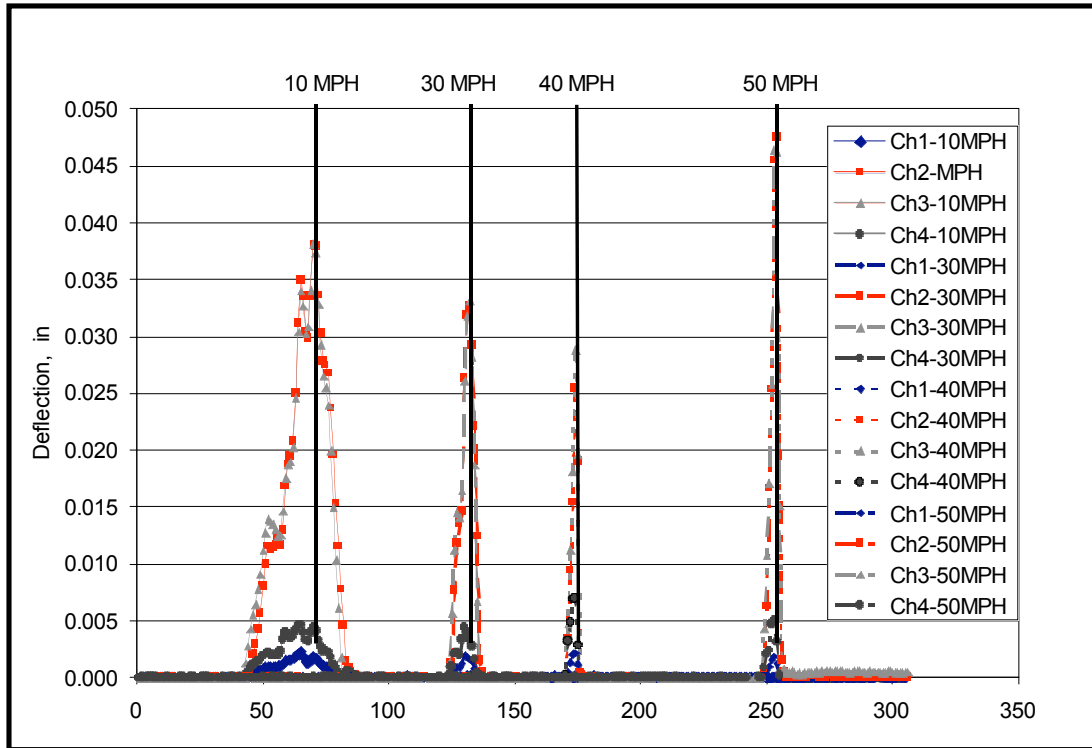


Figure 10.24: Deflection Measurements for Truck Velocities After Retrofit [1]

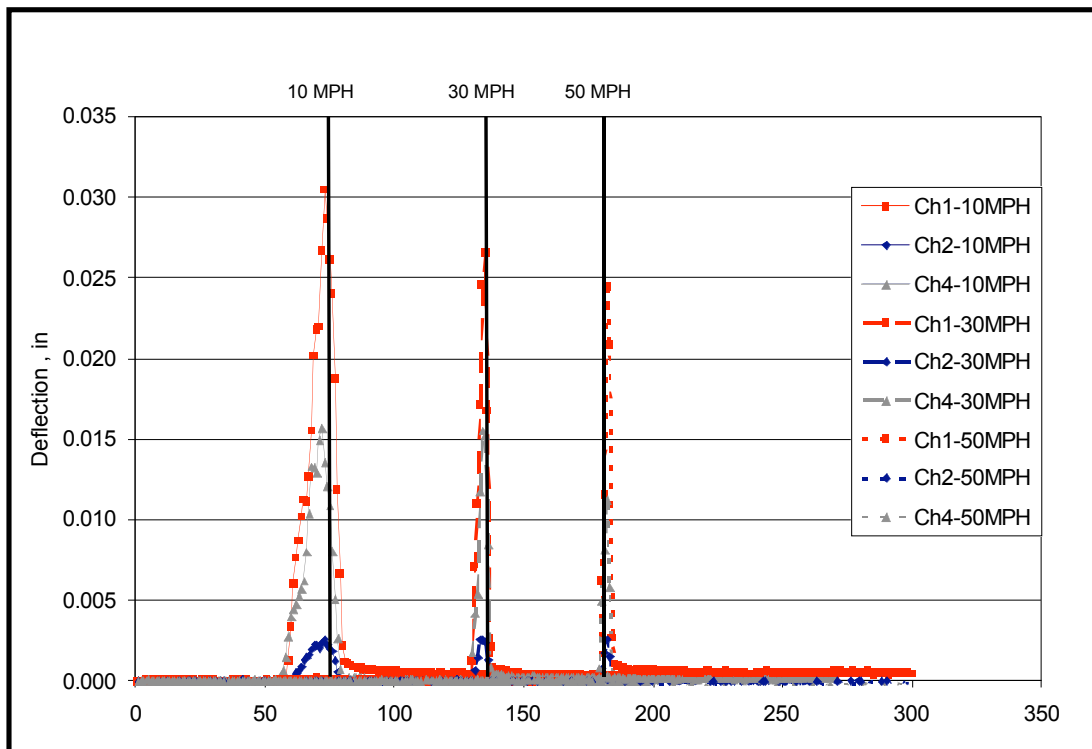
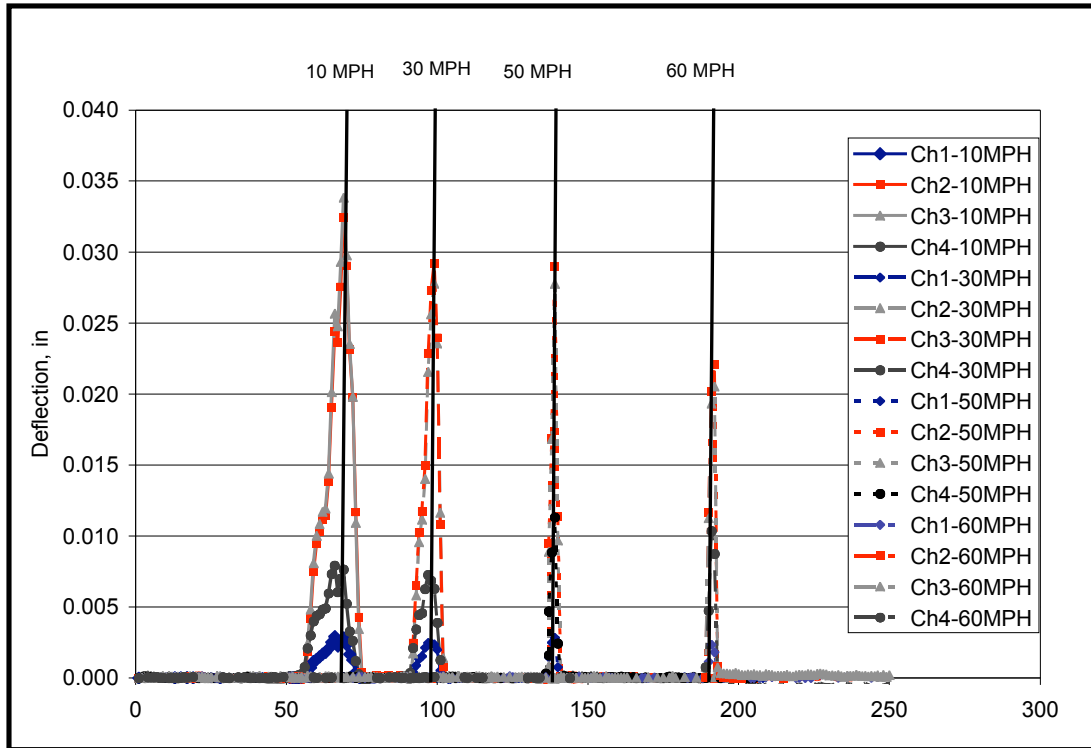


Figure 10.25: Deflection Measurements for Truck Velocities Before Retrofit [2]



**Figure 10.26: Deflection Measurements for Truck Velocities After Retrofit [2]**

The mid-span deflections experienced no amplification under the dynamic loading except at a 50 mph. truck velocity. The field impact factors determined for a truck speed of 50 mph were 1.21 without the retrofit and 1.32 after the retrofit.

For load position 2, none of the beams experienced an increase in deflection regardless of truck speed.

AASHTO states that field tests have indicated that the dynamic component of the response does not exceed 25% in the majority of highway bridges. Of the dynamic

response factors evaluated in this study, only one was found to be greater than this 25% value and none exceeded the 33% limiting AASHTO value.

## Chapter 11

### Summary and Conclusions

#### 11.1 Summary

In this study, a comprehensive investigation has been performed to develop a retrofit method to increase the shear capacity of PCBs designed without shear reinforcement. In addition, the study includes factors initiating beam deterioration. Most notably longitudinal reinforcing steel corrosion and concrete spalling were the major causes for beam deterioration. The primary objectives for this research include:

- Determining the extensiveness of PCB deterioration in Arkansas.
- Evaluating potential causes for longitudinal cracking and reinforcing steel corrosion.
- Evaluating shear strengthening techniques for precast channel beams.
- Develop a cost effective retrofit scheme that is easy to implement in the field.

The research objectives were accomplished in seven main parts.

1. A comprehensive literature review was performed to evaluate possible shear strengthening methods for concrete structures.
2. Thirty-three formerly in-service beams in varying deterioration states were load tested for their structural capacity. In these tests, a shear crack frequency distribution curve was developed to aid in determining adequate retrofit spacing.
3. Potential causes for longitudinal cracking and reinforcing steel corrosion were evaluated. This task included on-site bridge inspections, transverse traffic loading locations, relative humidity, in-situ moisture content, and concrete permeability.

4. The theoretical structural capacity of existing PCBs designed using the 1952 AHTD bridge details was determined. Three retrofit methods were designed based on the required shear improvement required for these beams to force failure in bending rather than in shear. Carbon fiber reinforced polymer strips and a sprayed epoxy coating were each examined as external shear strengthening methods. Conversely, the use of microcomposite multi-structural formable steel, MMFX, reinforcing bars was examined as internal shear reinforcement.
5. Structural load testing of twelve retrofitted beams and four control “un-retrofitted” beams were conducted to determine the effectiveness of each retrofit option.
6. A statistical analysis was used to select the optimal retrofit for field implementation.
7. A poor condition PCB bridge was retrofitted with the selected retrofit method.

## **11.2 Conclusions**

Conclusions made from this research include:

- At least fourteen states have used precast channel beams in their bridge inventory. In addition, eleven of the fourteen are experiencing similar deterioration found in Arkansas.
- Beam deterioration of in-service PCB bridges throughout Arkansas using the 1952 AHTD bridge details is much greater than originally suspected.
- Based on AHTD inspection reports, 28 bridges containing PCBs are in poor condition and therefore in need of shear strengthening.

- On-site UA bridge inspections revealed approximately equal amounts of longitudinal cracking and exposed reinforcing steel in both AHTD classified average and poor PCB bridges. Due to this level of subjectivity in field inspections, an additional 94 bridges having beams in average condition should be considered for shear strengthening.
- Load testing of thirty-three beams concluded that good condition beams were more ductile than poor condition beams. Further, six poor condition beams failed in shear without exhibiting longitudinal reinforcing steel yielding.
- The mid-height of a shear crack will most likely be within the range of 32 to 48in. from the beam end. The shear crack angle was typically less than 45°.
- There is over a 99% probability that a shear crack will develop within 50in. of the beam end.
- Flexure cracking is the result of heavier than initially designed for live loads. Moisture travels between adjacent beams and into flexure cracks causing reinforcing steel corrosion.
- Reinforcing steel corrosion causes longitudinal cracking. This deterioration eventually results in concrete spalling and exposed reinforcing steel.
- Humidity at bridge sites consistently rose above 70%. These humidity levels create ideal conditions for reinforcing steel corrosion.
- With the exception of a single sprayed epoxy coating retrofitted beam, all retrofitted beams increased deflection and energy ductility when compared to un-retrofitted beams.

- Statistically, the sprayed epoxy coating retrofit was found to be not significantly different than un-retrofitted beams.
- The CFRP and shear bar retrofits significantly increased the load carrying capacity of the beams when compared to the control unretrofitted beams.
- Although not statistically different, beams retrofitted with the diagonal CFRP strips produced greater load carrying capacities than using vertical CFRP strips.
- The deflection response was approximately equal for both CFRP strip orientations.
- The shear bar retrofit produced the highest mean values for both load capacity and deflection.
- The shear bar retrofit was selected as the optimal retrofit method based on improved structural behavior, economy, and ease of implementation.
- Excluding traffic control, a two person crew can easily perform the shear bar retrofit application in the field.
- Of the dynamic response factors calculated in the field examination, none exceeded the 33% limiting AASHTO value.

To substantiate the need for a retrofit approach, load testing results in the Phase I study found that the weakest beam, R1, failed at an applied load of  $P = 20k$ . This beam was taken from Jenkins' Ferry. It had been repaired earlier in the field with shotcrete, however was still in poor condition due to spalling and extensive lengths of exposed longitudinal reinforcing steel. This low failure load of  $P = 20k$  exceeds

the live load which the beam was initially designed for, H15 truck loading (16.6k). Although adequate for H15 truck loading, the beam was found inadequate for weight limit posting vehicles. Considering the applied load,  $P = 20$ -kip, the rating factors are 0.620, 0.507, and 0.533 for T3, T4, and T3S2 weight limit posting vehicles respectively [Durham, Heymsfield, and Schemmel, 2003].

Converse to the behavior of beams R1 and RC, both in “poor” condition and taken from the Jenkins’ Ferry Bridge site, the majority of the load tested beams failed at a shear force approximately equal to the beam’s theoretical shear strength ( $V_n$ ). Since no shear reinforcement exists in these beams, the theoretical shear strength is a function of the beam’s concrete compressive strength. This behavior is shown in the Phase I Final Report, Figure 42 [Durham, Heymsfield, and Schemmel, 2003].

A 4-in diameter core taken from the R1 beam had a compressive strength of  $f'_c = 9.216$ -ksi. Based on its theoretical shear strength ( $V_c = 46.08$  k), the beam should have failed at 42.1 kip instead of prematurely failing at  $P = 20$  kip. Therefore, although the beam was adequate for H15 loading, if the beam were strengthened to prevent premature shear failure, higher live loads could be carried.

Consequently, there were two objectives in developing a retrofit for beams in “poor” condition:

- prevent sudden shear failure and instead cause the beam to fail in ductile behavior and

- increase beam load capacity

Of the three retrofit procedures examined, the shear bar retrofit is the recommended method for increasing shear capacity and producing ductile behavior of deteriorated PCBs cast without shear reinforcement. A statistical analysis of results obtained from load testing retrofitted beams along with field implementation of an existing bridge substantiates this recommendation.

## References

- AASHTO (1994). "Manual for Condition Evaluation of Bridges", 2<sup>nd</sup> edition. American Association of State Highway and Transportation Officials, Washington D.C.
- AASHTO (1996). "Standard Specifications for Highway Bridges", 16<sup>th</sup> Edition. American Association of State Highway and Transportation Officials, Washington D.C.
- AASHTO (1998). "LRFD Bridge Design Specifications", 2<sup>nd</sup> edition. American Association of State Highway and Transportation Officials, Washington D.C.
- ACI (2002). "Building Code Requirements for Structural Concrete (318-02) and Commentary (318R-02)," American Concrete Institute, Farmington Hills, Michigan.
- Alkhrdaji, T. (2002). "Strengthening highway bridges with CFRP composites", Concrete Repair Bulletin, Vol. 15, Issue 3, pp 12-17. International Concrete Repair Institute, Des Plaines, Illinois.
- Al-Sulaimani, G., Kaleemullah, M., Basunbul, I., Rasheeduzzafar, (1990) "Influence of Corrosion and Cracking on Bond Behavior and Strength of Reinforced Concrete Members", ACI Structural Journal, Vol. 87, No. 2, March-April 1990. American Concrete Institute, Farmington Hills, Michigan.
- Auyeung, Y., Balaguru, P., Chung, L., (2000). "Bond Behavior of Corroded Reinforcement Bars", ACI Materials Journal, Vol. 97, No. 2, March-April 2000. American Concrete Institute, Farmington Hills, Michigan.
- Banthia, N., Boyd, A. (2000). "Sprayed Fibre-Reinforced Polymers for Repair", Canadian Journal of Civil Engineering, Vol. 27. pp. 907-915, 2000. NRC Research Press.
- Banthia, N., Nandakumar, N., and Boyd, A. (2002). "Sprayed fiber-reinforced polymer: from laboratory to a real Bridge", Concrete International, Vol. 24, Issue 11, pp 47-52. American Concrete Institute, Farmington Hills, Michigan.
- Batchelor, B., Kwun, M., (1981), "Shear in Reinforced Concrete Beams without Web Reinforcement," Proceedings of ASCE Journal of Structural Division, Vol. 107, No. ST5, pp. 907-921.

Bousselham, A., Chaallal, O. "Shear Strengthening Reinforced Concrete Beams with Fiber Reinforced Polymer: Assessment of Influencing Parameters and Required Research" *ACI Structural Journal*. Vol. 101, No. 2. March-April 2004. pp. 219-227. American Concrete Institute, Farmington Hills, Michigan.

Bungey, J., (1993), "Partially Destructive Methods for Assessing the In-Situ Strength of Concrete", *Proceedings of the Institution of Civil Engineers. Structures and Buildings*. Vol. 99, Issue 1., Institution of Civil Engineers. London, UK.

Chaallal, O., Nollet, M., Perraton, D., (1998) "Shear Strengthening of RC Beams by Externally Bonded Side CFRP Strips", *Journal of Composites for Construction*, Vol. 2, No. 2, pp. 111-113. American Society of Civil Engineers. New York.

Czaderski, Christoph. (2000), "Shear Strengthening of Reinforced Concrete With CFRP." 45<sup>th</sup> International SAMPE Symposium. May 21-25, 2000. pp 880-894.

Durham, S., Heymsfield, E., Schemmel, J., (2003). "The Structural Evaluation of Precast Concrete Channel Beams in Bridge Superstructures," *Transportation Research Record*, Vol. 1845, 2003, National Research Council, Washington D.C.

Durham, S., Heymsfield, E., Schemmel, J., Jones, J., (2003). "The Structural Evaluation of Precast Concrete Slab Panels in Bridge Superstructures", AHTD Final Report – TRC 0204, University of Arkansas, Fayetteville, AR.

El-Hacha, R., Rizkalla, S., (2002), "Fundamental Material Properties of MMFX Steel Rebars," North Carolina State University – Constructed Facilities Laboratory, No. 02-04. 2002.

Emmons, Peter H., (1993) Concrete Repair and Maintenance Illustrated. R.S. Means Company, Inc. Kingston, MA. 1993. pp. 7-27.

Emmons, P., Vaysburd, A., Thomas, J., (1998), "Strengthening Concrete Structures, Part I", *Concrete International*, Vol. 20, Issue 3, pp 53-58. American Concrete Institute, Farmington Hills, Michigan.

Federal Highway Administration (1988). "Recording and Coding Guide for the Structure Inventory and appraisal of the Nation's Bridges," Report No. FHWA-ED-89-044, OMB No. 2125. U.S. Department of Transportation.

Hale, W., Kuss, M., (2004) "A New In-Situ Test for Determining the Permeability of Concrete," *Transportation Research Record*, 2004, National Research Council, Washington D.C.

Harries, K., and Young, S. (2003). "Sprayed-fiber-reinforced composite materials for infrastructure rehabilitation", *Concrete International*, Vol. 25, Issue 1, pp 47-51, American Concrete Institute, Farmington Hills, Michigan.

Ibell, T., Morley, C., Middleton, C., (1997), "A Plasticity Approach to the Assessment of Shear in Concrete Beam-and-Slab Bridges", *The Structural Engineer; Journal of the Institution of Structural Engineers*. Vol. 75, Issue 19. pp. 331-338. 1997.

Jones, R., Swamy, R., Charif, A., (1988), "Plate Separation and Anchorage of Reinforced Concrete Beams Strengthened by Epoxy-Bonded Steel Plates", *The Structure Engineer, Journal of the Institute of Structural Engineers*, Vol. 66, Issue 5, pp. 85-94, The Institution of Structural Engineers, London, UK

Jones, J., (2004), "Fiber Reinforced Polymer Shear Strengthening of Short Span of Precast Concrete Channel Beams," MSCE Thesis, May 2004, University of Arkansas, Fayetteville, AR.

Jones, J., Heymsfield, E., Durham, S., (2004), "Fiber Reinforced Polymer Shear Strengthening of Short Span Precast Channel Beams in Bridge Superstructures," *Transportation Research Record*, 2004, National Research Council, Washington D.C.

Klaiber, F. W., Wipf, T. J., Nahra, M. J., Ingersoll, J. S., Sardo, A.G., and Qin, S. (2001). "Field and Laboratory Evaluation of Precast Concrete Bridges", Iowa State University, Ames, Iowa.

Lee, H., Avila, G., Montanez, C., (2004), "Numerical Study on Retrofit and Strengthening Performance of Sprayed Fiber Reinforced Polymer", submitted to *Engineering Structures*, 2004.

Menzel, C., (1955), "A Method for Determining the Moisture Condition of Hardened Concrete in Terms of Relative Humidity," *ASTM Proceedings*, Vol. 55, pp. 1085-1109.

Montgomery, D., (2001) *Design and Analysis of Experiments*, 5<sup>th</sup> Edition, John Wiley and Sons, Inc.

Mufti, A., Labossiere, P., Neale, K., (2002), "Recent Bridge Applications of FRP's in Canada", *Structural Engineering International: Journal of the International Association*

for Bridge and Structural Engineering., Vol. 12, No. 2, pp. 96-98., International Association for Bridge and Structural Engineering, Zurich, Switzerland.

National Bridge Inventory Study Foundation. “*National Bridge Inventory.*” <http://www.nationalbridgeinventory.com>. June 15, 2002.

Norris, T., Saadatmanesh, H., Ehsani, M., (1997), “Shear and Flexural Strengthening of R/C Beams with Carbon Fiber Sheets”, Journal of Structural Engineering, Vol. 123, No. 7, pp. 903-911. American Society of Civil Engineers. New York.

Rebeiz, K. S.; Fente, J.; Frabizzio, M; “New Shear Strength Prediction For Concrete Members Using Statistical and Interpolation Function Techniques,” Proceedings from the 8<sup>th</sup> ASCE Specialty Conference on Probabilistic Mechanics and Structural Reliability, South Bend, IN, 2000.

Soutsos, M., Bungey, J., Long, A., Henderson, G., (2000), “In-Situ Strength Assessment of Concrete – The European Concrete Frame Building Project”, Proceedings of the Non-Destructive Testing in Civil Engineering Symposium., Insight, Vol. 42, No. 7., pp. 432-435. July 2000

Stallings, J., Tedesco, J., El-Mihilmy, M., McCauley, M., (2000), “Field Performance of FRP Bridge Repairs”, Journal of Bridge Engineering, Vol. 5, No. 2, May 2000, pp. 107-113. American Society of Civil Engineers. New York.

Stark, D. (1989), “Influence of Design and Materials on Corrosion Resistance of Steel in Concrete,” PCA Research and Development Bulletin, No. RD098, 1989, Portland Cement Association, Skokie, IL.

Swamy, R. Qureshi, S., (1973), “Shear Behaviour of Reinforced Concrete T-Beams with Web Reinforcement.” Proceedings of the Institute of Civil Engineers, Paper No. 7656, pp. 35-49.

Taljsten, B., (2003). “Strengthening Concrete Beams for Shear with CFRP Sheets”, Construction and Building Materials, Vol. 17 No. 1. Elsevier Science Ltd. 2002.  
Tencleve, K., (2005), “Potential Causes for Longitudinal Reinforcing Steel Corrosion in Precast Channel Beams,” MSCE Thesis, May 2005, University of Arkansas, Fayetteville, AR.

Tsukahara, E., Uomoto, T., (2000). “Corrosion Rate of Reinforcing Steel Bars in Cracked Concrete”, Transactions of the Japan Concrete Institute, Vol. 22. 2000 Japan Concrete Institute.

Valerio, P., Ibell, T., (2003), “Shear Strengthening of Existing Concrete Bridges”, Proceedings of the Institute of Civil Engineers. Structures and Buildings Vol. 156, Issue 1. Institute of Civil Engineers. London, UK.

Wang, C., Salmon, Charles G. Reinforced Concrete Design. Sixth Edition. Addison Wesley Educational Publishers, Inc. 1998. pp 140-149

Yoon, S., Wang, K., Weiss, J., Shah, S., (2000). “Interaction between Loading, Corrosion, and Serviceability of Reinforced Concrete”, ACI Materials Journal, Vol. 97, No. 6, November-December 2000. American Concrete Institute, Farmington Hills, Michigan.

Zararis, P., Papadakis, G., (2001), “Diagonal Shear Failure and Size Effect in RC Beams without Web Reinforcement”, Journal of Structural Engineering, Vol. 127, No. 7, July 2001, pp. 733 – 742, American Society of Civil Engineers, New York.

**Appendix A**  
**Bridge Inspection Report**

>>>> INSPECTIONS >>>> REVISIONS 1/2  
 52E. INSPECTED BY RLL LET & GWF  
 90. DATE INSPECTED (M/D/Y) 04/25/2000 05/02/2002  
 91. INSPECTION FREQUENCY (HOS) 24  
 92./93. CRITICAL FEATURE

	INSP	FREQ	DATE MADE	INSP	FREQ	DATE MADE	INSP
	REQD	(NO)	(M/Y)	REQD	(NO)	(M/Y)	BY
A. FRAC CRIT	N						
B. U*WATER	Y	48	04/1998			05/02	LET
C. SPECIAL	N						

>>>> IDENTIFICATION <<<<  
 1. STRUCTURE NUMBER 00881  
 5A. ON/UNDER STR 1  
 2. HWY DISTRICT 64  
 3. COUNTY (65) SEBASTIAN  
 4. CITY (0000) RURAL  
 5B. ROUTE NO 00052  
 5E. DIRECTION (D) NA  
 5D2. SECTION/ZONE 01/1  
 11. LOG MILE 006.630  
 6. FEATURE INTERSECT: CREEK  
 7. FACILITY ON STR: SH 45  
 8. LOCATION: JCT SH 45 & SH 242-SEC 6  
 \* 16. LATITUDE: 35 DEG 06.2 MIN DEG MIN  
 \* 17. LONGITUDE: 91 DEG 22.0 MIN DEG MIN

BORDER BRIDGE:  
 98A. STATE CODE  
 98B. X SHARE RESPONSIBILITY  
 99. STRUCTURE NUMBER

>>>> CLASSIFICATION <<<<  
 \*184. HIGHWAY SYSTEM 1  
 \* 26. FUNCTIONAL CLASS 02  
 \*100. DEFENSE HIGHWAY 1  
 \*110. DESIGNATED NATIONAL NETWORK 1  
 101. PARALLEL STRUCTURE CODE N  
 102. DIRECTION OF TRAFFIC (2) 2-WAY  
 103. TEMPORARY STRUCTURE  
 21. MAINT. RESPONSIBILITY (01) STATE  
 22. OWNER (01) STATE  
 \* 37. HISTORICAL SIGNIFICANCE 5  
 112. NBIS BRIDGE LENGTH (Y/N) Y

>>>> MISCELLANEOUS <<<<  
 \*511. OLD BRIDGE NUMBER  
 \*512. NEW BRIDGE NUMBER  
 \* 23. CONTRACT JOB NUMBER N.S.  
 523. DATE LAST DRAWINGS (M/Y) 02/1999  
 524. WEATHERING STEEL (Y/N) N  
 \*510. PIN/HANGER

>>>> LOAD RATING/POSTING DATA <<<<  
 \*508. RATING ENGR DLY  
 \*507. RATING DATE 05/2000  
 \* 64. OPERATING RATING 2/31  
 \* 66. INVENTORY RATING 2/12  
 \* 67. STRUCTURAL EVALUATION 4  
 \* 70. BRIDGE POSTING CODE 5  
 41. OPERATIONAL STATUS A

VEHICLE CODE	COMPUTED (TONS)	POSTED (TONS) BEG.	END	*COMPUTED (TONS)
519. 4		27	27	
518. 9		27	27	
520. 5	NR	27	27	27

\* TO BE COMPLETED BY CENTRAL OFFICE  
 REMARKS:

DIST- 04; CO- 65; RTE- 00052; SECT/ZONE- 01/1; LOG- 006.630; STR #- 00881  
 SEBASTIAN

>>>> STRUCTURE/GEOMETRIC DATA <<<< REVISIONS 2/2

SUPERSTRUCTURE:

43. MAIN SPAN TYPE (1/22) R/C CHANNEL BR ✓  
 45. NUMBER OF SPANS 107 ✓  
 44. APPR SPAN TYPE (0/00) OTHER/OTHER ✓  
 46. NUMBER OF SPANS 0000 ✓

SUBSTRUCTURE:

526. ABUTMENT TYPE (1/10) C-1-PIOPEN W/ COLS/FIBR ✓  
 527. BENT TYPE-MAIN(1/92) C-1-PI2 COL W/D FILE ✓  
 528. BENT TYPE-APPR(2/92) NONE/NONE ✓

107. STRUCTURAL DECK TYPE 2 ✓  
 108. WEARING SURFACE/PROTECTION SYSTEM:  
 A. TYPE WEARING SURFACE 1 ✓  
 B. TYPE MEMBRANE 0 ✓  
 C. TYPE DECK PROTECTION 0 ✓

509. WEAR SURF THICK 80.0 IN ✓  
 48. MAXIMUM SPAN LENGTH 0012 FT ✓  
 49. STRUCTURE LENGTH 000185 FT ✓  
 50. CURB/SIDEWALK WIDTH (FT):  
 LEFT 10.8 RIGHT 00.0 ✓  
 51. BRIDGE RDWY WIDTH (C-C) 023.7 FT ✓  
 52. DECK WIDTH (OUT-OUT) 025.2 FT ✓  
 32. APPR RDWY WIDTH 032 FT ✓  
 35. MEDIAN TYPE (0) NONE ✓  
 34. SKEW (DEGREES) 00 ✓  
 35. STRUCTURE FLARED (0) NO ✓  
 10. LARGEST MIN VERT CLR 22 FT 22 IN ✓  
 47. TOTAL HORIZ CLR 25.6 FT ✓  
 53. MIN VERT CLR OVER BR RDWY 22 FT 22 IN ✓  
 54. MIN VERT UNDERCLR R / 00 FT 00 IN ✓  
 55. MIN LATERAL UNDERCLR-RT R / 29.9 FT ✓  
 56. MIN LATERAL UNDERCLR-LT 00.0 FT ✓

>>>> AGE AND SERVICE <<<<

27. YEAR BUILT 1958 / E ✓  
 106. YEAR RECONSTRUCTED 0000 / N ✓  
 42. TYPE SERVICE (15) HWY/WAY ✓  
 28. NUMBER OF LANES 02 / 00 ✓  
 29. AVERAGE DAILY TRAFFIC 00000 ✓  
 30. YEAR OF ADT 1998 ✓  
 M109. PERCENT TRUCK TRAFFIC 01 ✓  
 31. DESIGN LOAD (2) H 16 ✓  
 12. BYPASS DETOUR LENGTH (MILES) 05 ✓

>>>> NAVIGATION DATA <<<<

38. NAVIGATION CONTROL (0) NOT REQ ✓  
 111. PIER PROTECTION ✓  
 39. NAV VERT CLR (FT) 000 ✓  
 116. VERT-LIFT BRIDGE:  
 NAV MIN VERT CLR (FT) ✓  
 40. NAV HORIZ CLR (FT) 0000 ✓

>>>> CONDITION <<<<

58. DECK 5 ✓  
 59. SUPERSTRUCTURE 4 ✓  
 60. SUBSTRUCTURE 4 ✓  
 515. UNDERWATER 2 ✓  
 514. TYPE INSPECTION 5 ✓  
 61. CHANNEL/CHANNEL PROTECTION 2 ✓  
 62. CULVERTS 1 ✓

>>>> APPRAISAL <<<<

\* 68. DECK GEOMETRY 4 ✓  
 69. UNDERCLR, VERT/HORIZ 1 ✓  
 71. WATERWAY ADEQUACY 2 ✓  
 72. APPR RDWY ALIGNMENT 8 ✓  
 36. TRAFFIC SAFETY FEATURES 0/1/0/0 ✓  
 M113. SCOUR CRITICAL BRIDGE 8 ✓  
 504. PAINT CONDITION(X) 00 ✓

\* TO BE COMPLETED BY CENTRAL OFFICE

DIST- 01; CO- 65; RTE- 00045; SECT/ZONE- 01/0; LOG- 006.830; STR #- 00501  
 SEBASTIAN

Item 58 DECK	RATING	REMARKS
1. Deck-Structural Condition	5	<i>Some sand &amp; gravel patches to repair those to grade falling on sp. 4, unit #7 &amp; sp. 6, unit #1</i>
* 2. Wearing Surface	6	
* 3. Curbs	7	
* 4. Median	7	
* 5. Sidewalk	7	
* 6. Parapet	7	
* 7. Railing	7	
* 8. Drains	7	
* 9. Joint Leakage	7	
* 10. Expansion Joints/Devices	7	
Item 58 Condition Rating	5	

Item 59 SUPERSTRUCTURE	RATING	REMARKS
1. Stringers	7	<i>Completed 507 unit #2 has been loaded to the top of unit that indicates solder corrosion with No-Steel Corrosion.</i>
2. Girders or Beams	6	
3. Floorbeams	7	
4. Trusses- General	7	
- Portals	7	
- Bracing	7	
5. Rivets or Bolts	7	
6. Welds- Cracks	7	
7. Concrete Cracks	7	
8. Timber Decay	7	
9. Collision Damage	7	
10. Deflection Under Load	7	
11. Vibration Under Load	7	
12. Alignment of Members	7	
* 13. Bearing Devices	7	
Item 59 Condition Rating	6	

Item 60 SUBSTRUCTURE	RATING	REMARKS
1. Abutments- *Wings	7	<i>BTP 826 Columns have scaling.</i>
- Backwall	7	
- Footing	7	
- Piles	7	
- Scour	7	
- Settlement	7	
2. Piers or Bents- Caps	7	
- Column	7	
- Footing	7	
- Piles	7	
- Scour	7	
- Settlement	7	
3. Concrete Cracking/Spalling	7	
4. Timber Decay, etc.	7	
5. Collision Damage	7	
* 6. Debris on Seats	7	
* 7. Paint	7	
Item 60 Condition Rating	6	

\* These components shall have no effect on the inspectors condition rating.

BRIDGE INSPECTION REPORT  
NBIS-FORM II  
1 of 2

Inspected by LGW GWF  
Date 5-20-2007

Dist 4 Co 65 Rte 45 Sect 1 Log 603 Bridge # 00881

**Appendix B**  
**Structural Capacity Results for**  
**Thirty-Three PCB's**

## Jenkins' Ferry Bridge

**Table B1: Structural Load Results for Jenkins' Ferry Bridge Beams**

Beam ID	Beam Condition	Failure Mode	Load Capacity 2P (kip)	Mid-Span Deflection (in)															
RA	Poor	Shear	100	2.56															
RB	Poor	Shear	100	3.38															
RC	Poor	Shear	48	2.88	R1	Poor/Repaired	Shear	40	1.13	R2	Poor/Repaired	Flexural	95	4.56	R3	Poor/Repaired	Shear	86	1.19
R1	Poor/Repaired	Shear	40	1.13															
R2	Poor/Repaired	Flexural	95	4.56															
R3	Poor/Repaired	Shear	86	1.19															

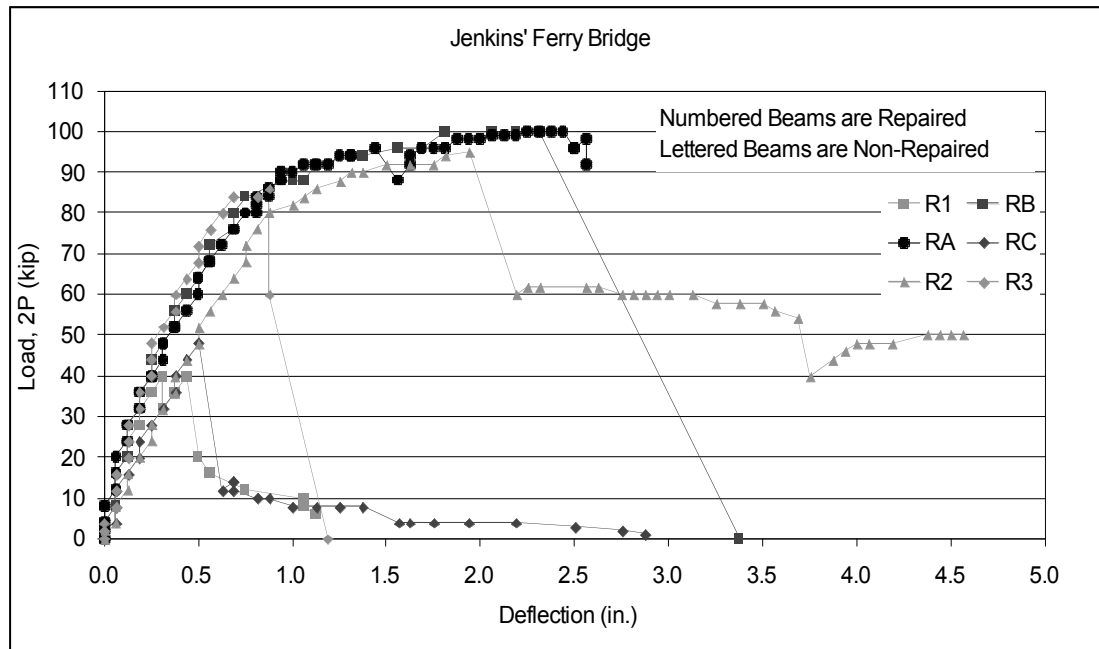


**Figure B1: Load vs. Deflection Curves for Jenkins' Ferry Bridge Beams**

## Little Osage Creek Bridge

**Table B2: Structural Load Results for Little Osage Creek Bridge Beams**

Beam ID	Beam Condition	Failure Mode	Load Capacity 2P (kip)	Mid-Span Deflection (in)
C1	Poor	Shear	64	0.88
C2	Poor	Shear	68	1.13
C3	Poor	Shear	44	1.19
C4	Poor	Shear	62	1.50
C5	Poor	Shear	84	2.00
C6	Poor	Shear	84	0.94
C7	Poor	Shear	84	1.03
C8	Poor	Shear	80	1.00

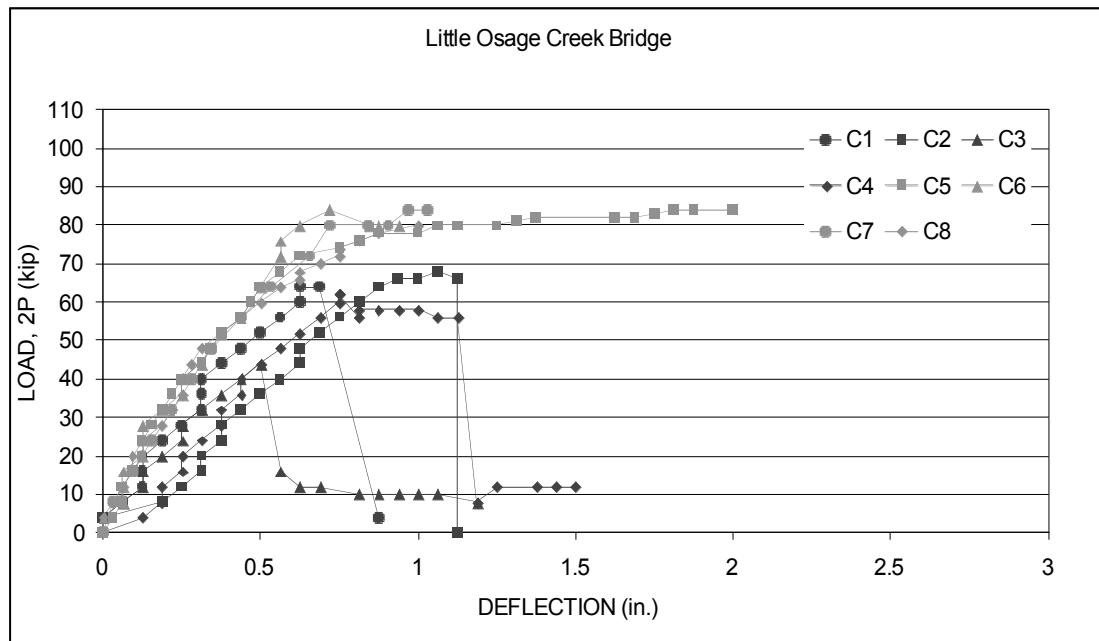


**Figure B2: Load vs. Deflection Curves for Little Osage Creek Bridge Beams**

## Gentry Maintenance Yard

**Table B3: Structural Load Results for Gentry Maintenance Yard Beams**

Beam ID	Beam Condition	Failure Mode	Load Capacity 2P (kip)	Mid-Span Deflection (in)
G1	Good	Shear	96	2.63
G2	Good	Flexural	104	5.69
G3	Good	Shear	98	5.13
G4	Good	Shear	106	6.13
G5	Good	Shear	84	1.50
G6	Good	Shear	94	3.06
G7	Good	Shear	94	2.81

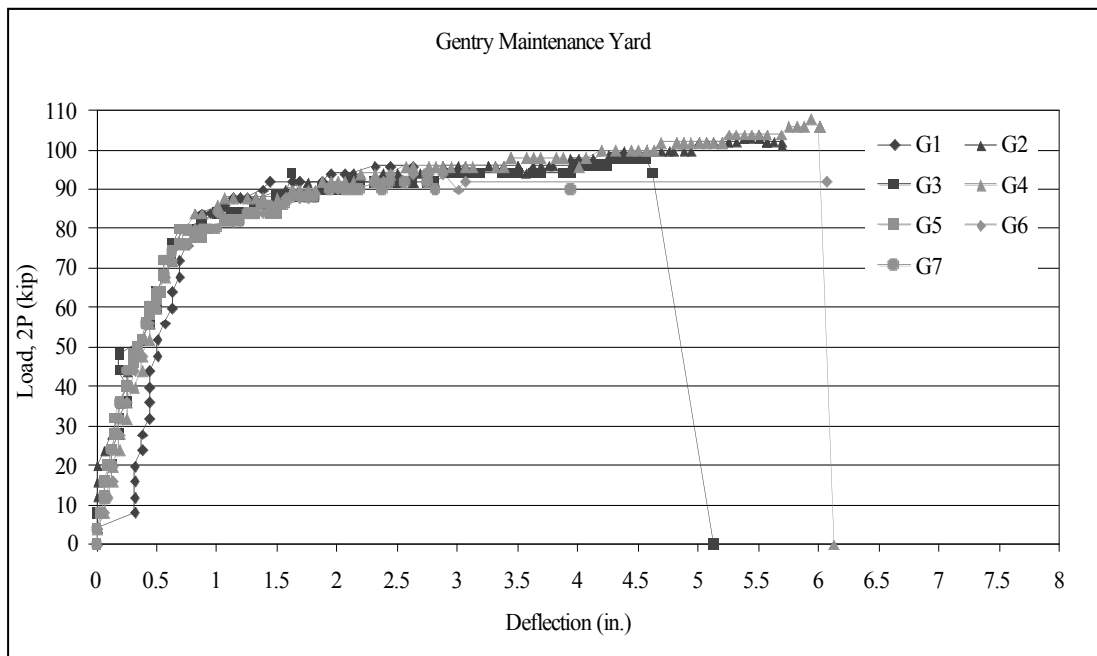


**Figure B3: Load vs. Deflection Curves for Gentry Maintenance Yard Beams**

## Carlisle Bridge

**Table B4: Structural Load Results for Carlisle Bridge Beams**

Beam ID	Beam Condition	Failure Mode	Load Capacity 2P (kip)	Mid-Span Deflection (in)
L1	Average	Shear	102	4.38
L2	Average	Shear	102	3.56
L3	Average	Shear	98	2.94
L4	Average	Shear	102	4.13
L5	Average	Shear	100	2.25
L6	Average	Shear	94	1.88
L7	Average	Shear	90	4.38
L8	Average	Shear	94	3.25
L9	Average	Shear	100	5.06
L10	Average	Shear	112	6.44
L11	Average	Shear	112	6.25
L12	Average	Shear	124	6.63

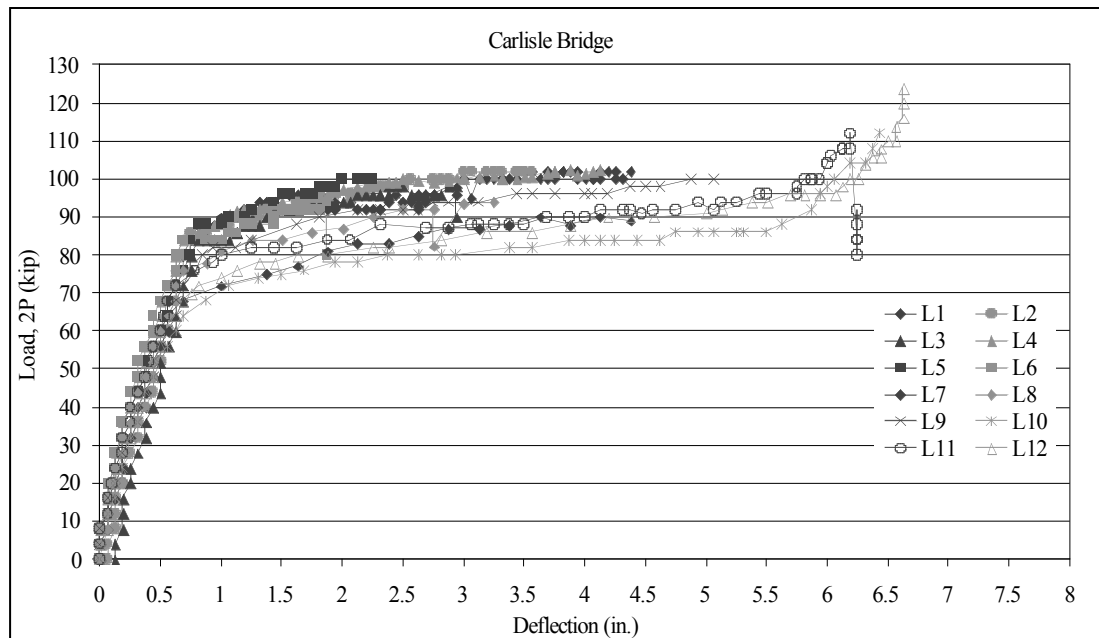


**Figure B4: Load vs. Deflection Curves for Carlisle Bridge Beams**

**Appendix C**  
**New Beams Load Data and**  
**Strain Gauge Results**

## New Beams

**Table C1: Structural Load Results for New Beams**

Beam ID	Beam Condition	Failure Mode	Load Capacity 2P (kip)	Mid-Span Deflection (in)
N1*	New	Flexure	140	6.06
N2*	New	Flexure	130	6.19
N3	New	Shear	80	1.00
N4	New	Shear	76	1.19

\* Indicates beams containing shear reinforcement.

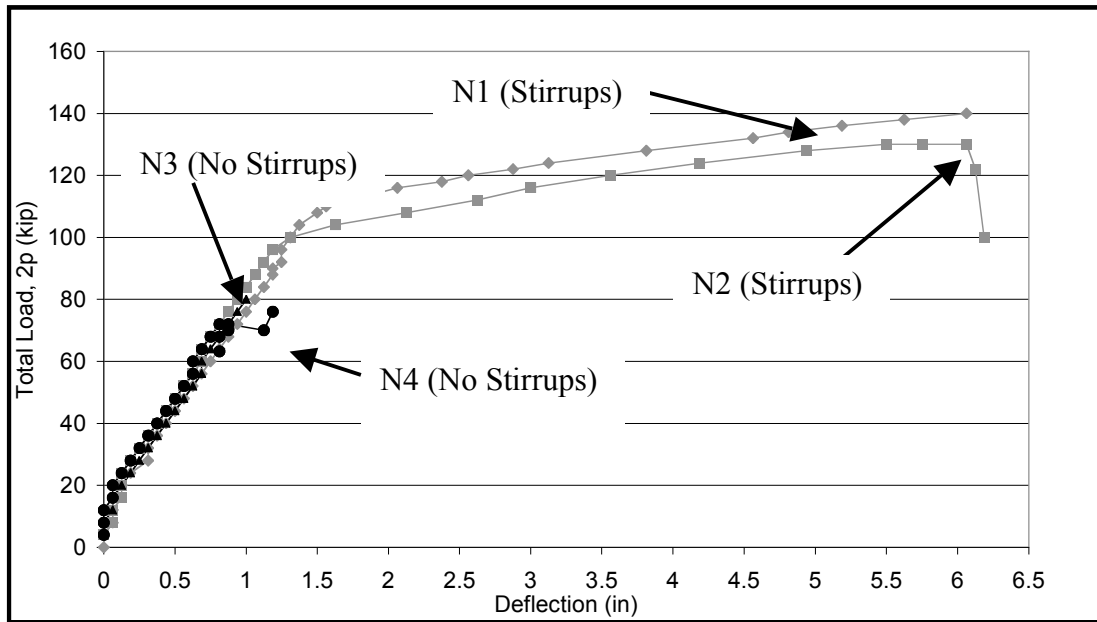
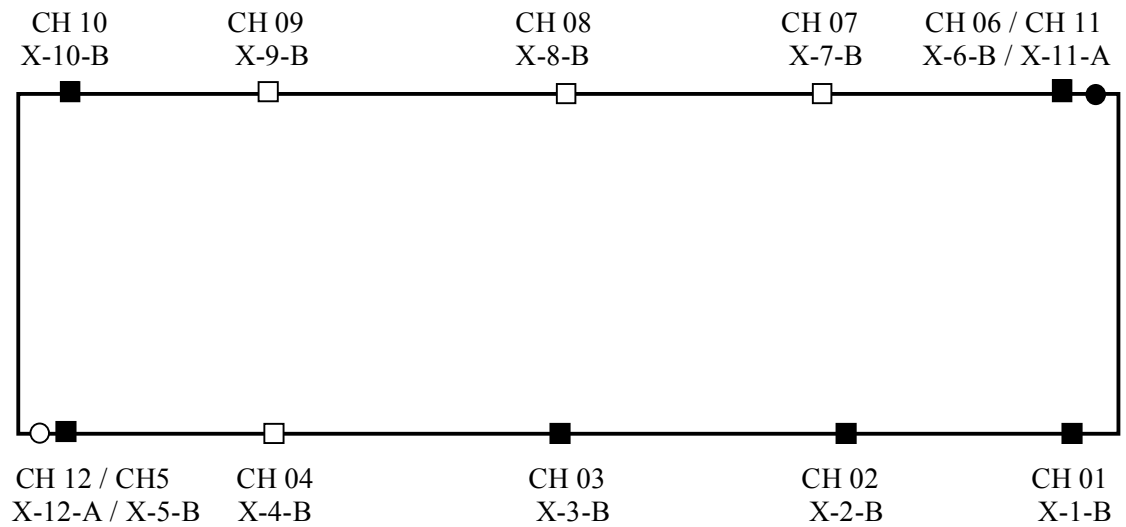


**Figure C1: Load vs. Deflection Curves for New Beams**

## Beam N1

H15 Loading w/ Stirrups

Cast on 03-17-03



- Functioning Strain Gauge on Longitudinal Reinforcement
- Non-Functioning Strain Gauge on Longitudinal Reinforcement
- Functioning Strain Gauge on Shear Reinforcement
- Non-Functioning Strain Gauge on Shear Reinforcement

**Beam Failure (2P) = 140kip**

**Type of Failure = Flexure (Deck Compression)**

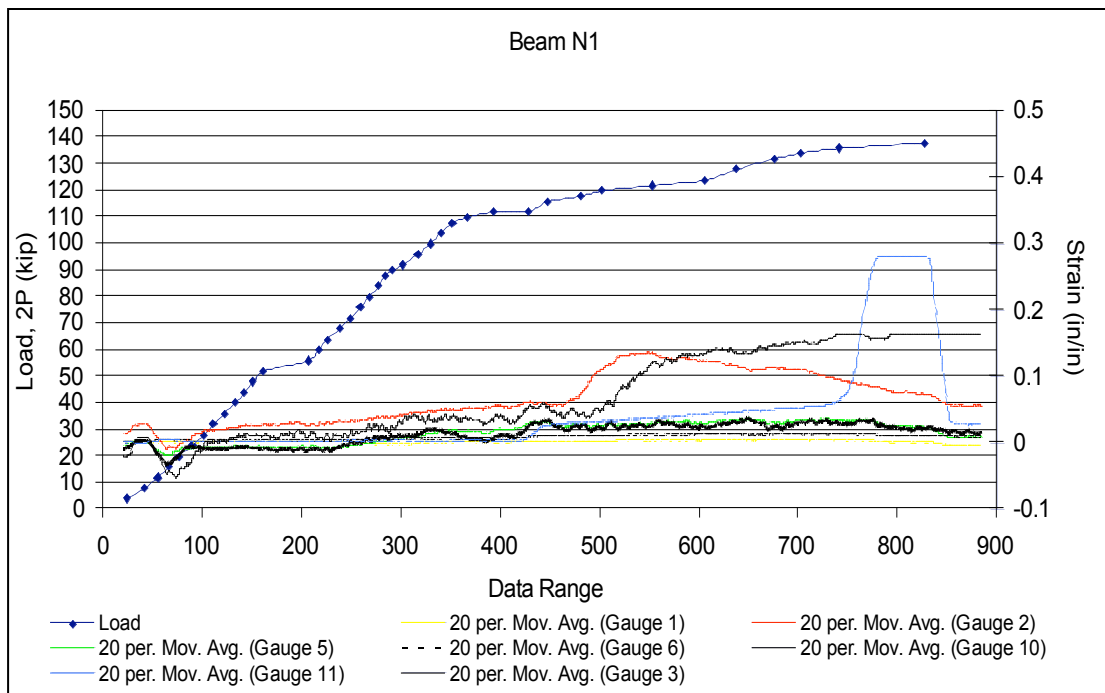
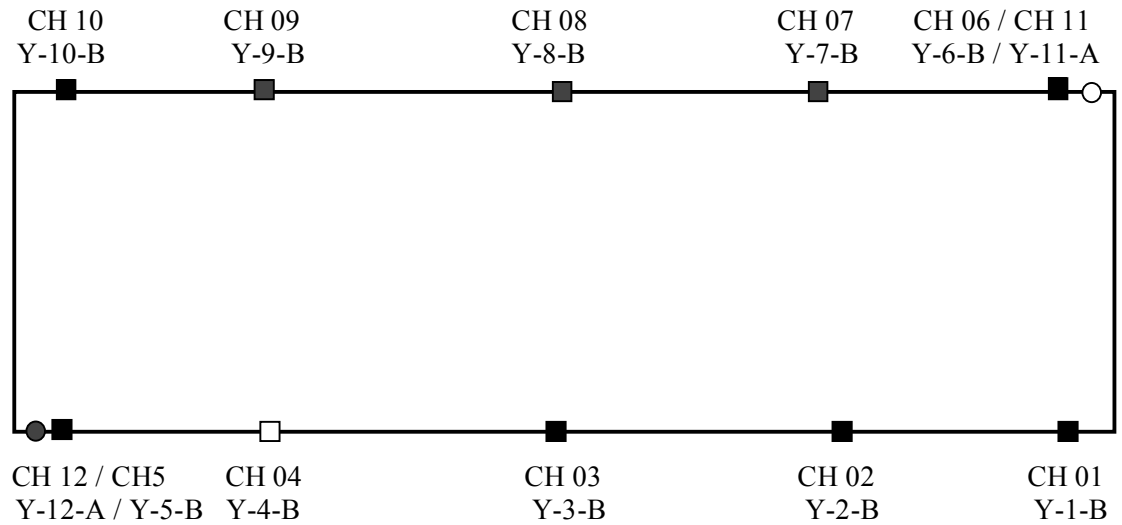


**Figure C2: Load and Strain Results for Beam N1 with Shear Reinforcement**

## Beam N2

### H15 Loading w/ Stirrups

Cast on 03-17-03



- Functioning Strain Gauge on Longitudinal Reinforcement
- Non-Functioning Strain Gauge on Longitudinal Reinforcement
- Functioning Strain Gauge on Shear Reinforcement
- Non-Functioning Strain Gauge on Shear Reinforcement

**Beam Failure (2P) = 130kip**

**Type of Failure = Flexure (Deck Compression)**

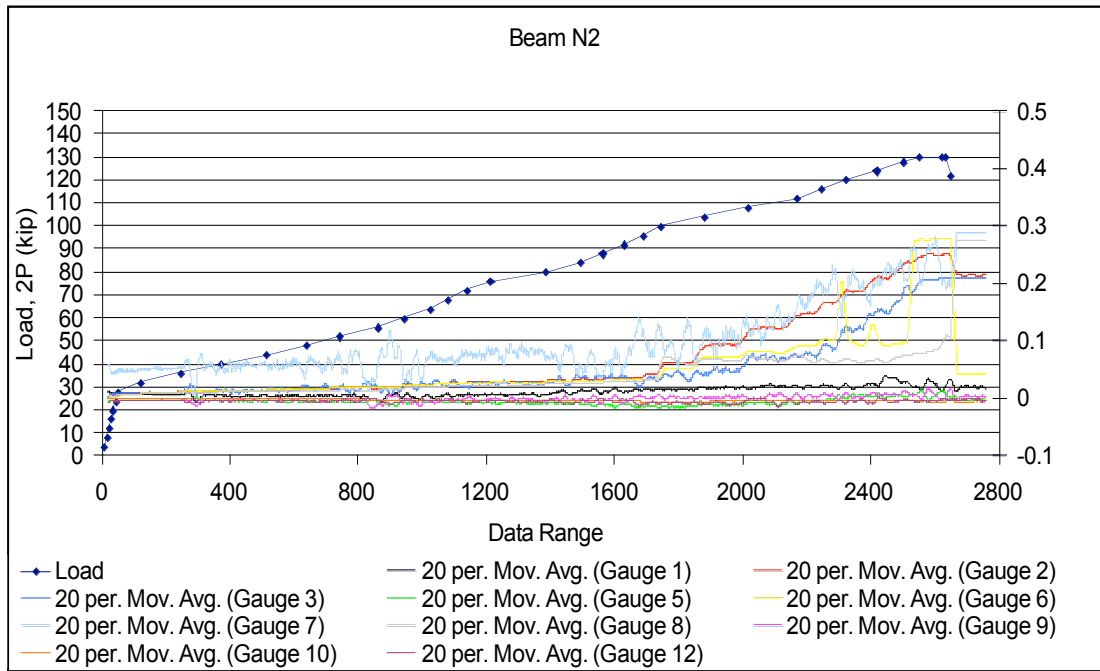
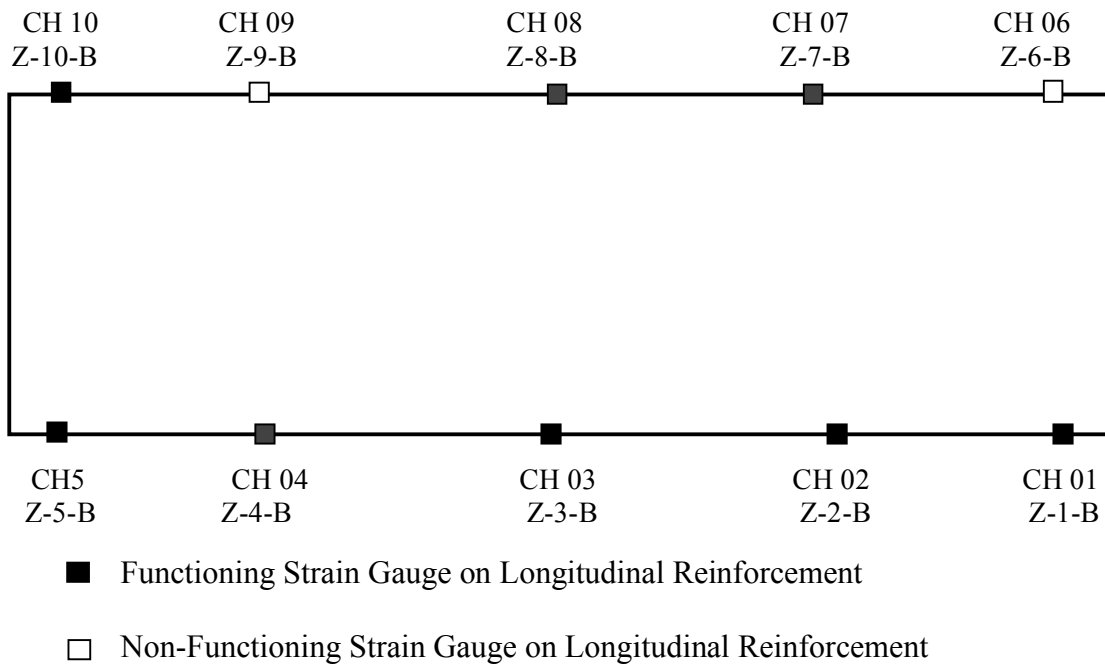


**Figure C3: Load and Strain Results for Beam N2 with Shear Reinforcement**

### Beam N3

**H15 Loading w/ No Stirrups**

**Cast on 03-18-03**



**Beam Failure (2P) = 80kip**

**Type of Failure = Shear**

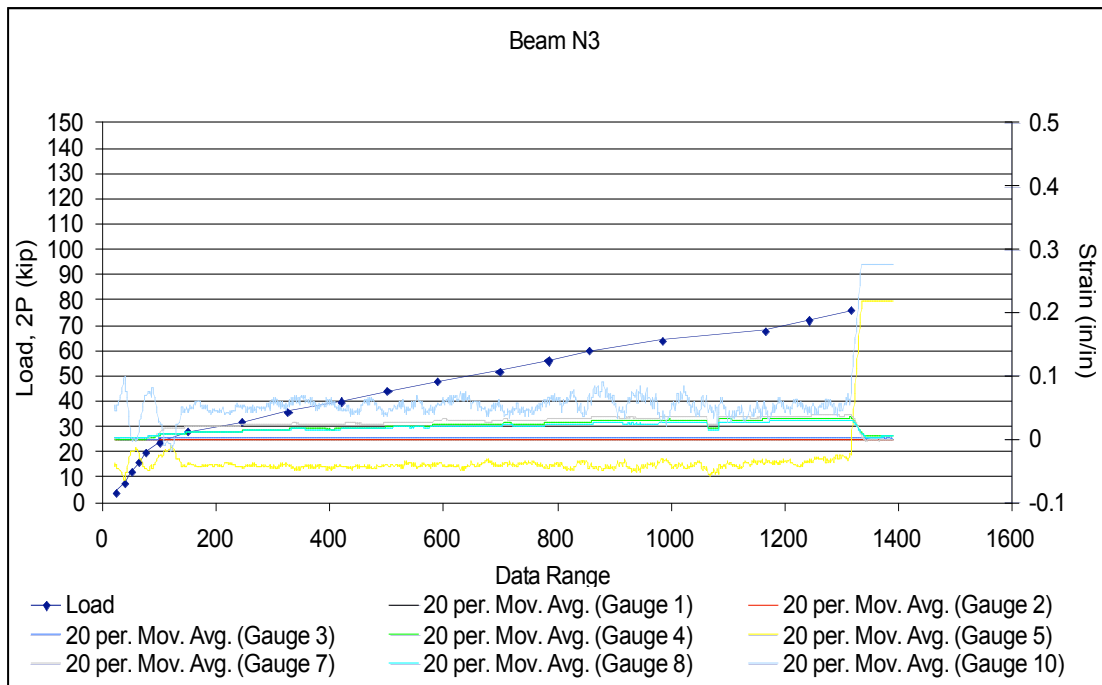
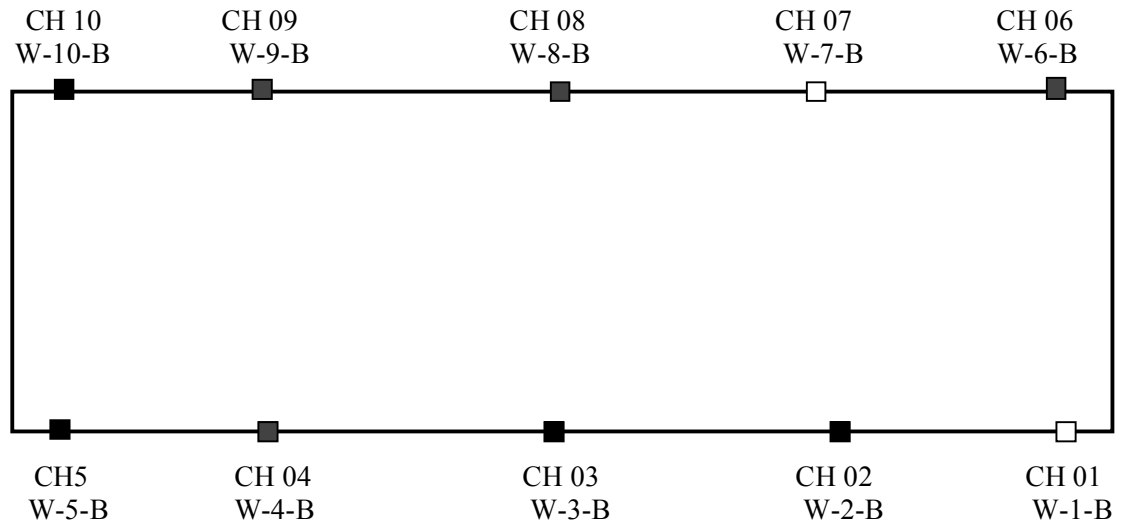


**Figure C4: Load and Strain Results for Beam N3 without Shear Reinforcement**

Beam N4

**H15 Loading w/ No Stirrups**

**Cast on 03-18-03**



■ Functioning Strain Gauge on Longitudinal Reinforcement

□ Non-Functioning Strain Gauge on Longitudinal Reinforcement

**Beam Failure (2P) = 77.6kip**

**Type of Failure = Shear**

Note: Shear crack began on right side of beam @ 63.2kip and on the left side of beam @ 70kip.

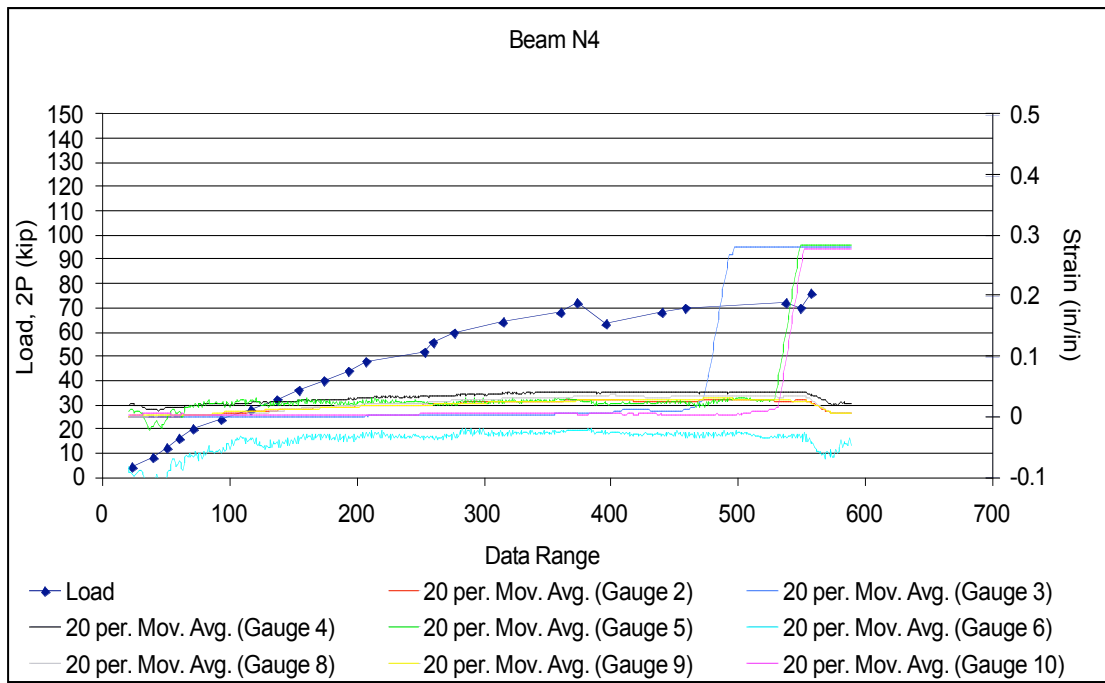
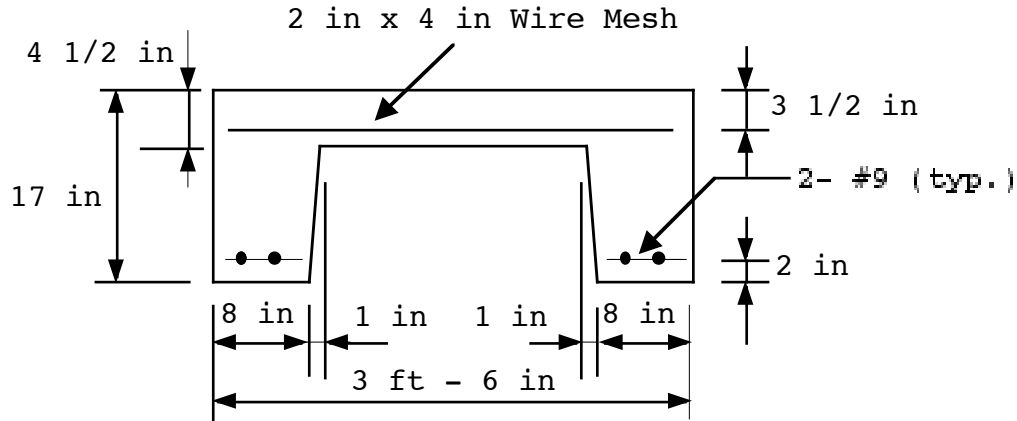


**Figure C5: Load and Strain Results for Beam N4 without Shear Reinforcement**

**Appendix D**  
**Retrofit Design Calculations**

## Moment Capacity and Equivalent HS Truck Loading

### Determine Dead Weight of Beam



$$\text{Volume (V}_{\text{bm}}) = \frac{[42 \times 17] - \frac{1}{2} [(42 - 18) + (42 - 16)] \times [17 - 5]}{144} \times 19 = 54.63 \text{ft}^3$$

*Does not include diaphragm*

$$\text{Volume (V}_d) = \frac{[6 + 9] \times [17 - 5]}{144} \times \frac{1}{2} \times 2 \times \frac{[42 - 16]}{12} + \frac{1}{2} \times \frac{[42 - 16]}{12} \times \frac{[17 - 5]}{12} \times \frac{[12 + 6]}{12} = 4.33 \text{ft}^3$$

$$\text{Total Volume of Concrete (V}_c) = 54.63 + 4.33 = 58.96 \text{ft}^3$$

$$\text{Beam Dead Weight (DL)} = \gamma_c V_c = 150 \text{pcf} \times 58.96 \text{cf} = 8.84 \text{kip}$$

Equivalent Uniform Load ( $w_{\text{DL}}$ )

$$w_{\text{DL}} = \frac{DL}{\text{Length}} = \frac{8.84}{19} = 0.465 \text{kip/ft}$$

### Beam Section Properties

Effective Depth ( $d$ ) = 17in – 2in = 15in.

Area of Flexural Reinforcing Steel ( $A_s$ )

$$A_s = 4 \times 1.0\text{in}^2 = 4\text{in}^2$$

No Shear Reinforcement

Span Length = 19ft

Width of Individual PCB = 42in.

Concrete Compressive Strength = 3000psi

Reinforcing Steel Yield Strength = 40ksi

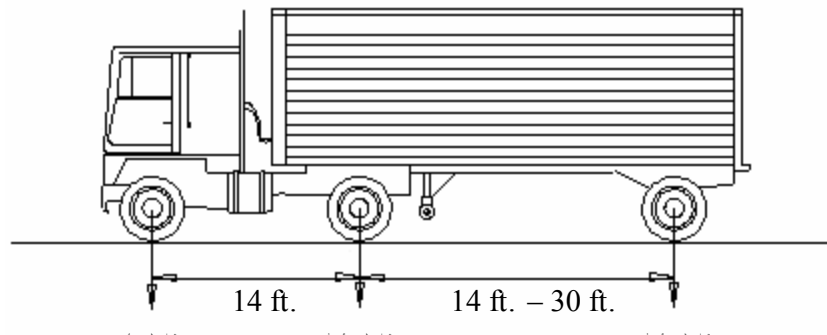
### Mid-Span Moment

**Moment Due to Dead Load ( $M_{DL}$ )**

$$MDL = \frac{w_{DL} L^2}{8} = \frac{0.46 \times 19^2}{8} = 20.7\text{kip-ft}$$

**Moment Due to Live Load ( $M_{LL}$ )**

Determine for HS-20 Truck Loading



Maximum Moment Occurs at Mid-Span

$$M_{LL} = \frac{pL}{4} = \frac{16 \times 19}{4} = 76 \text{kip-ft.}$$

(One Wheel Line without Impact and Distribution)

### Load Factor Rating

Impact Factor (I)

$$I = \frac{50}{L + 125} \leq 0.30 \quad (\text{AASHTO 3.8.2.1})$$

$$I = \frac{50}{19 + 125} = 0.347 > 0.30 \quad \text{Use } I = 0.30$$

Distribution Factor: Assume the load is carried by a single PCB. Thus DF=1.0.

Live Load + Impact Factor ( $M_{LL+I}$ )

$$M_{LL+I} = M_{LL}(1+I) \times (\text{DF}) = 76(1.30)(1.0) = 98.8 \text{kip-ft.}$$

Check Maximum Allowable Reinforcement Ratio ( $\rho_{\max}$ )

$$\rho_{\text{act}} = \frac{A_s}{bd} = \frac{4.0}{42 \times 15} = 0.00635$$

$$\rho_{\max} = 0.75\rho_{\text{bal}} = 0.75 \frac{0.85 \beta_1 f'_c}{f_y} \frac{87000}{87000 + f_y}$$

$$\beta_1 = 0.85 \text{ for } f'_c = 3000 \text{psi}$$

$$\rho_{\max} = 0.0278$$

$$\rho_{\text{act}} < \rho_{\max} \quad \text{OK}$$

### Section Moment Capacity

$$a = \frac{A_s f_y}{0.85 f'_c b} = \frac{4.0 \times 40}{0.85 \times 3 \times 42} = 1.49 \text{ in} < 5 \text{ in. OK}$$

$$M_n = A_s f_y \left[ d - \frac{a}{2} \right] = \frac{4.0 \times 40 \left[ 15 - \frac{1.49}{2} \right]}{12} = 190.0 \text{ kip-ft}$$

### Factored Moment Capacity

$$M_u = \phi M_n \quad (\text{AASHTO 8.16.1.2 } \phi = 0.90)$$

$$M_u = 0.9(190.0) = 171.0 \text{ kip-ft.}$$

### Inventory Level Rating

$$RF_I^{LF} = \frac{M_u - A_1 M_{DL}}{A_2 M_{LL+I}}$$

where:

- $RF_I^{LF}$  = load factor rating at inventory level
- $M_u$  = factored nominal moment capacity
- $M_{DL}$  = moment due to dead load
- $M_{LL+I}$  = moment due to live load and impact
- $A_1$  = load factor of dead load, 1.3
- $A_2$  = load factor of live load, 2.17

$$RF_I^{LF} = \frac{171.0 - 1.3(20.7)}{2.17(98.8)} = 0.672$$

### Operating Level Rating

$$RF_O^{LF} = \frac{M_u - A_1 M_{DL}}{A_2 M_{LL+I}}$$

where:

- $RF_O^{LF}$  = load factor rating at operating level
- $A_1$  = load factor of dead load, 1.3
- $A_2$  = load factor for live load, 1.3

$$RF_o^{LF} = \frac{171.0 - 1.3(20.7)}{1.3(98.8)} = 1.122$$

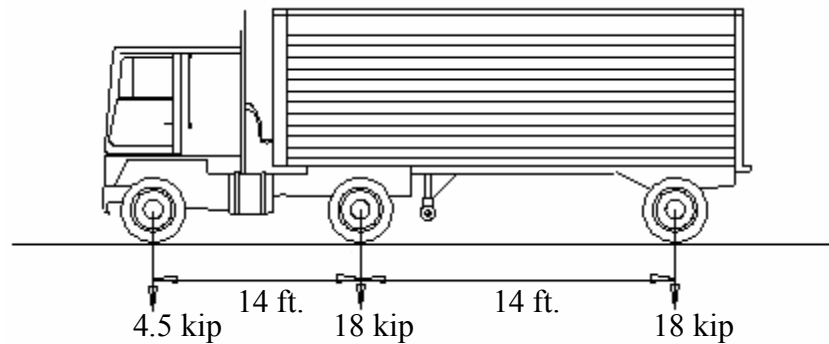
Load Capacity Based on Load Factor Ratings (HS-20 Truck Loading)

Inventory = 0.67 x 36Ton = 24.12Ton HS

Operating = 1.12 x 36Ton = 40.32Ton HS Use 40.5

Equivalent HS Truck

Live Load HS 40.5

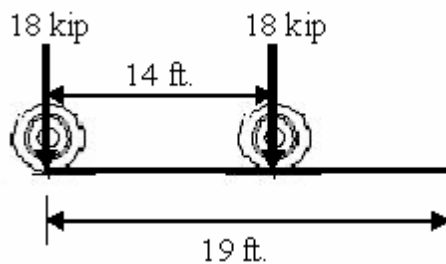


**Shear Capacity**

Maximum Dead Load Shear Force ( $V_{DL}$ )

$$V_{DL} = \frac{DL}{2} = \frac{8.84}{2} = 4.42\text{kip}$$

Maximum Live Load Shear Force ( $V_{LL}$ )



$$V_{LL} = 18 + 18 \frac{5}{19} = 22.74 \text{kip (One Wheel Line)}$$

$$V_{LL+1} = 22.74(1.3) = 29.56 \text{kip}$$

### Maximum Factored Shear Force

$$V_{u(\max)} = 1.3V_{DL} + 1.67V_{LL+1}$$

$$V_{u(\max)} = 1.3(4.42) + 1.67(29.56) = 55.1 \text{kip}$$

### Nominal Shear Strength Required

$$V_n = \frac{Vu}{\phi} = \frac{55.1}{0.85} = 64.8 \text{kip} = 65 \text{kip}$$

### Shear Strength (Actual)

$$V_c = 2 \times 2 \sqrt{f'_c} bd = 2 \sqrt{3000} \times 8 \times 15 = 26.3 \text{kip}$$

### Nominal Shear Capacity (Provided)

$$V_n = V_c + V_s$$

$$V_s = 0 \text{ (No Shear Reinforcement)}$$

$$V_n = V_c = 26.3 \text{kip}$$

### Shear Deficiency

$$V_n, \text{ required} - V_n, \text{ provided} = 64.8 - 26.3 = 38.5$$

$$\% \text{ Deficiency} = \frac{38.5}{64.8} \times 100 = 59.1\% \text{ Deficient}$$

## Design of CFRP Shear Strengthening Retrofit

### CFRP Material Properties

Carbon Fiber Reinforced Polymer Strip	
Design Tensile Strength	406 ksi (2799 MPa)
Design Modulus of Elasticity	$23.9 \times 10^3$ ksi (165 GPa)
Elongation at Break	1.69%
Thickness	0.047 in. (1.19 mm)
Width	1.97 in. (50.0 mm)
Fiber Volumetric Content	> 68%
Temperature Resistance	> 300°F (149°C)
Epoxy	
Tensile Strength @ 7 Days	3.6 ksi (24.8 MPa)
Elongation at Break @ 7 Days	1%
Modulus of Elasticity @ 7 Days	650 ksi (4482 MPa)
Flexural Strength @ 14 Days	6.8 ksi (46.9 MPa)
Tangent Modulus of Elasticity in Bending @ 14 Days	1700 ksi (11.7 GPa)
Shear Strength @ 14 Days	3.6 ksi (24.8 MPa)

### Vertical CFRP Orientation Application

$$V_{CFRP} = V_{n, \text{required}} = 65 \text{kip}$$

The design of the external CFRP strengthening technique was based on the AASHTO internal stirrup design procedure [AASHTO 1996].

$$V_{CFRP}(\text{vertical}) = \frac{A_{CFRP} f_{CFRP} d}{s}$$

where:

- $A_{CFRP}$  = area of the CFRP strip,  $2t_f w_f$
- $f_{CFRP}$  = CFRP design tensile strength
- $s$  = CFRP strip spacing
- $t_f$  = thickness of a single CFRP strip
- $w_f$  = width of the CFRP strip

$$s = \frac{A_{CFRP} f_{CFRP} d}{V_{CFRP}} = \frac{0.093 \times 406 \times 15}{65} = 8.71 \text{ in}$$

$$s_{\max} = w_{CFRP} + \frac{d}{4} = 1.97 + \frac{15}{4} = 5.72 \text{ in Use } 5.5 \text{ in.}$$

$$V_{CFRP}(\text{vertical}) = \frac{A_{CFRP} f_{CFRP} d}{s} = \frac{0.093 \times 406 \times 15}{5.5} = 103.0 \text{ kip}$$

Check:

$$8\sqrt{f'_c} bd = \frac{2 \times 8\sqrt{3000} \times 8 \times 15}{1000} = 105.2 \text{ kip} > 103.0 \text{ kip OK}$$

$$4\sqrt{f'_c} bd = \frac{2 \times 4\sqrt{3000} \times 8 \times 15}{1000} = 52.6 \text{ kip} < 103.0 \text{ kip OK}$$

**USE CFRP STRIPS PLACED VERTICALLY AT 5.5in SPACING C.C.**

#### Diagonal CFRP Orientation Application

$$V_{CFRP} = V_{n, \text{required}} = 65 \text{ kip}$$

The design of the external CFRP strengthening technique was based on the AASHTO internal stirrup design procedure [AASHTO 1996].

$$V_{CFRP}(\text{diagonal}) = \frac{A_{CFRP} f_{CFRP} (\sin \alpha + \cos \alpha) d}{s}$$

where:

$A_{CFRP}$  = area of the CFRP strip,  $2t_f w_f$

$f_{CFRP}$  = CFRP design tensile strength

$s$  = CFRP strip spacing

$\alpha$  = angle of CFRP strip (45 degrees)

$$S_{\max} = W_{CFRP} + \frac{1}{2} \frac{d}{\tan \alpha} = 1.97 + \frac{1}{2} \frac{15}{\tan 45} = 9.47 \text{ in Use } 8.0 \text{ in.}$$

$$V_{CFRP}(\text{diagonal}) = \frac{A_{CFRP} f_{CFRP} (\sin \alpha + \cos \alpha) d}{S}$$

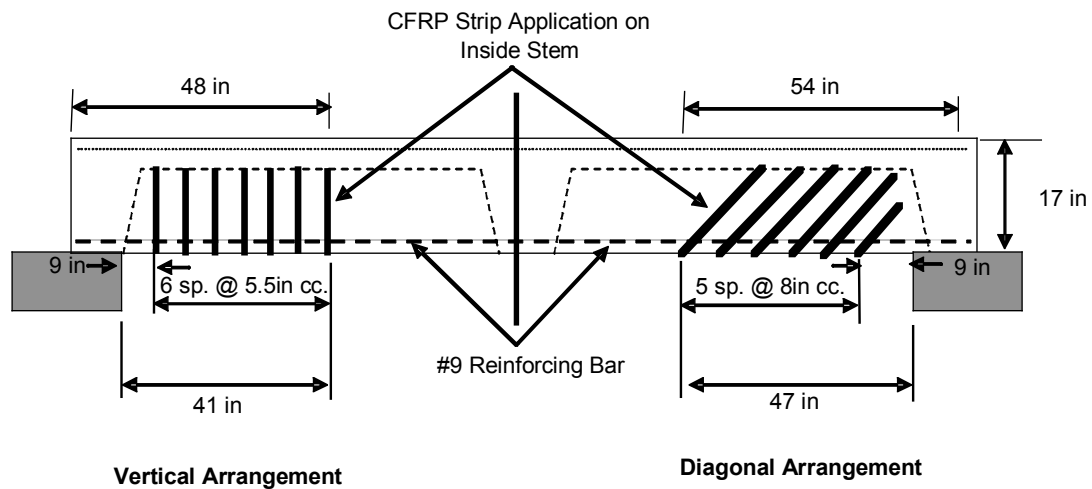
$$V_{CFRP}(\text{diagonal}) = \frac{0.093 \times 406 (\sin 45 + \cos 45) \times 15}{8.0} = 100.1 \text{ kip}$$

Check:

$$8\sqrt{f'_c} bd = \frac{2 \times 8 \sqrt{3000} \times 8 \times 15}{1000} = 105.2 \text{ kip} > 100.1 \text{ kip OK}$$

$$4\sqrt{f'_c} bd = \frac{2 \times 4 \sqrt{3000} \times 8 \times 15}{1000} = 52.6 \text{ kip} < 100.1 \text{ kip OK}$$

**USE CFRP STRIPS PLACED DIAGONALLY AT 8.0in SPACING C.C.**



## Design of MMFX Steel Shear Bar Retrofit

### Material Properties

<b>Microcomposite Multistructural Formable Steel (MMFX) Reinforcing Bar</b>	
Yield Tensile Strength (0.2% Offset)	120 ksi (1111 MPa)
Strain @ 0.2% Offset Yield Strength	0.60%
Ultimate Tensile Strength	177 ksi (1220 MPa)
Strain @ Ultimate Stress	12%
Young's Modulus of Elasticity (Tension)	29,000 ksi (200 GPa)
Yield Compressive Strength (0.2% Offset)	145 ksi (1000 MPa)
Young's Modulus of Elasticity (Compression)	29,000 ksi (200 GPa)
Shear Strength	110 ksi (758 MPa)
Poisson's Ratio	0.26
<b>Epoxy</b>	
Shrinkage During Cure	0.00051 (in/in)
Compressive Strength	10.3 ksi (71.0 MPa)
Heat Deflection Temperature	140°F (60°C)

### MMFX Shear Bar Application

$$V_{MMFX} = V_{n, \text{required}} = 65 \text{kip}$$

The design was based on the AASHTO internal stirrup design procedure [AASHTO 1996].

$$V_{MMFX} = \frac{A_b f_{mmfx} d}{s}$$

where:

- $A_b$  = area of the shear reinforcement
- $f_{MMFX}$  = MMFX steel design tensile strength
- $s$  = Bar spacing

$$s = \frac{A_b f_{MMFX} d}{V_{MMFX}} = \frac{2 \times 0.31 \times 120 \times 15}{65} = 17.1 \text{in} \quad \text{Use 12in.}$$

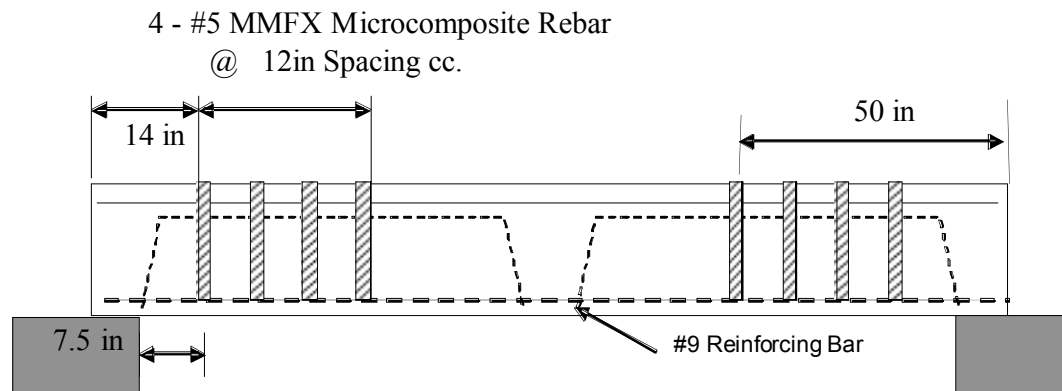
$$V_{CFRP}(\text{vertical}) = \frac{A_{CFRP} f_{CFRP} d}{s} = \frac{2 \times 0.31 \times 120 \times 15}{12} = 93.0 \text{ kip}$$

Check:

$$8\sqrt{f'_c} bd = \frac{2 \times 8\sqrt{3000} \times 8 \times 15}{1000} = 105.2 \text{ kip} > 93.0 \text{ kip OK}$$

$$4\sqrt{f'_c} bd = \frac{2 \times 4\sqrt{3000} \times 8 \times 15}{1000} = 52.6 \text{ kip} < 93.0 \text{ kip OK}$$

**USE MMFX STEEL SHEAR BARS AT 12in. SPACING C.C.**



## **Appendix E**

### **Retrofitted and Control Beam Load Testing Results**

## Carbon Fiber Reinforced Polymer Strip Retrofit Application

**Table E1: Structural Load Results for CFRP Retrofitted Beams**

Beam ID	Beam Condition (Retrofit Type)	Failure Mode	Load Capacity 2P (kip)	Mid-Span Deflection (in)
H1	Poor (FRP-Vert.)	Flexure	104	5.56
H4	Poor (FRP-Vert.)	Flexure	107	5.81
H2	Poor (FRP-Dia.)	Flexure	132	6.88
H6	Poor (FRP-Dia.)	Shear	110	4.34

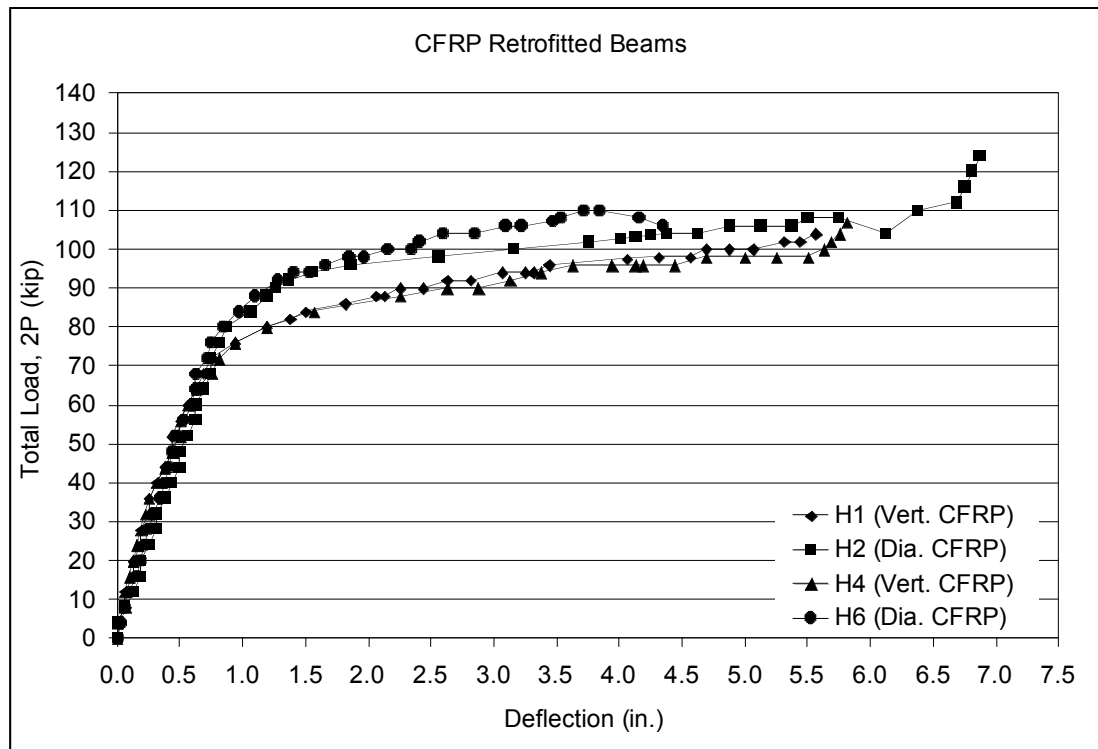


**Figure E1: Load vs. Deflection Curves for CFRP Retrofitted Beams**

## MMFX Steel Shear Bar Retrofit Application

**Table E2: Structural Load Results for MMFX Shear Bar Retrofitted Beams**

Beam ID	Beam Condition (Retrofit Type)	Failure Mode	Load Capacity 2P (kip)	Mid-Span Deflection (in)
H7	Poor (Shear Bar)	Flexure	130	6.19
H8	Poor (Shear Bar)	Flexure	132	6.63
H9	Poor (Shear Bar)	Flexure	104	6.50
H12	Poor (Shear Bar)	Flexure	102	6.19
H14	Poor (Shear Bar)	Flexure	130	6.19

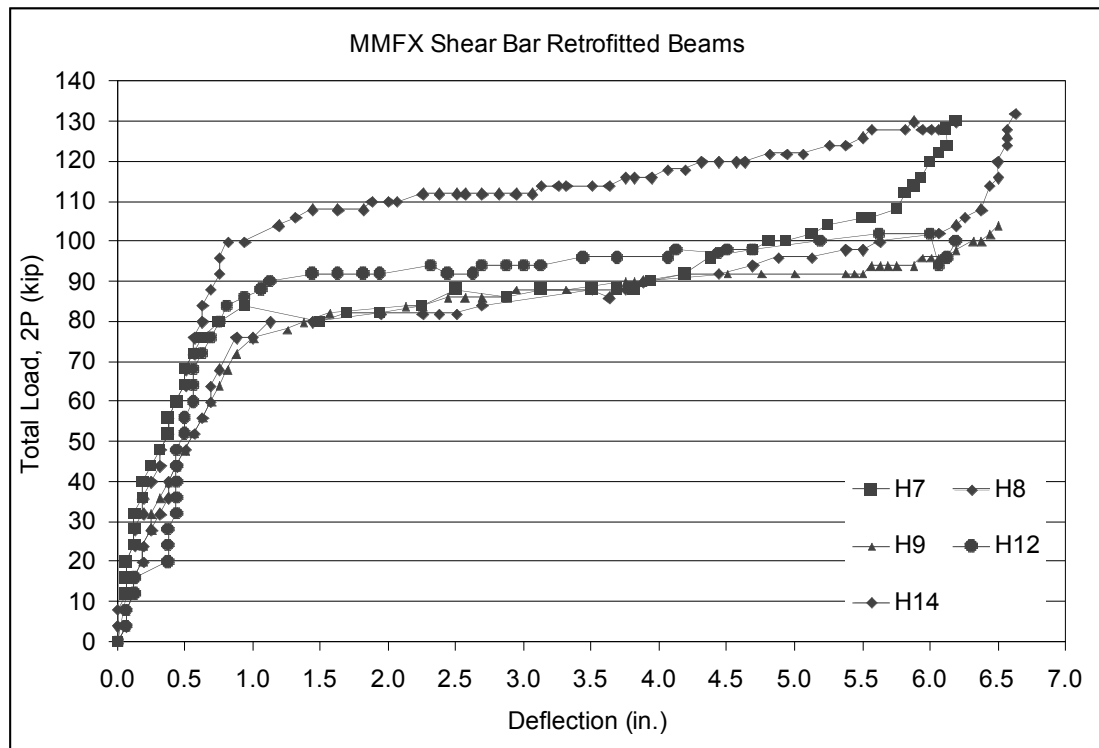


**Figure E2: Load vs. Deflection Curves for CFRP Retrofitted Beams**

## Sprayed Epoxy Coating Retrofit Application

**Table E3: Structural Load Results for Sprayed Epoxy Coating Retrofitted Beams**

Beam ID	Beam Condition (Retrofit Type)	Failure Mode	Load Capacity 2P (kip)	Mid-Span Deflection (in)
H10	Poor (Epoxy)	Flexure	112	6.25
H11	Poor (Epoxy)	Flexure	102	6.13
H13	Poor (Epoxy)	Shear	92	2.00

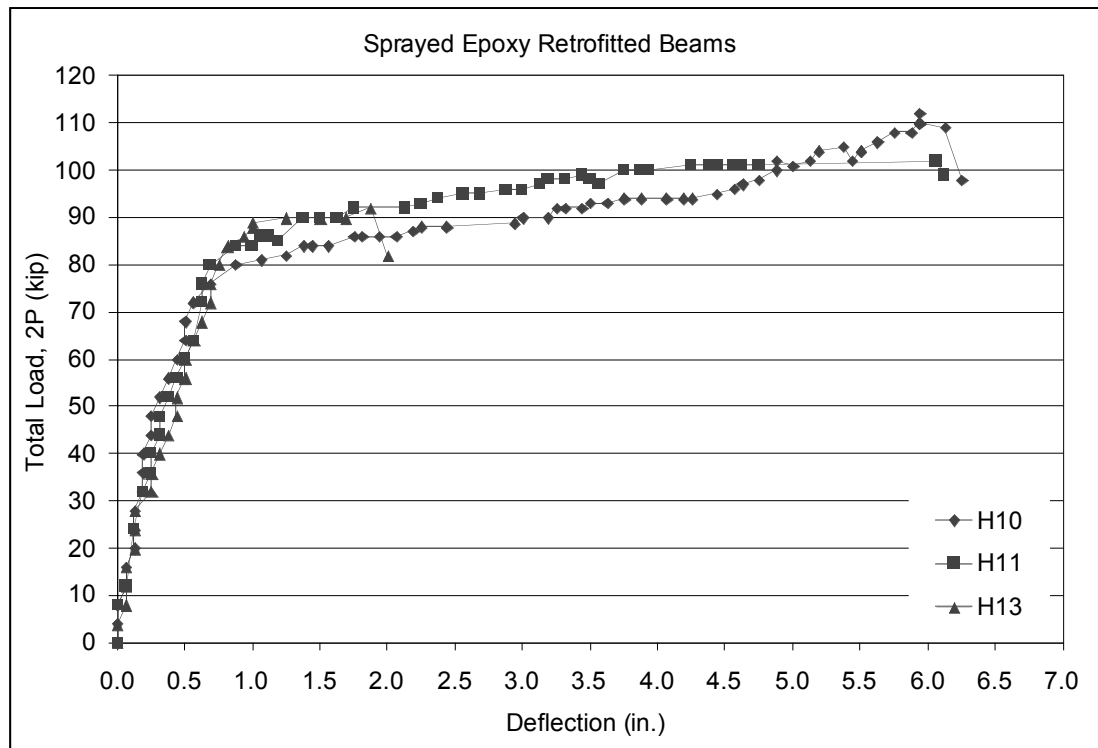


**Figure E3: Load vs. Deflection Curves for Sprayed Epoxy Retrofitted Beams**

## Control “Un-retrofitted” Beams

**Table E4: Structural Load Results for Control Beams**

Beam ID	Beam Condition (Retrofit Type)	Failure Mode	Load Capacity 2P (kip)	Mid-Span Deflection (in)
H3	Poor (Control)	Shear	82	1.69
H5	Poor (Control)	Shear	96	1.26
H14	Poor (Control)	Shear	100	4.06
H13	Poor (Control)	Shear	98	4.31

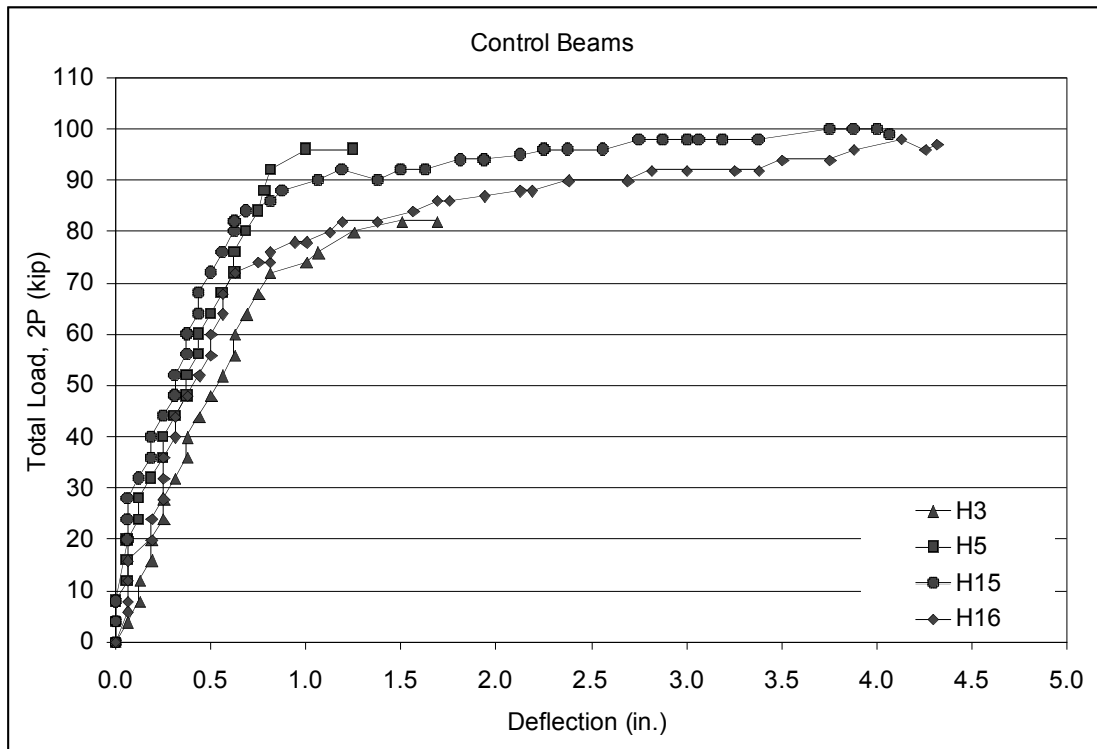


**Figure E4: Load vs. Deflection Curves for Control Beams**

<b>Beam:</b>	H1
<b>Retrofit:</b>	Vertical CFRP Strips
<b>Date Tested:</b>	8/27/2003

Pressure (psi)	P (lb)	2P (lb)	Displacement Measurement	Deflection (in)	Observation
0	0	0	30.31	0.00	
100	2	4	30.31	0.00	
200	4	8	30.25	0.06	
300	6	12	30.25	0.06	
400	8	16	30.19	0.13	
500	10	20	30.19	0.13	
600	12	24	30.13	0.19	
700	14	28	30.13	0.19	
800	16	32	30.06	0.25	
900	18	36	30.06	0.25	
1000	20	40	30.00	0.31	
1100	22	44	29.94	0.38	
1200	24	48	29.88	0.44	
1300	26	52	29.88	0.44	
1400	28	56	29.81	0.50	
1500	30	60	29.75	0.56	
1600	32	64	29.69	0.63	
1700	34	68	29.63	0.69	
1800	36	72	29.56	0.75	
1900	38	76	29.38	0.94	Yielding
2000	40	80	29.13	1.19	
2050	41	82	28.94	1.38	
2100	42	84	28.81	1.50	
2150	43	86	28.50	1.81	
2200	44	88	28.25	2.06	
2200	44	88	28.19	2.13	
2250	45	90	28.06	2.25	
2250	45	90	27.88	2.44	
2300	46	92	27.69	2.63	
2300	46	92	27.50	2.81	Shear Crack
2350	47	94	27.25	3.06	
2350	47	94	27.06	3.25	
2350	47	94	27.00	3.31	
2400	48	96	26.88	3.44	
2440	48.8	97.6	26.25	4.06	Debonding
2450	49	98	26.00	4.31	
2450	49	98	25.75	4.56	
2500	50	100	25.63	4.69	Debonding
2500	50	100	25.44	4.88	
2500	50	100	25.25	5.06	
2550	51	102	25.00	5.31	
2550	51	102	24.88	5.44	
2600	52	104	24.75	5.56	Shear Failure
0	0	0	25.56	4.75	Rebound

**Beam:** H2  
**Retrofit:** Diagonal CFRP Strips  
**Date Tested:** 8/27/2003

Pressure (psi)	P (lb)	2P (lb)	Displacement Measurement	Deflection (in)	Observation
0	0	0	30.50	0.00	
100	2	4	30.50	0.00	
200	4	8	30.44	0.06	
300	6	12	30.38	0.13	
400	8	16	30.31	0.19	
500	10	20	30.31	0.19	
600	12	24	30.25	0.25	
700	14	28	30.19	0.31	
800	16	32	30.19	0.31	
900	18	36	30.13	0.38	
1000	20	40	30.06	0.44	
1100	22	44	30.00	0.50	
1200	24	48	30.00	0.50	
1300	26	52	29.94	0.56	
1400	28	56	29.88	0.63	
1500	30	60	29.88	0.63	
1600	32	64	29.81	0.69	
1700	34	68	29.75	0.75	
1800	36	72	29.75	0.75	
1900	38	76	29.69	0.81	
2000	40	80	29.63	0.88	
2100	42	84	29.44	1.06	Yielding
2200	44	88	29.31	1.19	
2250	45	90	29.24	1.26	
2300	46	92	29.14	1.36	
2350	47	94	28.94	1.56	
2400	48	96	28.64	1.86	
2450	49	98	27.94	2.56	
2500	50	100	27.34	3.16	
2550	51	102	26.74	3.76	
2570	51.4	102.8	26.49	4.01	Deck Compression
2580	51.6	103.2	26.37	4.13	
2590	51.8	103.6	26.25	4.25	
2600	52	104	26.13	4.38	
2600	52	104	25.88	4.63	
2650	53	106	25.63	4.88	
2650	53	106	25.38	5.13	
2650	53	106	25.13	5.38	
2700	54	108	25.00	5.50	
2700	54	108	24.75	5.75	
2600	52	104	24.38	6.13	
2750	55	110	24.13	6.38	
2800	56	112	23.81	6.69	
2900	58	116	23.75	6.75	

3000	60	120	23.69	6.81	Limit of Pump Rebound
3100	62	124	23.63	6.88	
3200	64	128	23.63	6.88	
3300	66	132	23.63	6.88	
0	0	0	24.75	5.75	

<b>Beam:</b>	<b>H3</b>
<b>Retrofit:</b>	<b>Control</b>
<b>Date Tested:</b>	<b>9/2/2003</b>

Pressure (psi)	P (lb)	2P (lb)	Displacement Measurement	Deflection (in)	Observation
0	0	0	30.75	0.00	
100	2	4	30.69	0.06	
200	4	8	30.63	0.13	
300	6	12	30.63	0.13	
400	8	16	30.56	0.19	
500	10	20	30.56	0.19	
600	12	24	30.50	0.25	
700	14	28	30.50	0.25	
800	16	32	30.44	0.31	
900	18	36	30.38	0.38	
1000	20	40	30.38	0.38	
1100	22	44	30.31	0.44	
1200	24	48	30.25	0.50	
1300	26	52	30.19	0.56	
1400	28	56	30.13	0.63	
1500	30	60	30.13	0.63	
1600	32	64	30.06	0.69	
1700	34	68	30.00	0.75	
1800	36	72	29.94	0.81	
1850	37	74	29.75	1.00	
1900	38	76	29.69	1.06	Yielding
2000	40	80	29.50	1.25	
2050	41	82	29.25	1.50	Shear Crack
2050	41	82	29.06	1.69	Failure
0	0	0	29.06	1.69	

<b>Beam:</b>	<b>H4</b>
<b>Retrofit:</b>	<b>Vertical CFRP Strips</b>
<b>Date Tested:</b>	<b>9/2/2003</b>

Pressure (psi)	P (lb)	2P (lb)	Displacement Measurement	Deflection (in)	Observation
0	0	0	30.13	0.00	
100	2	4	30.13	0.00	
200	4	8	30.06	0.06	
300	6	12	30.06	0.06	
400	8	16	30.03	0.09	
500	10	20	30.00	0.13	
600	12	24	29.97	0.16	
700	14	28	29.94	0.19	
800	16	32	29.91	0.22	
900	18	36	29.88	0.25	
1000	20	40	29.81	0.31	
1100	22	44	29.75	0.38	
1200	24	48	29.69	0.44	
1300	26	52	29.63	0.50	
1400	28	56	29.63	0.50	
1500	30	60	29.56	0.56	Flexure Crack
1600	32	64	29.50	0.63	Long. Crack
1700	34	68	29.38	0.75	
1800	36	72	29.31	0.81	Yielding
1900	38	76	29.19	0.94	Shear Crack
2000	40	80	28.94	1.19	
2100	42	84	28.56	1.56	
2200	44	88	27.88	2.25	
2250	45	90	27.50	2.63	
2250	45	90	27.25	2.88	
2300	46	92	27.00	3.13	
2350	47	94	26.75	3.375	
2400	48	96	26.50	3.625	
2400	48	96	26.19	3.9375	
2400	48	96	26.00	4.125	
2400	48	96	25.94	4.1875	
2400	48	96	25.69	4.4375	
2450	49	98	25.44	4.6875	
2450	49	98	25.13	5	
2450	49	98	24.88	5.25	
2450	49	98	24.63	5.5	
2500	50	100	24.50	5.625	Deck compression
2550	51	102	24.44	5.6875	
2600	52	104	24.38	5.75	Limit of Pump
2675	53.5	107	24.31	5.8125	Rebound
0	0	0	25.38	4.75	

<b>Beam:</b>	<b>H5</b>
<b>Retrofit:</b>	<b>Control</b>
<b>Date Tested:</b>	<b>9/2/2003</b>

<b>Pressure (psi)</b>	<b>P (lb)</b>	<b>2P (lb)</b>	<b>Displacement Measurement</b>	<b>Deflection (in)</b>	<b>Observation</b>
0	0	0	30.13	0.00	
100	2	4	30.13	0.00	
200	4	8	30.13	0.00	
300	6	12	30.06	0.06	
400	8	16	30.06	0.06	
500	10	20	30.06	0.06	
600	12	24	30.00	0.13	
700	14	28	30.00	0.13	
800	16	32	29.94	0.19	
900	18	36	29.88	0.25	
1000	20	40	29.88	0.25	
1100	22	44	29.81	0.31	
1200	24	48	29.75	0.38	
1300	26	52	29.75	0.38	
1400	28	56	29.69	0.44	
1500	30	60	29.69	0.44	
1600	32	64	29.63	0.50	
1700	34	68	29.56	0.56	
1800	36	72	29.50	0.63	
1900	38	76	29.50	0.63	
2000	40	80	29.44	0.69	
2100	42	84	29.38	0.75	
2200	44	88	29.34	0.78	
2300	46	92	29.31	0.81	
2400	48	96	29.13	1.00	
2400	48	96	28.88	1.25	
0	0	0	28.88	1.25	Yielding Shear Crack Failure

<b>Beam:</b>	<b>H6</b>
<b>Retrofit:</b>	<b>Diagonal CFRP Strips</b>
<b>Date Tested:</b>	<b>9/23/2003</b>

Pressure (psi)	P (lb)	2P (lb)	Displacement Measurement	Deflection (in)	Observation
0	0	0	30.47	0.00	
100	2	4	30.44	0.03	
200	4	8	30.41	0.06	
300	6	12	30.38	0.09	
400	8	16	30.31	0.16	
500	10	20	30.28	0.19	
600	12	24	30.25	0.22	
700	14	28	30.22	0.25	
800	16	32	30.19	0.28	
900	18	36	30.13	0.34	
1000	20	40	30.09	0.38	
1100	22	44	30.06	0.41	
1200	24	48	30.03	0.44	
1300	26	52	30.00	0.47	
1400	28	56	29.94	0.53	
1500	30	60	29.88	0.59	
1600	32	64	29.84	0.63	
1700	34	68	29.84	0.63	
1800	36	72	29.75	0.72	
1900	38	76	29.72	0.75	
2000	40	80	29.63	0.84	
2100	42	84	29.50	0.97	Yielding
2200	44	88	29.38	1.09	
2300	46	92	29.19	1.28	
2350	47	94	29.06	1.41	
2350	47	94	28.94	1.53	
2400	48	96	28.81	1.66	
2450	49	98	28.63	1.84	
2450	49	98	28.50	1.97	
2500	50	100	28.31	2.16	
2500	50	100	28.13	2.34	
2550	51	102	28.06	2.41	
2600	52	104	27.88	2.59	
2600	52	104	27.63	2.84	
2650	53	106	27.38	3.09	
2650	53	106	27.25	3.22	
2680	53.6	107.2	27.00	3.47	
2700	54	108	26.94	3.53	Shear Crack
2750	55	110	26.75	3.72	
2750	55	110	26.63	3.84	
2700	54	108	26.31	4.16	
2650	53	106	26.13	4.34	
0	0	0	27.00	3.47	Rebound

<b>Beam:</b>	<b>H7</b>
<b>Retrofit:</b>	<b>MMFX Shear Bar</b>
<b>Date Tested:</b>	<b>2/3/2004</b>

Pressure (psi)	P (lb)	2P (lb)	Displacement Measurement	Deflection (in)	Observation
0	0	0	30.00	0.00	
300	6	12	29.94	0.06	
400	8	16	29.94	0.06	
500	10	20	29.94	0.06	
600	12	24	29.88	0.13	
700	14	28	29.88	0.13	
800	16	32	29.88	0.13	
900	18	36	29.81	0.19	
1000	20	40	29.81	0.19	
1100	22	44	29.75	0.25	
1200	24	48	29.69	0.31	
1300	26	52	29.63	0.38	
1400	28	56	29.63	0.38	
1500	30	60	29.56	0.44	
1600	32	64	29.50	0.50	
1700	34	68	29.50	0.50	
1800	36	72	29.44	0.56	Flexure Crack
1900	38	76	29.38	0.63	
2000	40	80	29.25	0.75	
2100	42	84	29.06	0.94	Yielding
2000	40	80	28.50	1.50	
2050	41	82	28.31	1.69	
2050	41	82	28.06	1.94	
2100	42	84	27.75	2.25	
2200	44	88	27.50	2.50	Shear Crack
2150	43	86	27.13	2.88	
2200	44	88	26.88	3.13	
2200	44	88	26.50	3.50	
2200	44	88	26.31	3.69	
2200	44	88	26.19	3.81	
2250	45	90	26.06	3.94	
2300	46	92	25.81	4.19	
2400	48	96	25.63	4.38	
2450	49	98	25.31	4.69	
2500	50	100	25.19	4.81	
2500	50	100	25.06	4.94	
2550	51	102	24.88	5.13	
2600	52	104	24.75	5.25	
2650	53	106	24.50	5.50	
2650	53	106	24.44	5.56	
2700	54	108	24.25	5.75	
2800	56	112	24.19	5.81	
2850	57	114	24.13	5.88	
2900	58	116	24.0625	5.94	
3000	60	120	24.00	6.00	

3000	60	120	24.00	6.00	Rebound
3050	61	122	23.94	6.06	
3100	62	124	23.88	6.13	
3200	64	128	23.88	6.12	
3250	65	130	23.81	6.19	
0	0	0	24.63	5.38	

<b>Beam:</b>	<b>H8</b>
<b>Retrofit:</b>	<b>MMFX Shear Bar</b>
<b>Date Tested:</b>	<b>2/3/2004</b>

Pressure (psi)	P (lb)	2P (lb)	Displacement Measurement	Deflection (in)	Observation
0	0	0	30.38	0.00	Existing Flexure Crack
100	2	4	30.31	0.06	
200	4	8	30.31	0.06	
300	6	12	30.25	0.13	
400	8	16	30.25	0.13	
500	10	20	30.19	0.19	
600	12	24	30.19	0.19	
700	14	28	30.13	0.25	
800	16	32	30.06	0.31	
900	18	36	30.00	0.38	
1000	20	40	30.00	0.38	
1100	22	44	29.94	0.44	
1200	24	48	29.88	0.50	
1300	26	52	29.81	0.56	
1400	28	56	29.75	0.63	
1500	30	60	29.69	0.6875	Flexure Crack
1600	32	64	29.69	0.6875	
1700	34	68	29.63	0.75	Shear Crack Yielding
1900	38	76	29.50	0.88	
1900	38	76	29.38	1.00	
2000	40	80	29.25	1.13	
2000	40	80	28.94	1.44	
2050	41	82	28.44	1.94	
2050	41	82	28.13	2.25	
2050	41	82	28.00	2.38	
2050	41	82	27.88	2.50	
2100	42	84	27.69	2.69	
2200	44	88	26.88	3.50	
2150	43	86	26.75	3.63	
2200	44	88	26.63	3.75	
2250	45	90	26.50	3.88	
2300	46	92	26.19	4.19	
2300	46	92	25.94	4.44	
2350	47	94	25.69	4.69	
2400	48	96	25.50	4.88	
2400	48	96	25.25	5.13	
2450	49	98	25.00	5.38	
2450	49	98	24.88	5.50	
2500	50	100	24.75	5.63	
2550	51	102	24.31	6.06	
2600	52	104	24.19	6.19	
2650	53	106	24.13	6.25	
2700	54	108	24.00	6.38	
2850	57	114	23.94	6.44	
2900	58	116	23.88	6.50	

3000	60	120	23.88	6.50	Rebound
3100	62	124	23.81	6.56	
3150	63	126	23.81	6.56	
3200	64	128	23.81	6.56	
3300	66	132	23.75	6.63	
0	0	0	24.63	5.75	

<b>Beam:</b>	<b>H9</b>
<b>Retrofit:</b>	<b>MMFX Shear Bar</b>
<b>Date Tested:</b>	<b>4/28/2004</b>

Pressure (psi)	P (lb)	2P (lb)	Displacement Measurement	Deflection (in)	Observation
0	0	0	30.25	0.00	
100	2	4	30.19	0.06	
200	4	8	30.19	0.06	
300	6	12	30.13	0.13	
400	8	16	30.13	0.13	
500	10	20	30.06	0.19	
600	12	24	30.06	0.19	
700	14	28	30.00	0.25	
800	16	32	30.00	0.25	
900	18	36	29.94	0.31	
1000	20	40	29.88	0.38	
1100	22	44	29.81	0.44	
1200	24	48	29.75	0.50	Flexure Crack
1300	26	52	29.69	0.56	
1400	28	56	29.63	0.63	
1500	30	60	29.56	0.69	Flexure Crack
1600	32	64	29.50	0.75	
1700	34	68	29.44	0.81	
1800	36	72	29.38	0.88	
1900	38	76	29.25	1.00	Yielding
1950	39	78	29.00	1.25	
2000	40	80	28.88	1.38	
2050	41	82	28.69	1.56	
2100	42	84	28.13	2.13	
2100	42	84	28.00	2.25	
2150	43	86	27.81	2.44	
2150	43	86	27.69	2.56	
2150	43	86	27.56	2.69	
2150	43	86	27.38	2.88	
2200	44	88	27.31	2.94	
2200	44	88	27.13	3.13	
2200	44	88	26.94	3.31	
2250	45	90	26.50	3.75	Shear Crack
2250	45	90	26.44	3.81	
2250	45	90	26.38	3.88	
2300	46	92	25.75	4.50	
2300	46	92	25.50	4.75	
2300	46	92	25.25	5.00	
2300	46	92	24.88	5.38	
2300	46	92	24.81	5.44	
2300	46	92	24.75	5.50	
2350	47	94	24.69	5.56	
2350	47	94	24.63	5.63	
2350	47	94	24.56	5.69	
2350	47	94	24.50	5.75	

2350	47	94	24.38	5.88	Limit of Pump
2400	48	96	24.31	5.94	
2400	48	96	24.25	6.00	
2400	48	96	24.19	6.06	
2400	48	96	24.13	6.13	
2450	49	98	24.06	6.19	
2500	50	100	23.94	6.31	
2500	50	100	23.88	6.38	
2550	51	102	23.81	6.44	
2600	52	104	23.75	6.50	
0	0	0	24.81	5.44	

<b>Beam:</b>	<b>H10</b>
<b>Retrofit:</b>	<b>Sprayed Epoxy Coating</b>
<b>Date Tested:</b>	<b>4/28/2004</b>

Pressure (psi)	P (lb)	2P (lb)	Displacement Measurement	Deflection (in)	Observation
0	0	0	30.13	0.00	
100	2	4	30.13	0.00	
200	4	8	30.13	0.00	
300	6	12	30.06	0.06	
400	8	16	30.06	0.06	
500	10	20	30.00	0.13	
600	12	24	30.00	0.13	
700	14	28	30.00	0.13	
800	16	32	29.94	0.19	
900	18	36	29.94	0.19	
1000	20	40	29.94	0.19	
1100	22	44	29.88	0.25	Flexure Crack
1200	24	48	29.88	0.25	
1300	26	52	29.81	0.31	
1400	28	56	29.75	0.38	
1500	30	60	29.69	0.44	Flexure Crack
1600	32	64	29.63	0.50	
1700	34	68	29.63	0.50	
1800	36	72	29.56	0.56	
1900	38	76	29.44	0.69	
2000	40	80	29.25	0.88	Yielding
2025	40.5	81	29.06	1.06	
2050	41	82	28.88	1.25	Shear Crack
2100	42	84	28.75	1.38	
2100	42	84	28.69	1.44	
2100	42	84	28.56	1.56	
2150	43	86	28.38	1.75	
2150	43	86	28.31	1.81	
2150	43	86	28.19	1.94	
2150	43	86	28.06	2.06	
2180	43.6	87.2	27.94	2.19	
2200	44	88	27.88	2.25	
2200	44	88	27.69	2.44	
2220	44.4	88.8	27.19	2.94	
2250	45	90	27.13	3.00	
2250	45	90	26.94	3.19	
2300	46	92	26.88	3.25	
2300	46	92	26.81	3.31	
2300	46	92	26.69	3.44	
2325	46.5	93	26.63	3.50	
2325	46.5	93	26.50	3.63	
2350	47	94	26.38	3.75	
2350	47	94	26.25	3.88	
2350	47	94	26.06	4.06	
2350	47	94	25.94	4.19	

2350	47	94	25.88	4.25	Deck Compression Rebound
2375	47.5	95	25.69	4.44	
2400	48	96	25.56	4.56	
2425	48.5	97	25.50	4.63	
2450	49	98	25.38	4.75	
2500	50	100	25.25	4.88	
2550	51	102	25.25	4.88	
2525	50.5	101	25.13	5.00	
2550	51	102	25.00	5.13	
2600	52	104	24.94	5.19	
2625	52.5	105	24.75	5.38	
2550	51	102	24.69	5.44	
2600	52	104	24.63	5.50	
2600	52	104	24.63	5.50	
2650	53	106	24.50	5.63	
2700	54	108	24.38	5.75	
2700	54	108	24.25	5.88	
2750	55	110	24.19	5.94	
2800	56	112	24.19	5.94	
2750	55	110	24.19	5.94	
2725	54.5	109	24.00	6.13	
2450	49	98	23.88	6.25	
0	0	0	24.81	5.31	

<b>Beam:</b>	<b>H11</b>
<b>Retrofit:</b>	<b>Sprayed Epoxy Coating</b>
<b>Date Tested:</b>	<b>4/28/2004</b>

Pressure (psi)	P (lb)	2P (lb)	Displacement Measurement	Deflection (in)	Observation
0	0	0	28.88	0.00	Yielding
200	4	8	28.88	0.00	
300	6	12	28.81	0.06	
600	12	24	28.75	0.13	
800	16	32	28.69	0.19	
900	18	36	28.63	0.25	
1000	20	40	28.63	0.25	
1100	22	44	28.56	0.31	
1200	24	48	28.56	0.31	
1300	26	52	28.50	0.38	
1400	28	56	28.44	0.44	
1500	30	60	28.38	0.50	
1600	32	64	28.31	0.56	
1800	36	72	28.25	0.63	
1900	38	76	28.25	0.63	
2000	40	80	28.19	0.69	
2100	42	84	28.00	0.88	
2150	43	84	27.88	1.00	
2150	43	86	27.81	1.06	
2125	42.5	86	27.75	1.13	
2100	42	85	27.69	1.19	
2250	45	90	27.50	1.38	
2250	45	90	27.38	1.50	
2250	45	90	27.25	1.63	
2300	46	92	27.13	1.75	
2300	46	92	26.75	2.13	
2325	46.5	93	26.63	2.25	
2350	47	94	26.50	2.38	
2375	47.5	95	26.31	2.56	
2375	47.5	95	26.19	2.69	
2400	48	96	26.00	2.88	
2400	48	96	25.88	3.00	
2425	48.5	97	25.75	3.13	
2450	49	98	25.69	3.19	
2450	49	98	25.56	3.31	
2475	49.5	99	25.44	3.44	
2450	49	98	25.38	3.50	
2425	48.5	97	25.31	3.56	
2500	50	100	25.13	3.75	
2500	50	100	25.00	3.88	
2500	50	100	24.94	3.94	
2525	50.5	101	24.63	4.25	
2525	50.5	101	24.50	4.38	
2525	50.5	101	24.44	4.44	
2525	50.5	101	24.31	4.56	

2525	50.5	101	24.25	4.63	Deck Compression Rebound
2525	50.5	101	24.13	4.75	
2550	51	102	24.06	6.06	
2475	49.5	99	24.00	6.13	
0	0	0	25.00	5.13	

<b>Beam:</b>	<b>H12</b>
<b>Retrofit:</b>	<b>MMFX Shear Bar</b>
<b>Date Tested:</b>	<b>4/29/2004</b>

Pressure (psi)	P (lb)	2P (lb)	Displacement Measurement	Deflection (in)	Observation
0	0	0	30.44	0.00	
100	2	4	30.38	0.06	
200	4	8	30.38	0.06	
300	6	12	30.31	0.13	
400	8	16	30.31	0.13	
500	10	20	30.06	0.38	
600	12	24	30.06	0.38	
700	14	28	30.06	0.38	
800	16	32	30.00	0.44	
900	18	36	30.00	0.44	
1000	20	40	30.00	0.44	
1100	22	44	30.00	0.44	Flexure Crack
1200	24	48	30.00	0.44	
1300	26	52	29.94	0.50	
1400	28	56	29.94	0.50	
1500	30	60	29.88	0.56	Flexure Crack
1600	32	64	29.88	0.56	
1700	34	68	29.88	0.56	
1800	36	72	29.81	0.63	
1900	38	76	29.75	0.69	
2000	40	80	29.69	0.75	
2100	42	84	29.63	0.81	
2150	43	86	29.50	0.94	
2200	44	88	29.38	1.06	
2250	45	90	29.31	1.13	Yielding
2300	46	92	29.00	1.44	
2300	46	92	28.81	1.63	
2300	46	92	28.63	1.81	
2300	46	92	28.50	1.94	
2350	47	94	28.13	2.31	
2300	46	92	28.00	2.44	
2300	46	92	27.81	2.63	
2350	47	94	27.75	2.69	
2350	47	94	27.56	2.88	
2350	47	94	27.44	3.00	
2350	47	94	27.31	3.13	
2400	48	96	27.00	3.44	
2400	48	96	26.75	3.69	
2400	48	96	26.38	4.06	
2450	49	98	26.31	4.13	
2425	48.5	97	26.00	4.44	
2450	49	98	25.94	4.50	
2450	49	98	25.75	4.69	
2500	50	100	25.25	5.19	
2550	51	102	24.81	5.63	

2550	51	102	24.44	6.00	Deck Compression Rebound
2350	47	94	24.38	6.06	
2400	48	96	24.31	6.13	
2500	50	100	24.25	6.19	
0	0	0	25.25	5.19	

<b>Beam:</b>	<b>H13</b>
<b>Retrofit:</b>	<b>Sprayed Epoxy Coating</b>
<b>Date Tested:</b>	<b>4/28/2004</b>

<b>Pressure (psi)</b>	<b>P (lb)</b>	<b>2P (lb)</b>	<b>Displacement Measurement</b>	<b>Deflection (in)</b>	<b>Observation</b>
0	0	0	30.50	0.00	
100	2	4	30.50	0.00	
200	4	8	30.44	0.06	
300	6	12	30.44	0.06	
400	8	16	30.44	0.06	
500	10	20	30.38	0.13	
600	12	24	30.38	0.13	
700	14	28	30.38	0.13	
800	16	32	30.25	0.25	
900	18	36	30.25	0.25	
1000	20	40	30.19	0.31	
1100	22	44	30.13	0.38	Flexure Crack
1200	24	48	30.06	0.44	
1300	26	52	30.06	0.44	
1400	28	56	30.00	0.50	
1500	30	60	30.00	0.50	
1600	32	64	29.94	0.56	
1700	34	68	29.88	0.63	
1800	36	72	29.81	0.69	
1900	38	76	29.81	0.69	Epoxy Crack
2000	40	80	29.75	0.75	
2100	42	84	29.69	0.81	Shear Crack
2150	43	86	29.56	0.94	
2200	44	88	29.50	1.00	Yielding
2225	44.5	89	29.50	1.00	
2250	45	90	29.25	1.25	
2250	45	90	29.00	1.50	
2250	45	90	28.81	1.69	
2300	46	92	28.63	1.88	
2050	41	82	28.50	2.00	Shear Failure

<b>Beam:</b>	<b>H14</b>
<b>Retrofit:</b>	<b>MMFX Shear Bar</b>
<b>Date Tested:</b>	<b>4/7/2005</b>

Pressure (psi)	P (lb)	2P (lb)	Displacement Measurement	Deflection (in)	Observation
0	0	0	30.06	0.00	
100	2	4	30.06	0.00	
200	4	8	30.06	0.00	
300	6	12	30.00	0.06	
400	8	16	30.00	0.06	
500	10	20	30.00	0.06	
600	12	24	29.94	0.13	
700	14	28	29.94	0.13	
800	16	32	29.88	0.19	
900	18	36	29.88	0.19	
1000	20	40	29.81	0.25	
1100	22	44	29.75	0.31	
1200	24	48	29.75	0.31	
1300	26	52	29.69	0.38	
1400	28	56	29.69	0.38	
1500	30	60	29.63	0.44	
1600	32	64	29.56	0.50	
1700	34	68	29.56	0.50	
1800	36	72	29.50	0.56	
1900	38	76	29.50	0.56	
2000	40	80	29.44	0.63	
2100	42	84	29.44	0.63	
2200	44	88	29.38	0.69	
2300	46	92	29.31	0.75	
2400	48	96	29.31	0.75	
2500	50	100	29.25	0.81	
2500	50	100	29.13	0.94	Yielding/Shear Crack
2600	52	104	28.88	1.19	
2650	53	106	28.75	1.31	
2700	54	108	28.63	1.44	
2700	54	108	28.44	1.63	
2700	54	108	28.25	1.81	
2750	55	110	28.19	1.88	
2750	55	110	28.06	2.00	
2750	55	110	28.00	2.06	
2800	56	112	27.81	2.25	
2800	56	112	27.69	2.38	
2800	56	112	27.56	2.50	
2800	56	112	27.50	2.56	
2800	56	112	27.38	2.69	
2800	56	112	27.25	2.81	
2800	56	112	27.13	2.94	
2800	56	112	27.00	3.06	
2850	57	114	26.94	3.13	
2850	57	114	26.81	3.25	

2850	57	114	26.75	3.31
2850	57	114	26.56	3.50
2850	57	114	26.44	3.63
2900	58	116	26.31	3.75
2900	58	116	26.25	3.81
2900	58	116	26.13	3.94
2950	59	118	26.00	4.06
2950	59	118	25.88	4.19
3000	60	120	25.75	4.31
3000	60	120	25.63	4.44
3000	60	120	25.50	4.56
3000	60	120	25.44	4.63
3050	61	122	25.25	4.81
3050	61	122	25.13	4.94
3050	61	122	25.00	5.06
3100	62	124	24.81	5.25
3100	62	124	24.69	5.38
3150	63	126	24.56	5.50
3200	64	128	24.50	5.56
3200	64	128	24.25	5.81
3250	65	130	24.19	5.88
3200	64	128	24.13	5.94
3200	64	128	24.06	6.00
3200	64	128	24.00	6.06
3250	65	130	23.88	6.19
0	0	0	25.19	4.88

Deck Compression  
Rebound

<b>Beam:</b>	<b>H15</b>
<b>Retrofit:</b>	<b>Control</b>
<b>Date Tested:</b>	<b>4/7/2005</b>

Pressure (psi)	P (lb)	2P (lb)	Displacement Measurement	Deflection (in)	Observation
0	0	0	29.88	0.00	
100	2	4	29.88	0.00	
200	4	8	29.88	0.00	
500	10	20	29.81	0.06	
600	12	24	29.81	0.06	
700	14	28	29.81	0.06	
800	16	32	29.75	0.13	
900	18	36	29.69	0.19	
1000	20	40	29.69	0.19	
1100	22	44	29.63	0.25	Flexure Crack
1200	24	48	29.56	0.31	
1300	26	52	29.56	0.31	
1400	28	56	29.50	0.38	
1500	30	60	29.50	0.38	
1600	32	64	29.44	0.44	
1700	34	68	29.44	0.44	
1800	36	72	29.38	0.50	
1900	38	76	29.31	0.56	
2000	40	80	29.25	0.63	
2050	41	82	29.25	0.63	
2100	42	84	29.19	0.69	
2150	43	86	29.06	0.81	
2200	44	88	29.00	0.88	
2250	45	90	28.81	1.06	
2300	46	92	28.69	1.19	Yielding
2250	45	90	28.50	1.38	
2300	46	92	28.38	1.50	
2300	46	92	28.25	1.63	
2350	47	94	28.06	1.81	
2350	47	94	27.94	1.94	
2375	47.5	95	27.75	2.13	
2400	48	96	27.63	2.25	
2400	48	96	27.50	2.38	
2400	48	96	27.31	2.56	
2450	49	98	27.13	2.75	
2450	49	98	27.00	2.88	
2450	49	98	26.88	3.00	
2450	49	98	26.81	3.06	
2450	49	98	26.69	3.19	
2450	49	98	26.50	3.38	Shear Crack
2500	50	100	26.13	3.75	
2500	50	100	26.00	3.88	
2500	50	100	25.88	4.00	
2475	49.5	99	25.81	4.06	Shear Failure

<b>Beam:</b>	<b>H16</b>
<b>Retrofit:</b>	<b>Control</b>
<b>Date Tested:</b>	<b>4/7/2005</b>

Pressure (psi)	P (lb)	2P (lb)	Displacement Measurement	Deflection (in)	Observation
0	0	0	30.25	0.00	Existing Flexure Crack
150	3	6	30.25	0.06	
200	4	8	30.19	0.06	
300	6	12	30.19	0.06	
400	8	16	30.19	0.06	
500	10	20	30.06	0.19	
600	12	24	30.06	0.19	
700	14	28	30.00	0.25	
800	16	32	30.00	0.25	
900	18	36	30.00	0.25	
1000	20	40	29.94	0.31	
1100	22	44	29.94	0.31	
1200	24	48	29.88	0.38	
1300	26	52	29.81	0.44	
1400	28	56	29.75	0.50	
1500	30	60	29.75	0.50	
1600	32	64	29.69	0.56	
1700	34	68	29.69	0.56	
1800	36	72	29.63	0.63	
1850	37	74	29.50	0.75	
1850	37	74	29.44	0.81	
1900	38	76	29.44	0.81	
1950	39	78	29.31	0.94	
1950	39	78	29.25	1.00	
2000	40	80	29.13	1.13	
2050	41	82	29.06	1.19	
2050	41	82	28.88	1.38	
2100	42	84	28.69	1.56	
2150	43	86	28.56	1.69	
2150	43	86	28.50	1.75	
2175	43.5	87	28.31	1.94	
2200	44	88	28.13	2.13	
2200	44	88	28.06	2.19	
2250	45	90	27.88	2.38	
2250	45	90	27.56	2.69	
2300	46	92	27.44	2.81	
2300	46	92	27.25	3.00	
2300	46	92	27.00	3.25	
2300	46	92	26.88	3.38	
2350	47	94	26.75	3.50	
2350	47	94	26.50	3.75	
2400	48	96	26.38	3.88	
2450	49	98	26.13	4.13	
2400	48	96	26.00	4.25	
2425	48.5	97	25.94	4.31	
0	0	0	26.56	3.69	Shear Crack
					Shear Failure
					Rebound

**Appendix F**  
**Statistical Analysis**

### Bartlett's Test for Equal Variances (5 Treatments) – Load Values

$$H_0: \sigma_1^2 = \sigma_2^2 = \sigma_3^2 = \sigma_4^2 = \sigma_5^2$$

Anova: Single Factor

#### SUMMARY

Groups	Count	Sum	Average	Variance
CFRP-Vert	2	211	105.5	4.5
CFRP-Dia.	2	234	117.0	98.0
Shear Bar	5	598	119.6	230.8
Epoxy	3	306	102.0	100.0
No Retrofit	4	376	94.0	66.7

$$S_p^2 = \frac{\sum_{i=1}^a (n_i - 1) S_i^2}{N - a}$$

$$S_p^2 = \frac{1(4.5) + 1(98.0) + 4(230.8) + 2(100.0) + 3(66.7)}{20} = 71.3$$

$$q = (N - a) \log_{10} S_p^2 - \sum_{i=1}^a (n_i - 1) \log_{10} S_i^2$$

$$q = 20 \log_{10} (71.3) - [\log_{10} 4.5 + \log_{10} 98.0 + 4 \log_{10} 230.8 + 2 \log_{10} 100.0 + 3 \log_{10} 66.7]$$

$$q = 15.49$$

$$c = 1 + \frac{1}{3(a-1)} \left( \sum_{i=1}^a (n_i - 1)^{-1} - (N - a)^{-1} \right)$$

$$c = 1 + \frac{1}{3(5-1)} ((1 + 1 + 0.25 + 0.50 + 0.33) - 0.05) = 1.25$$

$$\chi_0^2 = 2.3026 \left( \frac{q}{c} \right) = 2.3026 \left( \frac{15.49}{1.25} \right) = 28.54 > \chi_{0.05,4}^2 = 9.49$$

**Reject the Null Hypothesis: all five variances are not the same**

### Bartlett's Test for Equal Variances (4 Treatments) – Load Values

$$H_0: \sigma_1^2 = \sigma_2^2 = \sigma_3^2 = \sigma_4^2$$

Anova: Single Factor

#### SUMMARY

Groups	Count	Sum	Average	Variance
CFRP	4	445	111.3	78.3
Shear Bar	5	598	119.6	230.8
Epoxy	3	306	102.0	100.0
No Retrofit	4	376	94.0	66.7

$$S_p^2 = \frac{\sum_{i=1}^a (n_i - 1) S_i^2}{N - a}$$

$$S_p^2 = \frac{3(78.3) + 4(230.8) + 2(100.0) + 3(66.7)}{20} = 77.91$$

$$q = (N - a) \log_{10} S_p^2 - \sum_{i=1}^a (n_i - 1) \log_{10} S_i^2$$

$$q = 20 \log_{10} (77.91) - [3 \log_{10} 78.3 + 4 \log_{10} 230.8 + 2 \log_{10} 100.0 + 3 \log_{10} 66.7]$$

$$q = 13.22$$

$$c = 1 + \frac{1}{3(a-1)} \left( \sum_{i=1}^a (n_i - 1)^{-1} - (N - a)^{-1} \right)$$

$$c = 1 + \frac{1}{3(4-1)} ((0.33 + 0.25 + 0.50 + 0.33) - 0.05) = 1.15$$

$$\chi_0^2 = 2.3026 \left( \frac{q}{c} \right) = 2.3026 \left( \frac{13.22}{1.15} \right) = 26.48 > \chi_{0.05,3}^2 = 7.81$$

**Reject the Null Hypothesis: all four variances are not the same**

**Bartlett's Test for Equal Variances (5 Treatments) – Deflection Values**

$$H_0: \sigma_1^2 = \sigma_2^2 = \sigma_3^2 = \sigma_4^2 = \sigma_5^2$$

Anova: Single Factor

SUMMARY

Groups	Count	Sum	Average	Variance
CFRP-Vert	2	11.4	5.7	0.03
CFRP-Dia.	2	11.2	5.6	3.23
Shear Bar	5	31.7	6.3	0.04
Epoxy	3	14.4	4.8	5.86
No Retrofit	4	11.3	2.8	2.49

$$S_p^2 = \frac{\sum_{i=1}^a (n_i - 1) S_i^2}{N - a}$$

$$S_p^2 = \frac{1(0.03) + 1(3.23) + 4(0.04) + 2(5.86) + 3(2.49)}{20} = 1.13$$

$$q = (N - a) \log_{10} S_p^2 - \sum_{i=1}^a (n_i - 1) \log_{10} S_i^2$$

$$q = 20 \log_{10} (1.13) - [\log_{10} 0.03 + \log_{10} 3.23 + 4 \log_{10} 0.04 + 2 \log_{10} 5.86 + 3 \log_{10} 2.49]$$

$$q = 4.95$$

$$c = 1 + \frac{1}{3(a-1)} \left( \sum_{i=1}^a (n_i - 1)^{-1} - (N - a)^{-1} \right)$$

$$c = 1 + \frac{1}{3(5-1)} ((1+1+0.25+0.50+0.33) - 0.05) = 1.25$$

$$\chi_0^2 = 2.3026 \left( \frac{q}{c} \right) = 2.3026 \left( \frac{4.95}{1.25} \right) = 9.11 < \chi_{0.05,4}^2 = 9.49$$

**Cannot reject the Null Hypothesis: all five variances are the same**

### Bartlett's Test for Equal Variances (4 Treatments) – Deflection Values

$$H_0: \sigma_1^2 = \sigma_2^2 = \sigma_3^2 = \sigma_4^2$$

Anova: Single Factor

#### SUMMARY

Groups	Count	Sum	Average	Variance
CFRP	4	22.6	5.6	1.09
Shear Bar	5	31.7	6.3	0.04
Epoxy	3	14.4	4.8	5.86
No Retrofit	4	11.3	2.8	2.49

$$S_p^2 = \frac{\sum_{i=1}^a (n_i - 1) S_i^2}{N - a}$$

$$S_p^2 = \frac{3(1.09) + 4(0.04) + 2(5.86) + 3(2.49)}{20} = 1.13$$

$$q = (N - a) \log_{10} S_p^2 - \sum_{i=1}^a (n_i - 1) \log_{10} S_i^2$$

$$q = 20 \log_{10} (1.13) - [3 \log_{10} 1.09 + 4 \log_{10} 0.04 + 2 \log_{10} 5.86 + 3 \log_{10} 2.49]$$

$$q = 3.82$$

$$c = 1 + \frac{1}{3(a-1)} \left( \sum_{i=1}^a (n_i - 1)^{-1} - (N - a)^{-1} \right)$$

$$c = 1 + \frac{1}{3(4-1)} ((0.33 + 0.25 + 0.50 + 0.33) - 0.05) = 1.15$$

$$\chi_0^2 = 2.3026 \left( \frac{q}{c} \right) = 2.3026 \left( \frac{3.82}{1.15} \right) = 7.64 < \chi_{0.05,3}^2 = 7.81$$

**Cannot reject the Null Hypothesis: all five variances are the same**

### Sample Size Adequacy – Deflection Response

<b>Retrofit Method</b>	<b>Deflection Values</b>				
CFRP-Vert	5.56	5.81			
CFRP-Dia.	6.88	4.34			
Shear Bar	6.19	6.63	6.5	6.19	6.19
Epoxy	6.25	6.13	2		
No Retrofit	1.69	1.26	4.06	4.31	

Anova: Single Factor

#### SUMMARY

<i>Groups</i>	<i>Count</i>	<i>Sum</i>	<i>Average</i>	<i>Variance</i>
CFRP-Vert	2	11.4	5.69	0.03
CFRP-Dia.	2	11.2	5.61	3.23
Shear Bar	5	31.7	6.34	0.04
Epoxy	3	14.4	4.79	5.86
No Retrofit	4	11.3	2.83	2.49

#### ANOVA

<i>Source of Variation</i>	<i>SS</i>	<i>df</i>	<i>MS</i>	<i>F</i>	<i>P-value</i>	<i>F crit</i>
Between Groups	29.62	4	7.41	3.60	0.04	3.36
Within Groups	22.61	11	2.06			
Total	52.24	15				

#### *Variables*

$n = 5, a = 5, \sigma^2 = 2.06$  (from MSE in the ANOVA table)

$$\Phi^2 = \frac{(5)(7.38)}{5(2.06)} = 3.58$$

$$\Phi = 1.89$$

#### *Chart V (Text)*

$$v_1 = a - 1 = 4$$

$$v_2 = a(n - 1) = 20$$

$$\text{Probability} = 0.11$$

**Power = 1 –  $\beta$  = 0.89 ~ 0.90 Sample Size is Adequate**

### Sample Size Adequacy – Load Response

<b>Retrofit Method</b>	<b>Load Capacity Values</b>				
CFRP-Vert.	104	107			
CFRP-Dia.	124	110			
Shear Bar	130	132	104	102	130
Epoxy	112	102	92		
No Retrofit	82	96	100	98	

#### **Anova: Single Factor**

##### SUMMARY

<i>Groups</i>	<i>Count</i>	<i>Sum</i>	<i>Average</i>	<i>Variance</i>
CFRP-Vert	2	211	105.5	4.5
CFRP-Dia.	2	234	117.0	98.0
Shear Bar	5	598	119.6	230.8
Epoxy	3	306	102.0	100.0
No Retrofit	4	376	94.0	66.7

##### ANOVA

<i>Source of Variation</i>	<i>SS</i>	<i>df</i>	<i>MS</i>	<i>F</i>	<i>P-value</i>	<i>F crit</i>
Between Groups	1738.74	4	434.68	3.35	0.05	3.36
Within Groups	1425.70	11	129.61			
Total	3164.44	15				

##### *Variables*

$n = 5, a = 5, \sigma^2 = 129.61$  (from MSE in the ANOVA table)

$$\Phi^2 = \frac{(5)(453.1)}{5(129.61)} = 3.50$$

$$\Phi = 1.87$$

##### *Chart V (Text)*

$$v_1 = a-1 = 4$$

$$v_2 = a(n-1) = 20$$

$$\text{Probability} = 0.11$$

**Power = 1 –  $\beta$  = 0.89 ~ 0.90 Sample Size is Adequate**

## **Appendix G**

### **Deflection Results from Field Implementation**

## Span 4 – Beam 2 without Retrofit

**Table G1: S4B2 Mid-Span Deflection Values**

Position ft.	Deflection			
	Beam 2L	Beam 2R	Beam 2 Avg.	Beam 3
1.2	0.0180	0.0297	0.0239	0.0041
2.2	0.0219	0.0340	0.0279	0.0053
3.2	0.0252	0.0377	0.0314	0.0066
4.2	0.0276	0.0403	0.0340	0.0076
6.8	0.0323	0.0453	0.0388	0.0089
9.5	0.0360	0.0493	0.0426	0.0093
12.2	0.0322	0.0442	0.0382	0.0092
14.9	0.0233	0.0327	0.0280	0.0072
15.9	0.0191	0.0275	0.0233	0.0067
16.9	0.0135	0.0207	0.0171	0.0054
17.9	0.0076	0.0136	0.0106	0.0037

**Table G2: S4B2 Quarter-Span Deflection Values**

Position ft.	Deflection			
	Beam 2L	Beam 2R	Beam 2 Avg.	Beam 3
1.2	0.0100	0.0239	0.0169	0.0031
2.2	0.0165	0.0305	0.0235	0.0043
3.2	0.0185	0.0327	0.0256	0.0047
4.2	0.0206	0.0347	0.0276	0.0050
6.8	0.0222	0.0359	0.0290	0.0050
9.5	0.0223	0.0354	0.0288	0.0051
12.2	0.0185	0.0295	0.0240	0.0053
14.9	0.0139	0.0199	0.0169	0.0052
15.9	0.0117	0.0153	0.0135	0.0047
16.9	0.0085	0.0107	0.0096	0.0039
17.9	0.0051	0.0053	0.0052	0.0028

## Span 4 – Beam 2 with Retrofit

**Table G3: S4B2R Mid-Span Deflection Values**

	Deflection				
Position	Beam 1	Beam 2L	Beam 2R	Beam 2 Avg.	Beam 3
ft.					
1.2	0.0011	0.0158	0.0179	0.0169	0.0023
2.2	0.0013	0.0193	0.0205	0.0199	0.0024
3.2	0.0014	0.0229	0.0235	0.0232	0.0026
4.2	0.0014	0.0259	0.0264	0.0262	0.0025
6.8	0.0013	0.0303	0.0311	0.0307	0.0025
9.5	0.0013	0.0345	0.0365	0.0355	0.0023
12.2	0.0008	0.0306	0.0313	0.0310	0.0017
14.9	0.0002	0.0231	0.0216	0.0223	0.0008
15.9	-0.0001	0.0193	0.0167	0.0180	0.0003
16.9	-0.0006	0.0130	0.0090	0.0110	-0.0004
17.9	-0.0009	0.0078	0.0028	0.0053	-0.0009

**Table G4: S4B2R Quarter-Span Deflection Values**

	Deflection				
Position	Beam 1	Beam 2L	Beam 2R	Beam 2 Avg.	Beam 3
ft.					
1.2	0.0010	0.0108	0.0147	0.0127	0.0035
2.2	0.0010	0.0141	0.0176	0.0158	0.0038
3.2	0.0010	0.0168	0.0199	0.0184	0.0037
4.2	0.0010	0.0187	0.0222	0.0205	0.0036
6.8	0.0009	0.0205	0.0239	0.0222	0.0033
9.5	0.0008	0.0206	0.0242	0.0224	0.0031
12.2	0.0005	0.0170	0.0202	0.0186	0.0025
14.9	0.0001	0.0119	0.0129	0.0124	0.0017
15.9	-0.0002	0.0096	0.0086	0.0091	0.0014
16.9	-0.0003	0.0072	0.0044	0.0058	0.0012
17.9	-0.0007	0.0036	-0.0016	0.0010	0.0008

**Span 4 – Beam 6 without Retrofit**

**Table G5: S4B6 Mid-Span Deflection Values**

Position ft.	Deflection		
	Beam 5	Beam 6R	Beam 7
1.2	0.0078	0.0125	0.0017
2.2	0.0094	0.0151	0.0020
3.2	0.0102	0.0180	0.0022
4.2	0.0109	0.0211	0.0024
6.8	0.0118	0.0266	0.0027
9.5	0.0133	0.0320	0.0029
12.2	0.0123	0.0310	0.0029
14.9	0.0093	0.0229	0.0024
15.9	0.0079	0.0195	0.0023
16.9	0.0054	0.0143	0.0019
17.9	0.0034	0.0098	0.0017

**Table G6: S4B6 Quarter-Span Deflection Values**

Position ft.	Deflection		
	Beam 5	Beam 6R	Beam 7
1.2	0.0041	0.0090	0.0014
2.2	0.0051	0.0109	0.0017
3.2	0.0060	0.0125	0.0019
4.2	0.0068	0.0140	0.0020
6.8	0.0081	0.0164	0.0021
9.5	0.0089	0.0205	0.0024
12.2	0.0082	0.0220	0.0023
14.9	0.0065	0.0191	0.0018
15.9	0.0056	0.0167	0.0017
16.9	0.0043	0.0128	0.0014
17.9	0.0031	0.0094	0.0011

## Span 4 – Beam 6 with Retrofit

**Table G7: S4B6R Mid-Span Deflection Values**

Position ft.	Deflection				
	Beam 5	Beam 6L	Beam 6R	Beam 6 Avg.	Beam 7
1.2	0.0046	0.0111	0.0109	0.0110	0.0017
2.2	0.0060	0.0141	0.0140	0.0141	0.0020
3.2	0.0070	0.0177	0.0176	0.0176	0.0022
4.2	0.0076	0.0208	0.0206	0.0207	0.0024
6.8	0.0085	0.0262	0.0260	0.0261	0.0025
9.5	0.0085	0.0313	0.0311	0.0312	0.0022
12.2	0.0065	0.0288	0.0287	0.0288	0.0016
14.9	0.0037	0.0211	0.0211	0.0211	0.0007
15.9	0.0025	0.0164	0.0166	0.0165	0.0004
16.9	0.0016	0.0117	0.0121	0.0119	-0.0002
17.9	0.0006	0.0065	0.0071	0.0068	-0.0007

**Table G8: S4B6R Quarter-Span Deflection Values**

Position ft.	Deflection				
	Beam 5	Beam 6L	Beam 6R	Beam 6 Avg.	Beam 7
1.2	-0.0012	0.0059	0.0076	0.0067	0.0004
2.2	-0.0002	0.0076	0.0095	0.0085	0.0006
3.2	0.0007	0.0091	0.0111	0.0101	0.0008
4.2	0.0016	0.0106	0.0127	0.0116	0.0011
6.8	0.0033	0.0132	0.0152	0.0142	0.0013
9.5	0.0046	0.0168	0.0194	0.0181	0.0012
12.2	0.0041	0.0181	0.0213	0.0197	0.0011
14.9	0.0025	0.0142	0.0176	0.0159	0.0000
15.9	0.0013	0.0112	0.0144	0.0128	-0.0005
16.9	-0.0002	0.0079	0.0107	0.0093	-0.0008
17.9	-0.0021	0.0036	0.0057	0.0046	-0.0015